

Mimicking Microbial Membranes

by

Jakob Andersson

Thesis

Submitted to Flinders University

for the degree of

Doctor of Philosophy

College of Science and Engineering

December 2018

Contents

Declaration	iv
Acknowledgements	v
Abstract	vi
List of abbreviations	vii
1 Model Membrane Architectures	1
1.1 Introduction	1
1.2 The importance of temperature	2
1.3 Black lipid membranes	4
1.4 Solid supported membranes	8
1.5 Polymer supported membranes	12
1.6 Tethered membranes	15
1.7 Conclusion	21
1.8 References	22
2 Methods: Neutron Scattering and Electrochemical Impedance Spectroscopy	27
2.1 Neutron scattering in soft matter	27
2.1.1 Theory of neutron scattering	27
2.1.2 Neutron data analysis	34
2.1.3 Monte Carlo error analysis	37
2.1.4 Other approaches to fit neutron data	37
2.2 Electrochemical Impedance Spectroscopy	38
2.2.1 Theory of electrochemical impedance spectroscopy	38
2.2.2 Fitting and interpretation of EIS data	42
2.3 Experimental Protocols	45
2.3.1 Substrate preparation	46
2.3.2 Bilayer formation	48
2.4 References	49
3 Tethered Membranes to Study Artificial Ion Channels	51
3.1 Introduction	51
3.2 Ion transport studies by EIS	53

3.2.1	Ion transport of tricrown ethers.....	53
3.2.2	Ion transport of crown ether monomers.....	57
3.3	Conclusion.....	59
3.4	References.....	60
4	New Membrane Architectures for Tethered Bilayer Lipid Membranes.....	61
4.1	Introduction.....	62
4.2	Materials and methods.....	66
4.3	Results and discussion.....	68
4.3.1	Synthetic approach.....	68
4.3.2	Membrane formation and characterisation.....	70
4.4	Conclusion.....	79
4.5	References.....	80
4.6	Supporting information.....	82
4.6.1	Synthetic procedures and product characterisation.....	82
4.6.2	Electrochemical impedance spectroscopy.....	87
4.6.3	Neutron data.....	92
5	Mimicking Microbial Membranes.....	95
5.1	Introduction.....	96
5.2	Materials and methods.....	101
5.2.1	Chemicals.....	101
5.2.2	Bilayer formation.....	101
5.2.3	Neutron scattering experimental method and data analysis.....	102
5.3	Results and Discussion.....	104
5.3.1	Bilayer structure and formation.....	104
5.3.2	Electrical characterisation of the membranes.....	107
5.3.3	Interaction of Colistin Sulfate with the model membranes.....	112
5.4	Conclusion.....	119
5.5	References.....	120
5.6	Supplementary information.....	123
5.6.1	Neutron data.....	123

5.6.2	Electrochemical impedance spectroscopy data	133
6	Enhancing Antibiotics with Nanoparticles	138
6.1	Introduction to antimicrobial gold nanoparticles	138
6.2	Materials and methods	139
6.3	The effect of gold nanoparticles on LPS-tBLMs.....	140
6.4	Combining nanoparticles with antibiotics	144
6.5	Conclusion	150
6.6	References.....	151
6.7	Supplementary information.....	152
7	Summary, Future Directions and Outlook	155
7.1	Summary	155
7.2	Future developments	157
7.2.1	Exploring the effect of membrane structure and composition on antibiotic susceptibility	157
7.2.2	Large scale antibiotic screening	159
7.2.3	A platform to study bacterial membrane proteins.....	160
7.3	Conclusion.....	161
7.4	References	162

Declaration

I certify that this thesis does not incorporate without acknowledgment any material previously submitted for a degree or diploma in any university; and that to the best of my knowledge and belief it does not contain any material previously published or written by another person except where due reference is made in the text.

A handwritten signature in black ink, appearing to read "J. Anderson", with a long horizontal flourish extending to the right.

Acknowledgements

First, I would like to thank my supervisor Associate Professor Ingo Köper for his invaluable guidance, support and encouragement during my candidature. I owe many thanks also to my co-supervisor Dr Stephen Holt for his supervision of my neutron scattering work at the Australian Nuclear Science and Technology organisation and to Associate Professor Mike Perkins for his role as my co-supervisor and for guiding me during the synthesis work I conducted at the beginning of my doctoral work.

I am also grateful to have received a scholarship from the Australian Government Research Training Program as well as a top up scholarship from the Australian Institute of Science and Engineering. Next, I would like to acknowledge the assistance of the research groups of Ingo Köper and Mike Perkins and the staff at ANSTO for their technical support of my project and helping me solve all the problems that seemed to always come up when I least wanted them to.

I would like to thank my parents Kerstin and Gunther Andersson and the rest of my family for being there when things became difficult, particularly towards the end of my candidature always ready to advise and encourage me or just to listen whenever I needed to talk.

Last but far from least, I would like to thank my incredible group of friends, in particular Kasturi, Mike, Kate, Tracey, Jack, Nicola, Mel, Bec and Jesse. I can't begin to thank you for your friendship; I could not have done any of this without you.

Abstract

Model membranes provide a controlled environment in which biophysical studies of membrane processes and membrane proteins can be carried out. This is necessary as the cell membrane is a highly complex structure which makes systematic studies of its individual components very challenging. Tethered bilayer lipid membranes provide a stable self-assembled membrane platform that can be studied a wide range of analytical tools, but the range of studies that can be carried out is limited by the number of architectures that are currently available. A number of new tether architectures were designed in this project to better facilitate the study of membrane proteins and ion transport across lipid bilayers.

Chapter 3 presents the use of a well-established tethered membrane architecture to study the ability of novel crown ether compounds to selectively transport ions across a lipid membrane without damaging the membrane itself. Chapter 4 presents novel anchorlipids to increase the range of available membrane architectures. It examines the effect that chemical modifications to the anchorlipid molecule have on the electrical and structural properties of the membrane.

Based on the development of these novel architectures, a new type of self-assembled membrane was developed mimicking the outer membrane of Gram-negative bacteria, which is presented in chapter 5. This enabled for the first time the study of this membrane type by electrochemical impedance spectroscopy, and significantly simplified the assembly process of the membrane for other studies such as neutron scattering.

The new model membrane was used to study the effects of membrane-targeting antibiotics as well as the effect of gold nanoparticles on the electrical properties of the lipid bilayer. The development of this membrane architecture will enable a wide range of future studies to further investigate the effect of membrane-targeting antibiotics as well as providing a new avenue of approach to design novel membrane-targeting antibiotics to meet the increasingly urgent need for new antibiotics to combat the threat of multi-drug resistant bacteria.

Chapter 6 uses the membrane architectures developed in chapter 5 to investigate novel approaches to target the outer membrane of gram-negative bacteria using a combination of a well-known antibiotic and nanoparticles. Finally, in chapter 7 an outlook is presented for future developments based on the work presented in this thesis.

List of abbreviations

AC	Alternating Current
AFM	Atomic Force Microscopy
AuNP	Gold Nanoparticle
BLM	Black Lipid Membrane
CaCl ₂	Calcium Chloride
CPE	Constant Phase Element
DC	Direct Current
DMPC	dimyristoylphosphatidylcholin
DMPE	1,2-Dimyristoyl-sn-glycero-3-phosphoethanolamine
DOTAP	1,2-dioleoyl-3-trimethylammonium-propane
DPhyPC	1,2-diphytanoyl-sn-glycero-3-phosphocholine
EIS	Electrochemical Impedance Spectroscopy
GNB	Gram-negative Bacteria
KCl	Potassium Chloride
LB	Langmuir-Blodgett
LPS	Lipopolysaccharide
LPS-tBLM	Lipopolysaccharide-tethered bilayer lipid membrane
LS	Langmuir-Schaefer
NaCl	Sodium Chloride
NMR	Nuclear Magnetic Resonance
NR	Neutron Reflectometry
OM	Outer Membrane
OmpF	Outer Membrane Protein F
OMV	Outer Membrane Vesicle
PDADMAC	poly(dimethylammoniumchloride)
PEG	poly(ethylene glycol)
POPC	1-palmitoyl-2-oleoyl-sn-glycero-3-phosphocholine
SAM	Self-Assembled Monolayer
sBLMs	Supported Bilayer Membrane
SLD	Scattering Length Density
SOPC	1-stearoyl-2-oleoyl-sn-glycero-3-phosphocholine
SPR	Surface Plasmon Resonance
tBLM	Tethered Bilayer Lipid Membrane
βME	beta-Mercaptoethanol

1 Model Membrane Architectures

This section was published in: Biomimetic Membranes, Reference Module in Materials Science and Materials Engineering, Elsevier, 2018, ISBN 9780128035818,[1]

Abstract

Biological membranes host a significant portion of the cellular machinery, play an essential role in intercellular signalling and are the first line of defence against pathogens and toxins. Furthermore, a significant number of pharmaceuticals target membrane components (for example G-protein coupled receptors). It is therefore important to better understand the cellular membrane and its components – but studying the membrane is challenging as it is a highly complex architecture. Any study carried out on a natural cell membrane must contend with factors that cannot be controlled or fully known, such as the exact composition of the membrane. Furthermore, membrane proteins themselves are challenging to study as they do not crystallize easily and are not water soluble, which means traditional methods of studying proteins cannot be used effectively. To address this, model membranes have been developed that mimic the physicochemical characteristics of lipid bilayers, but do not exhibit the complexity inherent to the cellular membrane. This simplifies the biophysical study of membranes and membrane components and significantly enhances the range of analytical tools that can be used.

1.1 Introduction

In principle, the cell membrane is a phospholipid bilayer that serves as a host matrix for a wide range of membrane protein, carbohydrates, sterols and other membrane-bound compounds. The membrane serves as a protective shell around the cellular interior and its contents, isolating them from their environment.[2] The cellular membrane is a highly complex structure, composed of a large number of different components and it is essential for a large number of critical physiological processes.[3] For example, it contains crucial proteins responsible for cell-cell communication and signalling as well as transport of substances across the membrane.[4] Up to 5% of a cell's genes are used to produce large variety of lipid types[2] and one-third of its genes encode membrane-bound proteins[5]. This showcases the significant advantage organisms gain from possessing a diverse and highly regulated barrier between themselves and the environment. Patch-clamping is currently the most commonly used technique to study ion transport processes and ion channels. However, this technique does not allow for the complete control of the composition of the membrane and therefore experiments always have to be carried out without being able to fully control all parameters.

While the complexity of the membrane architecture is essential for its functional properties, it hinders systematic investigations into membrane-related processes as well as the use of membranes in practical applications, such as a biosensor. To overcome these issues, a range of model platforms have been developed that aim to mimic the essential properties of a cell membrane in a simplified, yet easily accessible system.

Here, a range of these model membrane systems are reviewed with a few highlighted examples. The different systems allow for the analysis of different membrane properties and processes. For example, ion transport across membranes is best measured using black lipid membranes, whereas solid supported membranes allow for the monitoring of binding events to the membranes.

1.2 The importance of temperature

In general, the temperature in which the lipid bilayer is formed significantly impacts the quality and stability of the lipid bilayers. A wide variety of lipids with different chemical structures exists, and their structure determines the ideal temperature range in which the lipid should be used. The length of the main carbon chain in phospholipids varies significantly among species and cell types and can range from around ten carbon atoms per chain to well above twenty. These carbon chains can be saturated or unsaturated, and they can contain a wide variety of side chains branching from the main lipid chains. The number as well as the structure of these side chains can vary significantly, from single methyl groups to one or more carbon chains that are comprised of two, three or even more carbon atoms. The chemical structure of these side chains affects the temperatures at which they form ordered or disordered structures. Figure 1.1 Shows an example of various phospholipid structures and their respective transition temperatures.

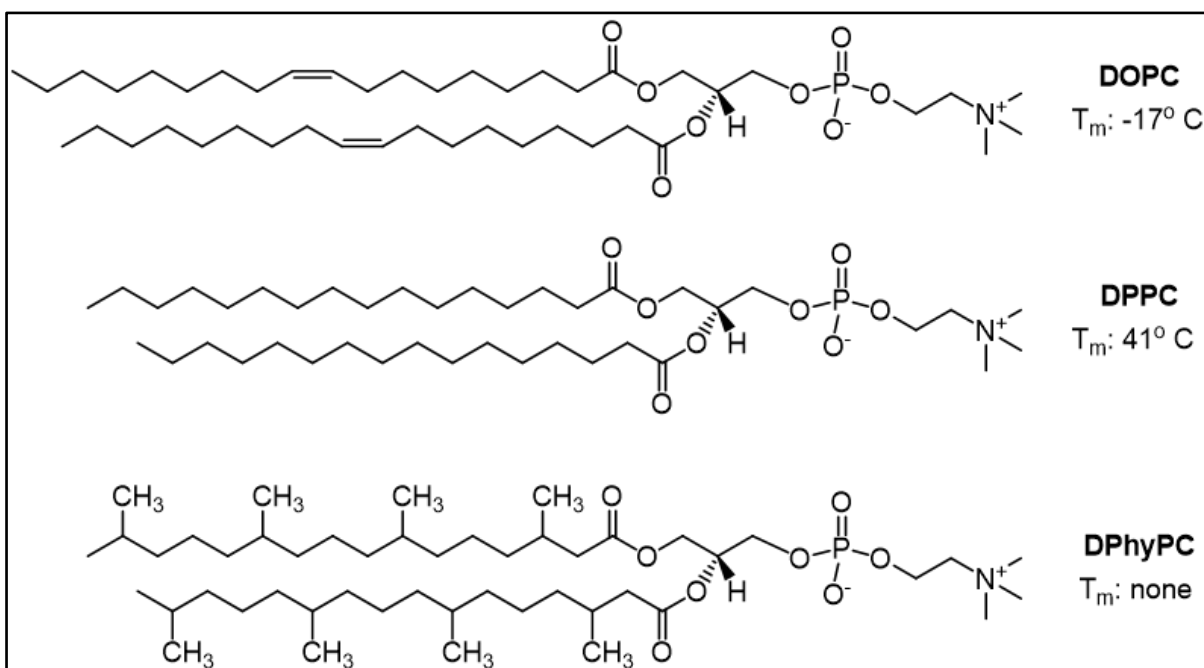


Figure 1.1: Examples of the effect that the hydrocarbon tail structure has on the lipids transition temperature from the P_β (gel) to the L_α (liquid crystalline) form. DOPC and DPPC differ only slightly in terms of tail length, and DOPC contains a single double bond in each tail. However, this difference has enormous ramifications in terms of the transition temperatures, with DOPC having a T_m that is 58° lower than DPPC.[6] DPhyPC has four branching methyl chains in each tail, and there is no observable transition temperature at all.[7] These data were taken from the website of Avanti Polar Lipids (<https://avantilipids.com>)

Below the transition temperature, lipid bilayers form a more ordered, crystalline structure which is more densely packed and where the lateral mobility of the lipids is strongly reduced.[8] The reduction in lipid mobility increases defect formation, as lipids can no longer move to compensate for perturbations to the bilayer structure.[8] There is a significant amount of information available on the thermodynamic properties of different lipids and lipid types. The database LIPIDAT (http://www.lmsd.tcd.ie/new_lipidat/homelipidat.asp) created by Ohio State University provides access to a wealth of information regarding the properties of different lipids.[9]

In addition to strictly controlling the ambient temperature of the model membrane, it is important to maintain the highest possible purity and cleanliness of reagents and glassware, as the model systems rely mostly on self-assembly. Particularly the presence of the surfactants and solvents used to clean laboratory glassware can disrupt the integrity of lipid bilayers or prevent their formation, as the detergents can disturb the hydrophobic interactions between lipid tails that are necessary to maintain the structure of the lipid bilayer.

1.3 Black lipid membranes

The spontaneous formation of lipid membranes in aqueous 0.1 M NaCl solutions at temperatures between 37 and 47° C containing extracted lipids was first reported in 1962.[10] When spread across a small (μm -scale) aperture, a lipid bilayer can form to separate two aqueous reservoirs (see Figure 1.2). The formation of a layer that is only a few nanometres thick causes destructive interference of light reflected from these interfaces, which leads to a black appearance of the film. Black lipid membranes (BLMs) have become the standard model system for the analysis of ion transport processes across lipid membranes, complementing the traditional patch-clamp approaches used on natural membranes and whole cells. BLMs have been used almost exclusively for the electrical study of pores and ion channels[5] as well as pore formation by antibiotics[11], peptides and electrical or physical stress[12] over very short periods of time, for which they are ideally suited. Additionally, the unhindered mobility of lipids in BLMs enables the study of protein diffusion behaviour in lipid membranes, for example *via* fluorescence correlation spectroscopy.[13]

In addition to phospholipids, a black lipid membrane formed from cholesterol derivatives has also been reported.[14] The authors observed that while fresh cholesterol was unable to form lipid bilayers, when the sample was left to 'age' – either by leaving it exposed to oxygen and light for a period of time or by heating it, membrane formation took place. While the authors were unable to determine the structure of every compound present in the sample, compounds that were identified in these cholesterol samples included dihydroxycholesterol and 7-ketocholesterol. These compounds possess additional polar functional groups compared to cholesterol (which only has a single hydroxyl group and is otherwise non-polar). It is likely that the increased amphiphilic character of the degraded cholesterol molecules is responsible for their improved ability to form black lipid membranes.

To form a BLM, Teflon is most frequently used as a substrate but other materials, for example porous alumina, can also be used for the formation of nano-scale BLMs.[15] The following general process is used for BLM formation[16]: lipids dissolved in chloroform are painted over the Teflon substrate and left to dry for around twenty minutes, as Teflon is lipophobic and thus has to be 'pre-treated' to allow bilayer adhesion.

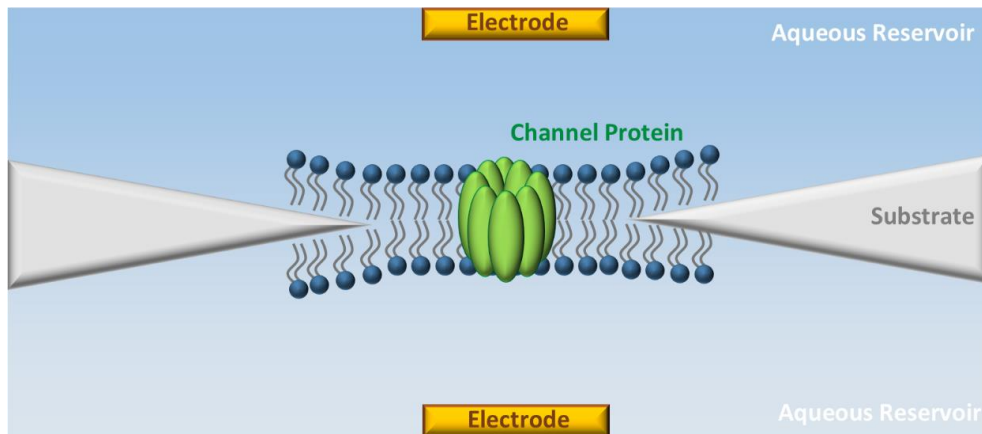


Figure 1.2: Schematic of a black lipid membrane containing a single channel protein. These lipid bilayers are free-standing architectures, attached only at the sides to a solid support. They are ideal for the characterisation of single ion channels

Black lipid membranes are prepared by coating the aperture (typically with a diameter from 100 μm up to several mm diameter[17, 18]) with a lipid dissolved in an organic solvent such as pentane[5], hexane[19], decane[17] or a chloroform-methanol mixture[20], allowing it to dry and then immersing the substrate into an aqueous medium.[20] The resulting BLMs (Figure 1.2) are an excellent tool to study the electrical properties of single pore proteins and ion channels[5, 19, 21] as they possess high electrical sealing properties with resistances of 10-100 $\text{M}\Omega\cdot\text{cm}^2$ and capacitances of 0.7-1.5 $\mu\text{F}\cdot\text{cm}^2$. These values are equivalent to those measured on natural membranes using patch-clamp techniques. Protein incorporation typically takes place after bilayer formation is complete.[22] By placing electrodes on both side of the membrane, trans-membrane currents can be recorded. Typically, patch-clamp amplifiers are used allowing to resolve transport through single ion channel proteins.

While black lipid membranes are the gold standard for ion channel measurements in model membrane systems, they generally lack long term stability, only remaining intact for a period of a few hours at most.[5] This makes them less suitable for sensing or screening application. However, there have been several attempts to address this stability issue.

The stability of black lipid membranes can for example be increased by encapsulating the bilayer within a hydrogel in place of the aqueous reservoir, enabling the retention of $\text{G}\Omega$ -resistances for more than a week.[23] The function of ion channels such as α -hemolysin and alamethicin was not altered when embedded into hydrogel-stabilised lipid membranes compared to their function in unstabilised BLMs. Other reports, however, only show an increase from several hours to several days when using an agarose gel for BLM stabilisation.[24]

Alternatively, the diameter of the membrane has been reduced in order to increase the stability. By reducing the aperture size to nano-scale pores and stabilising the bilayer with an agarose gel, single-channel measurements of α -hemolysin incorporated into the BLM could be made over a period of several weeks.[22]

Nano-black lipid membranes are a recently developed architecture in which BLMs are spread over nano-sized holes in a porous substrate such as polycarbonate filters or engineered substrates.[25, 26] Bilayers can be formed by adding large unilamellar vesicles with a diameter of 600 nm to a hydrophobic substrate. Bilayer formation required around 30 hours and the membranes were stable for up to 50 hours before beginning to disintegrate.

While the stability of the membrane can be increased significantly by surrounding it with a hydrogel and/or reducing the pore size, the assembly process of black lipid membranes still requires many steps and considerable expertise to carry out. Therefore, their application in biosensing and are limited compared with other systems. BLMs have been assembled in microfluidic devices, with bilayer resistances of up to 2 G Ω .[27] However, the BLMs remained intact only for 2-12 hours and therefore are not yet ideal for use in biosensors as the BLMs and their sensing element can only be assembled immediately prior to use.

Due to their spatial arrangement and the requirement for a significant aqueous reservoir on both sides of the membrane and the absence of a solid support, BLMs cannot be studied with techniques such as atomic force microscopy (AFM) or quartz crystal microbalance (QCM). Surface plasmon resonance (SPR) also cannot be applied as it requires a conductive substrate in the immediate vicinity of the membrane. Furthermore, as BLMs are free-standing membranes with poor long-term stability it is also challenging to apply neutron scattering measurements as they usually require 3-6 hours of continuous measurements and the black lipid membrane structure deteriorates too quickly to obtain good data sets.

Black Lipid membranes have been shown to be excellent tools for calibrating voltage-sensitive dyes (VSDs) – dyes that change their absorption properties (such as maximum absorbance, absorbance intensity or the width of the absorption peak).[28] Their benefit compared to vesicle-based calibration techniques or patch clamping is that both voltage and membrane composition can be precisely controlled. This has helped to simplify the otherwise arduous task of determining the response for VSDs to different membrane potentials which is an important aspect of many neurological studies. BLMs have also been used for a large number of biophysical studies of lipid bilayer behaviour and transport processes. BLMs were for example used to show that the antibiotic peptide nisin forms pores with a diameter of 2 – 2.5 nm in the cytoplasmic membrane that are stable for around 6 seconds.[29] A black lipid membrane modelling the outer membrane of Gram-negative bacteria has been used to study

the gating and conduction behaviour of the bacterial membrane protein OmpF.[16] The protein was incorporated into the membrane by adding detergent-stabilised protein to a pre-formed BLM. The concentration of the detergent was such that upon being added to the membrane bathing solution, it was below the critical micelle concentration. Consequently, the detergent gradually desorbed from the proteins and they were incorporated into the lipid membrane as a result of their hydrophobic domains.

BLMs are also highly useful for the study of membrane-related proteins. The unique and highly controlled environment afforded by BLMs has for example been used to better understand the structural and functional changes of Cry1A toxin[30]. Cry1A is an insecticidal compound produced by *Bacillus thuringiensis*. BLMs also served as platforms to study portal proteins, a class of membrane-related proteins expressed by many bacteriophages as well as herpesviruses.[31] The exact mechanism and activity of portal protein in the delivery of the genetic material of the virus was unclear due to the difficulty of studying the structure and behaviour of membrane-related proteins as they are not water-soluble.

BLMs also provide a platform with properties that are consistent between different laboratories, which is a feature not afforded by traditionally used techniques such as patch clamping. In another study, the membrane protein bacteriorhodopsin was integrated into nano-BLMS using porous alumina as a substrate.[32] Bacteriorhodopsin is a protein found in Archaea that transports proteins across lipid membranes using light as an energy source. It is of significant interest for a wide range of biotechnological applications, from optoelectronics to energy storage. BLMs have significantly simplified the analysis of this potentially important biomaterial.

1.4 Solid supported membranes

The generally poor stability of black lipid membranes can be improved by assembling the lipid bilayer on a solid support where it floats on a thin aqueous cushion with a thickness of 1-2 nm, creating a supported lipid bilayer (SLB, see Figure 1.3).[18] Hydrophilic supports such as gold[33, 34], silicon oxide[35] and glass[35] are commonly used as substrates for SLBs.

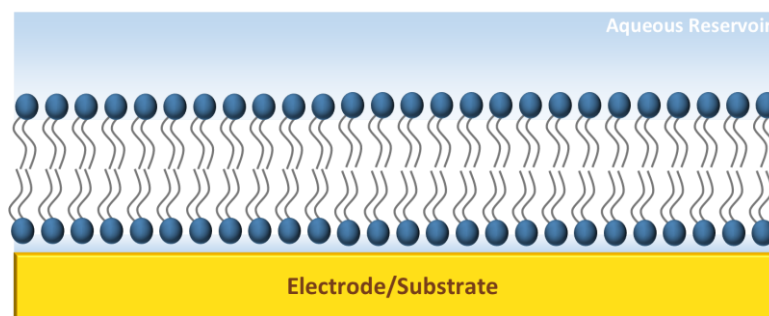


Figure 1.3: Schematic of a solid supported model membrane. The lipid bilayer is deposited, but not bound to, a solid support. This increases its stability and the number of analytical techniques that can be used to study the membrane. It is not suitable for the incorporation of proteins with large sub-membrane domains as they would be adversely affected by contacting the solid support.

Solid supported lipid membranes are generally formed using Langmuir-Blodgett (LB) film transfer followed by Schaefer dipping[18] or *via* vesicle fusion[36]. Langmuir-Blodgett film transfer is a method of transferring a phospholipid monolayer from an air-water interface onto a solid support.[35] A hydrophilic substrate (such as freshly cleaned gold, mica or SiO₂) is pulled through a lipid monolayer formed at the air-liquid interface, forming a lipid monolayer at the gold interface. This is followed by Schaefer dipping, during which the pre-formed monolayer is then “pushed” through the same lipid monolayer, forming a solid-supported lipid bilayer. Figure 1.4 shows schematics of the Langmuir-Blodgett film transfer and Schaefer dipping processes.

To form the lipid monolayer used for both Langmuir-Blodgett film transfer and Schaefer dipping, a lipid is dissolved in an organic solvent that is nonpolar and has a higher density than water, for example chloroform.[37] The dissolved lipid is then added dropwise to a water solution. The amphiphilic molecules will arrange themselves such that the hydrophilic head groups of the lipids are located in the aqueous phase and the tail regions are in the organic solvent. Once the solvent has evaporated, the tail regions are exposed to air. The lipid monolayer film is then compressed before the hydrophilic substrate is dragged through the film at the air-water interface to create the first leaflet of the lipid bilayer. It is important to note that some solvent residue may remain in the lipid bilayer after assembly, which may be a concern depending upon the intended application of the membrane. The second leaflet is formed by pushing the substrate surface through the lipid monolayer a second time.

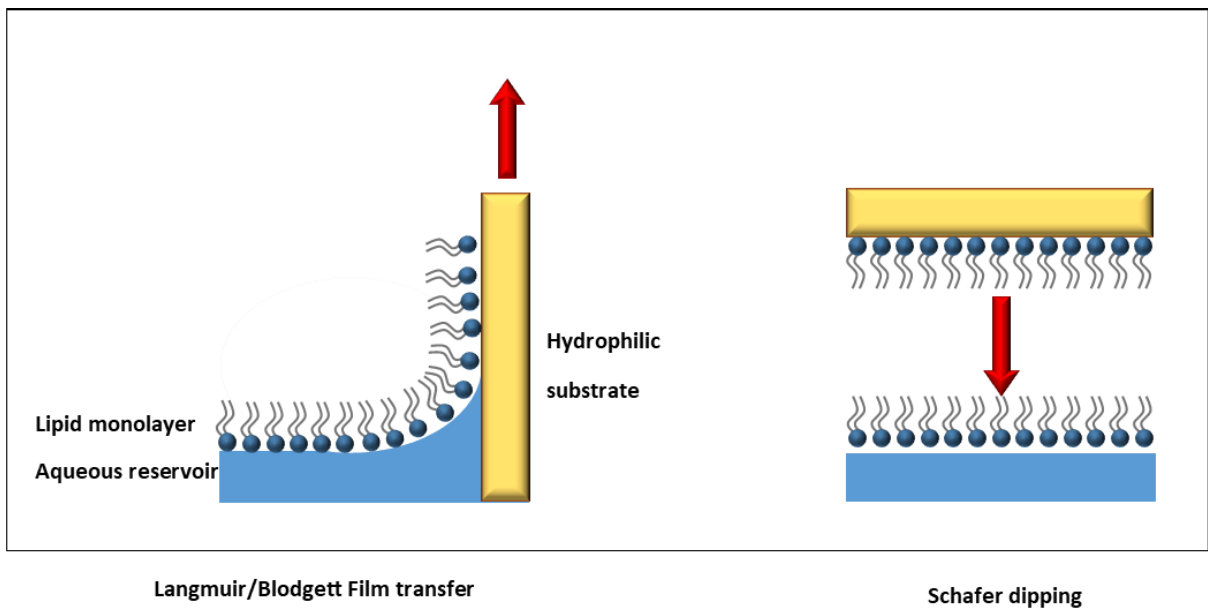


Figure 1.4: Schematic of the Langmuir-Blodgett process (left) and Schaefer dipping (right) to assemble a solid-supported lipid bilayer membrane.

In vesicle fusion, lipid vesicles are added to the solid support immersed into an aqueous buffer or salt (typically NaCl or CaCl₂). Over time, vesicles adsorb to the support. They rupture, fusing into a continuous lipid bilayer on the surface (see Figure 1.5). Divalent ions such as Ca²⁺ and Mg²⁺ can speed up the fusion process.[38]

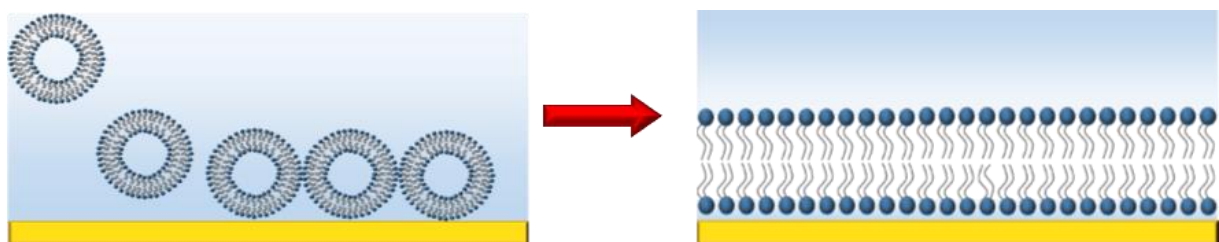


Figure 1.5: During vesicle fusion, extruded vesicles adsorb to the surface before rupturing and fusing into a continuous lipid bilayer over the period of several hours

There are many methods to prepare lipid vesicles for vesicle fusion. In principal, lipids must be dissolved in water or a buffer and extruded through a filter paper with 50-100 nm pores. To promote dispersion of the lipid in the solvent, they can first be dissolved in an organic solvent (such as chloroform) which is then evaporated, leaving a lipid film in the container. This lipid film is then resuspended in water or a buffer by sonication and/or heating, which is then

followed by extrusion of the vesicles or a series of freeze/thaw cycles in which monodisperse lipid vesicles are formed. Lipid vesicles can be frozen at -20° and re-used. However, to ensure optimal bilayer formation, the vesicles should be re-extruded prior to use every time.

These vesicles are then added to the substrate immersed in an aqueous bathing solution containing a buffer or sodium/calcium chloride solution and left to form the lipid bilayer. This process is complete after around 4 hours.[36] Supported lipid bilayers can also be assembled *via* spin-coating.[39] Bilayer formation was possible on both silicon and glass substrates. The substrates were treated with either 5 M KOH, an oxygen plasma or UV/Ozone to obtain a more hydrophilic surface. Afterwards, the phospholipid of choice was added to the substrate at a concentration of 20 mg/mL and the sample was spun at 3000 RPM. Once excess solution was cleared from the substrate and the solvent had evaporated, the samples were stored under high vacuum to remove all traces of organic solvents. To achieve bilayer formation, the substrates were re-hydrated in a water vapour atmosphere at 20° C.

Supported lipid bilayer membranes can be studied with surface sensitive techniques such as SPR, QCM and AFM as well as ellipsometry. Another significant advantage of SLBs is that the solid support allows the assembly of membranes with a sufficient lifetime and stability to enable neutron scattering studies. Neutron scattering is a unique tool that allows for the study of the structure of a lipid bilayer while it is in its native environment (immersed in water) with sub-nanometre resolution.[33, 40, 41]

Because their long-term stability is limited[42], and these membranes are highly susceptible to damage from handling of the sample, studies that require several days or more cannot be undertaken. The stability of solid-supported membranes can be increased by using a polymerisable lipid such as 1,2-bis[10-(2C,4C-hexadienoxy)decanoyl] - sn-glycero-3-phosphocholine (bis-SorbPC) which contains several double bonds in its tail region.[43] A solid-supported lipid bilayer is formed as normal, for example *via* vesicle fusion. The bilayer is then photopolymerised by irradiation with UV light, increasing the resistance of the membrane to degradation and defect formation. The disadvantage of a polymerised lipid bilayer is that subsequent incorporation of membrane proteins into the bilayer could be challenging, and the diffusion of embedded membrane components may also be adversely affected.

Another consideration that has to be made if SLBs are assembled via LB-film transfer and Schaefer dipping, is that membrane proteins are challenging to incorporate. They must reside at the air-water interface during bilayer formation which could denature the protein as its chemical environment is no longer suitable. Furthermore, as solid-supported lipid bilayers provide only very little space between the lipid bilayer and its support, embedded proteins could be denatured as a result of contacting the solid support.[44] This can be mitigated to

some extent by covalently modifying the solid support prior to the deposition of the lipid bilayer, for example by modifying a gold surface with 1-thio-glucose.[45] This provides a cushion underneath the membrane such that any proteins that are incorporated into the bilayer do not contact the gold surface directly and are thus less likely to be denatured. However, the available space underneath the membrane remains small (around 2 nm) so that proteins with large sub-membrane domains would likely be adversely affected, nonetheless. This issue can be circumvented by using vesicle fusion with protein-functionalised vesicles to form the lipid bilayer.

While there are some studies that have characterised the electrical properties of polymer-supported lipid bilayers,[46] the electrical characteristics of these types of model membranes have not been thoroughly investigated. Due to the difficult to control nature of the polymer support, it would likely be challenging to obtain bilayers with reproducible electrical properties. As a result, these model systems are best used for the study of membrane-related processes that do not involve charge transport. For example, a model of the outer membrane of Gram-negative bacteria has been developed.[33] The model used an asymmetric lipid bilayer with the inner leaflet comprised of 1,2-dipalmitoyl-*sn*-glycero-3-phosphocholine (DPPC) and the outer leaflet containing lipopolysaccharides (LPS) – large, lipid-like molecules found in the outer membrane of gram-negative bacteria. Using neutron scattering, the authors showed that the removal of divalent cations such as magnesium and calcium strongly affects the structure of the lipid bilayer.[47] The experiment showed that upon removal of the cations, significant irreversible mixing of lipids between the leaflets of the membrane took place. In another study, the interaction of differently charged ions with various lipid types was investigated using an SLB.[48] This study demonstrated that the Gouy-Chapman field theory cannot account for the membrane binding and translocation behaviour of ions across lipid membranes. The authors found a trend for ions to bind to lipid membranes that was the opposite to what is predicted by the Hofmeister series.

An SLB was also used to gain an understanding of the effect that fullerenes have on living organisms.[49] As there is an ever-increasing amount of nano-engineered substances entering the environment due to human activities, understanding their interactions with living organisms is of significant importance. The cell membrane is one of the first points of contact that nanomaterials have with an organism, thus the interaction of fullerenes with a lipid bilayer is an important aspect of understanding the interaction between fullerenes and a cell. The study concluded that fullerenes tend to accumulate in lipid bilayers comprised primarily of unsaturated lipids. Furthermore, positively charged lipid membranes attract the nanoparticles more strongly than membranes containing negatively charged or neutral lipids.

An SLB was also used to understand the interaction of polycationic polymers that are commonly used for drug delivery. Mica-supported lipid bilayers comprised of DMPC were studied with AFM to show that the polycations caused the formation of holes with diameters of 4-8 nm in the lipid bilayer. No holes were formed when neutral polymers such as poly(ethylene glycol) and poly(vinyl alcohol) were added to the membrane.

By using the polymerisable phospholipid containing four diacetylene groups in their tail region, it is possible to create micropatterned phospholipid bilayers.[50] First, a lipid bilayer is deposited as normal using LB-Schaefer film transfer. Subsequently, the lipid bilayer is photopolymerised by exposure to UV light through a mask in the desired pattern. The polymerised lipid becomes insoluble in organic solvents and can also no longer be solubilised by detergents. The lipid that was not polymerised is then washed away, leaving behind a lipid bilayer with the desired pattern.

A solid-supported lipid bilayer was also used to test for the lipophilicity of various drug candidates.[51] As some pharmaceuticals must traverse the cell membrane to be effective, lipophilicity is an important property that should be tested for early in the drug development cycle. By using model membranes, the impact of various lipid types and membrane composition on the ability of the drug to cross the membrane can be systematically examined in a readily accessible manner.

1.5 Polymer supported membranes

To avoid denaturation of proteins in solid-supported lipid membranes, polymer cushions can be used between the lipid bilayer and the solid support to reduce or eliminate interactions between the lipid bilayer and its support (a schematic of a polymer-supported lipid bilayer is shown in Figure 1.6). Polymer-supported lipid bilayer membranes are therefore ideally suited to study membrane processes involving proteins with large sub-membrane domains that would be adversely affected by contacting the supporting material. The polymer support can also function as an approximation of the cytoskeleton.[52] A major challenge facing polymer-supported lipid bilayers is that their structure and properties are difficult to control, as the thickness and uniformity of the supporting polymer cushion depends strongly on the degree of polymerisation and the polydispersity of the polymer. The unevenness of the supporting polymer adversely affects the electrical sealing properties of the deposited lipid bilayer, which means that the electrical properties of polymer-supported lipid bilayers are generally not suitable for applications that depend on controlled charge transport.[53]

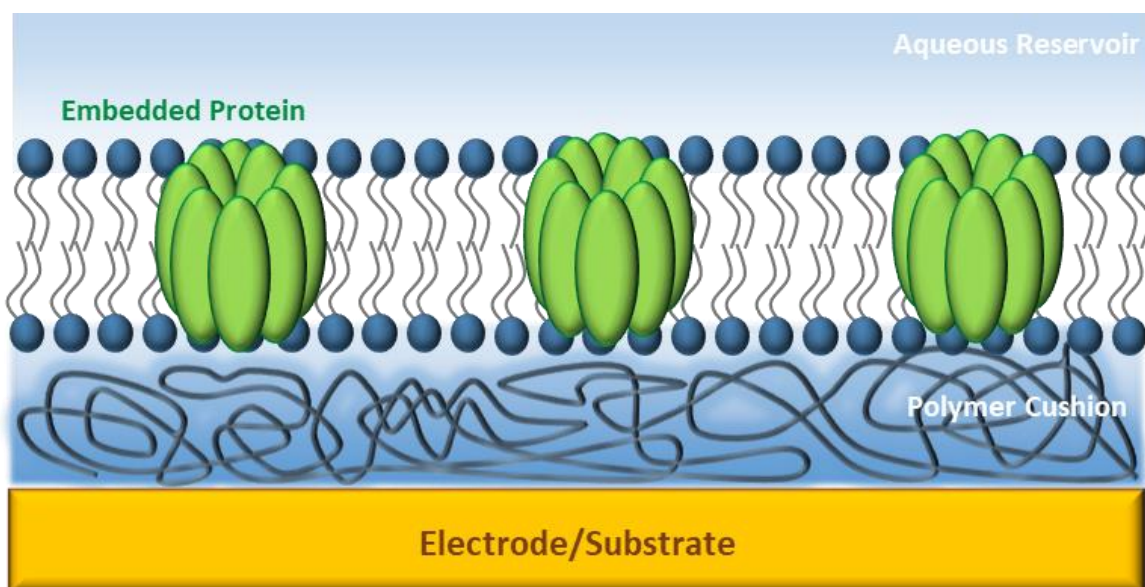


Figure 1.6: Schematic of a polymer-supported lipid membrane where a hydrophilic long-chain polymer such as poly(ethylene glycol) provides a cushion between the lipid bilayer and the support such that an embedded protein does not contact the underlying support material.

One of the most frequently used polymers to support a bilayer lipid membrane is poly(ethylene-glycol), which provides a hydrophilic cushion of up to 10 nm underneath the lipid membrane.[54] Other polymers that can be used are poly(amino acid methacrylate)[55] or a maleic acid-based copolymer.[56] It has been shown that the polymer support strongly affects the mobility and diffusion rate of the lipid bilayer. The stronger the interaction between the bilayer and its polymer support, the slower the diffusion rates of the lipid bilayer.

The average diffusion rate (this study did not distinguish between diffusion rates of the inner and outer leaflet of the lipid bilayer) of individual lipids in a bilayer comprised of 1,2-dimyristoyl-sn-glycero-3-phosphocholine (DMPC) is around $4 \mu\text{M}^2\text{s}^{-1}$. [56] When the supporting glass slide was functionalised with a maleic acid-based hydrogel, the diffusion was reduced to $3 \mu\text{M}^2\text{s}^{-1}$. The bilayer was then further stabilised *via* the addition of N-succinidomyristidic ester. This compound binds covalently to the polymer support while its long aliphatic chain integrates into the lipid bilayer, effectively tethering the membrane to the solid support. The addition of 20 mol-% of this linker group reduced the lipid diffusion rate to $1.3 \mu\text{M}^2\text{s}^{-1}$. A careful balance should thus be maintained between membrane stability and membrane fluidity.

When functionalising the glass support with a benzophenone silane, there was an even more significant effect on lipid mobility with varying tethering density.[57] The inner leaflet of the membrane contained a mixture of lipopolymers and phospholipid while the outer leaflet consisted of a mixture of DMPC and 1,2-dimyristoyl-sn-glycero-3-phosphoethanolamine

(DMPE). The lipopolymer could be coupled to the benzophenone groups of the support via photocrosslinking. When the inner leaflet contained 5% lipopolymer, the diffusion rate in the outer leaflet at 40°C was $18 \mu\text{M}^2\text{s}^{-1}$. An increase of lipopolymer content to 30% reduced the diffusion rate to $1 \mu\text{M}^2\text{s}^{-1}$.

Bilayers can also be attached to the solid support electrostatically rather than covalently. Depending on the side chains of the polymer (for example ethene, propene or octadecene), the cushion thickness can be varied from 4 to 60 nm.[58] The lipid bilayers were assembled from egg phosphatidylcholine. However, increasing the cushion thickness from 4 to 60 nm reduced diffusion coefficients of the lipid bilayer from 1.1 to $0.26 \mu\text{M}^2\text{s}^{-1}$. Lipid bilayers comprised of 1-palmitoyl-2-oleoyl-*sn*-glycero-3-phosphocholine (POPC) tethered by 25% 1,2-dioleoyl-3-trimethylammonium-propane (DOTAP) can be formed on a cushion of poly(amino acid methacrylate) with a thickness of 12 nm. The membrane retained a mobile lipid fraction of 70% with lipid diffusion rates of $1.5 \mu\text{M}^2\text{s}^{-1}$.

Another method of assembling a polymer cushion with variable thickness is by using layer-by-layer deposition of polyelectrolytes. The thickness of the support can be increased simply by adding additional layers of polymer. For example, alternating layers of the polymers poly(allylamine hydrochloride) (PAH) and poly(styrene sodium sulfonate) (PSS) can be used as a support upon which a lipid bilayer comprised of a mixture of 30% DOPC and 70% 1,2-dioleoyl-*sn*-glycero-3-phospho-L-serine can be assembled *via* vesicle fusion.[46] Bilayer formation was followed by QCM-D and electrochemical impedance spectroscopy. Sealing lipid bilayers formed on cushions of up to 11 layers of polyelectrolyte (a single polyelectrolyte layer is comprised of one layer of PAH and one layer of PSS). The frequency shift during bilayer formation was around 26 Hz and the resistance of the resulting bilayer around $20 \text{ M}\Omega \text{ cm}^2$. These properties are characteristic for the formation of a complete and sealing lipid bilayer.

To study the effect of the polymer cushion on incorporated proteins, Cytochrome b(5) and annexin V were embedded into polymer-supported lipid bilayer membranes.[53] The use of a polymer cushion enabled the diffusion of these proteins at the same velocities as in their natural environment of up to $4 \times 10^{-10} \text{ cm}^2\text{s}^{-1}$. However, incorporation of high quantities of proteins into polymer-supported lipid membranes results in abnormal diffusion behaviour, where proteins and polymer chains obstruct diffusion pathways.[59]

Polymer-supported lipid membranes have served as platforms for a large number of studies. For example, the sodium-based conductive polymer polypyrrole-dodecylbenzenesulfonate (PPy(DBS)) was used as a support for a DPhyPC lipid bilayer functionalised with alamethicin, a voltage-gated ion channel protein.[60] The activity of alamethicin regulates the electrical properties of the supporting polymer, increasing or decreasing charge transport depending on

the amount of sodium pumped across the bilayer. This architecture could serve as the platform for novel biosensing devices. Another report demonstrates the use of a polymer-supported lipid bilayer as a platform for urea-and ammonia sensing.[61] The study used a polypyrrole-supported lipid bilayer which was functionalised with urease. The authors showed a concentration-dependent change in current across the membrane in the presence of urea. In another study, a polyethylene glycol-supported lipid bilayer membrane was used to study the role of SNARE proteins in the fusion of vesicles with lipid membranes.[62] The t-SNARE protein resides in the target membrane, and the v-SNARE protein is present in the vesicle. The precise sequence of events involving the SNARE complex formation followed by vesicle fusion was investigated with the model membrane. The authors showed that the SNARE complex is dissociated by a complex of the N-ethylmaleimide-sensitive factor and α -SNAP with the use of ATP.

1.6 Tethered membranes

To simplify the assembly process and increase the stability and quality of solid supported membranes, tethered lipid bilayer membranes (tBLMs) were developed. They are semi-synthetic lipid bilayers covalently bound to a solid support. The outer leaflet is comprised of a phospholipid while the inner leaflet consists of a synthetic anchorlipid covalently attached to a substrate. The assembly process of these model membranes is vastly simplified as the membrane can be formed using only self-assembly – no specific technique such as LB-film transfer is required to use this type of model membrane. Furthermore, the properties of tBLMs are not reliant on controlling the properties (such as polydispersity) of a polymer support, therefore membranes with more reproducible properties can be assembled. Figure 1.7 shows a schematic of a typical tBLM.

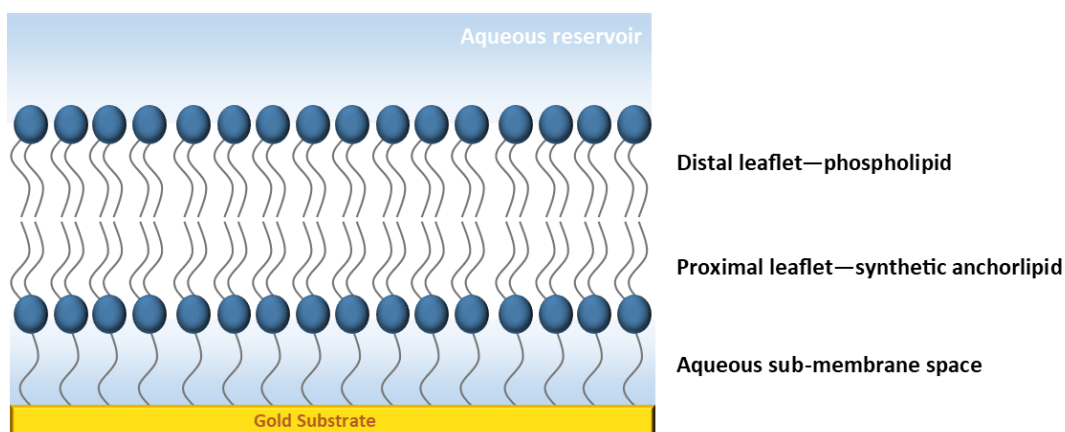


Figure 1.7: A tethered lipid bilayer membrane is an asymmetric lipid bilayer comprised of a phospholipid (or a mixture of phospholipids) in the distal leaflet and a synthetic proximal leaflet which has an anchoring segment, binding it covalently to the solid support.

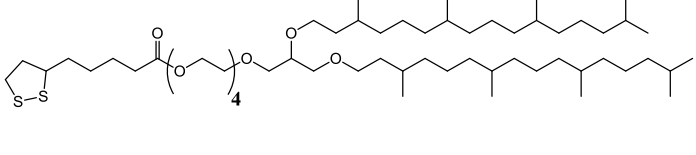
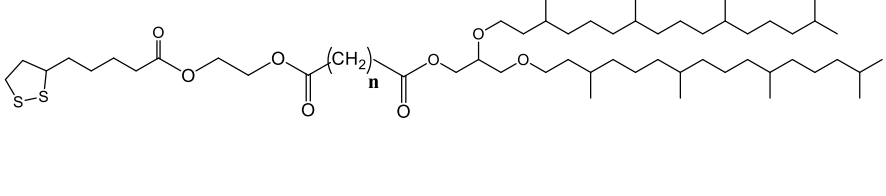
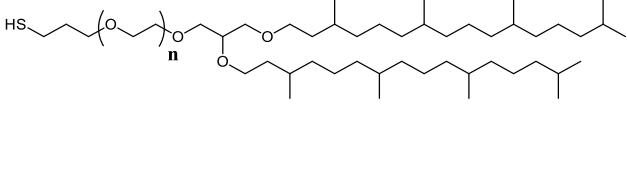
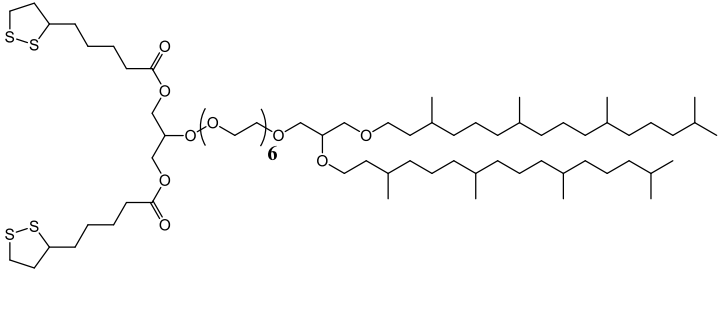
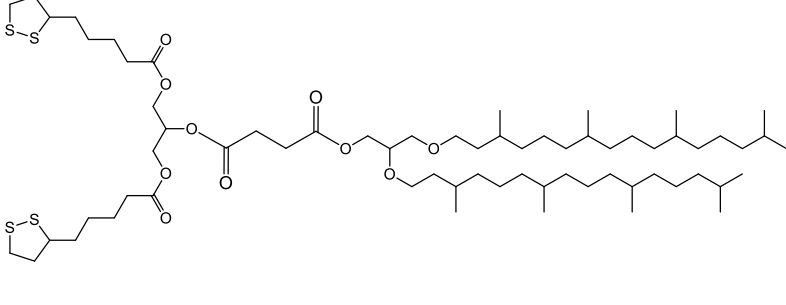
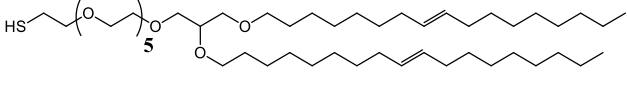
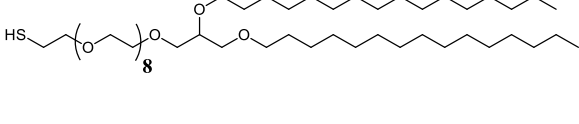
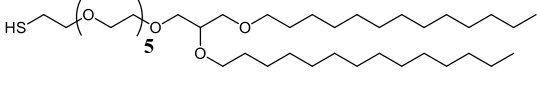
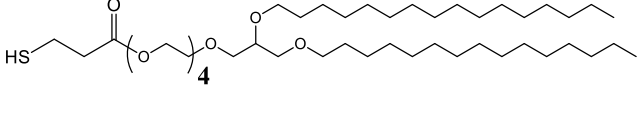
Gold is the most frequently used substrate for tBLMs[63-66] but other substrates such as mercury droplets[67, 68] and silicon oxide[69] have also been used. The covalent tethering of the lipid bilayer to a solid support, significantly increases its stability, with membranes remaining intact for several weeks or more.[70] It also enables the use of a significantly larger range of analytical tools such as AFM[71, 72], QCM[71, 73], (SPR)[74], electrochemical impedance spectroscopy (EIS)[41, 63, 70] and neutron scattering[41, 63, 75]. The anchoring molecule prevents the lipid bilayer from directly contacting the solid support, which makes them more suitable for the incorporation of proteins that extend below the lipid bilayer. Due to their ease of assembly, stability and flexible architectures, tBLMs are becoming increasingly popular.

When the proximal leaflet is comprised exclusively of an anchorlipid, the sub-membrane reservoir is densely packed and poorly hydrated, with only 5% of the volume underneath the membrane containing water.[41, 63] Structural analysis of the ethylene glycol segment of DPhyTL has shown that it assumes a coiled structure, exposing the hydrophobic carbon segments to its environment and thereby excluding water from the sub-membrane domain.[84] This does not provide ideal conditions for the incorporation of membrane proteins with sub-membrane domains that would require an aqueous environment.

The hydration of the sub-membrane space can be improved by mixing the anchorlipid with smaller “spacer” molecules, for example mercaptoethanol if a gold substrate is used for bilayer assembly. This spacer molecule can be mixed with the lipids shown in Table 1.1, for example DPhyTL[63], WC14 or FC16[85] as well as DPhySDL, DPhyGL and DPhyAL[63] to obtain a sparsely tethered tBLM (stBLM) in which up to 60% of the sub-membrane space is hydrated rather than around 5% in undiluted architectures. Lengthening the spacer segment, for example in DPhyOT and DPhyHT also increases sub-membrane hydration, but also reduces membrane resistance and stability.[41]

Reducing the tethering density by combining the anchorlipid with a smaller spacer results in significantly reduced membrane resistance. While tBLMs assembled purely on anchorlipids generally have resistances of 10-100 M Ω .cm² [41, 63], and can even be in the G Ω -range[86], reducing the tethering density also reduces membrane resistance to as low as 90 k Ω [75]. It has been shown that combining anchorlipids with spacer molecules increases sub-membrane hydration and must therefore reduce the number of anchorlipid molecules in the SAM. However, it has thus far not been possible to determine the exact composition of SAMs formed from these mixtures.

Table 1.1: Various structures that have been developed for gold-supported anchorlipids.

	<p>DPhyTL[64, 69, 76, 77]</p>
	<p>DPhySL (n = 2)[78] DPhyGL (n = 3)[78] DPhyAL (n = 4)[78]</p>
	<p>DPhyTT (n=4)[41] DPhyHT (n=6)[41] DPhyOT (n=8)[41]</p>
	<p>DPhyHDL[41]</p>
	<p>DPhySDL[78]</p>
	<p>HC 18[79]</p>
	<p>FC16[79]</p>
	<p>WC14[80-82]</p>
	<p>TEG-DP[83]</p>

The composition of the monolayer is likely a complex function of the relative solubilities of the two compounds, the stability of their interaction with the substrate, incubation time and temperature as well as their molecular sizes. An alternative approach to reducing the density of the tethering molecules in the SAM is to use anchorlipids with larger anchoring groups such that spatial constraints necessarily reduce the density of the SAM. When diluted, the contact angle of the SAMs is reduced from 105-110° to below 100°.[63] At lower contact angles, vesicle fusion no longer produces bilayers, instead, resulting in the adsorption of vesicles to the surface without subsequent fusion of the vesicles into continuous lipid bilayer. High quality bilayers can then only be formed *via* solvent-assisted bilayer formation.[63]

Two lipids with large anchoring groups, DPhyHDL and DPhySDL, (see Table 1.1) have been developed. The increased size of the anchoring molecule increased sub-membrane hydration to around 25%[41, 63] while also maintaining membrane resistances above 1 MΩ.cm². The incorporation of the pore α-Hemolysin into a fully tethered (DPhyTL) and sparsely tethered (DPhyHDL) membrane architecture showed that while DPhyTL forms higher-quality membrane, the activity of α-Hemolysin is significantly higher in the sparsely tethered lipid bilayer.[64] When α-Hemolysin inserted into a fully tethered membrane, the resistance was reduced by around half an order of magnitude, whereas in the case of a sparsely tethered membrane, the resistance was reduced by three orders of magnitude.

Instead of using a synthetic anchorlipid, a modified protein can also serve as a method of tethering the lipid membrane to its support. For example, detergent-solubilised cytochrome C oxidase modified to contain a his-tag can be attached to a support *via* nitrilo-triacetic acid.[87] The detergent is then displaced by a lipid bilayer *via* in-situ dialysis, creating a protein-tethered lipid bilayer. S-layer proteins can also be used to create protein-tethered lipid bilayer membranes.[88]

While gold is by far the most common substrate used for tBLM formation, the anchoring group of the lipids can be modified to be suitable for other surfaces. By using trichlorosilane instead of a disulfide as anchoring group, the anchorlipid can be used to form a tBLM on a silicon oxide surface.[89] This enables the use of tBLMs in the field of silicon-based microelectronics.

One of the disadvantages of the solid support is that partial or complete attachment of the inner leaflet of the membrane to a solid support reduces or even completely eliminates lipid mobility in one or both of the leaflets of the bilayer. This makes the model system less suitable as a model for membrane processes related to the diffusion of membrane components. However, by using mercury as a support, fluidity of the membrane can be restored while retaining some of the stability afforded by tethered membrane systems.[67, 68] The same anchoring chemistry that is suitable to gold (that is, either a thiol or disulfide-containing anchor group) can also be

applied to mercury. The anchoring lipid DPTL combined with DPhyPC as an outer leaflet was used to incorporate the OmpF porin in a functional state as a concept proving the viability of mercury as a support for a tBLM.

Tethered lipid bilayer membranes have proven themselves to be highly useful model membrane systems, and a wide variety of different studies have been carried out using these model systems. These studies include biophysical examinations of lipid bilayer behaviour as well as membrane proteins. Thus far, tBLMs have been used most commonly for the analysis of ion transport across the membrane *via* pore proteins and toxins such as α -haemolysin[64] and gramicidin.[90] However tethered membrane architectures have also been used to gain insight into common illnesses such as Alzheimer's disease. Using tBLMs, it has been shown that amyloid beta-oligomers directly affect the dielectric properties of lipid bilayers. In short, the adsorption of amyloid clusters to the lipid membrane causes the formation of defects in the membrane. This has significant implications on the disease model of Alzheimer's.[82, 91]

Tethered membranes have also been used to study the HIV-1 Gag protein, providing for the first time detail about the process by which the protein facilitates assembly of the virus.[92] As the protein has a disordered structure, it was impossible to study its structure *via* x-ray crystallography. However, by using a combination of small angle neutron scattering and molecular modelling, the authors were able to follow the conformational changes that the protein underwent when in contact with a lipid membrane. This demonstrates the benefit of model membranes in studying biological processes that cannot be properly understood using traditional methods of protein characterisation. The effect of aging due to oxidative stress on lipid bilayers was also studied using tBLMs.[93] By carrying out in-situ oxidation by exposing a lipid bilayer comprised of POPC to Fe(II) or 5 mM ascorbate and observing the structural changes in the lipid bilayer *via* neutron scattering, the authors showed that oxidative damage caused the lipid bilayer to become less tightly packed. Observing the same process with EIS, the authors also showed that oxidative damage caused the formation of holes in the lipid bilayer, significantly reducing its electrical resistance. This has important implications for the medical understanding of oxidative damage to cells, as tightly controlled ion transport across the membrane is essential for cell survival and function.

In another study, the interaction of β -lactoglobulin (a milk protein) with lipid bilayers was investigated.[94] Depending on its concentration, the protein exists either as a dimer or a monomer. It facilitates solubilisation of fat molecules in milk, but the exact nature of its interaction with lipids is not known. Using neutron scattering, the authors were able to show that depending on the concentration of the protein and whether it was denatured or in its native structure, it formed very different types of assemblies on phospholipid bilayers.

A tethered membrane was also used to investigate the effect of silver nanoparticles[66] on lipid membranes. As noted previously, the interaction of nano-scale materials with lipid membranes is poorly understood area, and further studies are urgently required. Nanomaterials have already been approved for use in many areas where they come into direct contact with humans and animals. For example, silver nanoparticles are used in bandages, items of clothing and toys already. The authors report that silver nanoparticles with a diameter of 2 nm lead to a small reversible disruption to the lipid membrane, temporarily reducing its electrical resistance.

More complex lipid membrane architectures comprised of a mixture of lipids have also been developed. For example, a sparsely tethered membrane mimicking the outer membrane of gram-negative bacteria has been developed which was used to study the activity of Colistin Sulfate and its effect on the membrane *via* neutron scattering and EIS.[95] Colistin acts by partially solubilising the lipids in the outer leaflet of the membrane and causing the formation of lesions in the lipid bilayer.

In addition to biophysical studies, tethered lipid membranes can also be used for more complex applications, for example in biosensing. One of the first reports of tBLMs used for biosensing is a membrane architecture using modified gramicidin to detect ferritin.[96] Gramicidin is a two-part ion channel which is only conductive when two pore proteins (one in the distal and one in the proximal leaflet of the membrane) are in the same location. The binding of ferritin prevents diffusion of the ion channels such that conductivity is 'switched off' in the presence of the analyte. The advantage of this type of biosensor is that by using different antibodies, it can be modified to detect any analyte for which there is a known antibody. In addition, aptamers (short DNA sequences that can be optimised to detect a large variety of different targets) could also be used to in this biosensor to enhance its potential.

One of the most promising aspects of tethered membranes is the possibility of preparing them by using only self-assembly, which makes it possible to incorporate them into microfluidic devices. It is conceivable, for example, to develop a microfluidic device containing tens or even hundreds of membrane patches in various stages of interaction with β -amyloid clusters. This device could then be used to test the effects of a large number of compounds on the aggregation and ability of these clusters to damage the membrane, which has the potential to significantly enhance the development of drugs to combat Alzheimer's Disease. A similar device could also be made containing tBLMs mimicking various bacterial membranes to screen large compound libraries for their ability to damage the membrane of bacteria.

1.7 Conclusion

Model membranes have shown themselves to be a powerful and versatile tool to study biological processes. As traditional methods of studying proteins have focused on water-soluble proteins, there is much information missing regarding the structure and function of membrane-bound proteins. Due to their ease of assembly and flexibility in terms of composition, model membranes can solve many of these problems. Black lipid membranes are uniquely suited for single-channel measurements but lack stability for longer-term studies or biosensing applications unless they are stabilised, for example with a hydrogel. Polymer-and-solid supported lipid membranes are highly suitable for the study of membrane processes are not related to charge transport, such as membrane binding events and the interaction of drugs or vesicles with lipid bilayers. Due to the difficulty of controlling the properties of the polymer support, the electrical properties of polymer-supported lipid bilayers are not well suited for ion channel studies, although some progress has been made in this area. Thanks to their high stability and ease of assembly, tethered membranes are uniquely suited for electrical studies of membranes and can be used in more complex applications such as microfluidic chips where lipid membranes are needed, but polymer-and solid supported lipid bilayers cannot easily be assembled, or lack sufficient long-term stability. However, tethered membranes only have a limited aqueous reservoir underneath the membrane, limiting their suitability for the incorporation of membrane proteins, as increasing the length of the tethering layer tends to deteriorate membrane quality.

1.8 References

1. *Comprehensive Nanoscience and Nanotechnology* 2ed. 2019: Academic Press.
2. van Meer, G., D.R. Voelker, and G.W. Feigenson, *Membrane lipids: where they are and how they behave*. *Nature Reviews Molecular Cell Biology*, 2008. **9**(2): p. 112-124.
3. Lingwood, D. and K. Simons, *Lipid Rafts As a Membrane-Organizing Principle*. *Science*, 2010. **327**(5961): p. 46-50.
4. Groves, J.T. and J. Kuriyan, *Molecular mechanisms in signal transduction at the membrane*. *Nature structural & molecular biology*, 2010. **17**(6): p. 659-665.
5. Römer, W. and C. Steinem, *Impedance analysis and single-channel recordings on nano-black lipid membranes based on porous alumina*. *Biophysical journal*, 2004. **86**(2): p. 955-965.
6. Lipids, A.P. *Phase Transition Temperatures for Glycerophospholipids*. Available from: <https://avantilipids.com/tech-support/physical-properties/phase-transition-temps/>.
7. Lipids, A.P. *16:0 PC (DPPC) | 850355*. [cited 2018 24.4.2018]; Available from: <https://avantilipids.com/product/850355/>.
8. Marrink, S.J., J. Risselada, and A.E. Mark, *Simulation of gel phase formation and melting in lipid bilayers using a coarse grained model*. *Chemistry and Physics of Lipids*, 2005. **135**(2): p. 223-244.
9. LIPIDAD. *LIPIDAT*. 2006 [cited 2018 23.4.2018]; Available from: http://www.lmsd.tcd.ie/new_lipidat/homelipidat.asp.
10. MUELLER, P., et al., *Reconstitution of Excitable Cell Membrane Structure in Vitro*. *Circulation*, 1962. **26**(5): p. 1167-1171.
11. Wiedemann, I., R. Benz, and H.-G. Sahl, *Lipid II-mediated pore formation by the peptide antibiotic nisin: a black lipid membrane study*. *Journal of bacteriology*, 2004. **186**(10): p. 3259-3261.
12. Tieleman, D.P., et al., *Simulation of Pore Formation in Lipid Bilayers by Mechanical Stress and Electric Fields*. *Journal of the American Chemical Society*, 2003. **125**(21): p. 6382-6383.
13. Weiss, K., et al., *Quantifying the Diffusion of Membrane Proteins and Peptides in Black Lipid Membranes with 2-Focus Fluorescence Correlation Spectroscopy*. *Biophysical Journal*, 2013. **105**(2): p. 455-462.
14. Tien, H.T., S. Carbone, and E. Dawidowicz, *Formation of "black" lipid membranes by oxidation products of cholesterol*. *Nature*, 1966. **212**(5063): p. 718.
15. Romer, W. and C. Steinem, *Impedance analysis and single-channel recordings on nano-black lipid membranes based on porous alumina*. *Biophysical Journal*, 2004. **86**(2): p. 955-965.
16. Van Gelder, P., F. Dumas, and M. Winterhalter, *Understanding the function of bacterial outer membrane channels by reconstitution into black lipid membranes*. *Biophysical Chemistry*, 2000. **85**(2-3): p. 153-167.
17. Winterhalter, M., *Black lipid membranes*. *Current Opinion in Colloid & Interface Science*, 2000. **5**(3): p. 250-255.
18. Sackmann, E., *Supported membranes: Scientific and practical applications*. *Science*, 1996. **271**(5245): p. 43-48.
19. Schulte, A., et al., *The outer membrane protein VhOmp of Vibrio harveyi: pore-forming properties in black lipid membranes*. *Journal of Membrane Biology*, 2009. **230**(2): p. 101-111.
20. Mueller, P., et al., *METHODS FOR THE FORMATION OF SINGLE BIMOLECULAR LIPID MEMBRANES IN AQUEOUS SOLUTION*. *The Journal of Physical Chemistry*, 1963. **67**(2): p. 534-535.
21. Boheim, G., *Statistical analysis of alamethicin channels in black lipid membranes*. *Journal of Membrane Biology*, 1974. **19**(1): p. 277-303.
22. Kang, X.-f., et al., *A storable encapsulated bilayer chip containing a single protein nanopore*. *Journal of the American Chemical Society*, 2007. **129**(15): p. 4701-4705.
23. Jeon, T.-J., et al., *Black lipid membranes stabilized through substrate conjugation to a hydrogel*. *Biointerphases*, 2008. **3**(2): p. FA96-FA100.

24. Shim, J.W. and L.Q. Gu, *Stochastic Sensing on a Modular Chip Containing a Single-Ion Channel*. Analytical Chemistry, 2007. **79**(6): p. 2207-2213.
25. Schmitt, E.K., et al., *Electrically insulating pore-suspending membranes on highly ordered porous alumina obtained from vesicle spreading*. Soft Matter, 2008. **4**(2): p. 250-253.
26. Aminipour, Z., et al., *Formation and electrical characterization of black lipid membranes in porous filter materials*. Physica Status Solidi a-Applications and Materials Science, 2017. **214**(9): p. 8.
27. Poulos, J.L., et al., *Electrowetting on dielectric-based microfluidics for integrated lipid bilayer formation and measurement*. Applied Physics Letters, 2009. **95**(1): p. 013706.
28. Tsemperouli, M. and K. Sugihara, *Characterization of di-4-ANEPPS with nano-black lipid membranes*. Nanoscale, 2018. **10**(3): p. 1090-1098.
29. Wiedemann, I., R. Benz, and H.G. Sahl, *Lipid II-mediated pore formation by the peptide antibiotic nisin: a black lipid membrane study*. Journal of Bacteriology, 2004. **186**(10): p. 3259-3261.
30. Rausell, C., et al., *Tryptophan Spectroscopy Studies and Black Lipid Bilayer Analysis Indicate that the Oligomeric Structure of Cry1Ab Toxin from Bacillus thuringiensis Is the Membrane-Insertion Intermediate*. Biochemistry, 2004. **43**(1): p. 166-174.
31. Jing, P., H. Paraiso, and B. Burris, *Highly efficient integration of the viral portal proteins from different types of phages into planar bilayers for the black lipid membrane analysis*. Molecular BioSystems, 2016. **12**(2): p. 480-489.
32. Leekumjorn, S. and A.K. Sum, *Molecular studies of the gel to liquid-crystalline phase transition for fully hydrated DPPC and DPPE bilayers*. Biochimica et Biophysica Acta (BBA) - Biomembranes, 2007. **1768**(2): p. 354-365.
33. Clifton, L.A., et al., *An Accurate In Vitro Model of the E. coli Envelope*. Angewandte Chemie International Edition, 2015: p. n/a-n/a.
34. Le Brun, A.P., et al., *Structural Characterization of a Model Gram-Negative Bacterial Surface Using Lipopolysaccharides from Rough Strains of Escherichia coli*. Biomacromolecules, 2013. **14**(6): p. 2014-2022.
35. Castellana, E.T. and P.S. Cremer, *Solid supported lipid bilayers: From biophysical studies to sensor design*. Surface Science Reports, 2006. **61**(10): p. 429-444.
36. Koutsioubas, A., M.S. Appavou, and D. Lairez, *Time-Resolved Neutron Reflectivity during Supported Membrane Formation by Vesicle Fusion*. Langmuir, 2017. **33**(40): p. 10598-10605.
37. Girard-Egrot, A.P. and L.J. Blum, *Langmuir-Blodgett technique for synthesis of biomimetic lipid membranes*, in *Nanobiotechnology of biomimetic membranes*. 2007, Springer. p. 23-74.
38. Csúcs, G. and J.J. Ramsden, *Solubilization of planar bilayers with detergent*. Biochimica et Biophysica Acta (BBA) - Biomembranes, 1998. **1369**(2): p. 304-308.
39. Mennicke, U. and T. Salditt, *Preparation of solid-supported lipid bilayers by spin-coating*. Langmuir, 2002. **18**(21): p. 8172-8177.
40. Kučerka, N., et al., *Lipid bilayer structure determined by the simultaneous analysis of neutron and X-ray scattering data*. Biophysical journal, 2008. **95**(5): p. 2356-2367.
41. Junghans, A. and I. Koper, *Structural Analysis of Tethered Bilayer Lipid Membranes*. Langmuir, 2010. **26**(13): p. 11035-11040.
42. Knoll, W., et al., *Solid supported lipid membranes: New concepts for the biomimetic functionalization of solid surfaces*. Biointerphases, 2008. **3**(2): p. FA125-FA125.
43. Ross, E.E., et al., *Formation of Self-Assembled, Air-Stable Lipid Bilayer Membranes on Solid Supports*. Langmuir, 2001. **17**(8): p. 2305-2307.
44. Puu, G., et al., *Distribution and stability of membrane proteins in lipid membranes on solid supports*. Biosensors & Bioelectronics, 2000. **15**(1-2): p. 31-41.
45. Kycia, A.H., et al., *Atomic force microscopy studies of a floating-bilayer lipid membrane on a Au (111) surface modified with a hydrophilic monolayer*. Langmuir, 2011. **27**(17): p. 10867-10877.
46. Diamanti, E., et al., *High Resistivity Lipid Bilayers Assembled on Polyelectrolyte Multilayer Cushions: An Impedance Study*. Langmuir, 2016. **32**(25): p. 6263-6271.
47. Clifton, L.A., et al., *Effect of Divalent Cation Removal on the Structure of Gram-Negative Bacterial Outer Membrane Models*. Langmuir, 2014. **31**(1): p. 404-412.

48. Garcia-Celma, J.J., et al., *Specific Anion and Cation Binding to Lipid Membranes Investigated on a Solid Supported Membrane*. Langmuir, 2007. **23**(20): p. 10074-10080.
49. Ha, Y., L.E. Katz, and H.M. Liljestrand, *Distribution of Fullerene Nanoparticles between Water and Solid Supported Lipid Membranes: Thermodynamics and Effects of Membrane Composition on Distribution*. Environmental Science & Technology, 2015. **49**(24): p. 14546-14553.
50. Morigaki, K., et al., *Patterning solid-supported lipid bilayer membranes by lithographic polymerization of a diacetylene lipid*. Angewandte Chemie International Edition, 2001. **40**(1): p. 172-174.
51. Loidl-Stahlhofen, A., et al., *Solid-supported lipid membranes as a tool for determination of membrane affinity: High-throughput screening of a physicochemical parameter*. Journal of Pharmaceutical Sciences, 2001. **90**(5): p. 599-606.
52. Tanaka, M. and E. Sackmann, *Polymer-supported membranes as models of the cell surface*. Nature, 2005. **437**(7059): p. 656-663.
53. Wagner, M.L. and L.K. Tamm, *Tethered polymer-supported planar lipid bilayers for reconstitution of integral membrane proteins: silane-polyethyleneglycol-lipid as a cushion and covalent linker*. Biophysical Journal, 2000. **79**(3): p. 1400-1414.
54. Ye, Q., et al., *Liposomes Tethered to Omega-Functional PEG Brushes and Induced Formation of PEG Brush Supported Planar Lipid Bilayers*. Langmuir, 2009. **25**(23): p. 13534-13539.
55. Blakeston, A.C., et al., *New Poly(amino acid methacrylate) Brush Supports the Formation of Well-Defined Lipid Membranes*. Langmuir, 2015. **31**(12): p. 3668-3677.
56. Beyer, D., et al., *Influence of anchor lipids on the homogeneity and mobility of lipid bilayers on thin polymer films*. Angewandte Chemie International Edition in English, 1996. **35**(15): p. 1682-1685.
57. Naumann, C.A., et al., *The polymer-supported phospholipid bilayer: tethering as a new approach to substrate-membrane stabilization*. Biomacromolecules, 2002. **3**(1): p. 27-35.
58. Renner, L., et al., *Controlled enhancement of transmembrane enzyme activity in polymer cushioned supported bilayer membranes*. Soft Matter, 2010. **6**(21): p. 5382-5389.
59. Deverall, M.A., et al., *Membrane Lateral Mobility Obstructed by Polymer-Tethered Lipids Studied at the Single Molecule Level*. Biophysical Journal. **88**(3): p. 1875-1886.
60. Zhang, H., S. Salinas, and V.B. Sundaresan, *Conducting polymer supported bilayer lipid membrane reconstituted with alamethicin*. Smart Materials and Structures, 2011. **20**(9): p. 9.
61. Hianik, T., et al., *Conductance and electrostriction of bilayer lipid membranes supported on conducting polymer and their application for determination of ammonia and urea*. Materials Science and Engineering: C, 1998. **5**(3): p. 301-305.
62. Wagner, M.L. and L.K. Tamm, *Reconstituted Syntaxin1A/SNAP25 Interacts with Negatively Charged Lipids as Measured by Lateral Diffusion in Planar Supported Bilayers*. Biophysical Journal, 2001. **81**(1): p. 266-275.
63. Andersson, J., et al., *Synthesis and Characterization of Novel Anchorlipids for Tethered Bilayer Lipid Membranes*. Langmuir, 2017. **33**(18): p. 4444-4451.
64. Vockenroth, I.K., et al., *Incorporation of alpha-hemolysin in different tethered bilayer lipid membrane architectures*. Langmuir, 2008. **24**(2): p. 496-502.
65. Vogel, N., J. Zieleniecki, and I. Köper, *As flat as it gets: ultrasoft surfaces from template-stripping procedures*. Nanoscale, 2012. **4**(13): p. 3820-3832.
66. Goreham, R.V., et al., *Interaction of silver nanoparticles with tethered bilayer lipid membranes*. Langmuir, 2015.
67. Becucci, L. and R. Guidelli, *Mercury-supported biomimetic membranes for the investigation of antimicrobial peptides*. Pharmaceuticals, 2014. **7**(2): p. 136-168.
68. Moncelli, M., L. Becucci, and S.M. Schiller, *Tethered bilayer lipid membranes self-assembled on mercury electrodes*. Bioelectrochemistry, 2004. **63**(1): p. 161-167.
69. Atanasov, V., et al., *A molecular toolkit for highly insulating tethered bilayer lipid membranes on various substrates*. Bioconjugate Chemistry, 2006. **17**(3): p. 631-637.

70. Vockenroth, I.K., et al., *Stable insulating tethered bilayer lipid membranes*. *Biointerphases*, 2008. **3**(2): p. FA68-FA73.
71. Dorvel, B.R., et al., *Formation of Tethered Bilayer Lipid Membranes on Gold Surfaces: QCM-Z and AFM Study*. *Langmuir*, 2007. **23**(13): p. 7344-7355.
72. Vockenroth, I.K., et al., *Formation of tethered bilayer lipid membranes probed by various surface sensitive techniques*. *Biointerphases*, 2009. **4**(2): p. 19-26.
73. Knoll, W., et al., *Functional tethered lipid bilayers*. *Reviews in Molecular Biotechnology*, 2000. **74**(3): p. 137-158.
74. Naumann, R., et al., *The peptide-tethered lipid membrane as a biomimetic system to incorporate cytochrome c oxidase in a functionally active form*. *Biosensors and Bioelectronics*, 1999. **14**(7): p. 651-662.
75. McGillivray, D.J., et al., *Molecular-scale structural and functional characterization of sparsely tethered bilayer lipid membranes*. *Biointerphases*, 2007. **2**(1): p. 21-33.
76. Schiller, S.M., et al., *Archaea analogue thiolipids for tethered bilayer lipid membranes on ultrasoother gold surfaces*. *Angewandte Chemie International Edition*, 2003. **42**(2): p. 208-211.
77. Vockenroth, I.K., et al., *Functional incorporation of the pore forming segment of AChR M2 into tethered bilayer lipid membranes*. *Biochimica Et Biophysica Acta-Biomembranes*, 2007. **1768**(5): p. 1114-1120.
78. Andersson, J., *New Tether Structures of tethered bilayer lipid membranes*, in *Chemical and Physical Sciences*. 2013, Flinders University: Adelaide, Australia.
79. Budvytyte, R., et al., *Structure and Properties of Tethered Bilayer Lipid Membranes with Unsaturated Anchor Molecules*. *Langmuir*, 2013. **29**(27): p. 8645-8656.
80. Kibrom, A., et al., *Hydrogel-supported protein-tethered bilayer lipid membranes: A new approach toward polymer-supported lipid membranes*. *Soft Matter*, 2011. **7**(1): p. 237-246.
81. McGillivray, D.J., et al., *Structure of functional Staphylococcus aureus α -hemolysin channels in tethered bilayer lipid membranes*. *Biophysical journal*, 2009. **96**(4): p. 1547-1553.
82. Valincius, G., et al., *Soluble Amyloid beta-Oligomers Affect Dielectric Membrane Properties by Bilayer Insertion and Domain Formation: Implications for Cell Toxicity*. *Biophysical Journal*, 2008. **95**(10): p. 4845-4861.
83. Basit, H., et al., *Tethered Bilayer Lipid Membranes on Mixed Self-Assembled Monolayers of a Novel Anchoring Thiol: Impact of the Anchoring Thiol Density on Bilayer Formation*. *Langmuir*, 2011. **27**(23): p. 14317-14328.
84. Leitch, J., et al., *In Situ PM-IRRAS Studies of an Archaea Analogue Thiolipid Assembled on a Au(111) Electrode Surface*. *Langmuir*, 2009. **25**(17): p. 10354-10363.
85. Heinrich, F., et al., *A New Lipid Anchor for Sparsely Tethered Bilayer Lipid Membranes†*. *Langmuir*, 2009. **25**(7): p. 4219-4229.
86. Vockenroth, I.K., et al., *Tethered bilayer lipid membranes with giga-ohm resistances*. *Electrochemistry Communications*, 2008. **10**(2): p. 323-328.
87. Ataka, K., et al., *Oriented Attachment and Membrane Reconstitution of His-Tagged Cytochrome c Oxidase to a Gold Electrode: In Situ Monitoring by Surface-Enhanced Infrared Absorption Spectroscopy*. *Journal of the American Chemical Society*, 2004. **126**(49): p. 16199-16206.
88. Schrems, A., et al., *Bilayer lipid membrane formation on a chemically modified S-layer lattice*. *Langmuir*, 2011. **27**(7): p. 3731-3738.
89. Atanasov, V., et al., *Membrane on a chip: a functional tethered lipid bilayer membrane on silicon oxide surfaces*. *Biophysical journal*, 2005. **89**(3): p. 1780-1788.
90. Kozuch, J., et al., *Combined Electrochemistry and Surface-Enhanced Infrared Absorption Spectroscopy of Gramicidin A Incorporated into Tethered Bilayer Lipid Membranes*. *Angewandte Chemie International Edition*, 2012. **51**(32): p. 8114-8117.
91. Karaballi, R.A., et al., *Electrochemical surface-enhanced Raman spectroscopy (EC-SERS) study of the interaction between protein aggregates and biomimetic membranes*. *Physical Chemistry Chemical Physics*, 2018. **20**(6): p. 4513-4526.

92. Datta, S.A., et al., *HIV-1 Gag extension: conformational changes require simultaneous interaction with membrane and nucleic acid*. Journal of molecular biology, 2011. **406**(2): p. 205-214.
93. Knobloch, J.J., et al., *Oxidative Damage to Biomimetic Membrane Systems: In Situ Fe(II)/Ascorbate Initiated Oxidation and Incorporation of Synthetic Oxidized Phospholipids*. Langmuir, 2015. **31**(46): p. 12679-12687.
94. Junghans, A., et al., *Probing Protein-Membrane Interactions Using Solid Supported Membranes*. Langmuir, 2011. **27**(6): p. 2709-2716.
95. Andersson, J., et al., *A tethered bilayer lipid membrane that mimics microbial membranes*. Physical Chemistry Chemical Physics, 2018.
96. Cornell, B., et al., *A biosensor that uses ion-channel switches*. NATURE-LONDON-, 1997: p. 580-582.

2 Methods: Neutron Scattering and Electrochemical Impedance Spectroscopy

The two primary methods that were used in this work to characterise tBLMs were electrochemical impedance spectroscopy (EIS) and neutron scattering. These methods have been supplemented with other techniques such as contact angle measurements and X-ray reflectometry. The focus of this project was to develop a means of assembling tBLMs comprised of lipopolysaccharides *via* self-assembly and to study their structural and functional properties.

The structure of the lipid bilayers was studied using Neutron Scattering. This technique provides sub-nanometre structural information of an assembled tBLM at a solid-liquid interface. Neutron scattering is ideal to observe changes in the membrane that may not affect its electrical properties. These changes include, for example, morphological changes that do not result in defect formation as well as the binding of proteins, drugs or nanoparticles to the bilayer. However, small structural changes that take place in the lipid membranes are not always visible to neutron scattering. These can be detected much sensitively with EIS.

Electrochemical impedance spectroscopy provides information about the resistance and capacitance of a tBLM and is highly sensitive to small defects in the membrane structure.[1] Observations made with EIS can be understood better when the electrical data are complemented with neutron scattering measurements. For example, it is known that silver nanoparticles have an effect on the electrical properties of a lipid bilayer[2], but the location of the nanoparticles in the lipid bilayer cannot be elucidated from impedance data, nor can their effect on the structure of the lipid bilayer be determined.

2.1 Neutron scattering in soft matter

2.1.1 Theory of neutron scattering

This section is based largely on the work *Introduction to Small-Angle Neutron Scattering and Neutron Reflectometry* written by Andrew J Jackson.[3]

Neutron scattering is a technique often employed in soft matter studies as well as materials science due to the ability of neutrons to probe the structure of materials at scales less than 1 nm.[3] The ability of neutrons to study buried interfaces and multilayer systems makes neutron scattering a superior technique to methods such as AFM when it comes to the study of complex multilayer systems such as lipid bilayers because chemically distinct layers can be resolved, allowing the whole structure of the bilayer to be probed rather than only examining the surface topology.[4, 5] In addition, unlike XPS for example, neutron scattering does not require a high vacuum environment and can therefore be used on samples submerged in a solvent.[5-7]

Neutrons are subatomic particles with a spin of $\frac{1}{2}$ that are subject to refraction, reflection and diffraction. The scattering of neutrons upon interaction with atomic nuclei is exploited in neutron scattering, as the scattering event provides crucial information about the atom at which it occurred. There are two ways in which a neutron may be scattered upon interacting with matter. Firstly, nuclear scattering can occur when the neutron interacts with a nucleus. Secondly, magnetic scattering occurs when the neutron's magnetic moment interacts with the magnetic field of unpaired electrons. Both of these events can be exploited in neutron scattering experiments, but the study of lipid bilayers predominantly utilises nuclear scattering rather than magnetic scattering.

Neutron scattering upon interaction with an atomic nucleus is elastic, that is, the momentum of the particle is unchanged in magnitude, but its direction is altered by the collision. The scattering event depends upon the interaction potential between the nucleus and the incident neutron $V(r)$ where the r is the distance between the neutron and nucleus. The interaction potential is attenuated quickly, reaching 0 at around 10^{-15} m. As the neutron size is significantly smaller than the neutron wavelength of one to a few tens of Å, the nucleus acts as a point scatterer, creating a spherical scattering wave because the neutron undergoes isotropic scattering as it is equally likely to be scattered in all directions. Figure 2.1 shows a schematic representation of the scattering event.

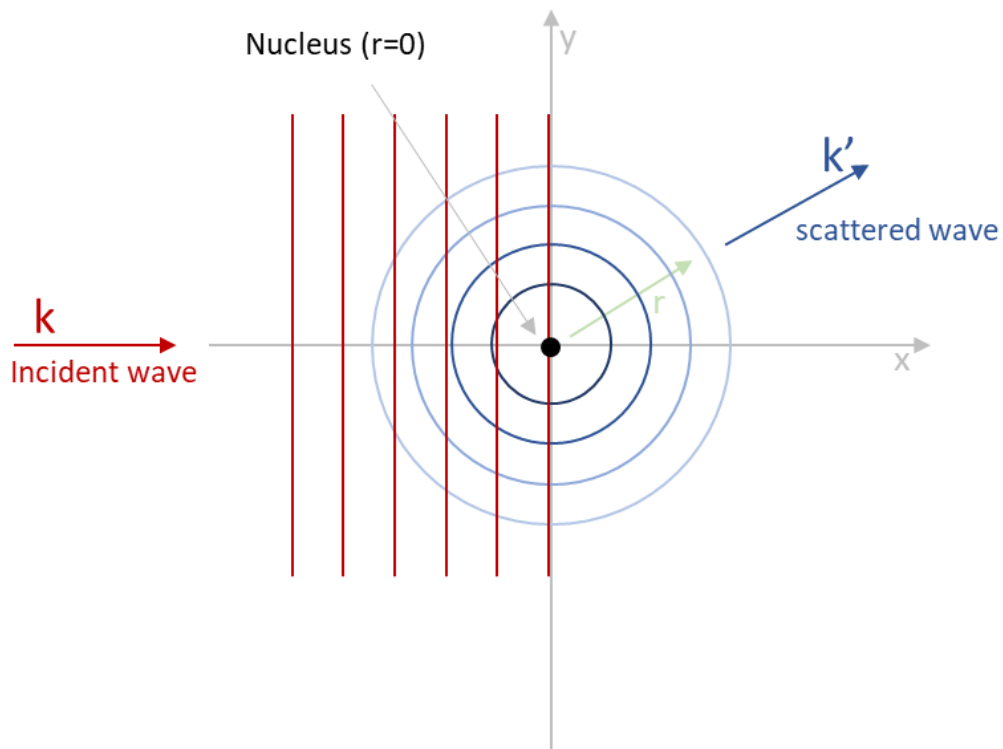


Figure 2.1: schematic of the incident neutron wave k and the scattered wave k' . Because of the large wave length, the incident wave can be considered planar relative to the diameter of an atomic nucleus.

The incident beam of neutrons can be approximated by a planar wave function (equation 2.1):

$$\Psi_i = e^{ikz} \quad (2.1)$$

in which \mathbf{z} is the distance between nucleus and incident neutron beam (in its direction of travel) and \mathbf{k} is the neutron wavenumber ($2\pi/\lambda$). The scattered wave is described by the wave function

$$\Psi_s = -\frac{b}{r} e^{ikr} \quad (2.2)$$

in which \mathbf{b} is the scattering length of the nucleus (see below for more detail) and \mathbf{r} is the distance between the wave front and the scattering origin (i.e. the nucleus). The imaginary component of the wave function is significant only in the case of a small number of nuclei not normally encountered in soft matter studies. The incident and reflected neutron waves can be described by their respective wave vectors (k_i and k_r), as shown in Figure 2.2.

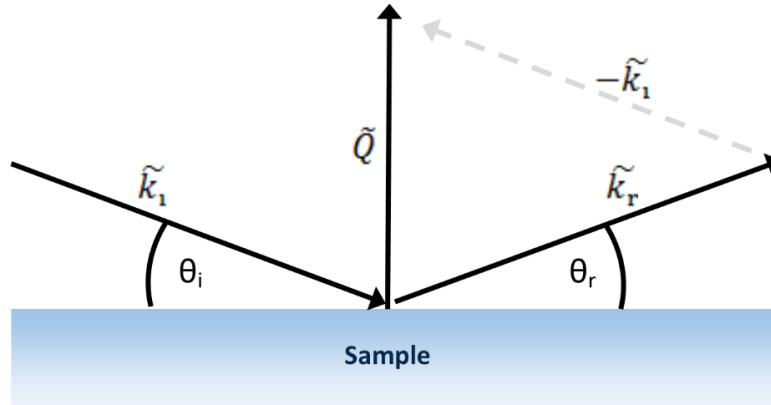


Figure 2.2: incident neutrons (k_i) and reflected neutrons (k_r), as it is an elastic scattering event, momentum is conserved. the momentum transfer vector q is perpendicular to the surface of the sample and can be obtained by subtracting k_i from k_r .

As ultra-flat samples are used for neutron scattering, specular reflection will occur at the interface and the reflected angle θ_r will be equal to the incident angle θ_i . The measured reflectivity is reported as a fraction of the incident neutron beam intensity:

$$R = \frac{I_i}{I_r} \quad (2.3)$$

Reflectivity data is plotted as a function of reflectivity (R) vs Q (momentum transfer, units of Å⁻¹). In specular reflection, the momentum transfer vector Q is always perpendicular to the surface (in the Z direction), making neutrons highly sensitive to structural differences in this direction. The magnitude of Q is calculated through subtraction of the wave vector of the incident neutron \mathbf{k}_i from the wave vector of the reflected neutron \mathbf{k}_r :

$$Q = | \mathbf{k}_r - \mathbf{k}_i | \quad (2.4)$$

As the two wave vectors are equal in magnitude ($k_i = k_r = 2\pi/\lambda$), trigonometric analysis quickly shows that

$$Q = \frac{4\pi \sin\theta}{\lambda} \quad (2.5)$$

Bragg's Law ($n\lambda = 2d \sin \theta$, where d is the spacing between atoms in the lattice) can be used to predict the appearance of fringes in a diffraction pattern. Maxima are predicted to appear whenever there is constructive interference between the two scattered particles (that is, if the path length between the diffracted particles differs by an integer multiple, n , of the wave length). Combination of Bragg's law with equation 2.5 predicts the positions of maxima in the observed interference pattern of scattered neutrons:

$$Q = \frac{2\pi}{d} n \quad (2.6)$$

Where d is the spacing between atoms in the substrate and a fringe appears whenever n is an integer. Inspection of equation 2.6 shows that the appearance of maxima (and the spacing between them) directly depends on the spacing between the layers of the sample. The intensity of the reflection maxima and the spacing between the peaks contains structural information about the sample.

To probe different length scales of the sample structure, either the incident angle θ or the wavelength of the neutrons (λ) can be varied. The Platypus instrument used to collect the neutron data in this work is a time-of-flight (TOF) reflectometer using cold neutrons with wavelengths of 2-20 Å.[8] The wavelength (λ) of a neutron is related to its speed (v) by the De Broglie equation: $\lambda = \hbar / mv$ where \hbar is Planck's constant and m is the mass of the neutron (1.675×10^{-27} kg).

By linking the chopper movement to detection events, the time of flight of the neutrons from the chopper to the detector can be determined (and thus their speed). The wavelength of the neutrons can thus be controlled by the chopper speed. As the wavelength of each neutron pulse is fixed, the incident angle (θ) can be varied by rotating the samples relative to the neutron beam.

Figure 2.3 shows a typical neutron data set (plotting the \log_{10} of the reflection intensity R against the momentum transfer vector Q). Alongside the experimental data, a fitting line is shown. The fit is generated using the method described in section 2.1.2: Neutron Data Analysis.

There is a point on the graph at which total reflection begins to occur is referred to as the critical edge. If a solvent is used, the position of the critical edge depends on the SLD of the solvent. This can be seen in Figure 2.3 (at $Q < 0.01 \text{ \AA}^{-1}$) where $\log R = 0$ (therefore the ratio of incident to reflected neutrons is 1 because all incident neutrons are reflected). This occurs below the critical angle, θ_c , calculated *via* Snell's Law: $\cos \theta_c = n_2/n_1$, where n_1 and n_2 are the respective refractive indexes of the two media at the interface (see Figure 2.3). From the following expression for the critical angle: $\theta_c = \sqrt{16 \pi (\Delta SLD)}$ in which ΔSLD is the change in SLD between the two media, it is clear that a critical angle only exists when there is an increase in SLD from the fronting to the backing media.

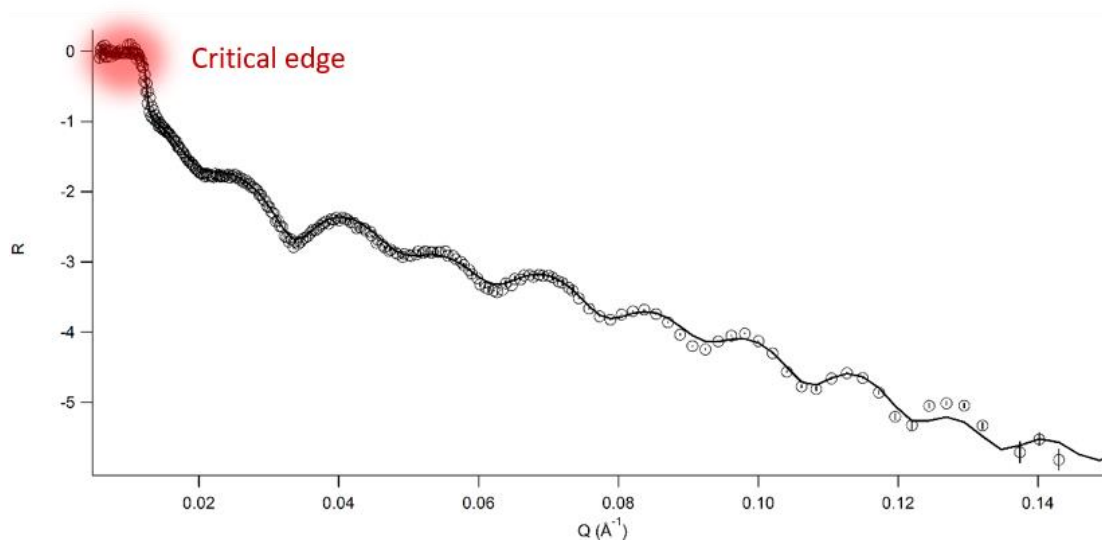


Figure 2.3: Experimental neutron data (circles) and fitted data (line). To increase the range of length scales measured in the experiment (increase in Q), three grazing angles are used. Reflectivity (R) is shown in \log_{10} (that is, $0 = \text{total reflectivity}$).

The degree to which a neutron is scattered depends upon the scattering length of a nucleus. The scattering length density of an element can in many ways be said to be analogous to the refractive index of a material, even though they are based on different physical processes. Neutron scattering events can be described using methods developed for optical phenomena such as Snell's law and the Fresnel equations.

A unique advantage of neutrons compared to other types of radiation in soft matter studies is that the scattering length varies significantly between elements, and randomly across the periodic table. This enables the differentiation between elements that cannot be distinguished with X-Rays. For example, ^1H has a scattering length of $-3.74 \times 10^{-5} \text{ \AA}$, while ^2H has a scattering length of $6.67 \times 10^{-5} \text{ \AA}$. [9]

To make use of the known scattering length for the purpose of analysing real systems, the scattering length density (SLD, ρ in equation 2.7) is used, calculated by summing up the scattering length (b) of n atoms (of element i) and averaging it over the occupied volume (V):

$$\rho = \frac{\sum_i^n b_i}{V} \quad (2.7)$$

At the atomic scale, the SLD is an inaccurate measure as the scattering length changes significantly with distance from the atom. But to describe a system on the nano-scale, averaging the SLD over a large distance and a large number of nuclei, the scattering length density is an accurate description of the properties of the system. The units of SLD are as described above are \AA^{-2} .

There is no correlation between atomic number and SLD (for example carbon has a coherent SLD of $7.0 \times 10^{-6} \text{ \AA}^{-2}$ whereas nitrogen has an SLD of $3.25 \times 10^{-6} \text{ \AA}^{-2}$). Furthermore, the significant variation in scattering length that can occur between isotopes means that for example, H_2O has an SLD of $-0.56 \times 10^{-6} \text{ \AA}^{-2}$ and D_2O has an SLD of $6.36 \times 10^{-6} \text{ \AA}^{-2}$. This phenomenon can be exploited in soft matter studies as it enables the differentiation of chemically similar components such as the inner and outer leaflet of lipid bilayers if one part of the bilayer is deuterated. [10]

As the scattering length density is simply the sum of scattering lengths averaged over a given volume, mixtures of elements and molecules can also be assigned an SLD. The difference in SLD between the isotopes of hydrogen enables the use of “contrast matching” – mixtures of solvents (typically H_2O and D_2O) tailored to specifically hide certain parts of a lipid bilayer or the substrate. For example, gold (which is commonly used as a substrate for tBLMs) has an SLD of $4.5 \times 10^{-6} \text{ \AA}^{-2}$. This can be matched with a mixture of 76% D_2O and 24% H_2O , which also has an SLD of $4.5 \times 10^{-6} \text{ \AA}^{-2}$. This type of solvent is sometimes referred to as “CM 4.5”. In a typical neutron experiment studying a tBLM system, three measurements with three different contrasts are used – H_2O , D_2O and CM4.5

The use of three contrasts allows for additional structural information to be elucidated from the neutron data. The change in SLD of any part of the lipid bilayer in response to a change of solvent contrast directly corresponds to the hydration of that part of the bilayer as an exchange of the solvent in the bilayer segment necessarily changes the SLD of that segment as well. Figure 2.4 shows a set of reflectivity plots measuring the same bilayer under three different contrasts.

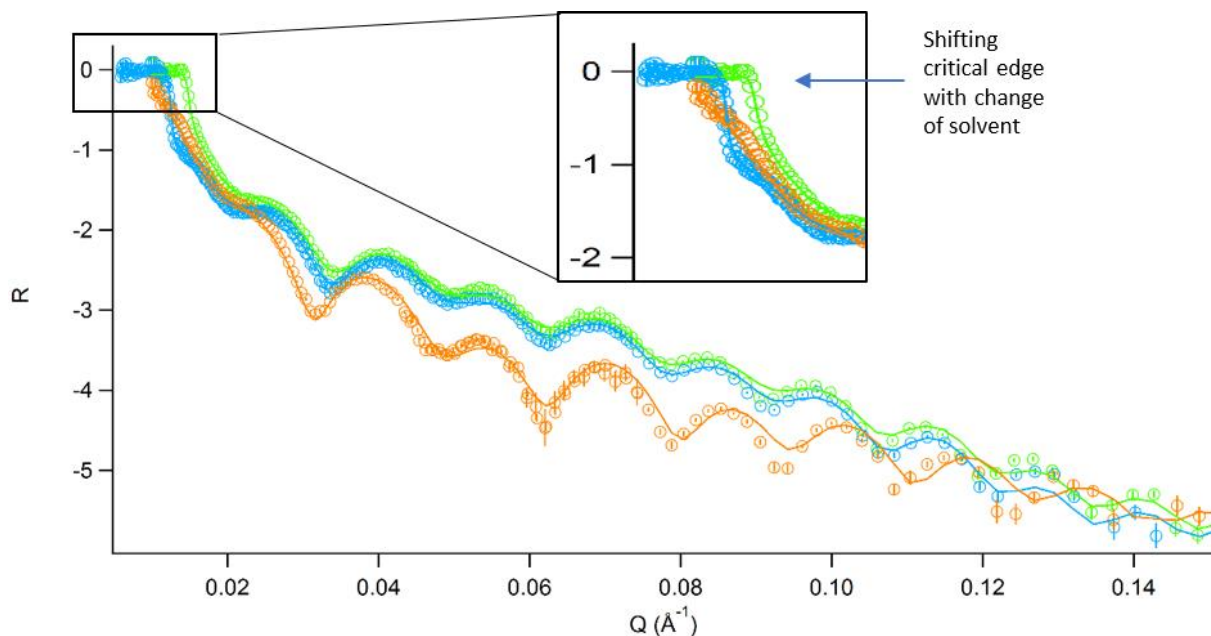


Figure 2.4: Reflectivity plot of a lipid bilayer under three different contrast agents: D₂O (green), CM4.5 (blue) and H₂O (orange). Experimental data are shown as circles and the fits are shown as straight lines. The inset shows the changing critical edge position which depends on the SLD of the solvent in use. When D₂O (green) is replaced with a mix of D₂O and water (blue) and is not visible when water is used (orange).

2.1.2 Neutron data analysis

Prior to fitting, the neutron data must be reduced. This requires direct beam measurements to be taken at the three grazing angles (if a fixed wavelength neutron source is used). Data reduction extracts the scattering intensity profile as a function of momentum transfer vector from the raw data collected by the detector, producing graphs such as that shown in Figure 2.4.

To fit neutron data, a theoretical fringe pattern is generated using a model system that approximates the structure of the lipid bilayer. A theoretical model describing the membrane divides the lipid bilayer into several distinct slabs or layers, using Abelès optical matrix approach to generate a matrix describing each layer of the membrane (see Figure 2.5).[11] The slabs are all assigned a thickness, SLD, roughness and hydration and a theoretical fringe pattern is generated from this system. The variables are then adjusted until the generated fringe pattern matches the experimental data. The initial accuracy of the fit is represented by a χ^2 value calculated using equation 2.11:

$$\chi^2 = \frac{1}{N-P} \sum_i^N \left(\frac{y_{obs_i} - y_{calc_i}}{\sigma_{obs_i}} \right)^2 \quad (2.8)$$

In which y_{obs} and y_{calc} are the values that were observed and calculated, respectively, and σ_{obs} is the standard deviation of y_{obs} . N represents the number of data points and P represents the parameters. Ideally, χ^2 will be 1, in case of a perfect fit. In real data sets, a value below 5 indicates a well-fitted data set and depending on the parameters and quality of the data, χ^2 values can be as high as 20 even with a good fit.[12] Once a satisfactory value for χ^2 has been achieved, the fit is evaluated using Monte Carlo error analysis (see chapter 2.1.3).

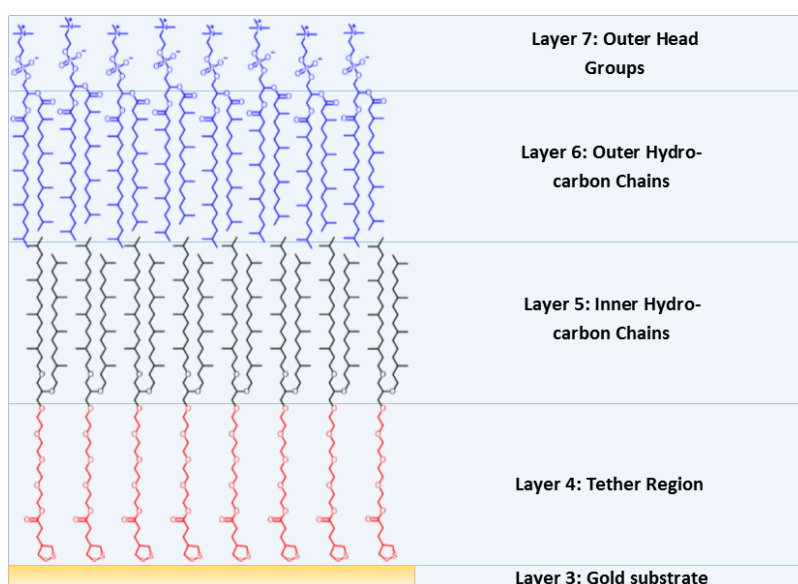


Figure 2.5: Layers of a theoretical bilayer used to model neutron data. Layers 1 and 2 are the oxide layer on the substrate and the chromium adhesion layer between silicon and gold and are not shown.

Some parameters of the sample are known and fixed (for example the SLD of silicon is always $2.07 \cdot 10^{-6} \text{ \AA}^{-2}$ and its hydration is 0%) and the remaining values are permitted to change within a certain assigned range (Table 2.1).

Table 2.1: Selected parameters of the theoretical slab-model used to model neutron data

	Typical SLD (10^{-6} \AA^{-2})	Typical Thickness (\AA)
Silicon Substrate (Backing plate)	2.07 (fixed)	infinite
Silicon Oxide	3.47 (fixed)	3 - 15
Chromium	3.03 (fixed)	20 - 80
Gold	4.1- 4.5	100 - 250
Tether Region	0.5 -2.0	12 - 18
Hydrocarbon chains (inner & outer)	-0.4 - 0	12 - 18
Outer head groups	1 – 3.5	7 - 12

The fitting process is done using the *MotoFit* plug in for Igor Pro.[12] From the fitted data, an SLD profile can be extracted as shown in Figure 2.6.

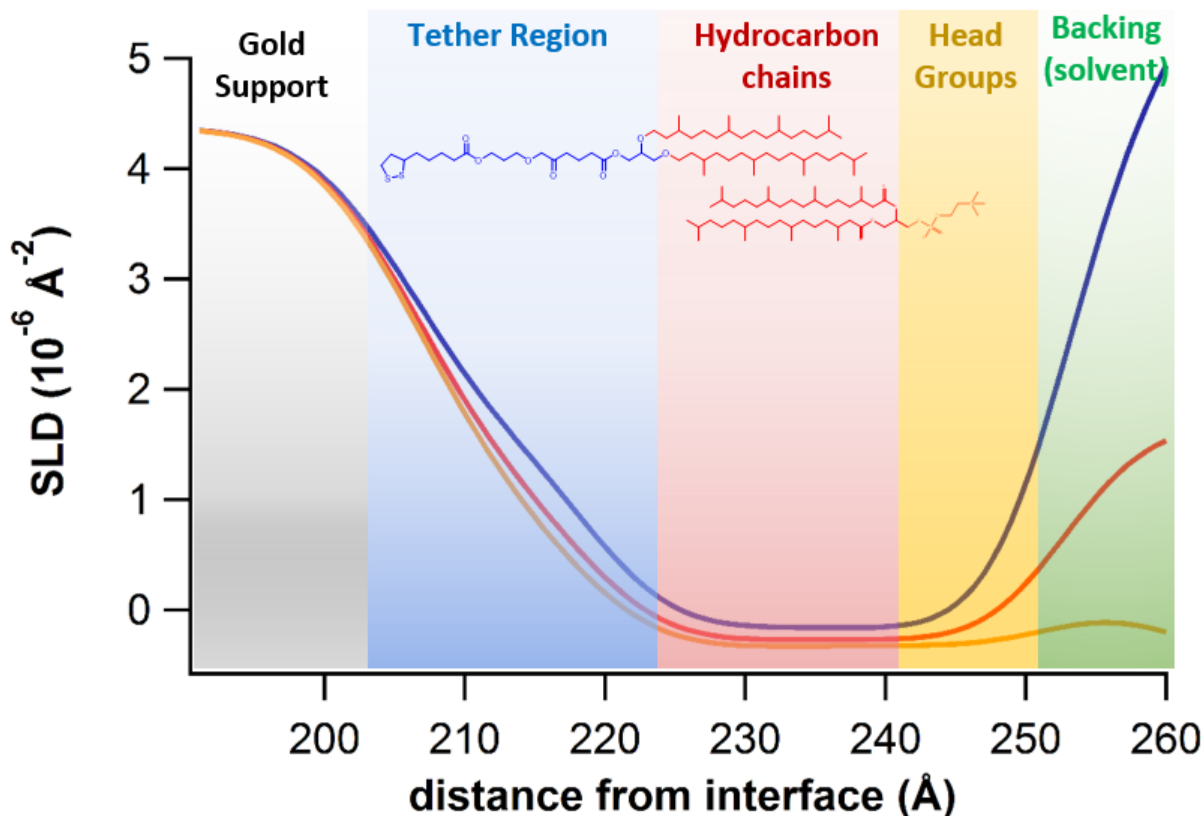


Figure 2.6: SLD profile of a tBLM on a silicon support. The SLD up to ca. 200 Å is that of the silicon backing wafer, chromium adhesion layer and gold substrate. The inset figure shows the part of the lipid bilayer corresponding to each section of the SLD profile.

Figure 2.6 shows smoothly changing SLD profiles rather than a series of sharp steps as one would expect if every segment of the bilayer were to be fitted with a discrete SLD value. The “smoothing” of the SLD profile is a result of roughness occurring between the interfaces of the assigned layers (Figure 2.5), causing gradual changes in SLD rather than distinct step-wise changes.[12] The observed roughness is a consequence of several factors including thermal movement of the nuclei in the bilayer, which is a significant factor given that measuring a lipid bilayer under three contrasts takes around 6 hours.

The roughness of the substrate (particularly roughness introduced by the sample preparation such as sputter coating) as well as defects of the bilayer and the inherent structural inhomogeneity of a self-assembled system. Roughness values around 3 - 8 Å are typical in a good sample.[13, 14]

2.1.3 Monte Carlo error analysis

The χ^2 value obtained during the fitting process is only an initial measure of fit quality. In order to obtain information on the variance of the individual parameters, Monte Carlo error analysis is carried out on each fitted data set.[15] As it is impossible to repeat neutron scattering experiments for the required number of times to obtain statistically significant data, Monte Carlo simulations provide a convenient alternative. In this method, gaussian noise is generated around every experimental data point and the resulting data set is fitted to the model. This is repeated a minimum of 1000 times and often up to 10,000 iterations are used. The parameters of the fitted data set (thickness, SLD, hydration and roughness for each layer) are then extracted from each fit and statistical analysis is carried out on the extracted parameters to obtain a mean and standard deviation for each parameter such that the data sets can be compared.

2.1.4 Other approaches to fit neutron data

Another method to fit neutron data has also been developed in which a space-filling model of the bilayer is generated using a combination of molecular dynamics simulations and statistical analysis, modelling the distribution of membrane components across the vertical axis.[16] This approach to fitting produces a plot of membrane composition along the vertical axis rather than plotting scattering length density. For example, rather than stating that the SLD of the sample at a distance of 210 Å from the interface is $1.5 \times 10^{-6} \text{Å}^{-2}$ and that it contains 5 volume-% water, the fit will state that the sample at this distance is comprised of 95% tether and 5% water.

This approach provides more nuanced information about membrane composition because rather than requiring a single slab with a hydration level and a distinct SLD, it allows the membrane composition to vary dynamically along the z axis. This means that the model is well-suited to study membranes with incorporated proteins, interactions of lipid membranes with proteins or very sparsely tethered membranes. Such membranes are not 96-99% complete but contain proteins and defects that must be accounted for and are thus more challenging to fit. The model systems under investigation in this thesis, however, have much lower defect densities and higher completion levels such that they can be described very accurately using the slab-based model. Therefore, the slab-model has been chosen instead of other methods as it was the approach best suited to study the membrane systems presented here.

2.2 Electrochemical Impedance Spectroscopy

2.2.1 Theory of electrochemical impedance spectroscopy

This chapter is largely based on the book *Impedance Spectroscopy: Theory, Experiment, and Applications*. [17]

Electrochemical impedance spectroscopy is a well-established technique to characterise a system with known resistive and/or capacitive elements. [1] In a typical EIS experiment, an alternating voltage is applied over a range of frequencies (typically 100 kHz – 3 mHz with an amplitude of 10 mV) and the resulting current is measured as well as the time delay between a change in the applied potential and the resulting current. Figure 2.7 shows a schematic of the instrumental setup used for impedance measurements. Impedance data can be fitted to an equivalent circuit of the system under investigation, which in the case of a tBLM provides information about the quality of the lipid bilayer and charge transport processes across the membrane, for example by defects or incorporated channel proteins. [1, 14, 18, 19]

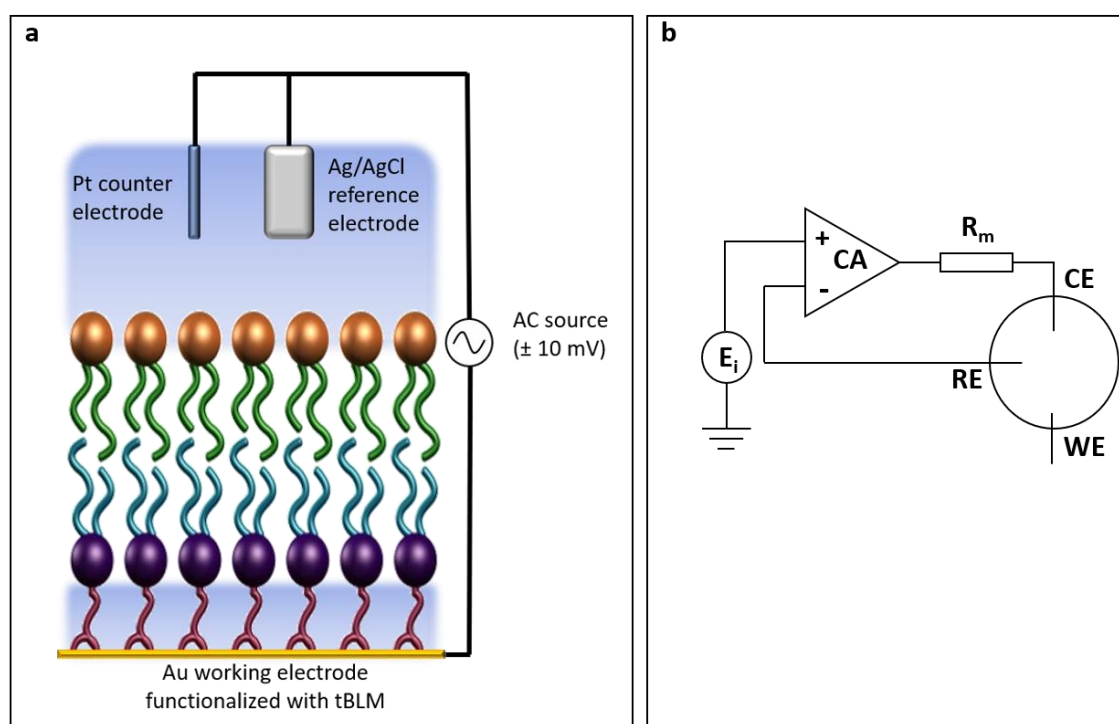


Figure 2.7: **a**: Schematic of the setup used for an EIS measurement of a tBLM. The working electrode is the surface upon which the tBLM is assembled (typically gold). The counter electrode (typically platinum due to its high chemical inertness) and the reference electrode (usually Ag/AgCl) are placed in the bathing solution above the lipid membrane such that the potential from the source is applied across the lipid bilayer. **b**: schematic of the potentiostat used for EIS measurements including the isolating amplifier (**CA**) that isolates the measurement cell from the supply and ensures that no current is drawn through the reference electrode (**RE**). The output current (through the counter electrode, **CE**, is measured as a voltage through a resistor (**R_m**). The bias voltage is applied between the reference electrode and the working electrode (**WE**).

Impedance is the analogue of electrical resistance in a direct current (DC) system when the applied potential is sinusoidal instead of constant. If only resistive elements were present and no charging or discharging of membrane components took place, the resistance of the bilayer to charge transport would be independent of the applied frequency and thus be constant. However, a lipid bilayer is comprised of resistive as well as capacitive elements.

If there are capacitors in an AC circuit, the change in current resulting from a change in the applied signal will be delayed. In a DC system, a capacitor will simply be charged to its maximum charge and then remain in this state until discharged. The resistance of the capacitor increases proportionally to the accumulated charge. If a sinusoidal alternating signal is applied, the capacitor is continually charged and discharged as the polarity switches and consequently also impedes current flow in the circuit.

Electrical impedance has two components: the real resistance (ohmic resistance impeding charge transport) of the resistive elements in the circuit and the imaginary resistance (causing a delayed shift in the magnitude of the current in response to voltage changes) caused by the capacitive elements:

$$\mathbf{Z = R + jX} \qquad \mathbf{(2.9)}$$

Where R is the real part of the impedance and X is the admittance, or the imaginary part of the impedance contributed by the capacitors in the circuit and $j = \sqrt{-1}$. The point on the complex plane corresponding to the vector sum can be expressed in its rectangular form: $Z = x + jy$ where x is the real component of the impedance and y is the imaginary component of the impedance caused by the capacitive elements in the circuit (see Figure 2.8). In electric circuits j is used instead of *i* for imaginary numbers to avoid confusion as *i* is also the symbol for electric current.

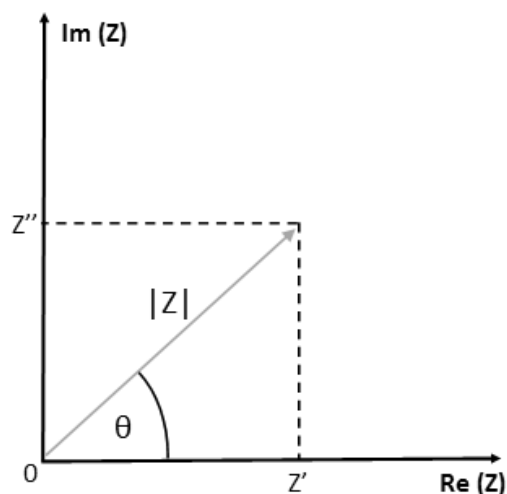


Figure 2.8: Impedance is the vector sum of the real and imaginary components. The y-axis plots the imaginary impedance caused by capacitive elements and the x-axis plots the real impedance caused by resistive elements of the circuit. The Phase angle θ is the delay between maximum current and maximum voltage

Instead of an ideal capacitor (C), a constant phase element (CPE) is often used to approximate lipid bilayers as an infinite series of non-ideal capacitors. A CPE has an additional factor associated with it (n or P), approximating its deviation from an ideal capacitor where $n=1$ describes a purely capacitive element and $n=0$ describes a purely resistive element. High quality lipid bilayers generally have n values above 0.95.[20]

The response of a capacitor to an AC signal is known as the capacitive reactance, X_c :

$$X_c = \frac{1}{2\pi f C} \quad (2.10)$$

Where f is the frequency of the applied signal and C is the capacitance of the circuit element. Examination of this relationship immediately shows that an increase of frequency at constant capacitance will lower the overall value of X_c such that at high frequencies, X_c is small and increases at low frequencies.

The potential that is applied to the cell as a function of time can be expressed as $E_t = E_0 \sin(\omega t)$ where E_t is the cell potential at a given time and E_0 is the amplitude of the applied signal and $\omega = 2\pi f$. The resulting current of the system fluctuates in the same manner as the applied potential, but its magnitude is delayed in phase (time) by ϕ : $I_t = I_0 \sin(\omega t + \phi)$. The total impedance at time t can then be expressed in a time-dependent form of Ohm's law:

$$Z = \frac{E_t}{I_t} = \frac{E_0 \sin(\omega t)}{I_0 \sin(\omega t + \phi)} \quad (2.11)$$

The impedance of a capacitor is proportional to the charge it has accumulated. The capacitor charges until the direction of the applied potential is switched, at which point it discharges and then begins charging again. At high frequencies, only a small amount of charge can accumulate in the capacitor before it is once again discharged. Therefore, its resistance is low. The lower the frequency, the longer the charging interval and thus the higher the measured resistance of the capacitor will be.

The resistance of (or conversely, conductance across) the membrane describes all “leaking” pathways, water-filled membrane defects, that allow charged species to cross the non-polar membrane interior.[1] While a detailed description of conduction mechanisms of ions across the membrane may not be available, the system can be reasonably described by an idealized approximation. Not every pathway for an ion across the membrane can be separately modelled, but all conduction across the membrane can be approximated by a single resistor. Similarly, all capacitive elements of the membrane may be approximated as either a single ideal capacitor or a constant phase element (CPE). In most cases a CPE is used instead of a single ideal capacitor to describe the imperfect nature of the membrane in terms of its ability to act as a capacitor. In an ideal system, the phase angle (of the current lag relative to the potential change) would be exactly 90° whereas in real systems a phase angle above 85° is acceptable.

In a system like a lipid bilayer, especially one designed as the basis for an electrochemical biosensor, resistance – or the degree to which the bilayer prevents the movement of electrical charges – is a key indicator of the quality of the bilayer – the higher the resistance, the fewer membrane defects there are. The lower the background current that can leak across the membrane, the smaller the detectable changes in membrane resistance and consequently the higher the sensitivity of the model to subtle changes affecting its conductivity.

The resistance and phase difference between voltage and current changes can be fitted to a equivalent circuit describing the membrane (shown in Figure 2.10) and are indicative of the quality of a lipid bilayer.[1, 20] EIS can also be used to observe charge transport across the membrane by incorporated proteins, ion channels or peptides.[18, 21] The typical resistance of a good tBLM is around $10\text{-}100\text{ M}\Omega\cdot\text{cm}^2$ and their capacitance should be around $0.5\text{-}1\text{ }\mu\text{F}\cdot\text{cm}^{-2}$. [22, 23]

2.2.2 Fitting and interpretation of EIS data

To interpret the experimental data *ZView2* (produced by Scribner Associates) was used (other software packages such as *NOVA* are also available). A theoretical circuit is created comprising different elements of the lipid bilayer and a Bode Plot (example shown in Figure 2.9) is generated to fit the experimental data as closely as possible.

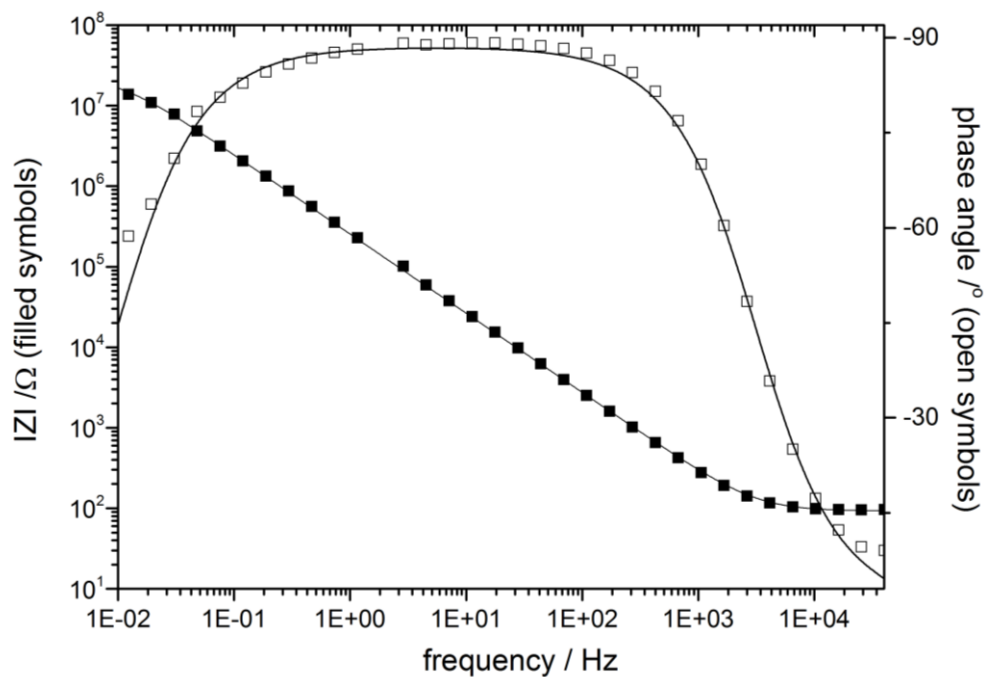


Figure 2.9: A typical Bode plot in which the absolute impedance (the vector sum of the real and imaginary resistance) is plotted against the frequency alongside the phase angle. Symbols represent experimental data and the fitted data is represented by a line.

If the experimental data and theoretically generated fit are in close agreement, the theoretical circuit is a good approximation of the lipid bilayer in terms of its electric properties. Numerous methods to modelling impedance data of model membranes have been developed. Some approaches treat lipid bilayers as perfect insulators with infinite resistance, choosing instead to model the bilayer defects with a certain resistance. Other approaches use highly detailed models that include elements for both leaflets of the lipid bilayer (including separate elements for the head and tail groups of the lipids) and also account for defect size, distribution and density.[1]

When a large number of membrane defects are present, a complex model accounting for membrane defects is useful as it can more accurately fit experimental data. However, these methods require assumptions to be made about the diameter and distribution of the defects. Allowances can be made for the size, distribution and mobility of the pores when fitting the data, and these assumptions can be reasonably made if the membrane contains well-defined pores, for example proteins.

However, when the formation of membrane defects is caused *via* the addition of drugs or nanoparticles (as is the case in the work reported in this thesis), it is unlikely that well-defined pores or defects are created, nor will they be evenly distributed and transport ions in a predictable manner.

Furthermore, before they are damaged *via* the addition of drugs or nanoparticles, the membranes used here contain very few defects such that a single resistor is sufficient to account for leakage pathways across the membrane and single capacitor can account for the accumulation of ions at the interfaces between the membrane and its surroundings. Figure 2.10 shows a schematic representation of a tBLM with the corresponding circuit elements used to the different components of the system.

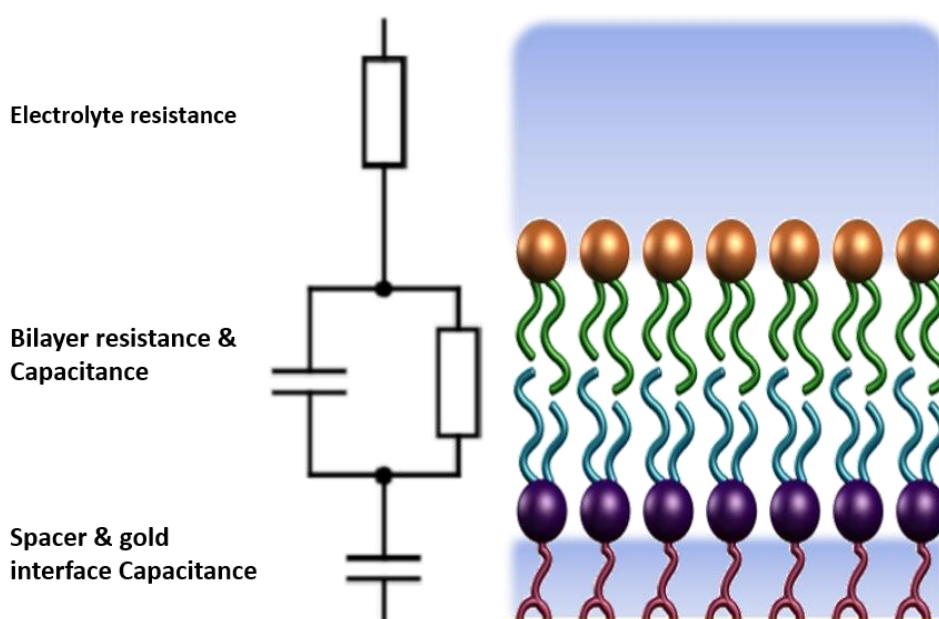


Figure 2.10: Schematic of a typical tBLM (right) and an example of a typical equivalent circuit modelling the resulting impedance data (left).

In addition to the circuit shown in Figure 2.10, two other equivalent circuits (shown in Figure 2.11) were used to fit EIS data. The most commonly used equivalent circuits used to fit high-quality tethered membranes are circuits 1 and 2 [7, 14, 24, 25]. In all circuits, R1 represents the resistance of the electrolyte which depends only on the composition and concentration of conductive species in the bathing solution (typically 100 mM NaCl, CaCl₂ or KCl).

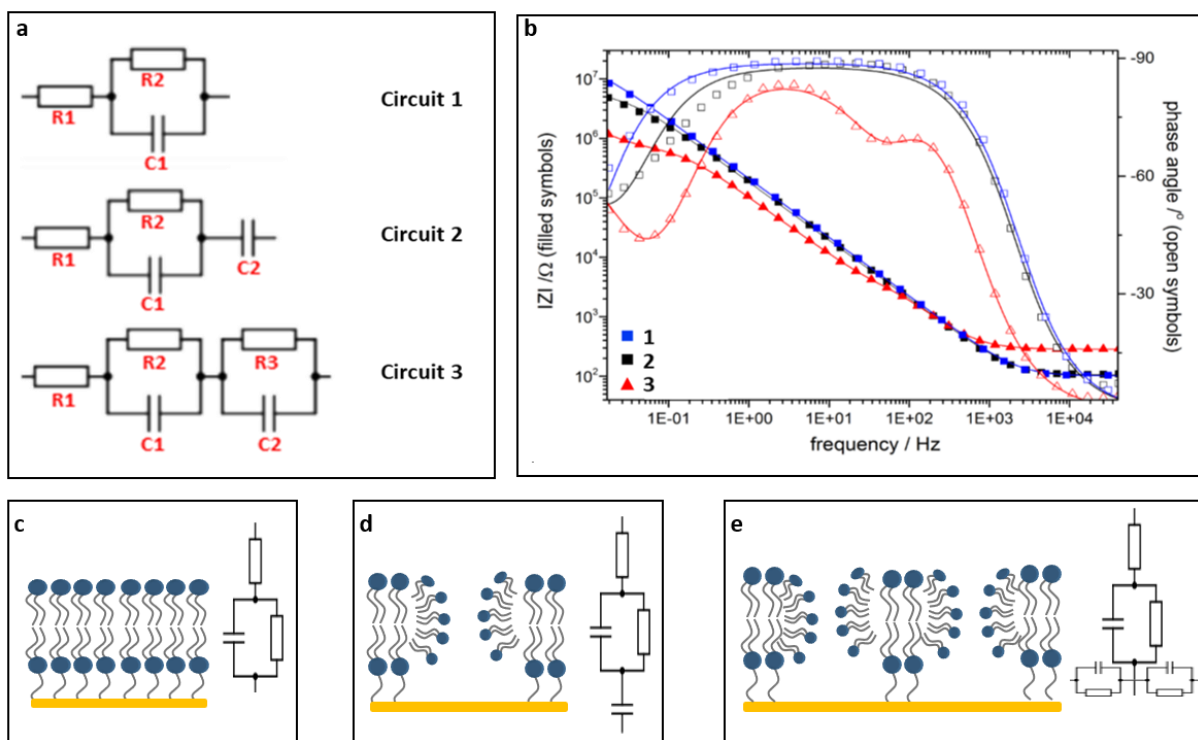


Figure 2.11: Electrical circuits used to fit EIS data (a) and examples of data fitted with each circuit (b). R1 represents the electrolyte resistance and C1 and R2 the membrane capacitance and resistance, respectively, in all circuits. Circuit 1 is used to fit data such as data set 1 on the right for a high-quality undamaged membrane (shown in c). In circuit 2, C2 represents the capacitance of the interface between the spacer and the gold substrate (used to fit data set 2) which is the case when a small number of defects are present (shown in d) and in circuit 3 (used to fit data set 3), R3 and C2 represent the combined capacitance and resistance of the spacer segment of the membrane when a significant amount of defects are present, allowing a large number of ions to populate the sub-membrane space such that lateral diffusion of the ions underneath the membrane is possible in addition of ion transport through the membrane (shown in e). Capacitors can be replaced by constant phase elements if the phase angle is not -90° , for example in the case of data set 3.

The remaining circuit elements are components of the lipid bilayer and the interface between the sub-membrane space and the gold support. A complete, undamaged lipid bilayer is generally modelled using circuit 1. If sufficient ions can be transported across the membrane to populate the sub-membrane domain, a second capacitor or constant phase element was added (C2 in circuit 2, used to fit data set 2 for example) to fit the data. If the phase delay caused by the capacitive element is less than 90° , the capacitor is replaced with a constant phase element (CPE). A constant phase element approximates an imperfect capacitor that allows some charge leakage, resulting from an inhomogeneous distribution of membrane composition. This is often the case when the membrane is damaged. A CPE contributes to the impedance of a circuit in a way that is similar to but not the same as a capacitor.

The admittance ($1/|Z|$) of a CPE can be calculated using equation 2.12:

$$Y_{CPE} = Q(j\omega)^\alpha \quad 2.12$$

Where $j = \sqrt{-1}$ as defined previously, Q is the capacitance of the CPE, ω is the angular frequency and α is a factor modifying the capacitance of the CPE. Generally, α is between -1 and 1. If $\alpha = -1$, the CPE acts as a perfect inductor. If α is 0, it acts as a resistor and if $\alpha = 1$, it acts like a capacitor.[26] Normally, α will lie somewhere between these two extremes and is therefore useful to approximate an infinite distribution of imperfect capacitors, as is the case for damaged membranes.

Some lateral mobility of ions along the gold interface below the membrane also exists in addition to the build-up of a Helmholtz double layer between the lipid membrane and the gold support.[1] Ions can be located near the ethylene glycol segment of the spacer, closer to the lipid membrane or closer to the gold substrate, depending on the hydration of the sub-membrane domain and the number of ions able to cross the lipid membrane. As it is unrealistic to attempt to draw a circuit diagram accounting for the vast number of possible charge transport and charging events that take place, a CPE is well-suited to approximate the sub-membrane domain. The CPE accounting for the population of the spacer with ions and the Helmholtz double layer can be seen even in undamaged lipid membranes if membrane resistance is below $10 \text{ M}\Omega\cdot\text{cm}^2$. [13] If pore proteins are incorporated into the membrane, or the bilayer is severely damaged and there is a further increase of ion transport across the lipid membrane (such as in data set 3), a resistive element is also added to the spacer (R_3 in circuit 3) where the sub-membrane space is populated with sufficient ions to observe ion movement in addition to charging and discharging along the spacer segment that is distinct from the Helmholtz layer at the gold/spacer interface (**e** in Figure 2.11).

ZView 2 calculates the errors of the fit by giving the range of values that can be used for each parameter without decreasing the quality of the fit. The quality of the fit is optimised by minimising the difference between the fit and the experimental data. For example, if the fit is equally good whether the resistance of the membrane is fitted as $10 \text{ M}\Omega$ or $5 \text{ M}\Omega$, the membrane resistance is reported as $7.5 \pm 2.5 \text{ M}\Omega \text{ cm}^2$.

2.3 Experimental protocols

This section describes the procedures followed for sample preparation, impedance measurements and the protocol for neutron scattering experiments. Chemicals were acquired from Sigma Aldrich or Avanti Polar Lipids and used without further purification. All electrolytes and buffers were prepared using MilliQ grade water. Unless otherwise stated, electrolyte concentrations are 100 mM . All EIS experiments were carried out at 25°C .

2.3.1 Substrate preparation

This section was published in: Biomimetic membranes in Comprehensive Nanoscience and Nanotechnology, Second Edition, Academic Press 2019[27]

A very low substrate roughness is crucial for the formation of high quality tBLMs, ideally below 1 nm.[28, 29] Normally a metallic surface is used to enable electrochemical methods such as EIS or current-voltage measurements. A metallic surface is also required for SPR measurements and suitable for neutron scattering studies. Due to its stability, gold is the most frequently used supporting material. Using the same supporting material also means that the tethering chemistry can be the same, such that the membrane architecture does not have to be altered for different experimental methods. Substrates can be prepared *via* two methods: by directly sputter coating or evaporating gold onto an ultra-flat surface or using the template-stripping procedure.

Typically, substrates for applications that require large surface areas are prepared by evaporating gold onto a polished silicon wafer, as the substrates for neutron scattering tend to require surface areas of at least 75 cm² compared to the samples for EIS or SPR experiments which only require 1-4 cm². When preparing substrates *via* sputter coating onto silicon or glass substrates, an adhesion layer is required due to the crystal lattice mismatch between gold and silicon which results in poor adhesion. The most commonly used materials for the adhesion layer are chromium or titanium. A typical sample prepared for neutron scattering is coated with 5 nm chromium followed by around 15 nm gold. Sputtering rates should be low, ideally no more than 2-3 Å/s if possible, to obtain the lowest possible surface roughness. A dual target sputter coater should be used for this process as exposure of the chromium layer to oxygen leads to immediate oxidation. This results in poorer adhesion of the gold layer and becomes a complicating factor during the neutron data analysis, as this extra layer has to be accounted for during the fitting process.

The sputter coating process tends to result in a higher surface roughness than template stripping, thus making the substrates less ideal for electrochemical measurements as they are highly sensitive to surface defects, where even a small number of defects that allow for ion travel across the membrane would compromise the resistance of the tBLM. Neutron scattering on the other hand is much less sensitive to small defects as the signal is collected over a much larger surface area, and a small number of defects is not usually visible.

To obtain substrates with the lowest possible surface roughness, the template-stripping procedure has been developed.[29] Compared to thermally evaporated gold surfaces, template-stripping produces surfaces with significantly lower roughness, reducing the peak-to-valley distance from around 7-8 nm in thermally evaporated surfaces to at most 2 nm. A schematic outline of the process is shown in Figure 2.12.

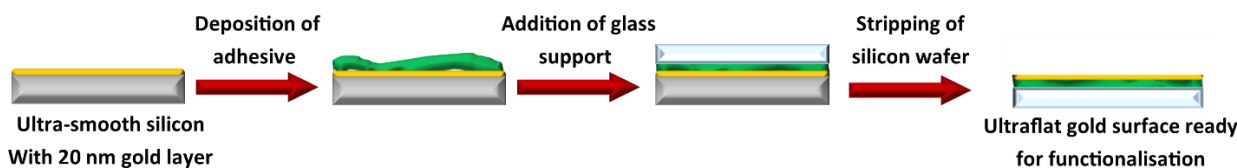


Figure 2.12: Schematic outline of the template stripping procedure

Prior to the deposition of gold, the silicon slide is cleaned by immersion into a basic piranha solution (typically a mixture of 1:1:5 $\text{H}_2\text{O}_2/\text{NH}_4^+/\text{H}_2\text{O}$) at 80 degrees for one hour. Afterwards, the gold is evaporated onto the slide. Control of the rate of evaporation is critical – the first 5 nm should be evaporated at a rate of 0.5-1 $\text{\AA}/\text{s}$ to obtain the best possible surface coverage. The rate can subsequently be increased to 5 $\text{\AA}/\text{s}$ for the remaining 10 nm.

As the gold surface of interest is now protected by the silicon slide and the sample can be handled without reducing the quality of the gold surface. Particular care should be taken when choosing the adhesive compound used to fix the glass support on the gold surface. Ideally, the glue when fully hardened should match the refractive index of glass to simplify SPR experiments. The glue should also be resistant to the solvent in which the tethering layer is deposited (generally ethanol). Suitable epoxy resins for the template stripping process are for example Epo-tek 377 and Epo-tek 301-2. Common microscopy slides are suitable to be used as glass supports, as their inherent surface roughness is compensated for by the glue.

Another important consideration when preparing the adhesive to attach the glass support is that there should be no pockets of air on the surface, as a small air bubble on the gold will result in a surface defect when “stripping” the silicon support. If lipid bilayers of poor quality are repeatedly formed on the prepared surface, it is possible that defects not visible to the eye resulting from microscopic air bubbles trapped in the glue are present on the surface.

To remove air, the glue should be gently warmed and placed under vacuum for 60 minutes until no visible pockets of air remain. Gently heating the substrate while depositing the glue (to no more than 40°C) aids the spreading of the glue and the removal of any remaining pockets of air trapped underneath the glass support. Excessive heating of the glue during these two steps could result in premature curing of the epoxide. In addition to preparing small surfaces, the template stripping method can also be used to deposit various patterns of electrodes on a surface, making this methodology suitable for the preparation of substrates for microfluidic applications and biosensing devices.[29]

After the surface is prepared, the assembly of a tBLM proceeds purely *via* self-assembly. First, the substrate is functionalised with the anchorlipid. Typically, the anchorlipid is dissolved in ethanol at 0.2 mg/mL and the substrate inserted into the solution for 18-24 hours, after which monolayer formation is complete.[30, 31] The proximal leaflet is then added either *via* vesicle fusion or another method known as rapid solvent exchange, or solvent-assisted bilayer formation.

2.3.2 Bilayer formation

Vesicle fusion can take place on a hydrophilic surface, as is the case in solid-supported lipid bilayers, where the vesicles will fuse into a lipid bilayer. It can also occur on a hydrophobic substrate, where vesicles will rupture and fuse into a lipid monolayer on the anchorlipid-SAM that was assembled previously. The vesicle fusion process typically requires around 12 hours to complete.[30] Vesicles are added to the solution (either NaCl, CaCl₂ or a buffer) at a concentration of 10 µg/mL.

In solvent-assisted bilayer formation (SALB), or rapid solvent exchange, a lipid is dissolved in ethanol (typically at a lipid concentration of 5-10 mg/mL) and incubated with the pre-formed SAM for 10-20 minutes.[31, 32] During this process, the dissolved lipids are thought to arrange themselves into an outer membrane leaflet at the interface between the SAM and the solvent. The organic solvent is then rapidly displaced by water, causing the pre-assembled lipids to “precipitate” out of solution into a lipid bilayer, while any lipids not associated with the surface are washed away. SALB is a faster method of assembling a lipid bilayer. However, as it typically requires 5-10 mg/mL of phospholipid for bilayer formation, it is also a more expensive procedure than vesicle fusion, which requires much smaller quantities of lipid for bilayer formation

2.4 References

1. Valincius, G., T. Meskauskas, and F. Ivanauskas, *Electrochemical Impedance Spectroscopy of Tethered Bilayer Membranes*. Langmuir, 2012. **28**(1): p. 977-990.
2. Goreham, R.V., et al., *Interaction of silver nanoparticles with tethered bilayer lipid membranes*. Langmuir, 2015.
3. Jackson, A.J., *Introduction to Small-Angle Neutron Scattering and Neutron Reflectometry*. NIST Center for Neutron Research, Gaithersburg, 2008: p. 12.
4. Knobloch, J.J., et al., *Oxidative Damage to Biomimetic Membrane Systems: In Situ Fe(II)/Ascorbate Initiated Oxidation and Incorporation of Synthetic Oxidized Phospholipids*. Langmuir, 2015. **31**(46): p. 12679-12687.
5. Clifton, L.A., et al., *An Accurate In Vitro Model of the E. coli Envelope*. Angewandte Chemie International Edition, 2015: p. n/a-n/a.
6. Koenig, B.W., et al., *Neutron Reflectivity and Atomic Force Microscopy Studies of a Lipid Bilayer in Water Adsorbed to the Surface of a Silicon Single Crystal*. Langmuir, 1996. **12**(5): p. 1343-1350.
7. Andersson, J., *New Tether Structures of tethered bilayer lipid membranes*, in *Chemical and Physical Sciences*. 2013, Flinders University: Adelaide, Australia.
8. James, M., et al., *The multipurpose time-of-flight neutron reflectometer "Platypus" at Australia's OPAL reactor*. Nuclear Instruments and Methods in Physics Research Section A: Accelerators, Spectrometers, Detectors and Associated Equipment, 2011. **632**(1): p. 112-123.
9. Kienzle, P., *Neutron activation and scattering calculator*. 2016, National Institute of Standards and Technology.
10. Yepuri, N.R., et al., *Stereoselective synthesis of perdeuterated phytanic acid, its phospholipid derivatives and their formation into lipid model membranes for neutron reflectivity studies*. Chemistry and Physics of Lipids, 2014. **183**(0): p. 22-33.
11. Heavens, O.S., *Optical properties of thin solid films*. 1991: Courier Corporation.
12. Nelson, A., *Co-refinement of multiple-contrast neutron/X-ray reflectivity data using MOTOFIT*. Journal of Applied Crystallography, 2006. **39**: p. 273-276.
13. Andersson, J., et al., *Synthesis and Characterisation of novel anchorlipids for tethered bilayer lipid membranes*. Langmuir, 2017.
14. Junghans, A. and I. Koper, *Structural Analysis of Tethered Bilayer Lipid Membranes*. Langmuir, 2010. **26**(13): p. 11035-11040.
15. Press, W.H., et al., *Numerical recipes 3rd edition: The art of scientific computing*. 2007: Cambridge university press.
16. Shekhar, P., et al., *Continuous distribution model for the investigation of complex molecular architectures near interfaces with scattering techniques*. Journal of Applied Physics, 2011. **110**(10): p. 102216-102216-12.
17. Evgenij Barsoukov, R.M., *Impedance Spectroscopy Theory, Experiment, and Applications*. 2005, United States: Wiley & Sons.
18. Vockenroth, I.K., et al., *Incorporation of alpha-hemolysin in different tethered bilayer lipid membrane architectures*. Langmuir, 2008. **24**(2): p. 496-502.
19. Valincius, G., et al., *Soluble Amyloid beta-Oligomers Affect Dielectric Membrane Properties by Bilayer Insertion and Domain Formation: Implications for Cell Toxicity*. Biophysical Journal, 2008. **95**(10): p. 4845-4861.
20. Vockenroth, I.K., et al., *Stable insulating tethered bilayer lipid membranes*. Biointerphases, 2008. **3**(2): p. FA68-FA73.
21. Zieleniecki, J.L., et al., *Cell-Free Synthesis of a Functional Membrane Transporter into a Tethered Bilayer Lipid Membrane*. Langmuir, 2016. **32**(10): p. 2445-2449.
22. Atanasov, V., et al., *A molecular toolkit for highly insulating tethered bilayer lipid membranes on various substrates*. Bioconjugate Chemistry, 2006. **17**(3): p. 631-637.
23. Koper, I., *Insulating tethered bilayer lipid membranes to study membrane proteins*. Molecular Biosystems, 2007. **3**(10): p. 651-657.
24. Andersson, J., et al., *A tethered bilayer lipid membrane that mimics microbial membranes*. Physical Chemistry Chemical Physics, 2018.
25. Giess, F., et al., *The Protein-Tethered Lipid Bilayer: A Novel Mimic of the Biological*

- Membrane*. Biophysical Journal, 2004. **87**(5): p. 3213-3220.
26. Zoltowski, P., *On the electrical capacitance of interfaces exhibiting constant phase element behaviour*. Journal of Electroanalytical Chemistry, 1998. **443**(1): p. 149-154.
 27. *Comprehensive Nanoscience and Nanotechnology* 2ed. 2019: Academic Press.
 28. Naumann, R., et al., *Tethered lipid bilayers on ultraflat gold surfaces*. Langmuir, 2003. **19**(13): p. 5435-5443.
 29. Vogel, N., J. Zieleniecki, and I. Köper, *As flat as it gets: ultrasmooth surfaces from template-stripping procedures*. Nanoscale, 2012. **4**(13): p. 3820-3832.
 30. Vockenroth, I.K., et al., *Formation of tethered bilayer lipid membranes probed by various surface sensitive techniques*. Biointerphases, 2009. **4**(2): p. 19-26.
 31. Andersson, J., et al., *Synthesis and Characterization of Novel Anchorlipids for Tethered Bilayer Lipid Membranes*. Langmuir, 2017. **33**(18): p. 4444-4451.
 32. McGillivray, D.J., et al., *Molecular-scale structural and functional characterization of sparsely tethered bilayer lipid membranes*. Biointerphases, 2007. **2**(1): p. 21-33.
 33. Lipids, A.P. *Phase Transition Temperatures for Glycerophospholipids*. Available from: <https://avantilipids.com/tech-support/physical-properties/phase-transition-temps/>.
 34. Lipids, A.P. *16:0 PC (DPPC) | 850355*. [cited 2018 24.4.2018]; Available from: <https://avantilipids.com/product/850355/>.
 35. Marrink, S.J., J. Risselada, and A.E. Mark, *Simulation of gel phase formation and melting in lipid bilayers using a coarse grained model*. Chemistry and Physics of Lipids, 2005. **135**(2): p. 223-244.
 36. LIPIDAD. *LIPIDAT*. 2006 [cited 2018 23.4.2018]; Available from: http://www.lmsd.tcd.ie/new_lipidat/homelipidat.asp.

3 Tethered Membranes to Study Artificial Ion Channels

3.1 Introduction

The transport of molecules across the cell membrane is an essential process for cell survival and growth.[1] While small nonpolar molecules can cross the membrane with relative ease[2], there is a large energy barrier against the traversal of ions and hydrophilic molecules across the membrane. A large number of physiological processes, such as the signalling process in nerve cells, including olfactory sensing and vision[3], rely on tightly controlled ion transport *via* ion channels and ion transporters across the cellular membrane. While significant progress has been made in the study of ion channels, with a Nobel Prize being awarded in this field in 2003, ion channels are not as well-understood as globular (water soluble) proteins.[5] This is partly because the study of ion channels is significantly more challenging than the study of soluble proteins, and partly because of the extremely large structural and functional diversity of ion transporters.[6] There is a need to better understand ion transporters, as defects in transport proteins can result in health conditions such as cystic fibrosis, colour blindness and vision loss.[7, 8] It may be possible to repair damaged ion transport pathways in conditions such as cystic fibrosis, for example through the insertion of artificial ion channels into the cell membrane.

Furthermore, a range of potent antibacterial compounds such as alpha-haemolysin[9], gramicidin[10] and valinomycin[11, 12] act by causing unregulated ion exchange and cell death with the surrounding medium. [13] Thus, there is also the potential for the use of artificial ion channels in the development of new antibiotics.

Muehlberg et. al. have synthesised several crown ethers designed for selective ion transport.[14]. The backbones connecting the crown ethers to one another and the number of oxygen atoms comprising the ring significantly affect its transport ability and its selectivity towards particular ions.[14] High selectivity of an ion channel is critical, as non-specific or unregulated ion transport can cause serious damage to the cell.

Two crown ethers and two tricrown ethers with small differences in their backbone structure were synthesised by Muehlberg et al. The key difference between monomers 1 and 2 tricrowns A and B is in the backbone structure (see Figure 3.1), with monomer 2 and tricrown A containing an additional ethene linkage, resulting in a slightly larger hydrophobic section of their backbone.

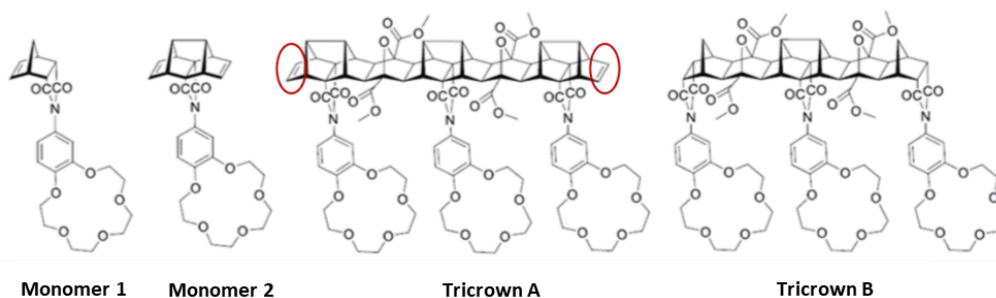


Figure 3.1: Schematic of the crown ether structures used in the ion transport studies. The key difference between monomers 1 and 2 and tricrowns A and B lies in an additional alkene group their backbone structure (highlighted in red on tricrown A).

Figure 3.2 shows a schematic of how a crown ether molecule might arrange in a lipid membrane to form an artificial ion channel and the charge transport mechanism it could facilitate.

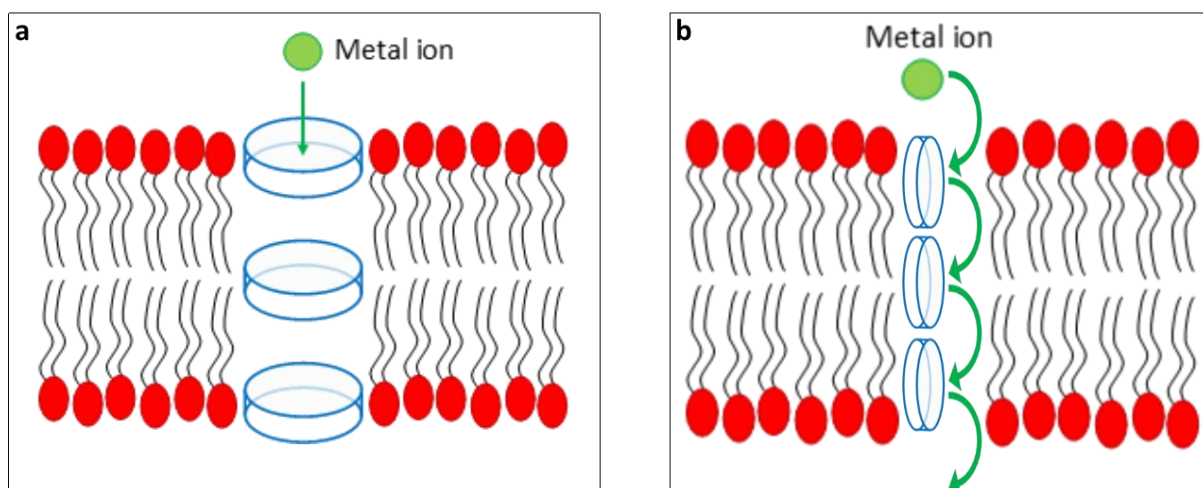


Figure 3.2: Three crown ethers (blue) stacked in a lipid bilayer forming a pore-like structure (a) that conducts ions or a scaffold (b) along which ions can ‘hop’ across the lipid membrane.[14]

The difference in their backbone structure of the tricrown compounds also forces a change in the spatial arrangements of the molecules, with the crown ether segments of tricrown A being oriented parallel to each other, while the ether segments of tricrown B are angled slightly towards each other. The structural differences may also have an impact on the orientation of the compounds in the lipid bilayer, which may affect their ion transport behaviour.

Using nuclear magnetic resonance (NMR) titration studies of potassium and sodium salts with Tricrown A and Monomers A and B, it was established that in solution, both monomers tend to form a 1:1 or 1:2 (crown/ion) complex with Na^+ . [14]

The interaction of the monomers with potassium ions could not be easily quantified, with the data fitting none of the ratios observed during sodium ion titrations. The data also was not described by a 1:3 or 1:4 binding ratio. Further NMR studies suggested a combination of 1:1, 1:2 and 2:3 complexation of crown ether and K^+ ions.[15] These results indicate a complex mechanism of interaction between the crown ethers and potassium ions, particularly because the crown ethers themselves are not large enough to accommodate a potassium ion.[14] A transient association between the crown ether also involving the carbonyl groups from the backbone has been suggested as a possible binding orientation.[14] To study the ability of the crown ethers to transport ions across a lipid bilayer, they were added to pre-formed tBLMs and studied with EIS.

3.2 Ion transport studies by EIS

3.2.1 Ion transport of tricrown ethers

The crown ethers were incorporated into pre-formed lipid bilayers by dissolving the compound in acetonitrile before addition to the bathing solution containing the membrane. Addition of small volumes (10-30 $\mu\text{L}/\text{mL}$) acetonitrile to the bathing solution covering the lipid bilayers had no effect on their electrical properties. After addition of the crown ether to the tBLM cell, the system was left to incubate overnight and rinsed with five cell volumes of electrolyte solution.

The bode plots of the lipid bilayers under NaCl and KCl electrolytes at increasing concentrations of tricrown A and tricrown B are shown in Figure 3.3.

Table 3.1 shows the change in membrane resistances under 100 mM NaCl and KCl bathing solutions after addition of the crown ethers to the lipid membrane and Table 3.2 shows the capacitance changes of the membranes. At least three experiments were carried out for each crown ether type and each change of electrolyte, and the best representative data sets were chosen to be shown here.

The membranes were rinsed with electrolyte prior to commencing EIS measurements. Therefore, any charge transport that was observed arises from crown ether compounds embedded into the membrane, as crown ethers only temporarily associated with the bilayer were been rinsed away prior to the measurements.

Table 3.1: Membrane resistances (in $M\Omega.cm^2$) of lipid bilayers with increasing concentrations of the Tricrown A and Tricrown B compounds under various 100 mM Electrolyte solutions. Errors are given as the range of values that can be fitted without decreasing the quality of the fit.

Concentration (μM)		Tricrown A	Tricrown B
	Bilayer (no CE)	2.8 ± 1.2	10.4 ± 1.2
30			
	NaCl	7.4 ± 1.1	8.6 ± 1.0
	KCl	4.7 ± 0.3	3.7 ± 0.6
60			
	NaCl	11.5 ± 0.5	6.5 ± 1.0
	KCl	1.9 ± 0.1	2.7 ± 0.4
120			
	NaCl	1.0 ± 0.1	10.3 ± 0.7
	KCl	0.4 ± 0.01	3.3 ± 0.3

Table 3.2: Capacitance data (in $\mu F.cm^2$) of lipid bilayers with increasing amounts of the Tricrown B compound under various 100 mM electrolyte solutions. Errors are given as the range of values that can be fitted without decreasing the quality of the fit.

		Tricrown A		Tricrown B	
Concentration (μM)		Bilayer	Spacer	Bilayer	Spacer
	bilayer	1.4 ± 0.4	1.8 ± 0.6	0.9 ± 0.04	0.9 ± 0.04
30					
	NaCl	1.0 ± 0.1	3.4 ± 1.1	0.9 ± 0.04	0.9 ± 0.04
	KCl	1.0 ± 0.01	3.9 ± 0.5	0.8 ± 0.05	0.8 ± 0.05
60					
	NaCl	0.8 ± 0.01	3.2 ± 0.9	1.1 ± 0.1	1.1 ± 0.1
	KCl	1.0 ± 0.02	4.4 ± 0.4	1.1 ± 0.1	1.1 ± 0.1
130					
	NaCl	1.2 ± 0.1	4.5 ± 0.6	1.0 ± 0.03	1.0 ± 0.03
	KCl	1.1 ± 0.01	4.6 ± 0.4	1.0 ± 0.04	1.0 ± 0.04

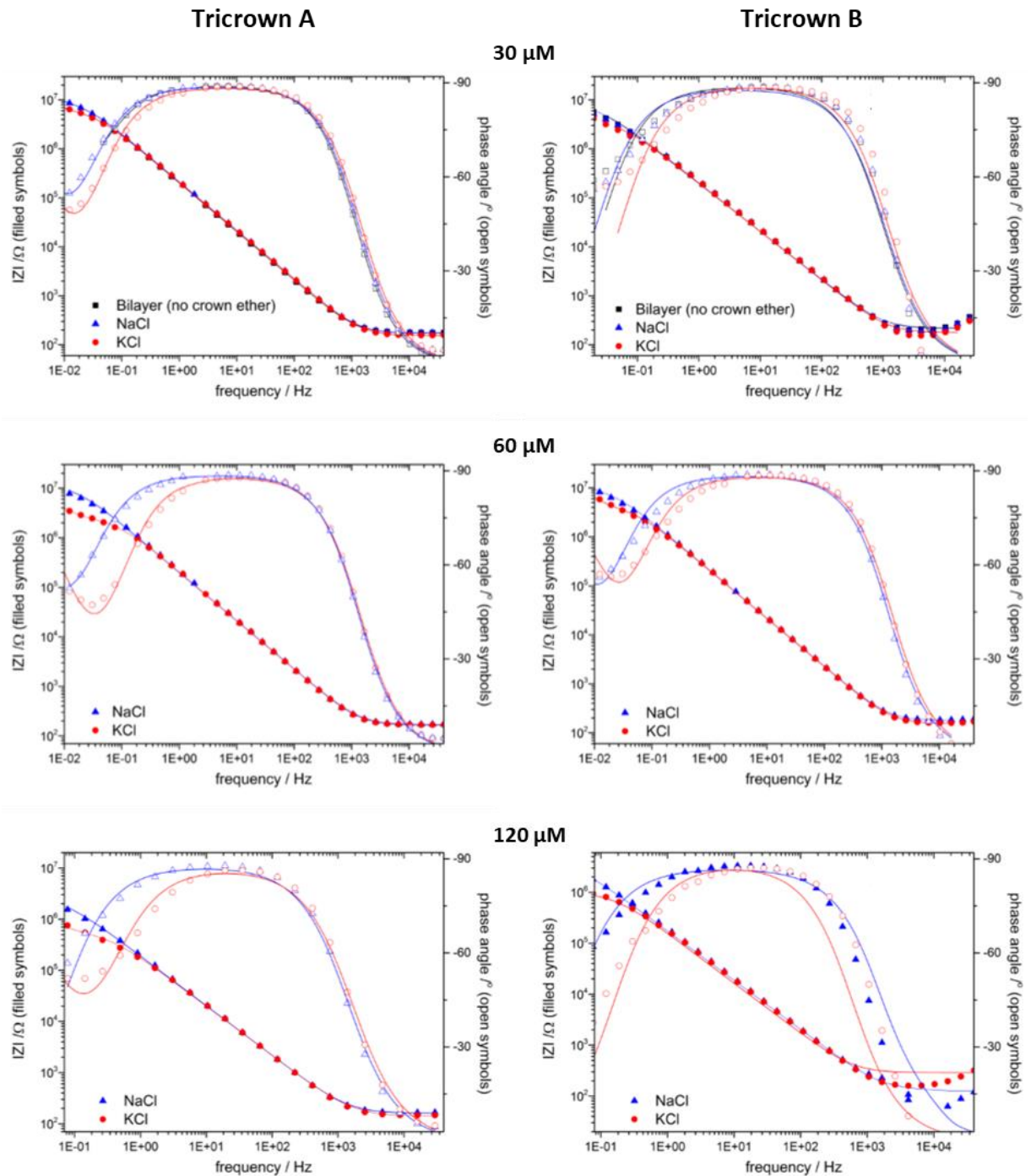


Figure 3.3: Bode plots of Lipid bilayer with increasing amounts of Tricrowns A (left) and B (right) under 100 mM NaCl (blue) and 100 mM KCl (red). Open symbols represent experimental phased data, filled symbols represent experimental impedance data and lines represent fitted data.

At crown ether concentrations of 60 μM , tricrown A selectively transported potassium across the lipid bilayer, as the membrane resistance under KCl was around one order of magnitude lower than the resistance under NaCl. The ion transport was not a result of the formation of lesions or defects in the membrane, as they would have resulted in an overall decrease of

membrane resistance rather than a reduction of membrane resistance only in the presence of KCl. Further increases in crown ether concentration to 120 μM did not result in additional ion transport. It is likely that the maximum amount of crown ether was already embedded into the membrane at a concentration of 60 μM .

There was no change in membrane capacitance with increasing amounts of crown ether or changes in electrolyte. However, there is a roughly two-fold increase in the capacitance of the spacer/gold interface, both in the presence of NaCl and KCl. This can be attributed to an increase in the number of ions binding to the spacer segment and the spacer/gold interface. It is possible that even when there was an insufficient number of crown ether molecules present in the membrane to significantly increase ion transport, some ions still travelled across the bilayer to populate the sub-membrane space.

Tricrown B had a similar slight preference for potassium transport to tricrown A, though there was no increase in spacer capacitance in this case. The overall level of ion transport facilitated by the modified crown ether structure was considerably lower than that of tricrown A, with membrane resistance being reduced by half an order of magnitude in the presence of KCl.

The apparent preference of the crown ethers to transport potassium rather than sodium in the EIS studies was unexpected as the NMR data clearly showed complexation of the crown ethers with Na^+ . Furthermore, MD simulations have shown that the crown ether is too small to accommodate the larger K^+ ion. It is possible that the association between the crown ether and sodium ions was too strong to facilitate ion transport, resulting in Na^+ ions permanently bound to the crown ether, thus not allowing sodium ions to cross the membrane. Being too large to fit inside the ring segments of the crown ether, K^+ ions may be only temporarily and weakly associated with the crown ether and can thus be transported along an electrochemical gradient by “hopping” between the rings of the crown ether (mechanism b shown in Figure 3.2).

It is unlikely that the structural changes to the crown ether backbone affect its ion selectivity, as the size of crown ether segment, which is responsible for ion binding, is not altered. However, given that only KCl was actively transported across the membrane and it cannot enter the crown ether structure, the difference in spatial arrangement of the crown ether is significant. If the K^+ ion is only transiently associated with the crown ether and the carbonyl segment of the backbone, the orientation of the crown ether groups with respect to the backbone may affect the strength and time scale of the binding event and therefore the efficiency of ion transport.

It was not possible to determine the exact location or orientation of the crown ether compounds in the lipid membrane without further experiments, for example quenching experiments with fluorescently labelled phospholipids[2], which were not carried out in this work.

3.2.2 Ion transport of crown ether monomers

Monomers 1 and 2 also differ from one another in the size of their backbone structure (see Figure 3.1). Monomer 2 contains two additional ethene linkages in its backbone that are not present in monomer 1. It is possible that this affects the membrane insertion process as well as the orientation of the crown ether molecules inside the lipid membrane, and as a result it might also affect if and how they facilitate ion transport across the membrane. To determine whether the backbone differences in the crown ether monomers influence their ability to transport ions across a tBLM, EIS studies were also carried out using monomers 1 and 2. Impedance data for monomer 1 are shown in table 3.3 and data for monomer 2 are shown in Table 3.4. Bode plots of EIS experiments after incubation with 0.5 mM of monomer 1 and 2 are shown in Figure 3.4.

Table 3.3: Electrical data of lipid bilayer with increasing concentrations of monomer 1 under various 100 mM NaCl and KCl electrolytes. Errors are given as the range of values that can be fitted without decreasing the quality of the fit.

		Bilayer		Gold/Spacer
Concentration (μM)		Impedance ($\text{M}\Omega$)	Capacitance (μF)	Capacitance (μF)
	Bilayer	2 ± 0.2	1.1 ± 0.04	3.9 ± 0.5
500				
	NaCl	3 ± 0.3	1 ± 0.05	3.8 ± 0.6
	KCl	0.1 ± 0.004	2.2 ± 0.1	6.6 ± 0.1
1000				
	NaCl	1.7 ± 0.1	1.1 ± 0.01	3.2 ± 0.3
	KCl	0.2 ± 0.006	1 ± 0.02	3.8 ± 0.1

Table 3.4: Electrical data of lipid bilayer with increasing amounts of monomer 2 under various 100 mM electrolyte solutions. Errors are given as the range of values that can be fitted without decreasing the quality of the fit.

		Bilayer	
Monomer Concentration (μM)		Impedance ($\text{M}\Omega$)	Capacitance (μF)
	Bilayer	115.5 ± 10.4	0.7 ± 0.004
125			
	NaCl	130.2 ± 75.1	0.7 ± 0.03
	KCl	58 ± 23.9	0.7 ± 0.04
250			
	NaCl	176.8 ± 320.5	0.7 ± 0.1
	KCl	26.3 ± 3.4	0.7 ± 0.02
	NaCl	172.8 ± 120.8	0.7 ± 0.04
500			
	NaCl	96.5 ± 12.4	0.7 ± 0.01
	KCl	31.6 ± 2.6	0.7 ± 0.01

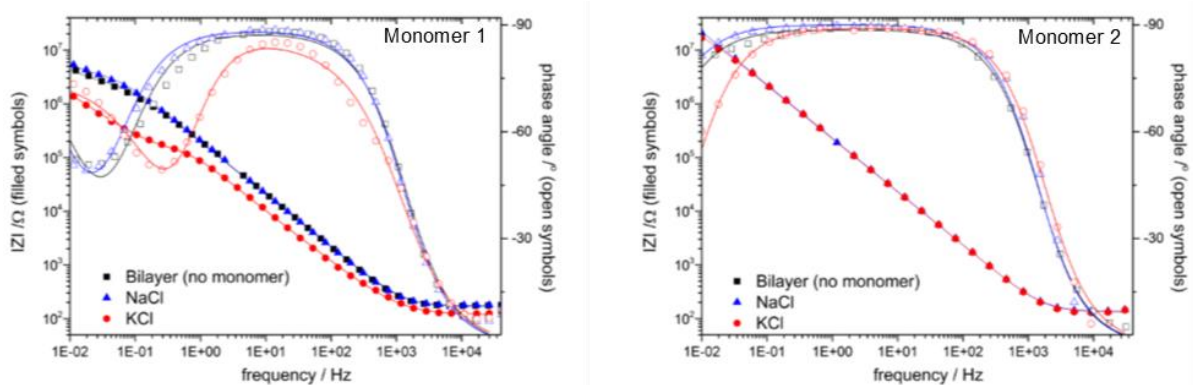


Figure 3.4: Bode plots of Lipid bilayers with 500 μM of monomer 1 (left) and monomer 2 (right) under 100 mM NaCl (blue) and KCl (red) solutions. Open symbols represent experimental phased data, filled symbols represent experimental impedance data and lines represent fitted data.

Ion transport under KCl was facilitated by monomer 1 when the membrane was incubated with 0.5 mM of the compound but did not increase when the concentration of monomer 1 was increased to 1 mM. Only minimal ion transport occurred when a tBLM was incubated with concentrations ranging from 125-500 μM of monomer 2. It is likely that the lipid bilayer was saturated with crown ether compounds after incubation with 0.5 mM crown ether solution and was therefore not able to accommodate further crown ether molecules.

Even at concentrations that were equivalent to those at which monomer 1 facilitated ion transport, no significant ion transport was facilitated by monomer 2. As the compound was available only in small quantities, the concentration could not be increased to 1000 μM .

This suggests that rather than affecting ion selectivity, the structure of the backbone affected the incorporation of the crown ether into the lipid bilayer. It is possible that the structural differences between monomers 1 and 2 affected the amount of monomer that could be incorporated into the lipid bilayer. However, as the difference was only a small increase (relative to the overall size of the molecule) in the size of the hydrophobic domain of monomer 2, it appears unlikely that the increased backbone size prevents the incorporation of the monomer 2 into the membrane. The larger backbone of monomer 2 may have prevented the aggregation of the monomers into a supramolecular assembly with the correct structure to facilitate potassium ion transport. Alternatively, the increased size of the hydrophobic segment of monomer 2 may force the monomer to remain predominantly in the hydrophobic core of the membrane, not allowing it to diffuse to the hydrophilic headgroups and bind ions in the aqueous reservoir.

Future studies should investigate whether other cations such as Li^+ or a divalent cation such as Ca^{2+} would be transported preferentially by one of the monomers. Neutron studies using deuterated versions of the crown ether molecules would be highly beneficial to determine the location of the crown ethers in the membrane.

3.3 Conclusion

While NMR studies showed that the crown ethers bind both Na^+ and K^+ ions, only potassium ions were transported across the lipid bilayer by both tricrown ether compounds, and crown ether A facilitated significantly more ion transport than tricrown B, likely as a result of the differences in the way the ions bind to the crown ether structure. The same trend was also observed in the case of the monomers, where monomer 1 was far superior to monomer 2 in transporting K^+ across the tBLM. This study has shown that tethered membranes can serve as easily accessible platforms to study ion transport of novel compounds.

3.4 References

1. Kasianowicz, J.J., *Introduction to Ion Channels and Disease*. Chemical Reviews, 2012. **112**(12): p. 6215-6217.
2. Fyles, T.M., *Synthetic ion channels in bilayer membranes*. Chemical Society Reviews, 2007. **36**(2): p. 335-347.
3. Wickman, K. and D.E. Clapham, *Ion channel regulation by G proteins*. Physiological Reviews, 1995. **75**(4): p. 865-885.
4. *The Nobel Prize in Chemistry 2003*. 2003 [cited 2018 23/03/2018]; Available from: https://www.nobelprize.org/nobel_prizes/chemistry/laureates/2003/.
5. White, S.H., *The progress of membrane protein structure determination*. Protein Science, 2004. **13**(7): p. 1948-1949.
6. Clapham, D.E., L.W. Runnels, and C. Strubing, *The trp ion channel family*. Nat Rev Neurosci, 2001. **2**(6): p. 387-396.
7. DiFrancesco, J.C. and D. DiFrancesco, *Dysfunctional HCN ion channels in neurological diseases*. Frontiers in Cellular Neuroscience, 2015. **9**: p. 10.
8. Kohl, S., et al., *Total colourblindness is caused by mutations in the gene encoding the α -subunit of the cone photoreceptor cGMP-gated cation channel*. Nature genetics, 1998. **19**(3): p. 257-259.
9. Vockenroth, I.K., et al., *Incorporation of alpha-hemolysin in different tethered bilayer lipid membrane architectures*. Langmuir, 2008. **24**(2): p. 496-502.
10. Kozuch, J., et al., *Combined Electrochemistry and Surface-Enhanced Infrared Absorption Spectroscopy of Gramicidin A Incorporated into Tethered Bilayer Lipid Membranes*. Angewandte Chemie International Edition, 2012. **51**(32): p. 8114-8117.
11. Becucci, L., et al., *Potassium ion transport by valinomycin across a Hg-supported lipid bilayer*. Journal of the American Chemical Society, 2005. **127**(38): p. 13316-13323.
12. Pinkerton, M., L. Steinrauf, and P. Dawkins, *The molecular structure and some transport properties of valinomycin*. Biochemical and biophysical research communications, 1969. **35**(4): p. 512-518.
13. Gilbert, R.J.C., *Pore-forming toxins*. Cellular and Molecular Life Sciences CMLS, 2002. **59**(5): p. 832-844.
14. Muehlberg, E.K., *The Modular Synthesis of Rigid Rod-like Scaffolds Towards Artificial Ion Channels*, in *Department of Physical and Chemical Sciences*. 2015, Flinders University: Adelaide, Australia. p. 221
15. Pelt, B.V., *Investigating Uncharacteristic Complexation of Alkali Metal Cations by Crown Ether Compounds*, in *College of Science and Engineering*. 2016, Flinders University: Adelaide, South Australia. p. 46.

4 New Membrane Architectures for Tethered Bilayer Lipid Membranes

This chapter has been published as:

Synthesis and Characterization of Novel Anchorlipids for Tethered Bilayer Lipid Membranes, Jakob Andersson, Jacqueline J. Knobloch, Michael V. Perkins, Stephen A. Holt, and Ingo Köper, *Langmuir* 2017 33 (18), 4444-4451.

Abstract

Tethered bilayer lipid membranes are versatile solid supported model membrane systems. Core to these systems is an anchorlipid that covalently links a lipid bilayer to a support. The molecular structure of these lipids can have a significant impact on the properties of the resulting bilayer.

Here, the synthesis of anchorlipids containing ester groups in the tethering part is described. The lipids are used to form bilayer membranes, and the resulting structures are compared with membranes formed using conventional anchorlipids or sparsely tethered membranes. All membranes showed good electrical sealing properties; the disulphide-terminated anchorlipids could be used in a sparsely tethered system without significantly reducing the sealing properties of the lipid bilayers. The sparsely tethered systems also allowed for increased ion transport across the membrane, in good correlation with a higher hydration of the spacer region as seen by neutron scattering.

4.1 Introduction

Tethered bilayer lipid membranes (tBLMs) are model systems that mimic the structure and function of a biological membrane. They consist of a lipid bilayer membrane, with the inner leaflet covalently attached to a solid substrate.[1-4] tBLMs have been shown to allow for the systematic investigation of membrane related processes, such as binding of drugs to membranes, the functioning of membrane proteins and membrane-protein interactions.[3, 5] Such studies are important, since membrane proteins are involved in wide range of fundamental physiological processes such as vision,[6] smell[7] and cardiac function.[8, 9] Furthermore, malfunction of membrane proteins can cause severe diseases such as cystic fibrosis[10] or muscular dystrophy.[11] A significant proportion of pharmaceuticals therefore target membrane proteins, particularly G-protein coupled receptors.[12, 13] The cell membrane also serves as the outermost barrier of the cell against pathogens. Pathogens and toxins as well as drugs must interact with or pass through the cell membrane in order to be effective. For example, some classes of antibiotics, e.g. such as polymyxins, aim to disrupt the membrane integrity[14] and beta blockers, one of the most commonly prescribed medications for hypertension and cardiac arrhythmia, target membrane-bound receptors.[15]

To understand the fundamentals of these membrane-related processes, a detailed description of membrane structure and function is necessary. However, most cellular membranes are highly complex architectures comprising a variety of components including receptors, transport proteins, ion channels as well as various lipids and carbohydrates. This complexity significantly hinders the study of membranes and membrane processes.[16] A range of model systems have been developed in order to simplify the complex membrane structure while retaining key chemical and physical characteristics of the membrane architecture,[17, 18] particularly membrane fluidity, hydration and electrical resistance.[2]

Among these model systems, tBLMs offer a very stable platform,[19, 20] while also allowing the use of various surface analytical techniques not available to other model systems to study membrane processes. For example, the structure of the membrane can be investigated using techniques such as surface plasmon resonance,[21] atomic force microscopy and neutron reflectivity,[22, 23] while the functionality of integrated membrane proteins can be assessed using electrochemical techniques.[24-26] Additionally, the covalent anchoring of the membrane to a support increases its stability for up to a month compared to hours or at most days in other membrane systems.[1, 19, 27] tBLMs also offer ease of assembly and significant flexibility in the composition of the distal leaflet to mimic a variety of cell membranes.

A tBLM is based on a self-assembled monolayer of anchorlipids which bind the membrane to the substrate and contain a spacer region that separates the lipid bilayer from the support. The structural and functional properties of the tBLM depend on the type of lipids used, the support material and on the available space underneath the membrane. Both the 2-dimensional packing density of the lipids in the inner membrane leaflet and the density and chemical nature of the sub-membrane space influence the intrinsic properties of the bilayer and its ability to host membrane proteins.[28] tBLMs have been characterised using a variety of techniques, and especially neutron scattering has been used extensively to assess the packing density and hydrophilicity of the tether region.[23, 29]

The chemical structure of the spacer of commonly used anchorlipids is mainly based on ethylene oxide moieties (Figure 1).[21, 30] Ethylene-oxide tethered lipid bilayers have been used in a variety of studies, however the sub-membrane space is typically poorly hydrated, with hydration levels as low as 5 volume% as seen by neutron reflectivity studies.[23] Polarisation-modulation infrared reflection absorption spectroscopy studies have shown that the tetraethylene glycol tether segment adopts a helical conformation when assembled into a tBLM, exposing hydrophobic regions of the tether to the surrounding medium.[31]

The low hydration and high packing density of the anchorlipids can hinder the incorporation and function of membrane proteins.[28] Sub-membrane hydration is of significant importance when studying proteins embedded into the membrane that have larger sub-membrane domains as the sub-membrane reservoir approximates the aqueous interior of a cell. The transport of ions across the membrane and into the spacer region can also be affected by the nature of the sub-membrane domain. There have been two approaches to address this issue: changes to the tether chemistry and length, and the use of diluting molecules. However, changes in those properties can affect the structural and functional properties of the membrane. For example, it has been shown that a disulphide heterocycle-terminated anchorlipids form more electrically insulating bilayers than thiol-terminated lipids.[23] Electrically sealing bilayers are essential if ion transport across the membrane, for example due to protein function, is studied.

An increase in tether length led to an increase in the hydration of the spacer region, from around 5% in a 4-ethylene glycol system to 40% with 8 ethylene glycol units.[23] However, a simultaneous significant decrease of membrane impedance by more than two orders of magnitude was observed, indicating the formation of significant defects in the membrane. This was also supported by molecular dynamics simulations of the effects on spacer length on bilayer structure.[32] Simply lengthening the tether length significantly is therefore not the most optimal approach to increasing sub-membrane space and hydration.

Furthermore, the capacity of the aqueous reservoir for ion storage is also not optimally increased by lengthening the tether, as doubling the length of the spacer segment in tBLMs assembled on mercury droplets did not lead to proportionally increased levels of ions in the sub-membrane reservoir.[33]

The density of the spacer can also be decreased by diluting the anchorlipid forming the proximal leaflet with a second, shorter surface-active backfilling molecule such as β -mercaptoethanol (β ME)[22] or mercaptoacetic acid disulphide.[1] tBLMs with as much as 64% hydration of the sub-membrane compartment have been reported using such sparsely tethered membranes assembled on thiol-terminated anchorlipids.[22] However, the insulating properties of the membranes were reduced significantly from 0.5 M Ω to 93 k Ω in membranes formed from a solution containing 30% tethered lipid and 70% backfiller.[22] This highly hydrated system is optimal for the study of membrane properties that are not related to its electrical sealing properties, as a very fluid bilayer is created with high hydration levels,[34] suggesting the presence of significant sub-membrane space for protein incorporation.

There have been fewer studies investigating the effect of the tether chemistry on the membrane properties. The use of building blocks other than all-ether moieties such as the ethylene glycol units might lead to different structure and to different interactions with ions and water molecules.

Here, the synthesis of several new anchorlipids containing ester-based tether segments is presented. The different molecules (Figure 4.1) were used to form tBLMs and the resulting membranes have been compared with sparsely tethered membranes formed with the anchorlipid DPhyTL or DPhySL and β ME. Finally, a self-diluting anchorlipid (DPhySDL), containing two anchor groups was synthesised and characterised

All approaches resulted in electrically insulating membranes, yet the new tether chemistry did not lead to a significantly higher hydration of the submembrane space. The use of diluting molecules on disulphide-terminated anchorlipids led to a significant increase in tether hydration while still enabling the formation of highly sealing bilayers.

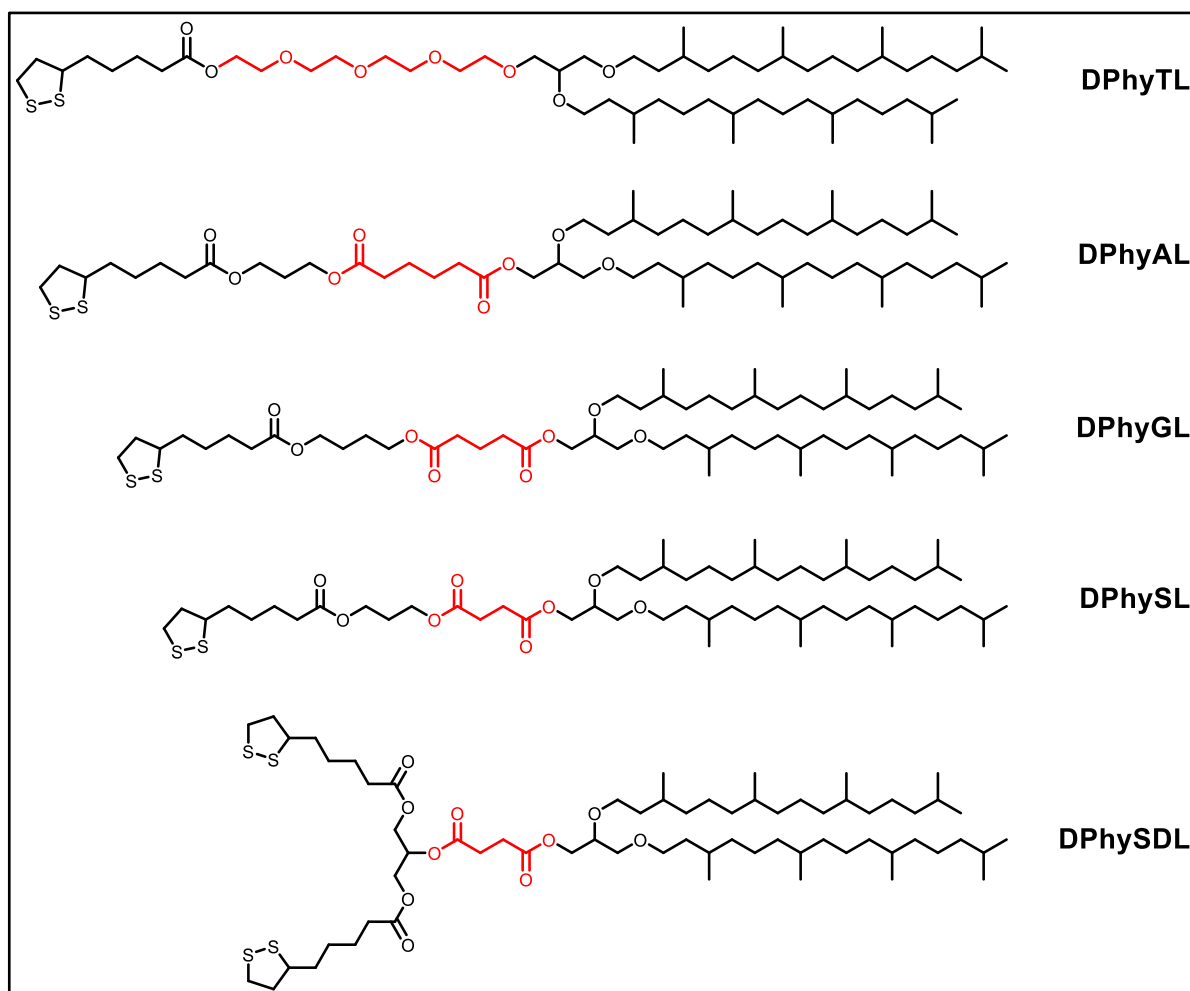


Figure 4.1: Structures of the commonly used anchorlipid DPhyTL (top)[21] and novel lipids, DPhyAL, DPhyGL and DPhySL as well as the self-diluting molecule DPhySDL. All lipids are composed of one (or two for DPhySDL) anchor groups, a spacer moiety and a lipid part. The key structural difference between DPhyTL and the new lipids is the replacement of the ethylene glycol tether segment with ester groups (highlighted in red). The number of carbon atoms in the highlighted segments of the new lipids was changed to determine the effect of this segment on bilayer formation, structure and sub-membrane hydration.

4.2 Materials and methods

Lipids were purchased from Avanti Polar lipids. All other chemicals were purchased from Sigma-Aldrich. Unless specified otherwise, all materials were used without further purification.

Bilayer formation: Template-stripped gold, (preparation described elsewhere)[21] was inserted into a solution of HPLC-grade ethanol containing 0.2 mM of the tether-lipid or a mixture of tether and spacer molecule (0.12 mM and 0.08 mM anchorlipid and spacer for 60% and 40% tether, respectively) for 16 hours, rinsed thoroughly with 100% ethanol and dried under a stream of nitrogen. Bilayers were formed via rapid solvent exchange or vesicle fusion. For the first process, the monolayer is incubated under DPhyPC in ethanol (5 mg/mL) for 15 minutes and then rinsed rapidly with 100 mM NaCl. Vesicle fusion was achieved by adding 20 μ L of vesicles generated *via* extrusion of 2 mg/mL DPhyPC in MilliQ through 50 nm filters to the monolayer under 100 mM NaCl and incubating over night at 25°C.

Ion Transport Studies: tBLMs were prepared in 100 mM NaCl solution and 5 μ L of a valinomycin solution (10 mg/mL in ethanol) was added and incubated for 2 hours. Afterwards, the membrane was rinsed with 5 mL 100 mM electrolyte solution (KCl or NaCl) prior to each measurement.

Electrochemical Impedance Spectroscopy: Measurements were performed as discussed elsewhere[29] using an Autolab PGSTAT30 impedance spectrometer. Data were recorded between 3 mHz and 100 kHz with 0V potential vs Ag/AgCl at a 10 mV AC modulation amplitude. Raw data were analysed using ZVIEW (version 3.3B by Scribner Associates) and fitted to an equivalent circuit comprising resistors and constant phase elements (see Figure 4.2 for the circuits used to fit the data and the supplementary information for further details) with final values normalised to an electrode area of 0.283 cm². All measurements were taken under 100 mM NaCl or 100 mM KCl solution. To exchange the electrolyte, the cell was rinsed with five cell volumes of the new electrolyte.

Neutron Reflectometry experimental method and data analysis: Specular neutron reflectometry (NR) measurements were carried out using the PLATYPUS time-of-flight neutron reflectometer at the 20 MW OPAL reactor (Australian Nuclear Science and Technology Research Organisation, Lucas Heights, Sydney NSW)[35]. The instrument provides cold neutrons with wavelengths ranging from 2.5 to 18Å. The reflected intensity was measured at three glancing (0.5°, 0.85° and 3.8°) under D₂O, H₂O and CM4 (a mixture of D₂O and H₂O with a combined SLD of 4) in the presence of 100 mM NaCl.

The substrates were prepared as follows: polished circular crystal Silicon discs (10 cm diameter, 1 cm thickness) were coated with 5 nm chromium followed by 15 nm gold at the South Australian node of the ANFF located at Mawson Lakes (South Australia). The tBLM was then assembled as described above. Neutron data were gathered for a total of 2h per contrast (for a total of 6h per sample).

The data was spliced together after data reduction (normalisation to direct beam and background subtraction) and fitted using the Motofit plugin for IgorPro (available at <https://sourceforge.net/projects/motofit/>). The SLD of the silicon wafer was fixed at $2.07 \times 10^6 \text{ \AA}^{-2}$ and the SLD of chromium at $3.03 \times 10^6 \text{ \AA}^{-2}$. The SLD of gold was allowed to vary between 4.3 and $4.5 \times 10^6 \text{ \AA}^{-2}$, the SLD of the tether segment was fitted between 0.5 and $2 \times 10^6 \text{ \AA}^{-2}$ and the SLD of the hydrocarbon chains was fitted between -0.4 and $0 \times 10^6 \text{ \AA}^{-2}$. The inner head groups (approximating either the glycerol segment of the anchor group or the incorporation of some DPhyPC in the lower leaflet of the membrane in the sparsely tethered systems) were fitted between 0.5 and $1.5 \times 10^6 \text{ \AA}^{-2}$. The outer head groups were fitted between 1 and $3.5 \times 10^6 \text{ \AA}^{-2}$. Error analysis was performed *via* Markov Chain Monte Carlo resampling. This method randomly fits the data 1000-2000 times to estimate the error associated with each fit.

¹H NMR spectroscopy: Measurements were carried out using a 400 or 600 MHz Bruker Avance III NMR spectrometer using CDCl₃ as a solvent. The internal lock was referenced to 7.26 ppm.

4.3 Results and discussion

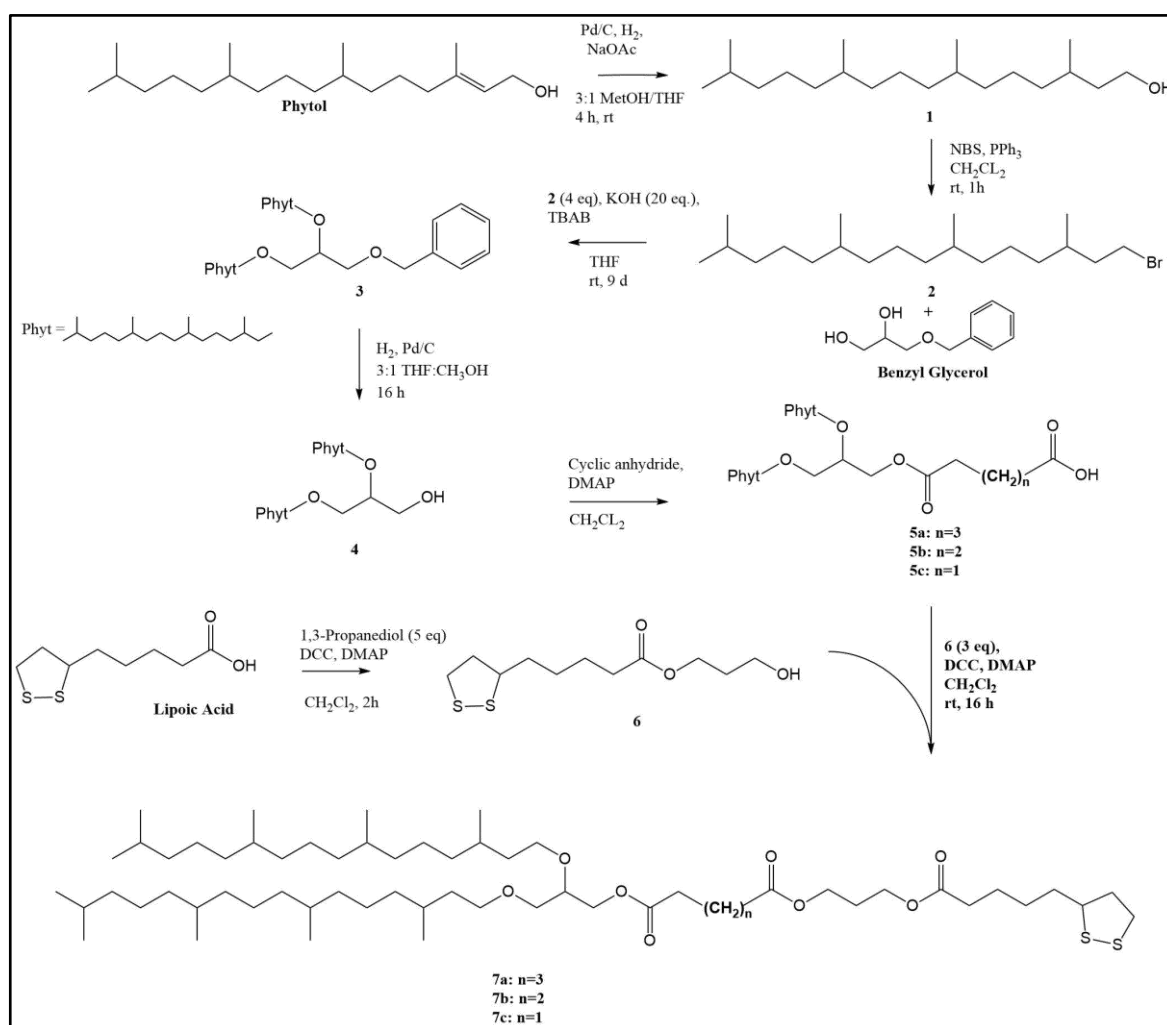
4.3.1 Synthetic approach

The synthesis of the lipids described in **section 4.3.1** was carried out in 2013 during the honours project of Jakob Andersson and has been submitted as part the following thesis:

Andersson, J., *New Tether Structures of tethered bilayer lipid membranes*, in *Chemical and Physical Sciences*. 2013, Flinders University: Adelaide, Australia.

A brief overview of the synthetic approach in a different form to that present in the thesis is presented here for the sake of completion.

Four different anchorlipids have been synthesised using a modular synthetic approach. Starting from commercially available phytol, the synthesis was achieved in 7 steps (Scheme 1 and supporting information for synthetic procedures).



Scheme 1: Synthetic Approach for the novel tether lipids DPhyAL (n=3), DPhyGL(n=2) and DPhySL(n=1). Benzyl Glycerol and Lipoic Acid were purchased from a commercial supplier.

To synthesise the saturated alkyl halide **1**, phytol was reduced *via* palladium-mediated hydrogenation. Complete reduction of the double bond occurred after 4 hours. However, there was a simultaneous loss of the hydroxyl functionality after this time, as seen by NMR analysis, probably due to the acidity of the methanol solvent. A more details analysis showed that after 1 hour, there was no significant presence of either alkene or hydroxyl functionality remaining in phytanol, indicating that the removal of the hydroxyl group (dehydration) took place independently of the reduction of the double bond. Dehydration of phytanol occurred even after the solvent was distilled over calcium hydride onto 3Å molecular sieves immediately prior to use. Loss of the hydroxyl functionality was prevented by addition of a small amount of sodium acetate to remove residual acid. It is important to note that under these conditions, permitting the reaction to proceed for more than 4 hours still led to the dehydration of phytol despite the presence of sodium acetate.

The alkyl halide **2** was synthesised in 1h *via* triphenylphosphine-mediated bromination. This approach was faster and gave better yields than bromination with CBr₄. Synthesis of the universal lipid precursor **3** was time consuming, and generally afforded poor yields of 30% or less. In addition to poor yields, a mixture of mono- and di-alkylation products was obtained. These could not be separated by column chromatography, resulting in the loss of starting reagents in subsequent reactions as both mono- and di-alkylated compounds underwent subsequent reactions but only one product was desirable. Addition of the phase transfer catalyst tetrabutylammonium bromide enabled a reasonable yield of product as well producing virtually no mono-alkylated product. Upon introduction of the ester groups in compounds **5** and onwards, buffered silica was required for column chromatography to avoid decomposition of the product.

Traditional ester synthesis was not feasible for the production of compounds **5a-5c** as the reaction would result in the formation of dimers consisting of two equivalents of compound **4** connected by dicarboxylic acid (eg. adipic acid). Cyclic anhydrides were used instead to ensure that only mono-substitution could occur, as only a cyclic anhydride would present a suitable starting material for the reaction and become unreactive once coupled with the alcohol **4**. The remainder of the synthetic procedure followed established methods for ester and anchorlipid synthesis[36] and did not present any unique challenges.

4.3.2 Membrane formation and characterisation

All new anchorlipids and mixtures of the lipids with β -ME were used to form self-assembled monolayers (SAMs). The SAMs were analysed by contact angle measurements (Table 4.1). While a pure β -ME layer was hydrophilic, all lipid containing monolayers showed hydrophobic characteristics. Even the monolayers with high content of β ME showed contact angles close to a pure lipid layer, suggesting that the ratio of β ME and anchorlipid on the surface might be different to that in solution. It is also likely that the presence of mercaptoethanol in the SAM would have been obscured by the much larger phytanyl chains and therefore not affect the measured contact angle as significantly as expected. The assembly time for all SAMs was kept constant at 24 hours. For shorter assembly times, smaller contact angles can be observed, however the resulting tBLMs typically show poor electrical properties (data not shown).

Table 4.1: Selected contact angle data of SAMs assembled from different lipids and lipid mixtures. (Average of at least 5 data sets with standard deviation shown as error)

monolayer architecture	Contact Angle ($^{\circ}$)
100% β -ME	45.7 ± 1.1
100% DPhyAL	110.2 ± 2.1
100% DPhyGL	106.2 ± 0.2
100% DPhySL	110.8 ± 2.4
40% DPhyTL, 60% β -ME	96.4 ± 1.3
60% DPhyTL, 40% β -ME	99.4 ± 1.7
80% DPhyTL, 20 % β -ME	102.8 ± 0.6
100% DPhyTL	103.8 ± 0.8
100% DPhySDL	108.7 ± 0.2

All monolayers were completed to bilayers. Bilayer formation *via* vesicle fusion was only successful for contact angles higher than 100°. For the 40% and 60% diluted DPhyTL and DPhySL systems, bilayers were formed by rapid solvent exchange instead.[22] The mechanism of lipid bilayer formation *via* vesicle fusion with a hydrophobic interface is not properly understood. However, a SAM with a contact angle of less than 100° appears to have insufficient surface energy to promote the fusion of vesicles into a continuous lipid bilayer. The resulting membranes were analysed using electrochemical impedance spectroscopy (EIS). EIS data was fitted using an equivalent circuit, where the bilayer is represented by resistor and capacitor in parallel (Figure 4.2).

All tBLMs showed high electrical sealing properties, with values similar to results reported on similar systems for fully tethered systems and higher than reported values for diluted systems.[22, 23, 37] The resistance values were in the M Ω range, while the capacitances for the non-diluted systems were below 1 μFcm^{-2} , and slightly higher for the diluted systems. While the electrical properties of the membrane are a good quality indicator, a good model system should be able to host peptides and proteins and allow for their function. This was investigated by incorporation of the ion-transporting peptide valinomycin. The peptide selectively transports potassium ions across bilayers, and its functional incorporation can be probed by exposing a valinomycin-containing tBLM to different electrolyte solutions and monitoring the electrical properties.[38] In the absence of potassium ions, a high resistance is to be expected, whereas the presence of potassium ions should result in a drop in the membrane resistance.[39]

The different tBLMs were exposed to either 100mM NaCl or 100 mM KCl solution. The latter resulted in a significant but reversible drop in the membrane resistance (Table 4.2, see supplementary information for Bode plots of all EIS data), indicating a successful incorporation of the peptide into the membrane. The difference in membrane resistance between NaCl and KCl solution is in principle proportional to the number of ions transported across the membrane. This will depend on the amount of peptide incorporated into the membrane and on the possibility to transport ions across the bilayer and into the tether region. The same amount of peptide was added to each membrane, and it can be assumed that the concentration of the peptide inside each tBLM is similar.

Table 4.2: Area normalised impedance and capacitance data for fully tethered tBLMs as a function of the electrolyte composition. Resistance values are expressed in $M\Omega\text{cm}^2$, capacitance values in μFcm^{-2} . Errors are given as the range of values that can be fitted without decreasing the quality of the fit.

	DPhyTL	DPhyAL	DPhyGL	DPhySL
Bilayer prior to valinomycin addition				
Bilayer resistance	23.0 ± 1.1	13.3 ± 1.1	7.24 ± 0.2	6.1 ± 0.4
Bilayer capacitance	0.6 ± 0.01	0.8 ± 0.03	0.7 ± 0.01	0.8 ± 0.02
Bilayer with valinomycin in NaCl				
Bilayer resistance	2.4 ± 0.1	2.67 ± 0.06	0.54 ± 0.01	1.5 ± 0.53
Bilayer capacitance	0.68 ± 0.01	0.69 ± 0.01	0.73 ± 0.02	0.94 ± 0.14
Bilayer with valinomycin in KCl				
Bilayer resistance	0.07 ± 0.01	0.070 ± 0.01	0.23 ± 0.03	0.1 ± 0.03
Bilayer capacitance	1.75 ± 0.1	1.74 ± 0.12	1.01 ± 0.07	1.98 ± 0.23
Bilayer with valinomycin in NaCl				
Bilayer resistance	2.4 ± 0.2	2.70 ± 0.1	0.44 ± 0.01	1.38 ± 0.4
Bilayer capacitance	0.75 ± 0.02	0.76 ± 0.02	0.72 ± 0.01	1.08 ± 0.12

There was no observable correlation between tether length and bilayer resistance in tBLMs formed using the novel anchorlipids. Incorporation of valinomycin into full tethered lipid bilayers caused a small reduction in membrane resistance which is likely caused by structural rearrangements of the membrane to incorporate the peptide into the lipid bilayer. It is also possible that some small degree of ion transport across the lipid bilayer takes place in the absence of potassium, despite the high selectivity of valinomycin for K^+ ions.

The fully tethered systems showed a reduction in membrane resistance by one or two orders of magnitude, in good agreement with previously reported results.[4, 21] Replacing the KCl bathing solution with NaCl immediately restored membrane resistance to the level seen prior to rinsing with KCl.

The sparsely tethered membranes also showed relatively high electrical sealing properties (See Table 4.3 for impedance data and Figure 4.2 for Bode plots). It is worth noting, that under the EIS settings used, resistances above $10 \text{ M}\Omega \text{ cm}^2$ are only visible at very low frequencies and therefor almost impossible to fit with a high degree of confidence. The very high membrane resistance of sparse DPhySL membranes is such a case and likely also a consequence of the natural variation of properties in tBLM systems.[23]

In contrast to the fully tethered membranes, the resistance in the sparsely tethered membranes did not drop upon the initial addition of valinomycin to the system. This suggests that most, if not all, impedance reduction of the fully tethered membranes upon valinomycin incorporation was caused by structural rearrangements of the bilayers, as nonspecific transport of ions across the membranes should otherwise be observed in sparsely tethered systems as well.

Exchange of the electrolyte to KCl to the sparsely tethered and self-diluted architectures led to a decrease in resistance by up to four orders of magnitude. This may be a consequence of the larger aqueous reservoir[28] which was also shown by neutron scattering studies (see later). It is also possible that a larger amount of valinomycin is incorporated into the sparsely tethered membranes, however the high affinity of the peptide towards the hydrophobic core of the bilayer makes this argument not very plausible

Table 4.3: Area normalised impedance data of sparsely tethered membrane systems as well as the self-diluting lipid DPhySDL. Resistance values are expressed in $M\Omega\text{cm}^2$, capacitance values in μFcm^{-2} . Errors are given as the range of values that can be fitted without decreasing the quality of the fit.

	60% DPhyTL	40% DPhyTL	DPhySDL	60% DPhySL	40% DPhySL
Bilayer prior to valinomycin addition					
Bilayer resistance	1.3 ± 0.1	0.6 ± 0.4	1.8 ± 0.07	40.5 ± 4.2	>100
Bilayer capacitance	1.8 ± 0.08	1.2 ± 0.2	0.9 ± 0.02	0.8 ± 0.011	0.8 ± 0.01
Bilayer with valinomycin in NaCl					
Bilayer resistance	1.61 ± 0.52	1.54 ± 0.27	1.81 ± 0.08	60 ± 9.1	>100
Bilayer capacitance	1.67 ± 0.15	1.52 ± 0.27	1.22 ± 0.04	0.8 ± 0.01	0.8 ± 0.01
Bilayer with valinomycin in KCl					
Bilayer resistance	0.001 ± 0.00001	0.0023 ± 0.00006	0.0007 ± 0.0001	0.01 ± 0.0006	0.014 ± 0.001
Bilayer capacitance	1.23 ± 0.1	2.17 ± 0.18	7.62 ± 2.14	1.2 ± 0.1	1.2 ± 0.1
Bilayer with valinomycin in NaCl					
Bilayer resistance	2.70 ± 0.43	0.8 ± 0.3	2.17 ± 0.52	93 ± 17	96.5 ± 11.9
Bilayer capacitance	1.33 ± 0.18	1.3 ± 0.05	1.06 ± 0.02	0.78 ± 0.01	0.9 ± 0.01

The larger accumulations of ions in the diluted systems also resulted in a significant change in the observed membrane capacitance under KCl, while the capacitances for the fully tethered membranes remained fairly constant. Similarly, DPhyAL with the longest tether moiety showed a larger effect than DPhyGL and DPhySL with shorter units.

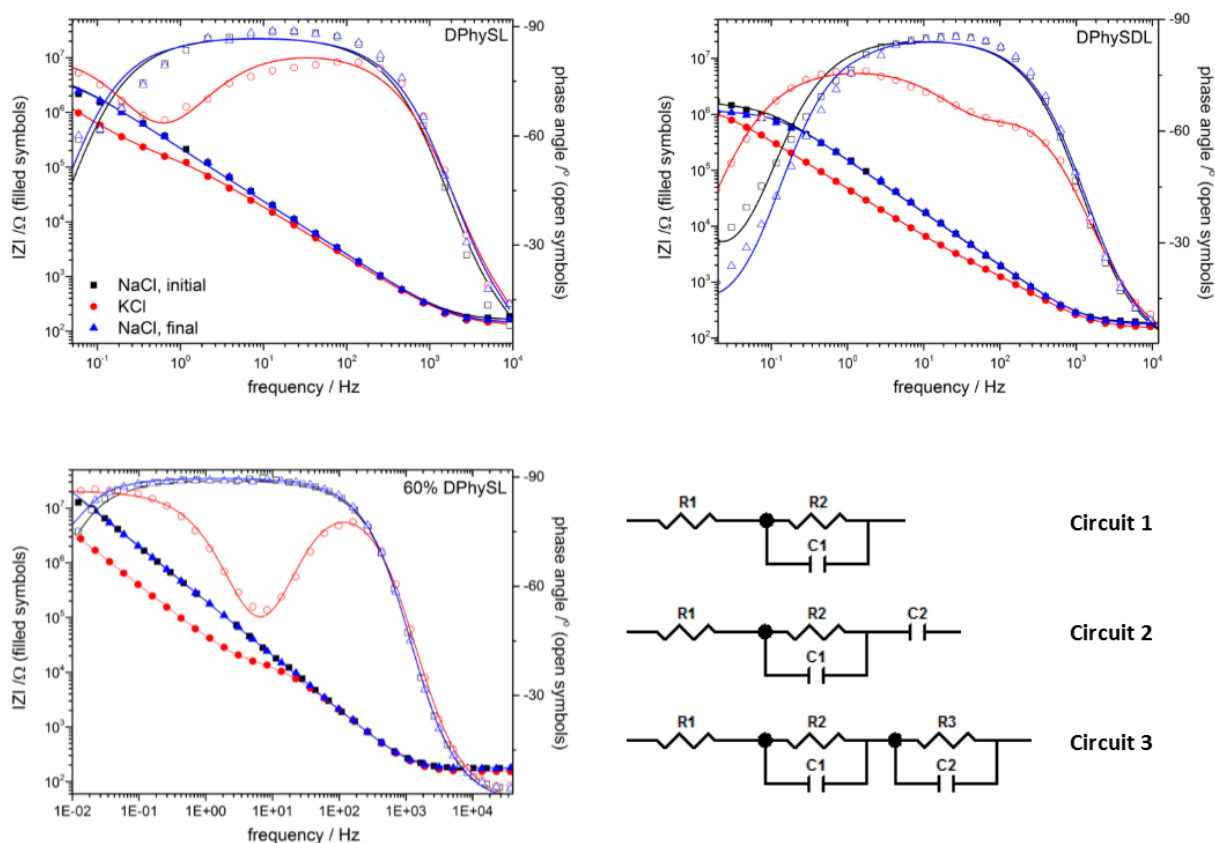


Figure 4.2: Bode plots for tBLMs formed on DPhySL, DPhySDL and 60% DPhySL after valinomycin incorporation in 100 mM NaCl (black squares), under 100 mM KCl (red circles) and after returning to NaCl (blue triangles). Experimental data are presented as symbols (impedance: filled, phase angle: open) and fits are presented as lines. The various equivalent circuits used are also shown. R1 is the electrolyte resistance, R2 and C1 are the resistance and capacitance of the lipid bilayer, respectively (in all circuits). In circuit 2, C2 represents the capacitance of the gold interface and in circuit 3, R2 and C2 represent the resistance and capacitance of the tether, respectively. For information regarding which circuit was used to fit each data set please refer to the supplementary information.

A single resistor/capacitor (R/C) element (with the addition of a second capacitor in some cases to account for the gold interface) was adequate to model fully tethered membranes. A second R/C element in series was required for the dilute tether systems as well as DPhySDL under KCl. The second R/C element accounts for the resistance and capacitance of the spacer segment that are seen due to the increased accumulation of ions under the membranes due to the increased amount of sub-membrane space afforded by these architectures. These elements can be seen in the Bode plot at low frequencies and are represented by few data points only, which leads to significant errors in the fitting.

Rinsing the DPhyTL-based architectures with NaCl solution immediately restored membrane resistance to levels prior to the addition of KCl. In fully tethered systems with ester-based spacers, storage under MilliQ for up to 24h was required to restore membrane resistance. As ester groups possess partial negative charges, it is conceivable that they are able to retain K^+ ions much more strongly than the ethylene oxide-based tethers, such that a significant electrochemical gradient is required to remove all ions from the system. In the sparsely tethered DPhySL membranes, recovery upon rinsing with NaCl was immediate. The dilution of the proximal leaflet with mercaptoethanol reduces the number of carbonyl groups in the sub-membrane space, probably allowing for an easier efflux of ions out of the spacer region.

While the electrical properties of the membrane can give an indication about the membrane structure and the size and hydration of the submembrane reservoir, neutron reflectivity experiments allow for a more direct analysis. Thus, in order to analyse the structural differences between the different tethering architectures, the tBLM systems were investigated using neutron scattering. Neutron reflectivity is an ideal tool to study buried interfaces or, as in the current case, study multi-layered systems. DPhySDL data was of insufficient quality to be analysed. Formation of tBLMs for EIS experiments is typically more reproducible, since the area used is significantly smaller compared to neutron experiments. Additionally, repeating neutron experiments is often not feasible due to beamtime restrictions. The latter also only allowed for only sparsely tethered DPhyTL systems to be investigated.

The tBLMs were analysed using a layer model (Figure 4.3 and supporting information) that describes the membrane structure perpendicular to the substrate. Each layer was fitted with a thickness, scattering length density (SLD), hydration and roughness (Table 4.4). The substrate was characterised by 3 layers (silicon wafer, chromium adhesion layer and gold), whereas the membrane was divided in 5 layers.

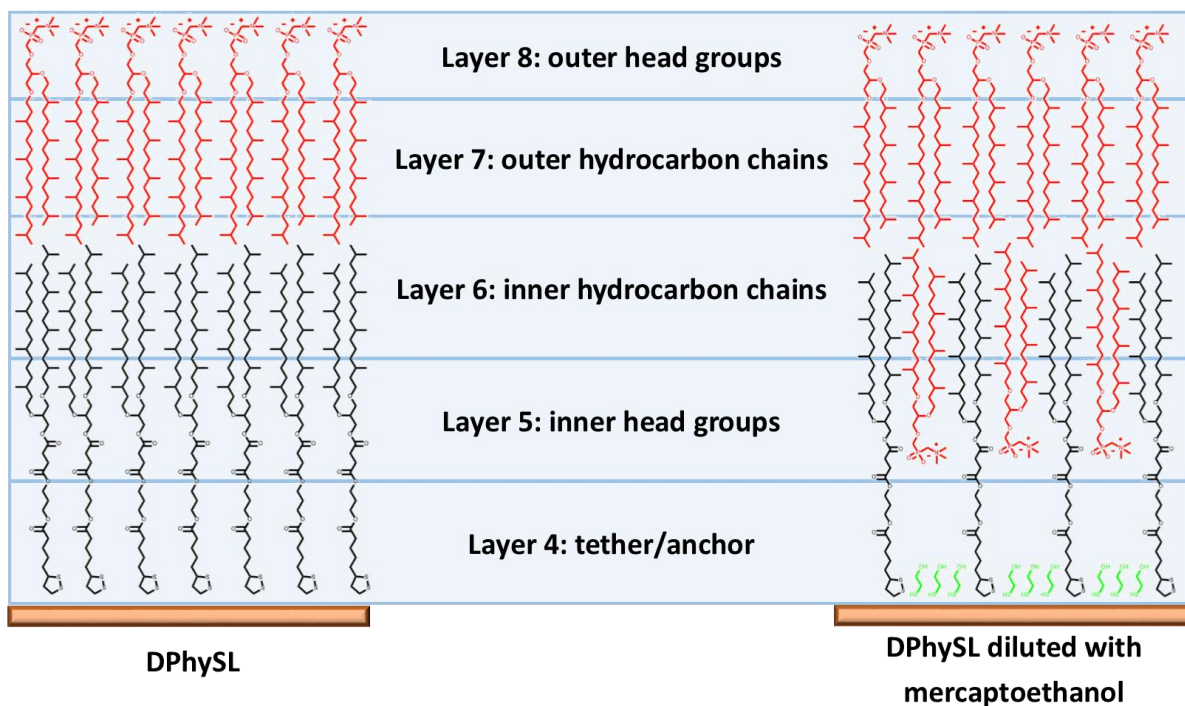


Figure 4.3: Schematic of the layer model for two different systems. Left: a fully tethered proximal leaflet (in this case formed by DPhySL, black) and right: a DPhySL layer diluted with mercaptoethanol (black and green, respectively). In both cases the distal leaflet is completed with DPhyPC (red). Layers 1-3 are omitted as they refer to substrate components.

The neutron data are in good agreement with the chemical structures of the different lipids. The anchor segment (layer 4) of DPhyAL, DPhyGL and DPhySL showed similar and low hydration levels of around 5%, indicating that the chemical changes to the sub-membrane domain do not impact the hydration of this segment of the tBLM. The length of ester segments (layer 5) correlated with the length of the carbon chain.

The level of hydration of the inner and outer hydrocarbon chains is indicative of bilayer quality. An ideal membrane should contain no water within the hydrophobic core, with the presence of water suggesting defects in the bilayer. Both DPhyAL and DPhyGL based bilayers showed a very low level of hydration, while the DPhySL based bilayer was of lower quality with only about 91% completion. This is likely due to defects in the DPhySL monolayer of the sample rather than caused by the difference in lipid structures as impedance data showed that all three lipids formed virtually equivalent bilayers. It is worth noting that for the neutron experiments, membranes had to be formed over much larger areas than for the EIS experiments, increasing the likelihood of defect formation in the membrane.

Table 4.4: Selected structural parameters of the novel tethering systems. (Thicknesses are expressed in Å, hydration in % and SLD in 10^{-6} \AA^{-2}). Values for DPhyTL have been reported elsewhere.[41] Errors are the standard deviation obtained from Monte Carlo calculations

	DPhyAL	DPhyGL	DPhySL	60% DPhyTL	40% DPhyTL
Anchor thickness	10.3 ± 0.9	8.5 ± 0.9	8.5 ± 0.7	10.2 ± 0.8	10.8 ± 0.6
Anchor hydration	5.9 ± 2.2	8.7 ± 1.1	6.8 ± 2.1	23.2 ± 5.4	26.2 ± 3.8
Inner head groups thickness	8.4 ± 0.9	5.2 ± 0.9	4.1 ± 0.5	7.2 ± 0.8	8.0 ± 0.6
Inner head groups SLD	0.09 ± 0.07	0.8 ± 0.2	0.7 ± 0.23	1.0 ± 0.3	0.7 ± 0.16
Inner head groups solvent	12.8 ± 3.3	11.8 ± 2.2	11.8 ± 2.3	15 ± 3.4	21.1 ± 4.3
Inner hydrocarbon chains thickness	15.4 ± 0.5	15.6 ± 0.3	14.2 ± 1.2	14.8 ± 1.9	15.2 ± 1.4
Inner hydrocarbon chains hydration	1.7 ± 0.6	1.4 ± 0.4	9.3 ± 0.6	3.1 ± 1.2	2.7 ± 1.3
Outer hydrocarbon chains thickness	15.3 ± 0.5	15.6 ± 0.3	13.9 ± 1.1	16.7 ± 1.7	15.3 ± 1.3
Outer hydrocarbon chains hydration	2.1 ± 0.9	2.0 ± 0.7	8.7 ± 1.0	2.7 ± 1.23	2.5 ± 1.3

Reducing the tethering density by diluting the tether-lipid with β ME increased the hydration of the anchor segment significantly to around 20-25%. Changing the tethering density from 60% to 40% had virtually no effect on the hydration of the anchor segment but caused a small increase in hydration of the inner head group layer.

The different approaches of tethering, i.e. fully tethered or sparsely tethered, thus both lead to comparably complete bilayers. The sparsely tethered systems however showed a significantly higher hydration in the tether region, which is in good correlation with the higher ion transport observed in the impedance data.

4.4 Conclusion

A series of new anchorlipids containing ester groups in the tethering region has been synthesized and characterised and compared to diluted tethering systems. All membrane architectures showed high electrical sealing properties and functional incorporation of valinomycin. The higher hydration of the diluted systems correlates with a higher ion transport into the spacer region as seen by the impedance data. The diluted systems, including the self-diluting structure are good candidates for protein incorporation, as has also been shown by others. The systems presented here, however, show higher overall sealing properties. The change in chemistry of the tether region seemed to have little effect on the electrical membrane properties, indicating that the tBLM architecture allows for significant tailoring of the sub-membrane domain depending upon its intended purpose, without affecting bilayer formation or the fundamental structure of the lipid bilayers.

4.5 References

1. Cornell, B.A., et al., *A biosensor that uses ion-channel switches*. Nature, 1997. **387**: p. 580-583.
2. Chan, Y.H.M. and S.G. Boxer, *Model membrane systems and their applications*. Current Opinion in Chemical Biology, 2007. **11**(6): p. 581-587.
3. Castellana, E.T. and P.S. Cremer, *Solid supported lipid bilayers: From biophysical studies to sensor design*. Surface Science Reports, 2006. **61**(10): p. 429-444.
4. Köper, I., *Insulating tethered bilayer lipid membranes to study membrane proteins*, in *Molecular BioSystems*. 2007. p. 651-657.
5. Terretaz, S. and H. Vogel, *Investigating the function of ion channels in tethered lipid membranes by impedance spectroscopy*. MRS Bulletin, 2005. **30**: p. 207-210.
6. Palczewski, K., et al., *Crystal structure of rhodopsin: A G protein-coupled receptor*. Science, 2000. **289**(5480): p. 739-745.
7. Leutenegger, M., et al., *Imaging of G protein-coupled receptors in solid-supported planar lipid membranes*. Biointerphases, 2008. **3**(2): p. FA136-FA145.
8. Kristiansen, K., *Molecular mechanisms of ligand binding, signaling, and regulation within the superfamily of G-protein-coupled receptors: molecular modeling and mutagenesis approaches to receptor structure and function*. Pharmacology & Therapeutics, 2004. **103**(1): p. 21-80.
9. Nakaya, M., et al., *Induction of Cardiac Fibrosis by beta-Blocker in G Proteinindependent and G Protein-coupled Receptor Kinase 5/beta-Arrestin2-dependent Signaling Pathways*. Journal of Biological Chemistry, 2012. **287**(42): p. 35669-35677.
10. Cheng, S.H., et al., *Defective intracellular transport and processing of CFTR is the molecular basis of most cystic fibrosis*. Cell, 1990. **63**(4): p. 827-834.
11. Emery, A.E.H., *The muscular dystrophies*. The Lancet, 2002. **359**(9307): p. 687-695.
12. Klabunde, T. and G. Hessler, *Drug design strategies for targeting G-protein-coupled receptors*. Chembiochem : a European journal of chemical biology, 2002. **3**(10): p. 928-44.
13. Guo, D., et al., *Drug-Target Residence Time-A Case for G Protein-Coupled Receptors*. Medicinal Research Reviews, 2014. **34**(4): p. 856-892.
14. Sahalan, A.Z. and R.A. Dixon, *Role of the cell envelope in the antibacterial activities of polymyxin B and polymyxin B nonapeptide against Escherichia coli*. International Journal of Antimicrobial Agents, 2008. **31**(3): p. 224-227.
15. Haeusler, G., *Pharmacology of beta-blockers - classical aspects and recent developments*. Journal of Cardiovascular Pharmacology, 1990. **16**: p. S1-S9.
16. Rolando, G. and B. Lucia, *Ion transport across biomembranes and model membranes*. Journal of Solid State Electrochemistry, 2011. **15**.
17. Jackman, J.A., W. Knoll, and N.J. Cho, *Biotechnology Applications of Tethered Lipid Bilayer Membranes*. Materials, 2012. **5**(12): p. 2637-2657.
18. Rebaud, S., O. Maniti, and A.P. Girard-Egrot, *Tethered bilayer lipid membranes (tBLMs): interest and applications for biological membrane investigations*. Biochimie, 2014. **107**: p. 135-142.
19. Vockenroth, I.K., et al., *Stable insulating tethered bilayer lipid membranes*. Biointerphases, 2008. **3**(2): p. FA68-FA73.
20. Andersson, J. and I. Köper, *Tethered and Polymer Supported Bilayer Lipid Membranes: Structure and Function*. Membranes, 2016. **6**(2): p. 30.
21. Naumann, R., et al., *Tethered lipid Bilayers on ultraflat gold surfaces*. Langmuir, 2003. **19**(13): p. 5435-5443.
22. McGillivray, D.J., et al., *Molecular-scale structural and functional characterization of sparsely tethered bilayer lipid membranes*. Biointerphases, 2007. **2**(1): p. 21-33.
23. Junghans, A. and I. Köper, *Structural Analysis of Tethered Bilayer Lipid Membranes*. Langmuir, 2010. **26**(13): p. 11035-11040.
24. Valincius, G., et al., *Enzyme Activity to Augment the Characterization of Tethered Bilayer Membranes*. J. Phys. Chem. B, 2006. **110**(21): p. 10213-10216.
25. Kwak, K.J., et al., *Formation and Finite Element Analysis of Tethered Bilayer Lipid Structures*. Langmuir, 2010. **26**(23): p. 18199-18208.

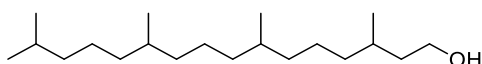
26. Steinem, C., et al., *Impedance analysis of supported lipid bilayer membranes: a scrutiny of different preparation techniques*. Biochimica et Biophysica Acta, 1996. **1279**: p. 169-180.
27. Knoll, W., et al., *Functional tethered lipid bilayers*. Reviews in Molecular Biotechnology, 2000. **74**(3): p. 137-158.
28. Vockenroth, I.K., et al., *Incorporation of alpha-hemolysin in different tethered bilayer lipid membrane architectures*. Langmuir, 2008. **24**(2): p. 496-502.
29. Vockenroth, I.K., et al., *Formation of tethered bilayer lipid membranes probed by various surface sensitive techniques*. Biointerphases, 2009. **4**(2): p. 19-26.
30. Schiller, S.M., et al., *Archaea analogue thiolipids for tethered bilayer lipid membranes on ultrasmooth gold surfaces*. Angewandte Chemie International Edition, 2003. **42**(2): p. 208-211.
31. Leitch, J., et al., *In Situ PM-IRRAS Studies of an Archaea Analogue Thiolipid Assembled on a Au(111) Electrode Surface*. Langmuir, 2009. **25**(17): p. 10354-10363.
32. Liu, C. and R. Faller, *Conformational, Dynamical. and Tensional Study of Tethered Bilayer Lipid Membranes in Coarse-Grained Molecular Simulations*. Langmuir, 2012. **28**(45): p. 15907-15915.
33. Becucci, L., R.J. Faragher, and A. Schwan, *The effect of the hydrophilic spacer length on the functionality of a mercury-supported tethered bilayer lipid membrane*. Bioelectrochemistry, 2015. **101**(0): p. 92-96.
34. Shenoy, S., et al., *In-plane homogeneity and lipid dynamics in tethered bilayer lipid membranes (tBLMs)*. Soft Matter, 2010. **6**(6): p. 1263-1274.
35. James, M., et al., *The multipurpose time-of-flight neutron reflectometer "Platypus" at Australia's OPAL reactor*. Nuclear Instruments and Methods in Physics Research Section A: Accelerators, Spectrometers, Detectors and Associated Equipment, 2011. **632**(1): p. 112-123.
36. Atanasov, V., et al., *A molecular toolkit for highly insulating tethered bilayer lipid membranes on various substrates*. Bioconjugate Chemistry, 2006. **17**(3): p. 631-637.
37. McGillivray, D.J., et al., *Solid-supported lipid membranes for protein incorporation*. Abstracts of Papers of the American Chemical Society, 2005. **230**: p. U1071-U1071.
38. Becucci, L., et al., *A metal-supported biomimetic micromembrane allowing the recording of single-channel activity and of impedance spectra of membrane proteins*. Bioelectrochemistry. **78**(2): p. 176-180.
39. Naumann, R., et al., *Kinetics of valinomycin-mediated K⁺ ion transport through tethered bilayer lipid membranes*. Journal of Electroanalytical Chemistry, 2003. **550-551**: p. 241-252.

4.6 Supporting information

This section contains the supporting information for the paper this chapter is based on, which can also be found on the journal website.

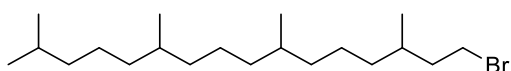
4.6.1 Synthetic procedures and product characterisation

1: 3,7,11,15-tetramethylhexadecan-ol



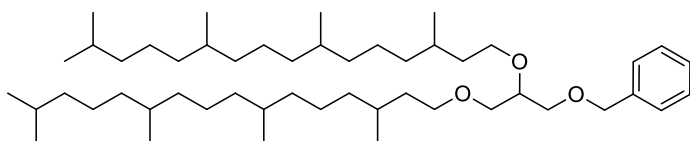
To a stirred solution of phytol (1.00 g, 3.4 mmol) in methanol (6 mL) was added palladium/carbon catalyst (15 mg, 1 mol %). Hydrogen gas was introduced from a balloon. The mixture was stirred vigorously for 24h. The catalyst is filtered over a short pad of celite and the solvent was removed via rotary evaporation, yielding the title compound as a clear oily liquid quantitatively. The product of this reaction was used without further purification. $^1\text{HNMR}$ (600 MHz, CDCl_3 , 26°C), ppm: 3.7 -3. 64 (m, 2H, $\text{CH}_2\text{-OH}$), 1.61-1.49 (m, 4 H, $\text{CH}_2\text{-CH}_2$), 1.06-1.38 (m, 21 H, $\text{CH}_2\text{-CH}_2$), 0.89-0.83 (m, 15 H, CH-CH_3)

2: 1-bromo-3,7,11,15-tetramethylhexadecane



To a stirred solution of **9** (5.00 g, 17 mmol) and triphenylphosphine (5.5 g, 21 mmol) in anhydrous CH_2Cl_2 (50 mL) at 5°C was added *N*-Bromosuccinimide (NBS) (6 g, 3.4 mmol) slowly in small portions. The addition of NBS caused the reaction mixture to bubble vigorously. The reaction mixture was allowed to warm up to room temperature and left to stir for 16 h. Hexane was added. The precipitate was removed via filtration and the solvent evaporated. Column chromatography (100% hexane) yielded 4.1 g (67 %) of the title compound as a clear colourless oil. R_F = 0.67 (100 % hexane), $^1\text{HNMR}$ (600 MHz, CDCl_3 , 26°C), ppm: 3.49-3.42 (m, 2 H, $\text{CH}_2\text{-Br}$), 1.92-1.90 (m, 1 H, $\text{CH}_2\text{-CH-CH}_3$), 1.70-1.59 (m, 2 H, $\text{CH}_2\text{-CH}_2\text{-Br}$), 1.56-1.54 (m, 2 H), 1.40-1.16 (m, 21 H, $\text{CH}_2\text{-CH}_2$), 0.92-0.86 (m, 16 h, CH-CH_3)

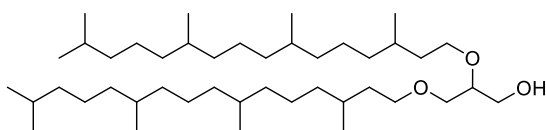
3: ((2,3-bis((3,7,11,15-tetramethylhexadecyl)oxy)propoxy)methyl)benzene



To a stirred solution of **6** (250 mg, 1.37 mmol) in benzene (7 mL) was added **7** (2.9 g, 8 mmol) and powdered KOH

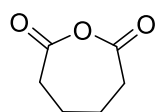
(670 mg, 12 mmol). The reaction mixture was set to reflux 48 h in a setup similar to a Dean Stark Trap to collect any water being produced by the reaction. The product was diluted with hexane (20 mL) and washed with water (3 x 20 mL). The solvent was evaporated. Column chromatography (50% EtOAc/hexane) yielded 630 mg (62 %) of the title compound as a clear pale yellow oil. R_f : = 0.31 (10% EtOAc/hexane), $^1\text{HNMR}$ (600 MHz, CDCl_3 , RT), ppm: 7.38-7.33 (m, 5H, Ar-H), 4.56 (s, 2H, Ar- CH_2), 3.63-3.57 (m, 3 H, $\text{CH}_2\text{-O-CH}$), 3.54-3.43 (m, 6H, $\text{CH}_2\text{-O}$), 1.64-1.49 (m, 12H, $\text{CH}_2\text{-CH}_2$), 1.36-1.05 (m, 84H, $\text{CH}_2\text{-CH}_2$), 0.9-0.84 (m, 30H, CH-CH_3)

4: 2,3-bis((3,7,11,15-tetramethylhexadecyl)oxy)propan-1-ol



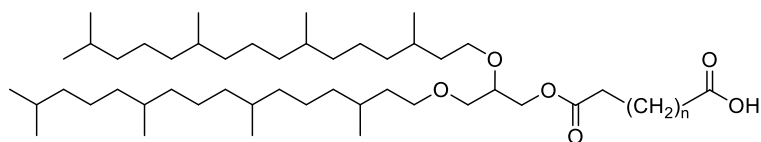
To a solution of **5** (630 mg, 0.9 mmol) in 10 mL of a 3:1 mixture $\text{CH}_3\text{OH}:\text{THF}$ was added palladium/carbon catalyst (60 mg, 1 mol %). Hydrogen gas was introduced from a balloon. The reaction was stirred for 16 h. The catalyst was removed via filtration through a short pad of celite. The solvent was evaporated, to give 540 mg (97%) of the title compound as a clear viscous oil. The product was used without further purification. $^1\text{HNMR}$ (600 MHz, CDCl_3 , 26°C), ppm: 3.71-3.46 (m, 9 H, $\text{CH}_2\text{-O-CH}$), 1.64-1.49 (m, 6H, $\text{CH}_2\text{-CH}_2$), 1.4-1.03 (m, 45H, $\text{CH}_2\text{-CH}_2$), 0.89-0.83 (m, 30H, CH-CH_3)

Oxepane-2,-7-dione (Other cyclic anhydrides were purchased from Sigma Aldrich)



The precursor acid (2g, 13.6 mmol) was dissolved in glacial acetic anhydride (35 mL) and refluxed under inert gas atmosphere for 4 h. The solvent was removed via rotary evaporation yielding 1.62 g (81%, determined from $^1\text{HNMR}$ spectrum) product as pale brown solid. The product was used without further purification. $^1\text{HNMR}$ (600 MHz, CDCl_3 , RT), ppm: 2.62-2.49 (m, 4H, 2 x C(O)O-CH_2), 1.74 (s, 4H, $\text{CH}_2\text{-CH}_2$)

5a, 5b, 5c, general method



To a solution of Diphytanyl glycerol (50 mg, 76 μ mol) in dichloromethane (1.5 mL) was

added the cyclic anhydride (20-30 mg, 0.2-0.3 mmol) and 4-Dimethylaminopyridine (1 eq). The reaction was left to stir overnight for 16 h. The reaction mixture was then diluted with CH_2Cl_2 (10 mL) and washed with water (2 x 20 mL) and with cold dilute citric acid (3 x 20 mL). The solvent was evaporated, yielding the desired product quantitatively. The product was used without further purification.

5a - 6-(2,3-bis((3,7,11,15-tetramethylhexadecyl)oxy)propoxy)-6-oxobutanoic acid:

1H NMR (600 MHz, $CDCl_3$, 26°C), ppm: 4.25 (dd, 1H, J = 11.6, 4.2 Hz, COO- CH_2), 4.13 (dd, J=11.4, 5.9 Hz, 1H, COO- CH_2), 3.63-3.56 (m, 3H, CH_2 -O), 3.50-3.44 (m, 4H, CH_2 -O), 2.69-2.64 (m, 4H, CH_2), 1.62-1.59 (m, 3H, CH_2 -CH), 1.55-1.49 (m, 6H, CH_2 - CH_2), 1.37-1.04 (m, 57H, CH_2 -CH), 0.89-0.83 (m, 39H, CH_2 -CH)

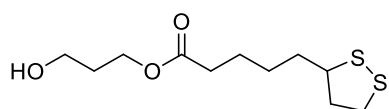
5b - 6-(2,3-bis((3,7,11,15-tetramethylhexadecyl)oxy)propoxy)-6-oxopentanoic acid:

1H NMR (400 MHz, $CDCl_3$, 26°C), ppm: 4.24 (dd, 1H, J = 11.6, 4.2 Hz, COO- CH_2), 4.1 (dd, J=11.4, 5.7 Hz, 1H, COO- CH_2), 3.63-3.42 (m, 7H, CH_2 -O), 2.45-2.37 (m, 4H, CH_2 - CH_2), 1.96 (quin, J=7.29 Hz, 2H, CH_2 - CH_2), 1.64-1.49 (m, 6H, CH_2 - CH_2), 1.37-0.99 (m, 51H, CH_2 - CH_2), 0.9-0.83 (m, 30H, CH- CH_3)

5c - 6-(2,3-bis((3,7,11,15-tetramethylhexadecyl)oxy)propoxy)-6-oxohexanoic acid:

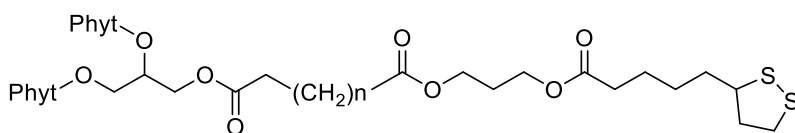
1H NMR (600 MHz, $CDCl_3$, 26°C), ppm: 4.22 (dd, 1H, J = 11.6, 4.2 Hz, COO- CH_2), 4.1 (dd, J=11.6, 5.7 Hz, 1H, COO- CH_2), 3.62-3.57 (m, 3H, CH_2 -O), 3.49-3.44 (m, 4H, CH_2 -O), 2.36 (q, 4H, CH_2 - CH_2), 1.70-1.67 (m, 4H, CH_2 - CH_2), 1.61-1.48 (m, 6H, CH_2 - CH_2), 1.37-1.03 (m, 47H, CH_2 - CH_2), 0.89-0.83 (m, 39H, CH_2 -CH)

6: 3-hydroxypropyl 6-(1,2-dithiolane-3-yl) pentanoate (lipoic diol ester)



To a solution of lipoic acid (200 mg, 1 mmol) and 1,3-propanediol (380 mg, 5 mmol) in CH_2Cl_2 (2 mL) were added DCC (200 mg, 1 mmol) and DMAP (25 mol-%). The reaction mixture was stirred for 16 h. The reaction mixture was then diluted with DCM to 5 mL and filtered under vacuum to remove any precipitate. The solution was washed with water (20 ml) followed by cold dilute citric acid (2x 20 mL) and water (20 mL). The solvent is evaporated and the compound purified via column chromatography (50% EtOAc/hexane) yielded 85 mg (32%) product as a clear yellow oil. R_f : 0.25 (50% EtOAc/hexane), $^1\text{H NMR}$ (600 MHz, CDCl_3 , RT), ppm: 4.21 (t, $J=6.2$ Hz, 2H, $\text{CH}_2\text{-COO}$), 3.67 (t, $J=6.1$ Hz, 2H, $\text{CH}_2\text{-OH}$), 3.57-3.53 (m, 1H, CH-SS), 3.17-3.14 (m, 1H, $\text{CH}_2\text{-SS}$), 3.12-3.07 (m, 1H, $\text{CH}_2\text{-SS}$), 2.47-2.42 (m, 1H, $\text{CH}_2\text{-CH}$), 2.31 (t, $J=7.3$, 2H, $\text{CH}_2\text{-COO}$), 2.07 (s, 1H, $\text{CH}_2\text{-COH}$), 1.92-1.88 (qq, 1H, $\text{CH}_2\text{-CH}$), 1.5 (quin, $J=6.1$ Hz, 2H, CH_2CH_2), 1.72-1.58 (m, 4H, CH_2CH_2), 1.51-1.39 (m, 2H, $\text{CH}_2\text{-CH}_2$)

7a-7c, general procedure



To a solution of **1a**, **1b**, **1c** (50 mg, ~60 μmol) in anhydrous dichloromethane (1.5 mL) under an inert gas atmosphere were added **Lipoic diol ester (6)** (50 mg, 0.2 mmol), DCC (100 mg, 0.5 mmol) and DMAP (25 mol-%). The reaction was left to stir for 16 h. The reaction is diluted with dichloromethane and then washed with water (20 mL), cold dilute citric acid (2 x 20 mL) and water (20 mL). The organic phase is dried over NaHSO_4 and the solvent removed via rotary evaporation. The crude product is taken up in a 1:1 mixture of ethyl acetate/hexane. The precipitate is removed by vacuum filtration. Column chromatography on buffered silica (100% dichloromethane) yields the pure product as clear pale yellow oil.

7a: 3-((5-(1,2-dithiolan-3-yl)pentanoyl)oxy)propyl (2,3-bis((3,7,11,15-tetramethylhexadecyl)oxy)propyl)succinate

Yield: 15%, ¹HNMR (600 MHz, CDCl₃, 26°C), ppm: 4.24 (dd, J=11.6, 4.2 Hz, 1H, COO-CH₂), 4.18-4.11 (m, 5H, COO-CH₂), 3.61-3.55 (m, 4H, CH₂-O), 3.48-3.46 (m, 4H, CH₂-O), 3.19-3.16 (m, 1H, CH₂-SS), 3.13-3.10 (m, 1H, CH₂-SS), 2.67-2.61 (m, 4H, CH₂-CH₂), 2.46 (dq, J=12.2, 6.3 Hz, 1H, CH-CH₂), 2.32 (t, J=7.5 Hz, 2H, CH₂-COO), 1.99-1.88 (m, 4H, CH₂-CH₂), 1.73-1.58 (m, 9H, CH₂-CH₂), 1.54-1.03 (m, 54H, CH₂-CH₂), 0.89-0.83 (m, 30H, CH-CH₃)

7b: 3-((5-(1,2-dithiolan-3-yl)pentanoyl)oxy)propyl (2,3-bis((3,7,11,15-tetramethylhexadecyl)oxy)propyl)glutarate

yield: 18%, ¹HNMR (600 MHz, CDCl₃, 26°C), ppm: 4.24 (dd, J=11.6, 4.2 Hz, 1H, COO-CH₂), 4.18-4.11 (m, 5H, COO-CH₂), 3.59-3.53 (m, 4H, CH₂-O), 3.45-3.42 (m, 4H, CH₂-O), 3.15-3.13 (m, 1H, CH₂-SS), 3.11-3.08 (m, 1H, CH₂-SS), 2.45-2.42 (m, 1H, CH₂-CH₂), 2.38 (m, CH-CH₂), 2.32 (t, J=7.5 Hz, 2H, CH₂-COO), 1.70-1.37 (m, 27H, CH₂-CH₂), 1.33-1.01 (m, 64H, CH₂-CH₂), 0.89-0.80 (m, 30H, CH-CH₃)

7c: 3-((5-(1,2-dithiolan-3-yl)pentanoyl)oxy)propyl (2,3-bis((3,7,11,15-tetramethylhexadecyl)oxy)propyl)adipate

Yield: 8%, ¹HNMR (600 MHz, CDCl₃, 26°C), ppm: 4.22 (dd, J=11.7, 4.0 Hz, 1H, COO-CH₂), 4.15-4.13 (m, 4H, COO-CH₂), 4.1 (dd, J=11.4, 5.5 Hz, 1H, CH₂-COO), 3.61-3.56 (m, 3H, CH₂-O), 3.48-4.45 (m, 4H, CH₂-O), 3.20-3.11 (m, 2H, CH₂-SS), 2.48-2.36 (m, 1H, CH-CH₂), 2.35-2.29 (m, 7H, CH-CH₂), 1.98-1.90 (m, 6H, CH₂-CH₂), 1.72-1.51 (m, 32H, CH₂-CH₂), 1.36-1.05 (m, 72H, CH₂-CH₂), 0.87-0.76 (m, 30H, CH-CH₃)

4.6.2 Electrochemical impedance spectroscopy

Details regarding which equivalent circuit was used to fit each data set can be found in the tables containing each data set. Impedance is shown in $M\Omega cm^2$ and capacitance is shown in $\mu F cm^{-2}$. Values marked with an asterisk are not reliable, as there are insufficient data points to fit this parameter (however, the parameter is required to achieve a reasonable fit).

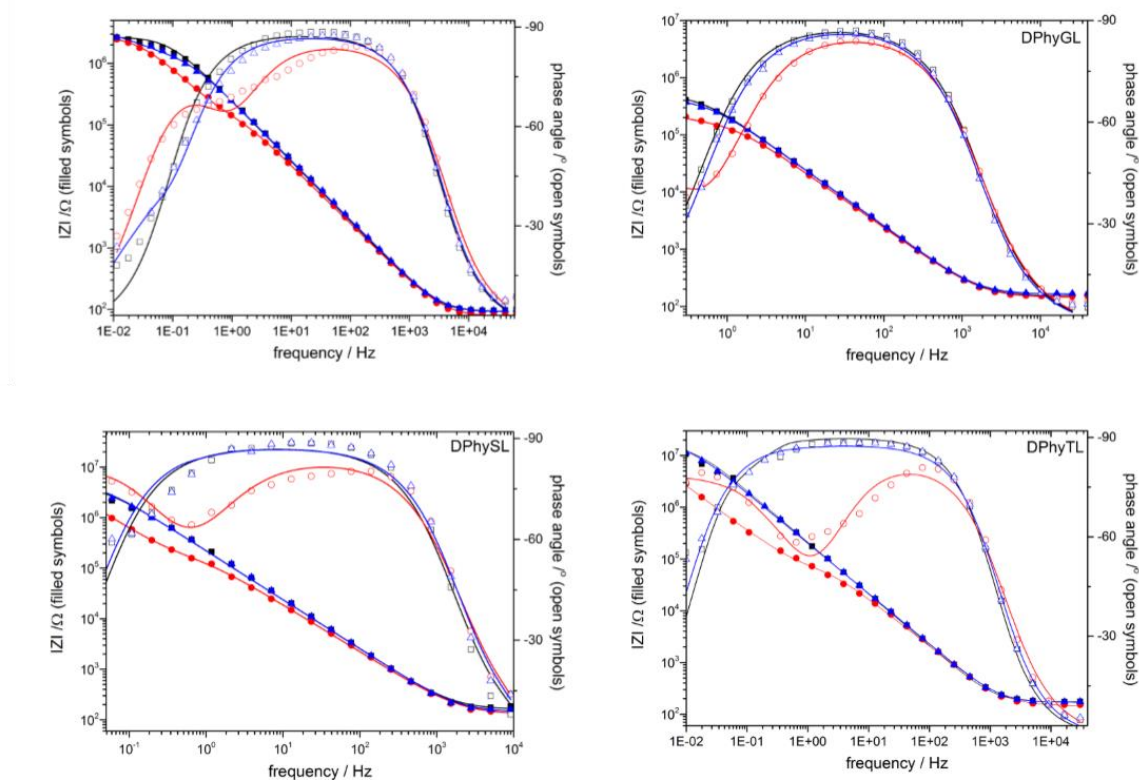


Figure S 4.1: Bode plots of the fully tethered tBLM architectures with incorporated valinomycin under NaCl (black squares), KCl (red circles) and under NaCl after KCl exposure (blue triangles). Empty symbols represent phase angle, fully symbols represent impedance and lines represent fits. Plots of bilayers prior to valinomycin incorporation not shown.

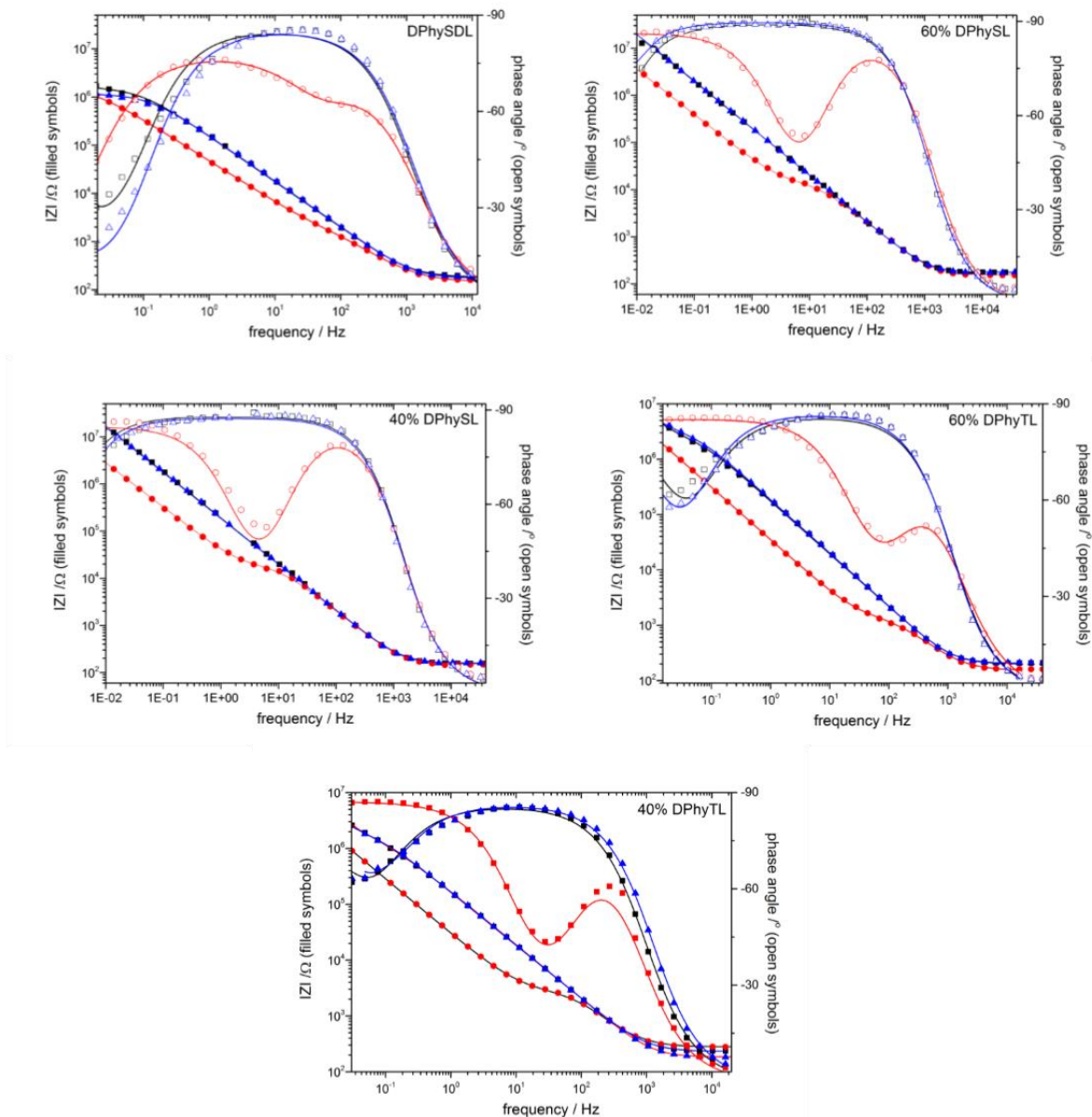


Figure S 4.2: Bode plots of the sparsely tethered tBLM architectures with incorporated valinomycin under NaCl (black squares), KCl (red circles) and under NaCl after KCl exposure (blue triangles). Empty symbols represent phase angle, fully symbols represent impedance and lines represent fits. Plots of bilayers prior to valinomycin incorporation not shown.

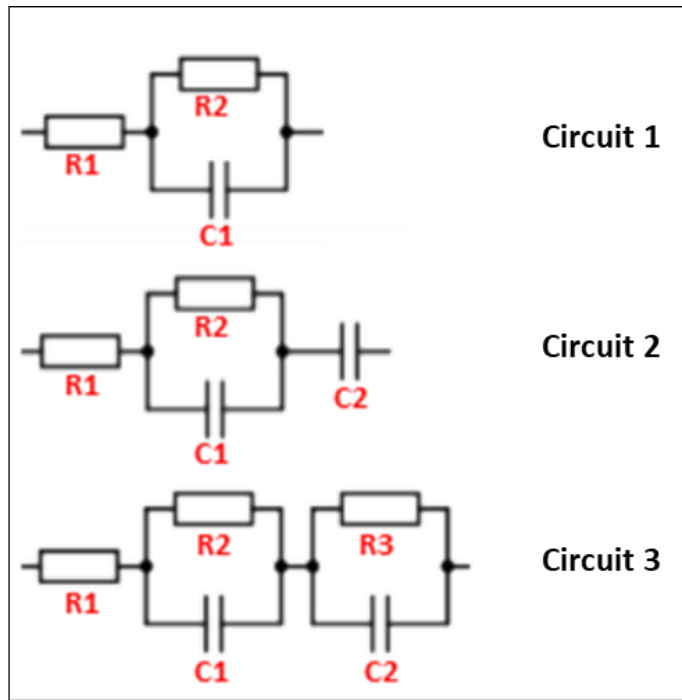


Figure S 4.3: Equivalent circuits used to fit EIS data.

Table S 4.1: Full set of EIS fitting data for fully tethered bilayer architectures.

DPhyAL					
	Bilayer		Spacer		Circuit #
	Resistance (M Ω)	Capacitance (μ F)	Resistance (M Ω)	Capacitance (μ F)	
Bilayer	13.3 \pm 0.8	0.8 \pm 0.03		*	1
Valinomycin (NaCl)	2.4 \pm 0.1	0.7 \pm 0.1		*	1
Valinomycin (KCl)	0.1 \pm 0.01	1.7 \pm 0.1	2.6 \pm 0.3	1.9 \pm 0.1	3
Valinomycin (NaI)	1.5 \pm 0.4	0.8 \pm 0.1		5.4 \pm 5.2	1
DPhyGL					
Bilayer	7.2 \pm 0.2	0.7 \pm 0.009		7.4 \pm 0.9	1
Valinomycin (NaCl)	0.5 \pm 0.1	0.6 \pm 0.007		50.8 \pm 4.7	1
Valinomycin (KCl)	0.1 \pm 0.1	0.8 \pm 0.015		5.1 \pm 0.4	2
Valinomycin (NaI)	0.4 \pm 0.1	0.6 \pm 0.006		30.9 \pm 5.9	1
DPhySL					
Bilayer	6.1 \pm 0.39	0.81 \pm 0.02			1
Valinomycin (NaCl)	1.52 \pm 0.13	0.88 \pm 0.03			1
Valinomycin (KCl)	0.09 \pm 0.013	1.95 \pm 0.12	54.4 \pm 28	2.56 \pm 0.8	3
Valinomycin (NaI)	1.62 \pm 0.12	0.9 \pm 0.3			1
DPhyTL					
Bilayer	23.0 \pm 1.1	0.6 \pm 0.01			1
Valinomycin (NaCl)	2.4 \pm 0.1	0.7 \pm 0.01	25.2 \pm 13		2
Valinomycin (KCl)	0.1 \pm 0.01	1.8 \pm 0.1	1.9 \pm 0.1	2.8 \pm 0.1	3
Valinomycin (NaI)	2.4 \pm 0.2	0.8 \pm 0.02	24.5 \pm v18		2

Table S 4.2: Full set of EIS fitting data for sparsely tethered bilayer architectures.

60% DPhyTL					
	Bilayer		Spacer		Circuit #
	Resistance	Capacitance	Resistance	Capacitance	
Bilayer	1.35 ± 0.1	1.8 ± 0.1		*	2
Valinomycin (NaCl)	1.17 ± 0.1	1.6 ± 0.1		*	2
Valinomycin (KCl)	0.001 ± 0.0001	2.2 ± 0.2	512.18 ± 1800	4.98 ± 0.03	3
Valinomycin (NaI)	1.86 ± 0.13	1.09 ± 0.03			2
60% DPhySL					
Bilayer	40.5 ± 4.2	0.82 ± 0.01			1
Valinomycin (NaCl)	60. ± 9.2	0.81 ± 0.01			1
Valinomycin (KCl)	0.01 ± 0.0001	1.16 ± 0.1	2.30E+08	3.96 ± 0.05	3
Valinomycin (NaI)	93.6 ± 17	0.79 ± 0.01			1
40% DPhySL					
Bilayer	178 ± 32	0.9 ± 0.01			1
Valinomycin (NaCl)	122 ± 8.6	0.9 ± 0.01			1
Valinomycin (KCl)	0.01 ± 0.001	1.2 ± 0.1	2.70E+09	4.8 ± 0.1	3
Valinomycin (NaI)	96.5 ± 12	0.9 ± 0.01			1
40% DPhyTL					
Bilayer	0.48 ± 0.047	1.2 ± 0.05			2
Valinomycin (NaCl)	1.52 ± 0.12	1.15 ± 0.04			2
Valinomycin (KCl)	0.002 ± 0.0001	1.2 ± 0.1	86.82 ± 31	5.5 ± 0.03	3
Valinomycin (NaI)	0.78 ± 0.1	1.3 ± 0.05			2

4.6.3 Neutron data

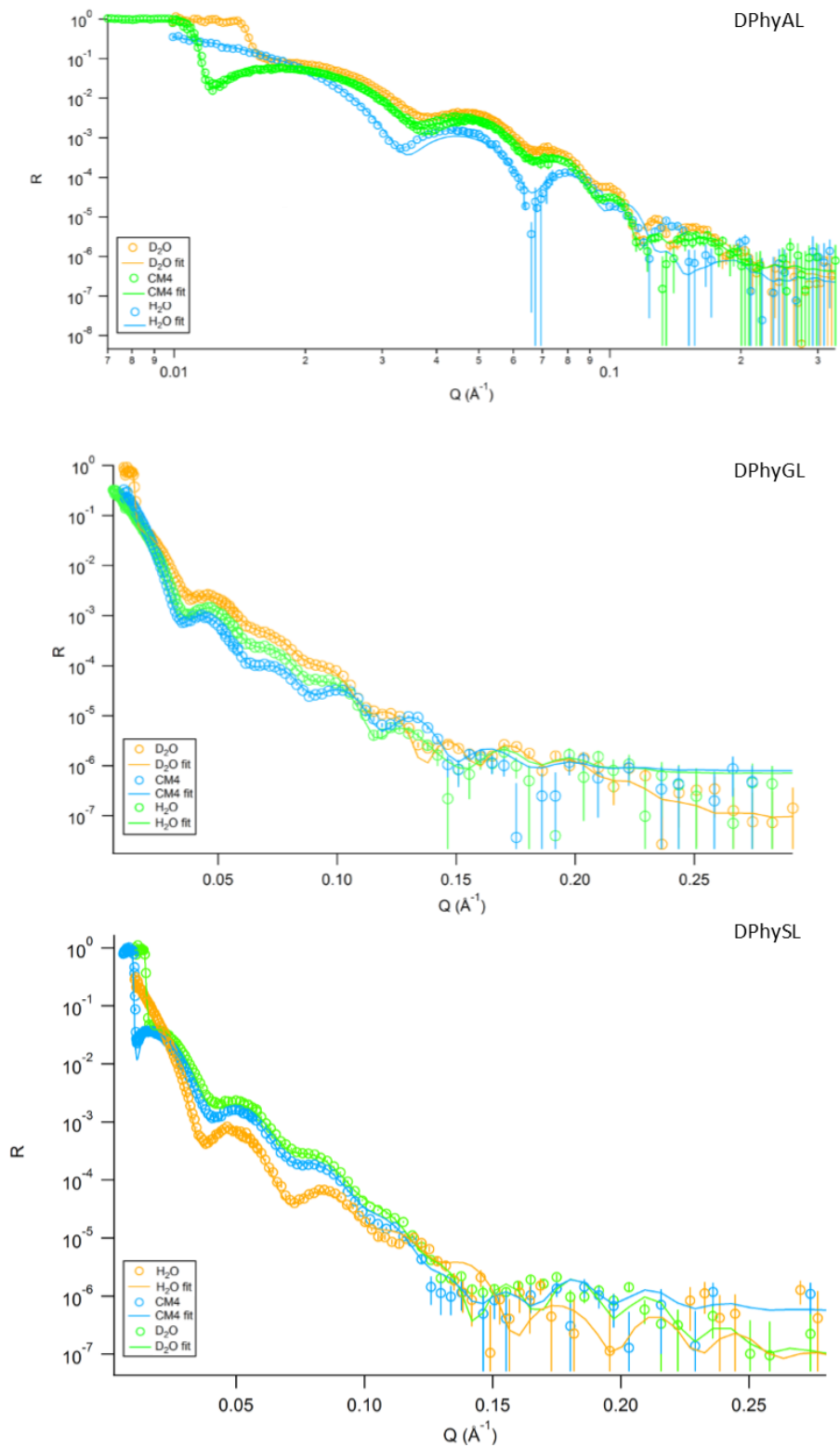


Figure S 4.4: Neutron data of DPhyGL, DPhyAL and DPhySL. Open symbols represent experimental data, solid lines represent fitted data

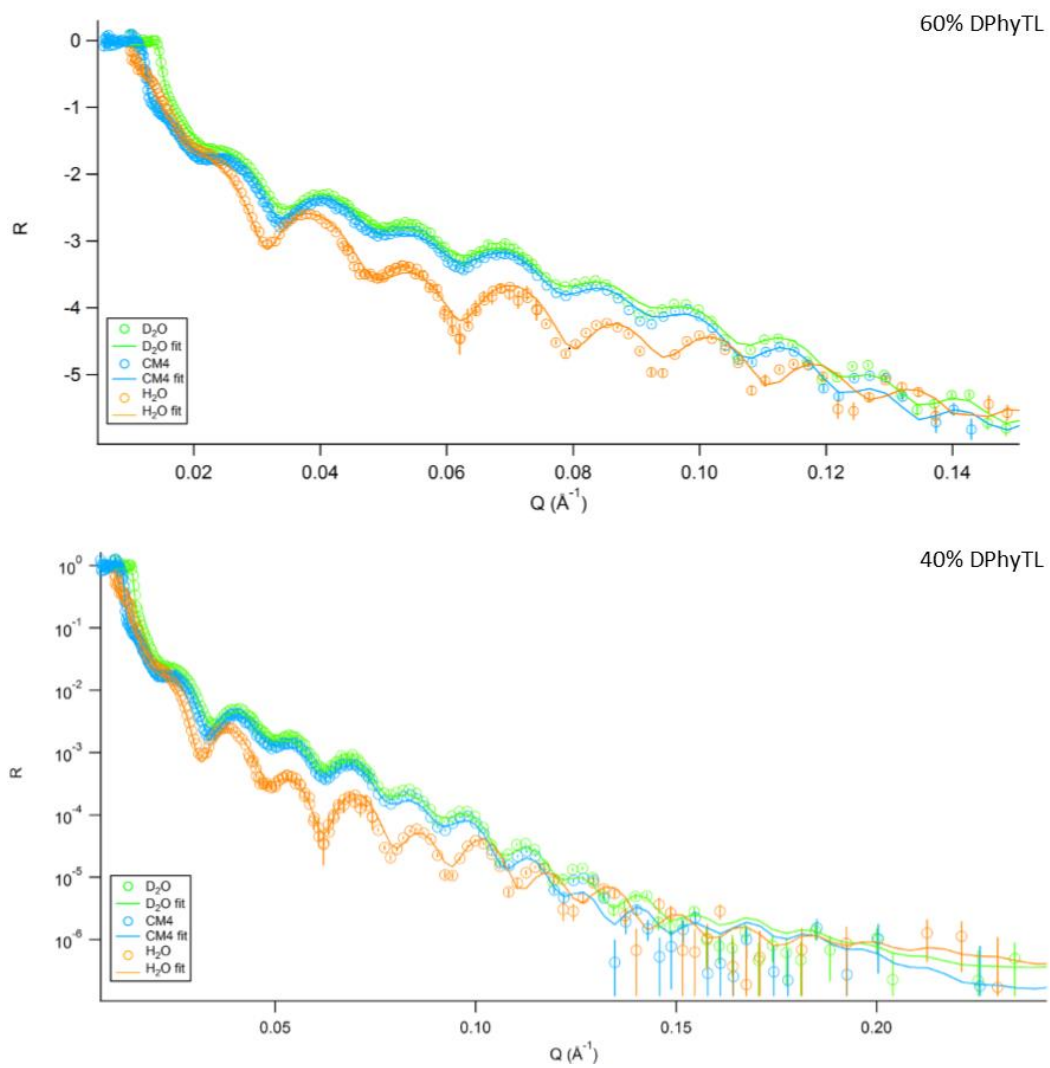


Figure S 4.5: Neutron data of 60% DPhyTL and 40% DPhyTL. Open symbols represent experimental data, solid lines represent fitted data

5 Mimicking Microbial Membranes

This chapter is published in the journal Physical Chemistry Chemical Physics under the following title:

A tethered bilayer lipid membrane that mimics microbial membranes, *Jakob Andersson*¹,
*Melanie A. Fuller*¹, *Kathleen Wood*², *Stephen A. Holt*², *Ingo Köper*¹

¹Flinders Centre for Nanoscale Science and Technology and College of Science and Engineering, Flinders University, Adelaide, Australia

²Australian Centre for Neutron Scattering, Australian Nuclear Science and Technology Organisation, Locked Bag 2001, Kirrawee DC, NSW, Australia

Abstract

A model membrane system has been developed, which mimics the outer membrane of Gram-negative bacteria. The structure is based on a tethered monolayer which has been fused with vesicles containing lipopolysaccharide molecules. The effect of the composition of the monolayer and the lipids in the outer layer on the structural and electrical properties of the membrane has been investigated. By using electrochemical impedance spectroscopy as well as neutron scattering techniques, it could be shown that a relatively high tethering density and a small amount of diluting lipids in the outer membrane leaflet leads to the formation of a stable solid supported membrane. The influence of divalent ions on the membrane stability has been probed as well as the interaction of the bilayer with the antibiotic colistin. A number of different architectures were developed, suited to both the study of bacterial membrane proteins and the screening of antimicrobial activity of potential drug candidates.

5.1 Introduction

The increasing prevalence of antibiotic resistance in bacteria poses a significant global health care problem.[1] While drug resistance occurs in both Gram-positive and Gram-negative bacteria (GNB), the latter are of particular concern since they tend to develop resistance more quickly.[2] This can be attributed to the unique structure of GNB cell walls, which consist of an inner and an outer cell membrane separated by a layer of peptidoglycans and lipoproteins.[3] The unique membrane of GNB provides a significant defensive barrier against most antibiotics,[4] which need to pass through the cell membrane in order to act against components of the cell machinery.[5]

Only very few antibiotics, particularly antimicrobial peptides such as polymyxins, target the cell membrane itself, [6, 7] yet targeting the cell membrane instead of biochemical pathways inside the cell can slow the development of drug resistance.[8] The bacterial membrane and its components are therefore highly viable targets for novel antibacterial treatments, and an improved understanding of the bacterial membrane, its components and their interactions with drugs is important for future drug discovery efforts. Furthermore, a better understanding of the mechanism of action of existing antibiotics targeting the cell membrane can improve their efficacy and may lead to the discovery of novel approaches to treat bacterial infections.

However, the systematic study of the cell membrane and embedded membrane proteins is difficult, mainly due to the complex membrane structure containing a wide variety of components including lipids, sugars, membrane proteins, transporters and peptides. Model membranes have been developed to mimic the fundamental chemical and physical properties of a cell membrane, while avoiding the intrinsic complexity of biological membranes.[9, 10] Such model systems enable the study of membrane proteins in a membrane-like environment without interference from other membrane components.[11-13] Most model membranes also enable the use of a wide range of analytical tools that cannot be used when studying live bacterial cells.[14, 15] Tools that can be applied to model membranes include atomic force microscopy, electrochemical impedance spectroscopy (EIS), surface plasmon resonance, quartz crystal microbalance and neutron scattering.. These tools can provide valuable insight into the mechanism of action of membrane-active drug candidates that would not otherwise be available. While a range of model membrane systems have been developed to date, only few mimic bacterial membranes, most likely due to their complex structure.

In addition to proving a platform that can be used to study the effect of membrane-targeting antibiotics, a realistic model of the outer membrane of GNB might also be used to study membrane proteins, particularly transport proteins and pores. The model membrane provides an environment that closely resembles the natural surroundings of bacterial membrane proteins while also providing easy access to a wide range of analytical tools. A suitable system should provide a reliable and stable platform; high electrical sealing properties are essential when studying ion transport processes across the membrane are studied.[11, 16]

The outer membrane (OM) of gram-negative bacteria contains roughly equal amounts of lipopolysaccharides (LPS), phospholipids and proteins.[17] Unlike other lipid membranes, the OM of gram-negative bacteria is highly asymmetrical. The inner leaflet of the OM is comprised of phospholipids as is typical for a lipid membrane, while the outer leaflet is dominated by LPS,[18] which covers up to 75% of the surface of *e. Coli* cells.[19]

Lipopolysaccharides are large, lipid like-molecules comprised of a hydrophobic core attached to a polysaccharide group and a negatively charged phosphate backbone, collectively known as Lipid A.[20] The highly negative charge on the phosphate backbone of LPS requires the presence of stabilising calcium or magnesium ions. The polysaccharide chain is covalently bound to an O-antigen comprised of oligosaccharide chains of varying lengths. Both the structure of the Lipid A moiety as well as the length and composition of the o-antigen vary significantly between bacterial strains and species.[21] Figure 5.1 shows a general schematic of some LPS molecules. Here, LPS from the *E. coli* J5 mutant (RcLPS) with a medium length sugar chain has been used as a model for most LPS molecules.

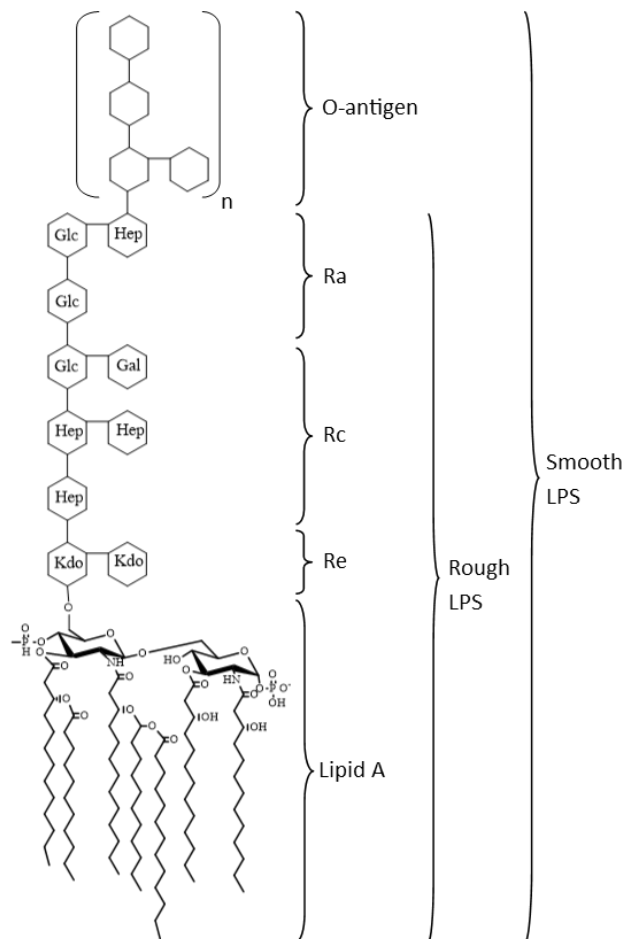


Figure 5.1: General schematic of LPS molecules found in *E. coli*. [22] The Rc strain contains the Lipid A moiety, two Kdo groups, three Hep groups and a single Gal and Glc group. Kdo: 2-keto-3-deoxycyonic acid; Hep: L-glycero-D-manno heptose; Glc: glucose; Gal: galactose.

Very few model membrane systems for GNB have been developed. For example, the outer membrane of GNB was mimicked using a hybrid bilayer comprised of an LPS-monolayer deposited on an alkanethiol surface. [23] The model has been used to show that polymixin B can extract of LPS from the membrane. While being suited for this specific study, the model system does not reflect some essential properties of a lipid bilayer. For example, it only allows only for limited protein incorporation into the membrane, as it lacks a hydrophilic reservoir underneath the membrane to accommodate proteins with sub-membrane domains. Furthermore, the alkanethiol monolayer does not approximate the inner leaflet of the membrane very well, as it is directly bound to a support and therefore highly inflexible.

In a different model system, the asymmetrical membrane structure of the OM was replicated using a Langmuir Blodgett/Langmuir Schaefer transfer of LPS onto a solid support. [22] The removal of the stabilising calcium ions from the LPS head groups caused significant structural changes in the membrane, resulting in a loss of bilayer asymmetry. [24] However, due to the

assembly process membrane proteins could not be incorporated into this bilayer architecture. This problem can be avoided by fusing native bacterial outer membrane vesicles (OMVs) that are created during cell growth into lipid bilayers on a planar glass support,[18] instead of assembling a lipid bilayer from isolated and purified membrane components.

The major disadvantage of solid supported bilayers is their lack of long-term stability,[13] and the complex assembly procedure in the case of films formed by Langmuir-Blodgett techniques. Furthermore, the composition of the membrane cannot be controlled when using bacterial OMVs. There is also often insufficient space between a solid supported membrane and the support, resulting in adverse effects on structure and function of incorporated membrane proteins with extended extramembrane domains.[12, 13]

Tethered bilayer lipid membranes (tBLMs) have been developed as a versatile, robust and stable solid supported model system.[25] In particular, they can provide excellent electrical sealing properties, similar to natural cell membranes.

A tBLM is a lipid bilayer, where the proximal leaflet is formed using a synthetic lipid analogue (anchorlipid) functionalised with a spacer molecule, which provides a cushion between the membrane and the solid support and anchors the membrane covalently to a solid support.[26] The composition of the distal leaflet of the tBLM can be varied depending upon the intended application; different lipids such as 1,2-Diphytanoylphosphatidylcholine (DPhyPC), 1-palmitoyl-2-oleoyl-sn-glycero-3-phosphocholine (POPC), Dipalmitoylphosphatidylcholine (DOPC) or synthetic phospholipids, for example to mimic a cell membrane damaged by oxidative stress.[27, 28]

A tBLM can provide some space underneath the membrane,[29, 30] facilitating the incorporation of larger membrane proteins into the lipid bilayer. Protein incorporation into tBLMs can take place even after bilayer formation has occurred, adding flexibility to the assembly process of the membrane.[31] A wide range of peptides and proteins has been functionally incorporated into tBLM architectures, including pore forming toxins[16], ion transporters[31] and ligand gated ion channels[32, 33]. However, the packing density of the inner leaflet can hinder the incorporation and proper function of complex membrane proteins.

To mitigate this, sparsely tethered tBLMs have been developed with increased membrane fluidity but reduced membrane impedance.[10] Sparsely tethered membranes are formed by either altering the structure of the anchorlipid,[34] or by mixing the anchorlipid with a small molecules such as mercaptoethanol (Figure 5.2). The small molecule competes with the lipid in binding to the gold support, diluting the tethering density of the proximal leaflet.[30] While longevity and membrane impedance of these sparsely tethered systems are reduced[30, 34], they still afford stable and electrically sealing tBLMs.[29, 30].

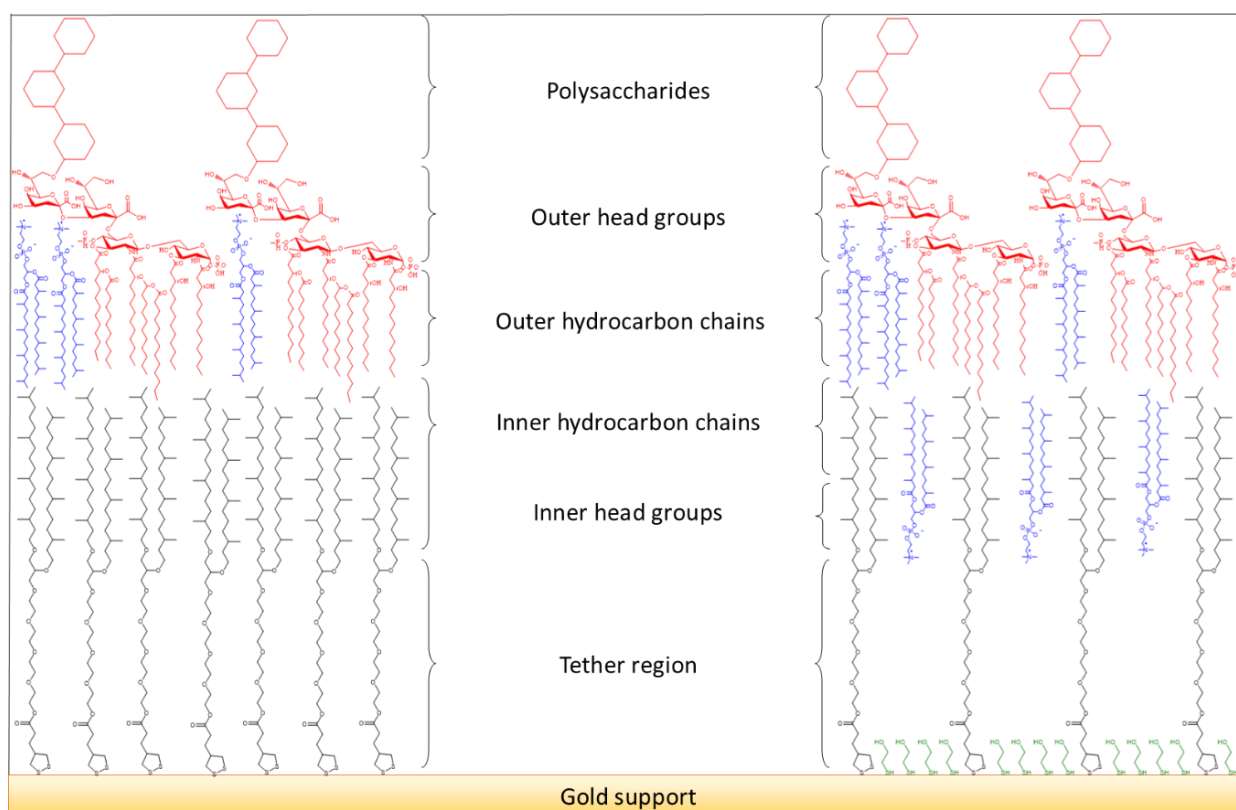


Figure 5.2: Schematics of a fully tethered (left) and sparsely tethered (right) tBLM. The inner leaflet of the sparsely tethered membrane is comprised of a mixture of DPhyTL (black) and mercaptoethanol (green), providing increased water content underneath the membrane to better facilitate the incorporation of membrane proteins into the tBLM. The outer leaflets of both bilayers are comprised of DPhyPC (blue) and LPS (red). The inner head groups are only present in a sparsely tethered tBLM where phospholipids are incorporated into the proximal leaflet during bilayer formation via vesicle fusion.

Here, the tBLM architecture has been adapted to mimic the outer membrane of gram-negative bacteria and the effect of diluting the proximal leaflet on the membrane properties has been systematically investigated. Tethering densities of 60% to 100% of the anchorlipid DPhyTL, diluted with mercaptoethanol have been studied.[30] DPhyTL is a thiolipid analogue modified with a tethering segment containing a disulphide anchor. Its synthesis has been described elsewhere.[35] The distal bilayer leaflet has been completed using RcLPS (Lipopolysaccharides extracted from Rc-strain *E. coli*) mixed with up to 6 mol-% 1,2-diphytanoyl-sn-glycero-3-phosphocholine (DPhyPC). The structural and functional properties of the resulting tBLMs have been analysed using electrical impedance spectroscopy and neutron reflectivity. The model system has then been used to study the effect of the antibiotic Colistin on the membrane.

5.2 Materials and Methods

5.2.1 Chemicals

1,2-diphytanoyl-sn-glycero-3-phosphocholine (DPhyPC) was purchased from Avanti Polar Lipids and was used without further purification. Rc-strain Lipopolysaccharides (Rc-LPS) from the J5 mutant of *E. coli* and colistin sulfate were purchased from Sigma Aldrich and used without further purification. Tail-deuterated DPhyPC was supplied by the National Deuteration Facility located at the Australian Nuclear Science and Technology Organisation in New South Wales, Australia under proposal NDF5829. Ultrapure water (18.2 M Ω cm resistance, obtained from a WaterPro PS reverse osmosis system by Labconco) was used for all experiments.

5.2.2 Bilayer formation

Silicon wafers were cleaned using a 1:1:5 mixture of aqueous NH₃/H₂O₂/MilliQ for 1h at 70°C, rinsed thoroughly with water and ethanol (Sigma Aldrich) and dried under a stream of nitrogen. A 5 nm chromium adhesion layer was deposited by sputter coating (with a current of 100 mA) followed by 20 nm gold (10 mA). The substrates were then rinsed with ethanol and inserted into an 0.1 mM ethanolic solution of a DPhyTL and mercaptoethanol mixture for 18 hours allowing for the formation of a tethered monolayer. The substrates were then removed from the solution and rinsed thoroughly with ethanol and dried under a stream of nitrogen. Bilayers were formed by fusion of vesicles with the pre-formed monolayer.

Vesicles containing various mol-ratios of DPhyPC and RcLPS from *E. coli* at a total concentration of 1 mg/mL were used. Mixtures containing 100%, 98% and 94% RcLPS and 2 or 6% DPhyPC, respectively, were dissolved in chloroform and evaporated under a stream of nitrogen for 15 minutes or until completely dry. 1 mL water was added to the dried lipid film and the lipid-water mixture was sonicated at 45°C for 1h and extruded 30 times through 200nm track-etched polycarbonate filter membranes. The vesicles can be stored at -18° C for later use, but should be extruded prior to each use.

For EIS experiments, 10 μ L/mL vesicles solution was added to the monolayer to an aqueous solution of 100 mM CaCl₂ (bilayer area: 0.283 cm²) and for neutron experiments 200 μ L/mL (due to the increased size of the membrane area of ca. 75 cm²) vesicle solution in 100 mM CaCl₂ was used. Bilayer formation was left to occur for 18h at 25°C and the resulting membranes were rinsed with 5 cell volumes of 100 mM CaCl₂. Colistin sulfate (source) was dissolved in water and incubated with the lipid bilayer for 18h prior to measurements.

5.2.3 Neutron scattering experimental method and data analysis

Neutron experiments were performed at the 20 MW OPAL reactor (Australian Nuclear Science and Technology Research Organisation, Lucas Heights, Sydney NSW).

Specular neutron reflectometry (NR) measurements were performed using the PLATYPUS time-of-flight neutron reflectometer.[36] The platypus instrument uses cold neutrons with wavelengths ranging from 2.5 to 18 Å. The reflected intensity was measured at three glancing angles (0.4°, 0.8° and 4°) under D₂O, H₂O and CM4.5, a mixture of D₂O and H₂O with a combined scattering length density (SLD) of $4.5 \times 10^{-6} \text{Å}^{-2}$, in the presence of 100 mM CaCl₂ for a total of 2 h per contrast. The substrates were prepared as follows: polished circular crystal Silicon discs (10 cm diameter, 1 cm thickness) were coated with 5 nm chromium and subsequently 20 nm gold at the South Australian node of the ANFF. The tBLM was then assembled as described above.

The data gathered at different angles was spliced after reduction (with normalisation to direct beam and background subtraction) and fitted with Motofit, a plugin for IgorPro (available at <https://sourceforge.net/projects/motofit/>).[37] The tBLM system was fitted to a multi-layer model.[38] The SLD of the silicon wafer was fixed at $2.07 \times 10^{-6} \text{Å}^{-2}$ and the SLD of chromium at $3.03 \times 10^{-6} \text{Å}^{-2}$. The SLD of gold was allowed to vary between 4.1 and $4.5 \times 10^{-6} \text{Å}^{-2}$, the SLD of the tether segment was fitted between 0.5 and $2 \times 10^{-6} \text{Å}^{-2}$ and the SLD of the hydrocarbon chains of the inner and outer leaflet was fitted between -0.4 and $0 \times 10^{-6} \text{Å}^{-2}$ for hydrogenous lipid bilayers and between -0.1 and $0.5 \times 10^{-6} \text{Å}^{-2}$ for partially deuterated lipid bilayers. The inner head groups, which approximate either the glycerol segment of the anchor group or the incorporation of some DPhyPC in the lower leaflet of the membrane in the sparsely tethered systems, were fitted with an SLD between 0.5 and $1.5 \times 10^{-6} \text{Å}^{-2}$. The outer head groups were fitted between 1.5 and $4.2 \times 10^{-6} \text{Å}^{-2}$. Colistin Sulfate was estimated to have a neutron SLD of $1.45 \times 10^{-6} \text{Å}^{-2}$ using the Neutron activation and scattering calculator tool provided by NIST[39], and based on an assumed density of 1.36g/cm^3 . [40] Error analysis was performed via Markov Chain Monte Carlo resampling. This method randomly fits the data 1000-10000 times to estimate the error associated with each fit.

Small angle neutron scattering (SANS) experiments were conducted on Quokka using a wavelength of 5 Å for sample to detector distances of 1.3 and 8 m and a wavelength of 8 Å for 20 m. This covered a Q range of 0.001 to 0.5Å^{-1} . To form the vesicles, 10mg of LPS from *Pseudomonas aeruginosa* was dissolved in 1mL D₂O and heated at ~40°C for 1 hour. The suspension was extruded 31 times through a 0.05 µm filter and transferred into quartz cells (Hellma, Müllheim, Germany), with a 1 mm optical path length. For the addition of Colistin, 300 µl of a Colistin solution (10 mg/mL) was added to the extruded vesicles before being transferred into the cells.

The data from different sample to detector lengths were merged into a single file after reduction, which included empty cell subtraction, normalisation to the empty beam and transmissions at 20 m and 8 m. The data was fitted using appropriate models developed by NIST's (National Institute of Standards and Technology) Center for Neutron Research through their macros for the Igor-PRO software [41].

Electrochemical Impedance Spectroscopy: Measurements were performed as discussed elsewhere[42] using an Autolab PGSTAT30 impedance spectrometer. Data were recorded between 3 mHz and 100 kHz with 0V potential vs Ag/AgCl at a 10 mV AC modulation amplitude. Raw data were analysed using ZVIEW (version 3.3B by Scribner Associates) and fitted to an equivalent circuit comprising resistors and constant phase elements (see Figure 4.2 for the circuits used to fit the data and the supplementary information for further details) with final values normalised to an electrode area of 0.283 cm². All measurements were taken under 100 mM NaCl or 100 mM KCl solution. To exchange the electrolyte, the cell was rinsed with five cell volumes of the new electrolyte.

5.3 Results and discussion

5.3.1 Bilayer structure and formation

tBLMs mimicking the membranes of Gram-negative bacteria have been assembled by fusion of LPS vesicles with pre-formed tethered monolayers. Bilayer formation requires the presence of calcium ions as counter ions for the negative charges in the phosphate head groups of LPS.[24] Vesicles were prepared in pure water and added to a 100 mM CaCl₂ solution for bilayer formation at a temperature above 25°C. The concentration gradient between the inside and outside of the vesicle likely provides additional driving force towards vesicle rupture and bilayer formation.

LPS vesicles were produced both by sonication of the lipid mixture and by extrusion. However, sonication alone resulted in highly inconsistent bilayer formation, most likely due to the formation of non-uniform vesicles containing uni- as well as multi-lamellar structures of varying sizes. This resulted in highly variable membrane structures and possibly the formation of multilayers rather than a single bilayer. Extrusion of the vesicles through 200 nm filters after sonication led to the consistent formation of bilayers with reproducible properties.

To study ion transport processes, a membrane resistance of 1-10 MΩ.cm² or higher is desirable.[11, 43] At lower resistances, the large number of defect sites allows for excessive background ion leakage across the bilayer and makes meaningful measurements of changes in membrane resistance difficult. Furthermore, pre-existing defects in the membrane could make it more susceptible to the effects of membrane-damaging compounds which would be undesirable. In such a case, it would be unclear whether the compound in question is damaging intact segments of the lipid bilayer or pre-existing defects. Bilayers containing a wide range of mixtures of DPhyPC and RcLPS could be formed on a 100% DPhyTL monolayer, but sparsely tethered inner leaflets comprised of 80% DPhyTL or less imposed some limitations on the composition of the membrane.

While lipid bilayers comprised of only DPhyPC formed sealing membranes at tethering densities as low as 60%,[30] bilayers comprised exclusively of LPS did not form on these tethering architectures. Vesicles containing 98% LPS and 2% DPhyPC formed low-quality bilayers via vesicle fusion at 60% tethering density (data not shown). Instead of further lowering the tethering density, 80% DPhyTL monolayer were used. High quality membranes from vesicles containing 94, 98 and 100% LPS could be formed on the small surface areas used in EIS, and bilayers containing 2-6% DPhyPC also formed on the larger substrates used for neutron scattering. Increasing the DPhyPC content in bilayers on 80% tethering densities above 6% resulted in poor quality membranes. Membranes with 100% LPS on 80% tethering densities were only analysed electrically, since this system does not represent a biomimetic system. As LPS is significantly larger than DPhyPC is unlikely, that the gaps in the monolayer

can be filled by LPS molecules. Their incorporation into the proximal leaflet of the membrane would likely result in an unstable assembly and an increase in the roughness of the inner leaflet of the membrane. Specific values for the resistance and capacitance of the membrane architectures under investigation are shown in Table 5.2 and Table 5.3, respectively. The structures of the various LPS-tBLM architectures were analysed at a sub-nanometer level using neutron scattering. The neutron data were fitted to a model using a number of “slabs” (Figure 5.2), each with a distinct thickness (given in Å), scattering length density (SLD, given in 10^{-6} \AA^{-2}), hydration (in volume-%) and roughness with respect to the preceding layer (in Å).

The exact composition of mixed LPS/DPhyPC layers can be determined by using the difference in SLD for tail-deuterated DPhyPC ($6.6 \times 10^{-6} \text{ \AA}^{-2}$ [44]) and the tails of non-deuterated LPS and the hydrocarbon chains of DPhyTL of $-0.39 \times 10^{-6} \text{ \AA}^{-2}$. [24, 30]

For example, the hydrocarbon segment of a membrane leaflet comprised exclusively of hydrogenous lipid tails has an average SLD of $-0.4 \times 10^{-6} \text{ \AA}^{-2}$. The introduction of 5% deuterated DPhyPC into the membrane will increase the SLD to $-0.05 \times 10^{-6} \text{ \AA}^{-2}$. Thus, even the presence of small percentages of DPhyPC in the lipid bilayer are easily visible by neutron scattering. Differences between theoretical and experimental predictions might be due to a relatively high uncertainty in the molecular weight of the LPS molecules, as their structure varies considerably even among the same bacterial strain.

Membranes with various DPhyTL/LPS ratios were formed on fully tethered and sparsely tethered monolayers (Table 5.1). Regardless of vesicle composition and tethering density, high quality bilayers with low defect densities and completion levels exceeding 95% were formed.

The hydration of the tether region of fully tethered tBLMs was around 5-9%, which is in good agreement with previously reported data. [34] The highest tether hydration of 9.3% for the fully tethered LPS bilayer comprised of 98% LPS was concurrent with an increased hydration of the inner and outer hydrocarbon chains of 5.5% and 4%, respectively. It is likely that the higher level of tether hydration is a result of slightly higher defect density in that particular sample as the hydration of the hydrocarbon segments should ideally be below 2%. [30, 34]

In the sparsely tethered architectures, the hydration of the tether region increased to around 10%. An additional layer was added to the model for sparsely tethered LPS-tBLMs to account for the head groups of DPhyPC incorporated into the proximal leaflet. The inner head groups had hydration levels of 10-17% and an SLD around $1.5 \times 10^{-6} \text{ \AA}^{-2}$. The increased hydration of the tether region did not cause the formation of defects in the bilayers, as seen by the constant hydration levels of the hydrocarbon chains in the inner (2%) and outer (2-3%) leaflets.

Table 5.1: Selected fitting parameters for fully and sparsely tethered LPS-tBLM architectures. Thickness and roughness values are given in Å, SLDs are given in 10^{-6}\AA^{-2} and hydration levels are given in volume-%. Errors are given as one standard deviation determined by Monte Carlo calculations. See Figures S1-S5 and Tables S1 and S2 in the supplementary information for graphs of the reflectivity plots, SLD profiles and for a full set of fitting parameters.

	100% DPhyTL, 100% LPS	100% DPhyTL, 98% LPS	100% DPhyTL, 94% LPS	80% DPhyTL, 98% LPS	80% DPhyTL, 94% LPS
Tether thickness	14.0 ± 1.1	12.2 ± 0.2	12.5 ± 0.4	8.3 ± 0.2	6.4 ± 0.3
Tether SLD	1.0 ± 0.3	1.1 ± 0.1	0.7 ± 0.1	1.0 ± 0.3	1.1 ± 0.2
Tether hydration	6.4 ± 1.0	9.3 ± 0.6	5.6 ± 1.5	11.1 ± 2.5	11.1 ± 2.3
Tether roughness	6.4 ± 0.9	3.2 ± 0.2	4.3 ± 0.2	4.8 ± 0.4	4.5 ± 0.7
Inner head group thickness				6.3 ± 0.2	6.3 ± 0.3
Inner head group SLD				1.3 ± 0.3	1.6 ± 0.7
Inner head group hydration				17.4 ± 2.7	10.1 ± 3.4
Inner head group roughness				8.0 ± 1.5	7.5 ± 1.9
Inner hydrocarbon chain thickness	15.9 ± 1.2	12.3 ± 0.2	13.1 ± 0.6	10.1 ± 0.8	12.6 ± 0.5
Inner hydrocarbon chain SLD	-0.3 ± 0.1	-0.3 ± 0.0	-0.3 ± 0.1	0.2 ± 0.01	0.3 ± 0.1
Inner hydrocarbon chain hydration	2.1 ± 1.1	5.5 ± 0.4	1.3 ± 0.9	1.8 ± 1.1	2.4 ± 1.4
Inner hydrocarbon chain roughness	5.9 ± 1.5	4.6 ± 1.0	6.2 ± 1.3	4.5 ± 0.4	4.0 ± 0.9
Outer hydrocarbon chain thickness	16.0 ± 1.2	12.2 ± 0.2	12.8 ± 0.5	15.7 ± 1.0	12.6 ± 0.5
Outer hydrocarbon chain SLD	-0.3 ± 0.0	-0.1 ± 0.0	0.1 ± 0.1	0.01 ± 0.01	0.4 ± 0.1
Outer hydrocarbon chain hydration	2.2 ± 0.8	4.1 ± 0.7	2.8 ± 1.8	2.2 ± 1.2	2.8 ± 1.3
Outer hydrocarbon chain roughness	6.6 ± 1.8	6.6 ± 1.8	6.7 ± 1.5	6.4 ± 1.4	6.1 ± 1.8
Outer head group thickness	8.4 ± 0.3	9.4 ± 0.8	7.3 ± 0.9	7.3 ± 0.3	13.8 ± 2.7
Outer head group SLD	2.8 ± 0.4	3.2 ± 0.3	3.3 ± 0.4	2.1 ± 0.01	2.6 ± 0.5
Outer head group hydration	60.2 ± 3.7	72.8 ± 1.7	69.3 ± 3.9	63.8 ± 1.0	78.4 ± 5.0
Outer head group roughness	3.4 ± 0.2	6.8 ± 0.5	4.5 ± 0.4	5.4 ± 0.5	7.3 ± 0.9

The fully tethered bilayers had inner hydrocarbon chain leaflets with SLDs of around $-0.3 \times 10^{-6} \text{Å}^{-2}$, confirming that incorporation of deuterated phospholipids into a densely packed proximal leaflet is not possible. In sparsely tethered LPS-tBLMs, the SLDs of the inner hydrocarbon chains of $0.2-0.3 \times 10^{-6} \text{Å}^{-2}$ suggest incorporation of around 10% deuterated DPhyPC into the proximal leaflet. The similarity between the roughness of the inner hydrocarbon chain segment of the fully and sparsely tethered architectures (around 4-6 Å in all cases) indicates that no LPS was able to incorporate into the proximal leaflet of the sparsely tethered membrane architecture.

In the fully tethered systems, the composition of the outer leaflets was in good agreement with the vesicle composition. With an increasing amount of DPhyPC in the vesicles, the SLD of the outer leaflets increased from $-0.3 \times 10^{-6} \text{Å}^{-2}$ to $-0.1 \times 10^{-6} \text{Å}^{-2}$ at 98% RcLPS content and from $-0.3 \times 10^{-6} \text{Å}^{-2}$ to $0.1 \times 10^{-6} \text{Å}^{-2}$ when the vesicles contained 94% RcLPS. Based on these SLDs, the distal leaflets contained 2% DPhyPC and 6% DPhyPC, respectively. The outer leaflets of the sparsely tethered LPS tBLMs contained around 6% and 10% DPhyPC, also in good correlation with the composition of the vesicles. The small differences between the composition of the vesicles and that of the membrane are likely the results of membrane inhomogeneity. Due to the time and preparation required for neutron scattering experiments, it is not possible to repeatedly examine the correlation between vesicle – and bilayer composition to determine whether there is any variation. The purpose of this study was primarily to determine whether DPhyPC would be present in the tBLM if it was added during vesicle preparation.

In previous experiments using floating lipid bilayers, it has been shown that removal of the calcium ions from the bilayer structure leads to significant structural changes in the membrane, including the transitioning of lipids between membrane leaflets.[24] However, rinsing the tBLM structures with EDTA in order to remove any calcium ions did not result in structural changes that were detectable *via* neutron scattering, regardless of membrane composition and tethering densities (data not shown). The more rigid tBLM architecture, compared to supported bilayer membranes, most likely results in a more compact lipid packing and tethering also reduces membrane fluidity, thus decreasing the likelihood of significant deformations of the membrane.

5.3.2 Electrical characterisation of the membranes

To see more subtle structural changes not visible to neutron scattering, the membranes were studied by EIS (Figure 5.3 & Tables 5.2 & 5.3). Bilayers were characterised by fitting frequency dependent impedance and phase shift data with an equivalent circuit composed of resistive and capacitive elements.[34, 45] The electrical properties of the lipid bilayer are represented by a resistor and a capacitor in parallel. A completely defect-free lipid membrane would act purely as a capacitor, but charge transport can take place across the bilayer through defects in the membrane. These defects are modelled by the membrane resistance. A lipid bilayer is

thus comprised of both capacitive and resistive circuit elements. An increase in membrane defects will be seen as a decrease in membrane resistance. All tBLM systems showed good electrical sealing properties in the M Ω -range, confirming the formation of well-sealed membranes.[34]

Fully tethered LPS-tBLMs had very high resistances in the range of 20-60 M Ω .cm², while sparsely tethered tBLMs with 80% DPhyTL had reduced resistances around 1-4 M Ω .cm², similar to previously published results.[16, 46]. The lower resistance is most likely due to the increased fluidity of sparsely tethered membranes which favours increased defect formation.[10] Changing the amount of LPS in the bilayer did not have a significant impact on bilayer sealing properties in either sparsely or fully tethered membrane architectures. To discriminate between effects of rinsing and calcium removal on the membrane properties, all membranes were rinsed with and measured under NaCl prior to being exposed to EDTA. Rinsing with NaCl led to a slight reduction in the membrane impedance for all tether density/membrane compositions (up to a factor of 10), however, this effect is also seen on DPhyPC bilayers (see supplementary information) and is probably due to the decreased ability of divalent cations to cross the hydrophobic membrane interior rather than to structural changes of the membrane.

At 100% tethering density, rinsing of the membrane system with EDTA had no significant impact on either the resistance or capacitance of the bilayer, regardless of the composition of the outer leaflet. The rigid structure of a fully tethered LPS-tBLMs most likely prevents the significant structural rearrangements due to calcium removal by EDTA seen in free-floating LPS bilayers.[24] Similarly, mixing of lipids between the outer and inner leaflet of the bilayer is unlikely in a tethered membrane architecture. This is also confirmed by the fact that the capacitance of the membranes remained fairly constant.

At 80% tethering density, and for membrane containing 100% LPS in the outer leaflet, the resistance decreased by three orders of magnitude upon removal of the calcium ions, suggesting that this architecture is very prone to defect formation. When small amounts of DPhyPC were incorporated into the sparsely tethered membrane architecture, this effect could no longer be observed. As seen from the neutron data, the DPhyPC molecules can integrate into the proximal leaflet of the bilayer, thus leading to a better packing density a more stable membrane. The addition of DPhyPC also reduces the negative charges in the membrane, making it less susceptible to changes upon ion removal.

In all cases, the changes in the electrical properties of membrane were fully reversible. It therefore appears that no LPS or phospholipid were removed from the membrane as a result of rinsing the bilayer with EDTA. In some cases, restoring CaCl_2 to the system after rinsing with EDTA resulted in slightly increased membrane impedance. Structural rearrangements upon restoring calcium to the system might have allowed for slightly improved lipid packing and a small reduction in defect density.

To use these bilayer architectures for the incorporation of membrane proteins, the increased packing density could present a challenge. This would be the case particularly if the proteins were added to pre-formed lipid bilayers. However, the membrane is quite susceptible to cation removal at 80% tethering density, suggesting that a reduction in tethering density could solve this problem. As an alternative to pre-formed lipid bilayers, it may also be possible to form protein-functionalised lipid bilayers by incorporating the proteins into the vesicles used to form the lipid bilayer. It is possible that intact membranes can form on lower tethering densities on which bilayers comprised only of LPS-phospholipid mixtures cannot easily form if proteins were added to the lipid bilayer.

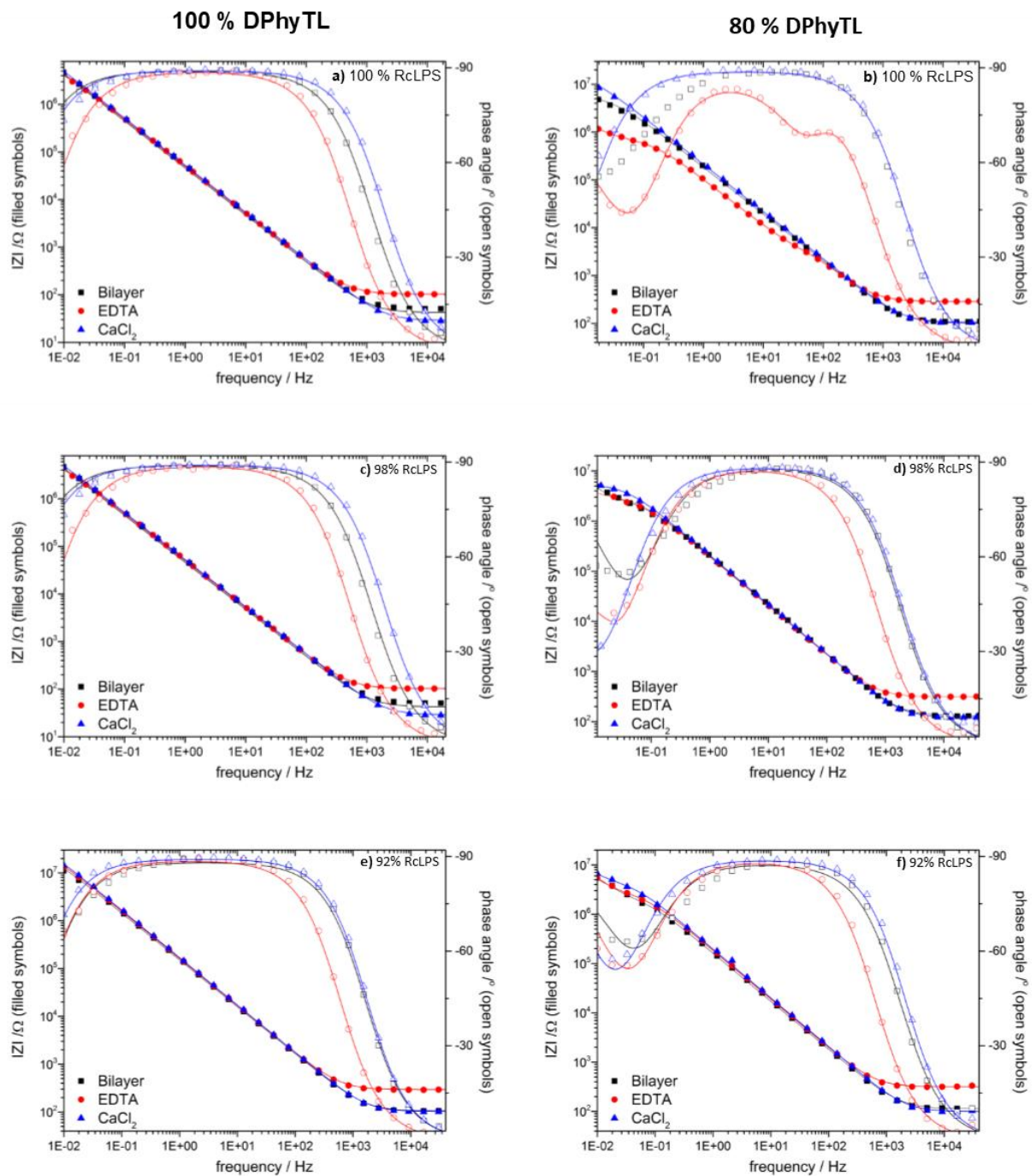


Figure 5.3: Bode plots of impedance data resulting from the cycling of electrolytes of various membrane architectures. Graphs on the left are of bilayers assembled on 100% DPhyTL and graphs on the right were assembled on 80% DPhyTL diluted with 20 mol-% mercaptoethanol. See individual graphs for details on the composition of the outer leaflets. Symbols represent experimental data and lines represent fitted data. Filled symbols represent impedance and empty symbols represent phase angle. See supplementary information for details on the circuits used to model each data set.

Table 5.2: Resistance of lipid bilayers of various compositions in response to electrolyte changes. All values are in $M\Omega\text{cm}^{-2}$. The errors are the values returned by the fitting program. Membrane resistance is modelled based on 2-4 data points at the lowest frequencies of the spectrum, hence the measurements are likely less accurate than the error value of the fitting program suggests in most cases, enabling only a qualitative interpretation of the data. Only the values for the lipid bilayer are shown. The full set of fitting data can be found in the supplementary information.

	100% Tether				80% tether			
	100% LPS	98% LPS	94% LPS	100% DPhyPC	100% LPS	98% LPS	94% LPS	100% DPhyPC
Bilayer (CaCl ₂)	26.2 ± 18.4	58.8 ± 4.15	31.1 ± 2.08	92.3 ± 5.22	3.52 ± 0.49	1.75 ± 0.22	1.24 ± 0.45	3.48 ± 0.83
NaCl	11.6 ± 0.42	34.9 ± 2.29	37.4 ± 2.05	10.7 ± 3.57	1.73 ± 0.12	1.01 ± 0.21	0.22 ± 0.04	1.79 ± 0.24
EDTA	8.33 ± 0.65	28.1 ± 1.38	34.4 ± 1.77		0.001 ± 0.0001	0.74 ± 0.07	1.88 ± 0.61	
CaCl ₂	23.6 ± 1.6	66.3 ± 4.37	50.6 ± 3.04		17.53 ± 0.81	4.89 ± 0.27	3.37 ± 1.11	

Table 5.3: Capacitance (in μFcm^{-2}) of lipid bilayers of various compositions in response to electrolyte changes. The errors are the range of values that could be fitted without decreasing the quality of the fit. Only the values the lipid bilayer are shown. The full set of fitting data can be found in the supplementary information.

	100% Tether				80% Tether			
	100% LPS	98% LPS	94% LPS	100% DPhyPC	100% LPS	98% LPS	94% LPS	100% DPhyPC
Bilayer (CaCl ₂)	0.9 ± 0.001	0.79 ± 0.01	1.09 ± 0.02	1.28 ± 0.35	1.25 ± 0.06	1.11 ± 0.6	1.66 ± 0.23	1.06 ± 0.22
NaCl	0.96 ± 0.01	0.78 ± 0.01	1.03 ± 0.02	0.84 ± 0.01	1.25 ± 0.09	1.20 ± 1.05	1.47 ± 0.13	1.15 ± 0.1
EDTA	0.91 ± 0.01	0.75 ± 0.01	1.00 ± 0.01		1.24 ± 0.23	0.98 ± 0.06	1.22 ± 0.18	
CaCl ₂	0.87 ± 0.01	0.71 ± 0.01	0.96 ± 0.01		0.77 ± 0.01	0.86 ± 0.05	1.12 ± 0.19	

5.3.3 Interaction of Colistin Sulfate with the model membranes

Aside from studying the structural aspects of a membrane mimicking a bacterial cell wall, it is interesting to investigate the behaviour of these membrane architectures when exposed to antibiotics. This will improve understanding of the mechanism of action of the antibiotic and might also lead to the development of a screening platform for potential new drugs.

Here, Colistin Sulfate, an antimicrobial peptide belonging to the polymyxin family, was used as it is one of only a small number of antibiotics directly targeting the membrane of GNB. Studies using a vesicle-based model of gram negative bacteria have shown that at low concentrations polymyxins promote inter-vesicle contact and lipid exchange between vesicles.[47] At higher concentrations, the antibiotics insert deeply into the membrane, increasing the packing density of the lipid. In addition, unspecific lipid mixing between leaflets and defect formation followed by leakage of cell contents has been observed at higher concentrations. Polymyxins seem to also promote contact and lipid exchange between the outer and inner membrane of gram-negative bacteria by acting as a solubilising agent, resulting in the extraction of lipids from the membrane into an aqueous environment.[48]

Initially, the effect of Colistin on LPS vesicles was studied by small angle neutron scattering. Prior to exposure to Colistin, the LPS vesicles had a unilamellar structure as no Bragg peaks resulting from the regular spacing of lipid layers in multilamellar vesicles were visible. The data was modelled using a three-shell smeared model, with an overall vesicle diameter of 120nm. After the addition of Colistin, the formation of a more ordered structure could be observed (see Figure S6 in the supporting information). These structures are most likely multilamellar vesicle with Bragg peaks occurring at $q=0.064$ and $q=0.107 \text{ \AA}^{-1}$. The first peak has a calculated d-spacing of 58 \AA^{-1} , which is in good agreement with literature.[49] The second peak can be attributed to a second order reflection. Additionally, the increased scattering intensity at low q , paired with a lack of an intensity plateau suggests the formation of larger particles or vesicle aggregates.[49, 50].

For a more detailed analysis of the drug-LPS interactions, the newly developed LPS-tBLM architectures were exposed to Colistin and changes in the electrical and structural properties of the membranes upon drug exposure were studied *via* neutron reflectivity and EIS (Figure 5.4 and Table 5.7). In NR experiments, structural changes to the membranes occurred over a period of 6-8 hours. The experimental data was fitted to the same layer models as before (Table 5.4 and 5.5). Colistin is most likely to affect mainly the outermost layers of the membrane as the inner leaflet is covalently bound to the solid support. The parameters for the inner membrane architecture (up to the inner hydrocarbon chains, see Figure 5.2) were therefore held constant.

Table 5.4: Parameter changes of fully tethered LPS-tBLMs (100% DPhyTL) exposed to Colistin Sulfate. Thickness and roughness are given in Å, SLD is given in 10^{-6}Å^{-2} and hydration is given in volume-%. Errors are given as one standard deviation determined by Monte Carlo calculations. See supplementary information for graphs of the reflectivity plots, SLD profiles and for a full set of fitting parameters.

	100% LPS		98% LPS		94% LPS	
	Bilayer	Colistin Addition	Bilayer	Colistin Addition	Bilayer	Colistin Addition
Outer hydrocarbon chain thickness	16.0 ± 1.2	16.3 ± 1.1	12.2 ± 0.2	12.5 ± 0.0	12.8 ± 0.5	12.4 ± 0.1
Outer hydrocarbon chain SLD	-0.3 ± 0.04	-0.4 ± 0.004	-0.1 ± 0.04	0.01 ± 0.05	0.12 ± 0.07	-0.05 ± 0.04
Outer hydrocarbon chain hydration	2.2 ± 0.8	0.1 ± 0.1	4.1 ± 0.7	4.5 ± 0.4	2.8 ± 1.8	1.4 ± 0.9
Outer hydrocarbon chain roughness	6.6 ± 1.8	7.7 ± 1.5	6.6 ± 1.8	7.0 ± 1.9	6.7 ± 1.5	6.8 ± 1.8
Outer head group thickness	8.4 ± 0.3	8.0 ± 0.1	9.4 ± 0.8	8.1 ± 0.1	7.3 ± 0.9	8.5 ± 0.1
Outer head group SLD	2.8 ± 0.4	2.1 ± 0.1	3.2 ± 0.3	2.2 ± 0.2	3.3 ± 0.4	2.3 ± 0.1
Outer head group hydration	60.2 ± 3.7	10.6 ± 0.5	72.8 ± 1.7	34.1 ± 0.7	69.3 ± 3.9	24.5 ± 2.7
Outer head group roughness	3.4 ± 0.2	3.1 ± 0.1	6.8 ± 0.5	6.9 ± 0.6	4.5 ± 0.4	3.6 ± 0.4

In all fully tethered LPS-tBLMs (Table 5.4), Colistin exposure led to a significant decrease in the hydration of the head groups. The most significant change in hydration occurred in a 100% LPS membrane, where the hydration decreased six-fold from 60% to 10%. This indicates a strong binding of the colistin molecule to the headgroup region, displacing the water molecules, as also indicated by the reduction in the head group SLD. The effect was less pronounced for lower LPS contents, as this results in fewer binding sites for colistin.

While the head group hydration changed, the hydration of the outer hydrocarbon chains remained fairly constant, showing that the binding of Colistin to the head groups did not cause any structural changes or defects within the lipid bilayer.

In sparsely tethered LPS-tBLMs, the exposure to colistin resulted in addition to the change in the headgroup hydration in a significant change in the roughness of the outer hydrocarbon chains from 6 Å to 14 – 19 Å (Table 5.5). The roughness exceeded the thickness of the layers themselves, showing significant structural disturbances of the outer leaflet. This is in accordance with the change from uni- to multilamellar vesicles observed in the small angle experiment. The tBLM systems are more stable than vesicles, thus the changes are less pronounced. The hydration of the membrane leaflets also remained constant on the sparsely tethered architectures, suggesting that no membrane defects were formed.

Table 5.5: Parameter changes of sparsely tethered LPS-tBLMs (80% DPhyTL, 20% mercaptoethanol) exposed to Colistin Sulfate. Thickness and roughness are given in Å, SLD is given in 10^{-6}Å^{-2} and hydration is given in volume-%. Errors are given as one standard deviation determined by Monte Carlo calculations. See supplementary information for graphs of the reflectivity plots, SLD profiles and for a full set of fitting parameters.

	98% LPS		94% LPS	
	Bilayer	Colistin Addition	Bilayer	Colistin Addition
Outer hydrocarbon chain thickness	15.7 ± 0.96	8.92 ± 2.8	12.6 ± 0.46	13.7 ± 0.82
Outer hydrocarbon chain SLD	0.01 ± 0.01	0.02 ± 0.55	0.41 ± 0.13	0.68 ± 0.09
Outer hydrocarbon chain hydration	2.24 ± 1.21	2.55 ± 2.54	2.83 ± 1.25	4.62 ± 1.73
Outer hydrocarbon chain roughness	6.35 ± 1.44	13.8 ± 3.47	6.13 ± 1.81	19 ± 2.50
Outer head group thickness	7.34 ± 0.27	10.2 ± 2.81	13.8 ± 2.66	15.8 ± 0.20
Outer head group SLD	2.05 ± 0.04	1.95 ± 0.6	2.57 ± 0.53	2.33 ± 0.15
Outer head group hydration	63.8 ± 0.98	47.1 ± 18.0	78.4 ± 5.04	62.2 ± 3.21
Outer head group roughness	5.43 ± 0.51	5.37 ± 2.3	7.26 ± 0.93	4.40 ± 0.34

To complement the neutron studies, EIS studies of tBLMs exposed to Colistin were performed on both fully and sparsely tethered bilayers. While changes in the neutron data were typically completed after an incubation period of 6-8 hours, changes in the EIS data could be seen over 18-48 hours. For the neutron experiments, membranes with a much higher surface area are required, which most likely leads to an increased number of membrane defects, making the membranes more susceptible to the effect of Colistin.

Table 5.6: Resistance (in $M\Omega \cdot \text{cm}^2$) of various bilayer architectures before and after being exposed to 10 or 20 mg/mL Colistin Sulfate. The errors are the range of values that could be fitted without decreasing the quality of the fit. Only the values for the lipid bilayer are shown. The full set of fitting data can be found in the supplementary information.

	100% Tether			80% Tether		
	100% LPS	98% LPS	94% LPS	100% LPS	98% LPS	94% LPS
Bilayer (CaCl ₂)	138 ± 13.5	102 ± 11.6	101 ± 10.1	5.71 ± 0.0001	1.75 ± 0.22	1.24 ± 0.45
10 mg/mL Colistin 18 h	197 ± 29.4	91.0 ± 19.0	73.4 ± 7.41	0.01 ± 0.000002	4.19 ± 1.77	2.26 ± 0.35
10 mg/mL Colistin 48 h	120 ± 15.3	83.6 ± 18.7	76.3 ± 1.85			
20 mg/mL Colistin 48 h	108 ± 2.3	71.6 ± 18.5	71.6 ± 18.5			

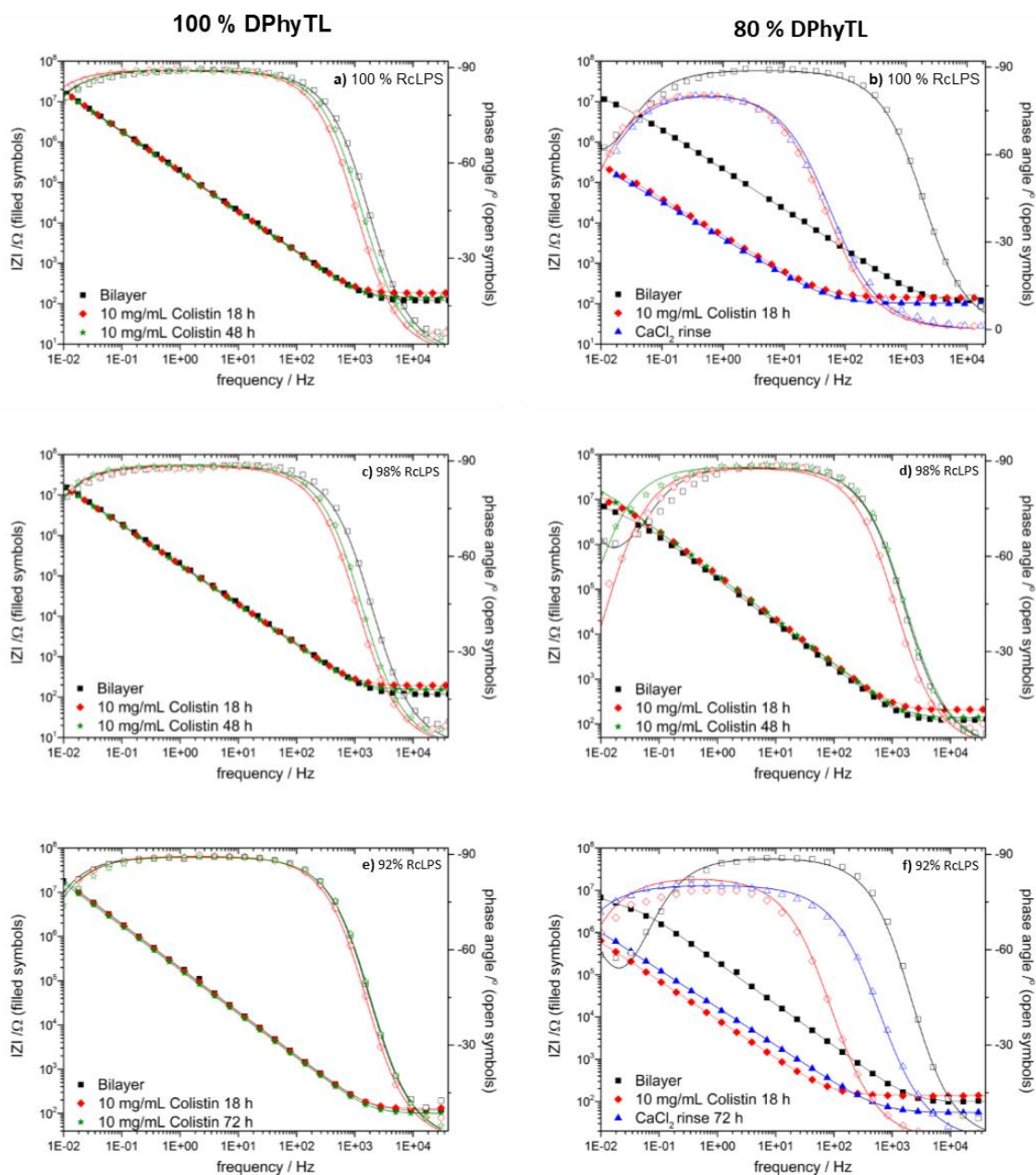


Figure 5.4: EIS data of various membrane architectures at 100% and 80% tethering density after exposure to 10 mg/mL colistin Sulfate for varying periods of time. Graphs on the left are of bilayers assembled on 100% DPhyTL and graphs on the right were assembled on 80% DPhyTL diluted with 20 mol-% mercaptoethanol. See individual graphs for details on the composition of the outer leaflets. Symbols represent experimental data and lines represent fitted data. Filled symbols represent impedance and empty symbols represent phase angle. See supplementary information for details on the circuits used to model each data set.

The resistance or capacitance of fully tethered membranes was unaffected by the addition of Colistin, regardless of the composition of the outer membrane leaflet (Figure 5.4 & Table 5.6). This is in good agreement with the lack of structural changes or defect formation seen in neutron scattering. The fully tethered membranes offer a very robust and stable platform, as previously reported.[25] While this system is too robust to serve as a platform for the study of membrane-damaging antibiotics, it could provide a highly sealing platform to study bacterial pore- and transport proteins.

At 80% tethering density and 100% LPS in the outer leaflet, exposure to 10 mg/mL Colistin sulfate for 18 hours reduced the membrane resistance by two orders of magnitude. For lower LPS contents, there was no significant change in the membrane resistance. This correlates with neutron data showing no increase in water-filled membrane defects, suggesting that there was no formation of additional pathways for charge transport across the membrane. As seen before, a membrane containing 100% LPS on a sparsely tethered monolayer is less stable than bilayers containing small amounts of DPhyPC, and therefore more susceptible to the removal of calcium ions as well as to the effect of drugs.

There was, however, a large and irreversible increase in the capacitance of bilayers containing 100% and 94% RcLPS (Table 5.7). The capacitance $C = \epsilon_r \epsilon_0 \frac{A}{d}$ depends on its dielectric constant ϵ_r , the area A and thickness d of the membrane. The three-fold increase in membrane roughness of the bilayer comprised of 94% LPS observed in the neutron data corresponds to an increase in membrane thickness and active area. This results most likely caused the large capacitance change observed in the EIS data. The smaller change in membrane roughness of the bilayer containing 98% LPS is in good agreement with the lack of change in the electrical properties of a bilayer with the same composition.

The article “Colistin: An Update on the Antibiotic of the 21st Century” (https://www.medscape.com/viewarticle/772588_4, accessed 05/12/18) by Biswas *et al* notes that the typical clinical dosage of Colistin is 2.5 – 5 mg/Kg. While this is far lower than the concentrations used here, it is difficult to estimate the concentration of antibiotic that bacteria are exposed to when the patient receives this dosage. This platform provides the opportunity to carry out proof-of-principle studies where the effect of Colistin on the membrane is examined and does not provide a detailed replicate of the environment in which the antibiotic is ultimately used. However, it is able to determine whether the drug candidate can damage a lipid membrane and should undergo further clinical evaluation. In addition, due to their simplicity and because they provide a controlled environment, model systems can provide insight into the fundamental biophysical process that occurs during the interaction between the drug and a lipid membrane.

Table 5.7: Capacitance (in $\mu\text{F}\cdot\text{cm}^{-2}$) of various bilayer architectures before and after being exposed to 5 or 10 mg/mL Colistin Sulfate. All values given. The errors are the values for each parameter that can be fitted without decreasing the quality of the fit. Only the values for the lipid bilayer are shown. The full set of fitting data can be found in the supplementary information

	100% Tether			80% Tether		
	100% LPS	98% LPS	94% LPS			
Bilayer (CaCl ₂)	0.8 ± 0.01	0.8 ± 0.01	0.81 ± 0.01	1.16 ± 0.67	3.14 ± 0.45	1.66 ± 0.23
10 mg/mL Colistin 18 h	0.9 ± 0.011	0.8 ± 0.01	0.85 ± 0.004	38.23 ± 0.18	3.02 ± 1.88	20.93 ± 0.45
10 mg/mL Colistin 48 h	0.9 ± 0.01	0.8 ± 0.01	0.93 ± 0.004			
20 mg/mL Colistin 48 h	0.9 ± 0.003	0.8 ± 0.01				

5.4 Conclusion

A tethered bilayer membrane architecture has been developed with the distal leaflet mimicking the outer membrane of Gram-negative bacteria. By varying lipid composition and tethering density, membranes with different properties can be achieved, ranging from very stably, highly resistive bilayers, to membranes, that are more susceptible to damage by antibiotics. Namely membranes with 80% tethering density and 100% or 94% LPS and 4% DPhyPC were significantly affected by colistin sulfate, with especially the outer leaflet of the lipid bilayer being damaged. These architectures might thus be used as a screening platform for potential antimicrobial agents, while the more stable architectures can be functionalised by incorporation of ion channel proteins and the high resistance of the membranes will allow analysis of ion transport phenomena.

5.5 References

1. *Antimicrobial Resistance*. World Health Organisation Website 2015 [cited 2016 01/02/2016]; Available from: <http://www.who.int/mediacentre/factsheets/fs194/en/>.
2. Vasoo, S., J.N. Barreto, and P.K. Tosh, *Emerging Issues in Gram-Negative Bacterial Resistance: An Update for the Practicing Clinician*. Mayo Clinic Proceedings, 2015. **90**(3): p. 395-403.
3. Brown, L., et al., *Through the wall: extracellular vesicles in Gram-positive bacteria, mycobacteria and fungi*. Nat Rev Micro, 2015. **13**(10): p. 620-630.
4. Delcour, A.H., *Outer Membrane Permeability and Antibiotic Resistance*. Biochimica et biophysica acta, 2009. **1794**(5): p. 808-816.
5. Tenover, F.C., *Mechanisms of antimicrobial resistance in bacteria*. American Journal of Infection Control, 2006. **34**(5): p. S3-S10.
6. Sahalan, A.Z. and R.A. Dixon, *Role of the cell envelope in the antibacterial activities of polymyxin B and polymyxin B nonapeptide against Escherichia coli*. International Journal of Antimicrobial Agents, 2008. **31**(3): p. 224-227.
7. Clausell, A., et al., *Gram-Negative Outer and Inner Membrane Models: Insertion of Cyclic Cationic Lipopeptides*. The Journal of Physical Chemistry B, 2007. **111**(3): p. 551-563.
8. Lam, S.J., et al., *Combating multidrug-resistant Gram-negative bacteria with structurally nanoengineered antimicrobial peptide polymers*. Nature Microbiology, 2016. **1**: p. 16162.
9. Jackman, J.A., W. Knoll, and N.J. Cho, *Biotechnology Applications of Tethered Lipid Bilayer Membranes*. Materials, 2012. **5**(12): p. 2637-2657.
10. Andersson, J. and I. Köper, *Tethered and Polymer Supported Bilayer Lipid Membranes: Structure and Function*. Membranes, 2016. **6**(2): p. 30.
11. Koper, I., *Insulating tethered bilayer lipid membranes to study membrane proteins*. Molecular Biosystems, 2007. **3**(10): p. 651-657.
12. Boxer, S.G., *Molecular transport and organization in supported lipid membranes*. Current Opinion in Chemical Biology, 2000. **4**(6): p. 704-709.
13. Castellana, E.T. and P.S. Cremer, *Solid supported lipid bilayers: From biophysical studies to sensor design*. Surface Science Reports, 2006. **61**(10): p. 429-444.
14. Wiebalck, S., et al., *Monitoring the Transmembrane Proton Gradient Generated by Cytochrome bo 3 in Tethered Bilayer Lipid Membranes Using SEIRA Spectroscopy*. The Journal of Physical Chemistry B, 2016. **120**(9): p. 2249-2256.
15. Zieleniecki, J.L., et al., *Cell-free synthesis of a functional membrane transporter into a tethered bilayer lipid membrane*. Langmuir, 2016. **32**(10): p. 2445-2449.
16. Vockenroth, I.K., et al., *Incorporation of alpha-hemolysin in different tethered bilayer lipid membrane architectures*. Langmuir, 2008. **24**(2): p. 496-502.
17. Lugtenberg, B. and L. Van Alphen, *Molecular architecture and functioning of the outer membrane of Escherichia coli and other gram-negative bacteria*. Biochimica et Biophysica Acta (BBA)-Reviews on Biomembranes, 1983. **737**(1): p. 51-115.
18. Hsia, C.-Y., et al., *A Molecularly Complete Planar Bacterial Outer Membrane Platform*. Scientific Reports, 2016. **6**: p. 32715.
19. Caroff, M. and D. Karibian, *Structure of bacterial lipopolysaccharides*. Carbohydrate Research, 2003. **338**(23): p. 2431-2447.
20. Seydel, U., M.H. Koch, and K. Brandenburg, *Structural polymorphisms of rough mutant lipopolysaccharides Rd to Ra from Salmonella minnesota*. Journal of structural biology, 1993. **110**(3): p. 232-243.
21. Banoub, J.H., et al., *Structural investigation of bacterial lipopolysaccharides by mass spectrometry and tandem mass spectrometry*. Mass spectrometry reviews, 2010. **29**(4): p. 606-650.
22. Le Brun, A.P., et al., *Structural characterization of a model gram-negative bacterial surface using lipopolysaccharides from rough strains of Escherichia coli*. Biomacromolecules, 2013. **14**(6): p. 2014-2022.
23. Thomas, C.J., N. Surolia, and A. Surolia, *Surface plasmon resonance studies resolve the enigmatic endotoxin neutralizing activity of polymyxin B*. Journal of Biological Chemistry, 1999. **274**(42): p. 29624-29627.
24. Clifton, L.A., et al., *Effect of Divalent Cation Removal on the Structure of Gram-Negative*

- Bacterial Outer Membrane Models*. Langmuir, 2014. **31**(1): p. 404-412.
25. Vockenroth, I.K., et al., *Stable insulating tethered bilayer lipid membranes*. Biointerphases, 2008. **3**(2): p. FA68-FA73.
 26. He, L.H., et al., *Tethered bilayer lipid membranes based on monolayers of thiolipids mixed with a complementary dilution molecule. 1. Incorporation of channel peptides*. Langmuir, 2005. **21**(25): p. 11666-11672.
 27. Knobloch, J.J., et al., *Oxidative Damage to Biomimetic Membrane Systems: In Situ Fe(II)/Ascorbate Initiated Oxidation and Incorporation of Synthetic Oxidized Phospholipids*. Langmuir, 2015. **31**(46): p. 12679-12687.
 28. Budvytyte, R., et al., *Structure and Properties of Tethered Bilayer Lipid Membranes with Unsaturated Anchor Molecules*. Langmuir, 2013. **29**(27): p. 8645-8656.
 29. McGillivray, D.J., et al., *Molecular-scale structural and functional characterization of sparsely tethered bilayer lipid membranes*. Biointerphases, 2007. **2**(1): p. 21-33.
 30. Andersson, J., et al., *Synthesis and Characterisation of novel anchorlipids for tethered bilayer lipid membranes*. Langmuir, 2017.
 31. Zieleniecki, J.L., et al., *Cell-Free Synthesis of a Functional Membrane Transporter into a Tethered Bilayer Lipid Membrane*. Langmuir, 2016. **32**(10): p. 2445-2449.
 32. Stora, T., J.H. Lakey, and H. Vogel, *Ion-Channel Gating in Transmembrane Receptor Proteins: Functional Activity in Tethered Lipid Membranes*. Angewandte Chemie International Edition, 1999. **38**(3): p. 389-392.
 33. Terrettaz, S., M. Mayer, and H. Vogel, *Highly Electrically Insulating Tethered Lipid Bilayers for Probing the Function of Ion Channel Proteins*. Langmuir, 2003. **19**(14): p. 5567-5569.
 34. Junghans, A. and I. Koper, *Structural Analysis of Tethered Bilayer Lipid Membranes*. Langmuir, 2010. **26**(13): p. 11035-11040.
 35. Schiller, S.M., et al., *Archaea analogue thiolipids for tethered bilayer lipid membranes on ultrasmooth gold surfaces*. Angewandte Chemie International Edition, 2003. **42**(2): p. 208-211.
 36. James, M., et al., *Platypus: a time-of-flight neutron reflectometer at Australia's new research reactor*. Journal of Neutron Research, 2006. **14**(2): p. 91-108.
 37. Nelson, A., *Co-refinement of multiple-contrast neutron/X-ray reflectivity data using MOTOFIT*. Journal of Applied Crystallography, 2006. **39**: p. 273-276.
 38. Nelson, A., *Co-refinement of multiple-contrast neutron/X-ray reflectivity data using MOTOFIT*. Journal of Applied Crystallography, 2006. **39**(2): p. 273-276.
 39. Kienzle, P., *Neutron activation and scattering calculator*. 2016, National Institute of Standards and Technology.
 40. De Boer, A., et al., *Dry powder inhalation of antibiotics in cystic fibrosis therapy, part 1: development of a powder formulation with colistin sulfate for a special test inhaler with an air classifier as de-agglomeration principle*. European journal of pharmaceuticals and biopharmaceutics, 2002. **54**(1): p. 17-24.
 41. Kline, S.R., *Reduction and analysis of SANS and USANS data using IGOR Pro*. Journal of Applied Crystallography, 2006. **39**: p. 895-900.
 42. Vockenroth, I.K., et al., *Formation of tethered bilayer lipid membranes probed by various surface sensitive techniques*. Biointerphases, 2009. **4**(2): p. 19-26.
 43. Andersson, J., *New Tether Structures of tethered bilayer lipid membranes*, in *Chemical and Physical Sciences*. 2013, Flinders University: Adelaide, Australia.
 44. Yepuri, N.R., et al., *Stereoselective synthesis of perdeuterated phytanic acid, its phospholipid derivatives and their formation into lipid model membranes for neutron reflectivity studies*. Chemistry and Physics of Lipids, 2014. **183**(0): p. 22-33.
 45. Valincius, G., T. Meskauskas, and F. Ivanauskas, *Electrochemical Impedance Spectroscopy of Tethered Bilayer Membranes*. Langmuir, 2012. **28**(1): p. 977-990.
 46. Andersson, J., et al., *Synthesis and Characterization of Novel Anchorlipids for Tethered Bilayer Lipid Membranes*. Langmuir, 2017. **33**(18): p. 4444-4451.
 47. Clausell, A., et al., *Influence of polymyxins on the structural dynamics of Escherichia coli lipid membranes*. Talanta, 2003. **60**(2): p. 225-234.
 48. Cajal, Y., et al., *Intermembrane Molecular Contacts by Polymyxin B Mediate Exchange of Phospholipids*. Biochemistry, 1996. **35**(1): p. 299-308.
 49. Roberts, J.L., et al., *In Vitro Evaluation of the Interaction of Dextrin–Colistin Conjugates*

- with Bacterial Lipopolysaccharide*. Journal of Medicinal Chemistry, 2016. **59**(2): p. 647-654.
50. Liu, Y., et al., *The effects of temperature, salinity, concentration and PEGylated lipid on the spontaneous nanostructures of bicellar mixtures*. Biochimica et Biophysica Acta (BBA) - Biomembranes, 2014. **1838**(7): p. 1871-1880.

5.6 Supplementary information

5.6.1 Neutron data

Table S 5.1: Substrate parameters of fully tethered bilayers and bilayers with 10 mg/mL Colistin. SLD given in 10^{-6} \AA^{-2} , Thickness and roughness given in \AA and hydration given in volume-%.

	100% DPhyTL, 100% RcLPS		100% DPhyTL, 98% RcLPS		100% DPhyTL, 94% RcLPS	
	Bilayer	Bilayer + 10 mg/mL Colistin	Bilayer	Bilayer + 10 mg/mL Colistin	Bilayer	Bilayer + 10 mg/mL Colistin
Scale factor	1.09 ± 0.01	1.00	0.88 ± 0.01	0.93	0.89 ± 0.01	0.92
fronting SLD	2.07	2.07	2.07	2.07	2.07	2.07
backing roughness	3.64 ± 0.51	6.26	5.79 ± 1.27	6.88	5.58 ± 1.28	7.55
SiO ₂ thickness	27.2 ± 1.35	20.0	38.2 ± 0.73	41.88	35.6 ± 0.81	32.76
SiO ₂ SLD	3.47	3.47	3.47	3.47	3.47	3.47
SiO ₂ hydration	0.00	0.00	0.00	0.00	0.00	0.00
SiO ₂ roughness	3.42 ± 0.33	4.90	3.21 ± 0.17	3.02	3.84 ± 0.61	5.64
Cr thickness	30.2 ± 1.60	35.34	5.12 ± 0.10	6.32	5.17 ± 0.15	5.01
Cr SLD	3.03	3.03	3.02 ± 0.01	3.01	3.02 ± 0.01	3.02
Cr hydration	0.00	0.00	0.00	0.00	0.00	0.00
Cr Roughness	4.40 ± 1.01	7.91	3.39 ± 0.32	4.65	3.64 ± 0.51	6.49
Cr Oxide thickness*	45.7 ± 1.58	46.71	*These layers are not present in the other samples.			
Cr Oxide SLD*	3.85 ± 0.03	3.88				
Cr Oxide hydration*	0.00	0.00				
Cr Oxide roughness	4.68 ± 1.09	3.92				
Cr Thickness*	38.3 ± 1.09	38.73				
Cr SLD*	3.03	3.03				
Cr hydration*	0.00	0.00				
Cr Roughness*	7.13 ± 0.76	7.04				
Au thickness*	210.46 ± 1.03	208.60	107.0 ± 0.83	102.42	231.4 ± 0.69	233.20
Au SLD	4.33 ± 0.01	4.32	4.35 ± 0.01	4.40	4.48 ± 0.01	4.49
Au hydration	0.00	0.00	0.00	0.00	0.00	0.00
Au roughness	7.90 ± 0.09	6.26	9.95 ± 0.04	9.79	11.9 ± 0.05	11.66

Table S 5.2: Bilayer parameters of fully tethered bilayers and bilayers with 10 mg/mL Colistin. SLD given in 10^{-6} \AA^{-2} , Thickness and roughness given in \AA and hydration given in volume-%.

100% DPhyTL, 100% RcLPS	100% DPhyTL, 98% RcLPS	100% DPhyTL, 94% RcLPS	100% DPhyTL, 100% RcLPS	100% DPhyTL, 98% RcLPS	100% DPhyTL, 94% RcLPS	100% DPhyTL, 100% RcLPS
Bilayer	Bilayer + 10 mg/mL Colistin	Bilayer	Bilayer	Bilayer + 10 mg/mL Colistin	Bilayer	Bilayer
Tether thickness	14.02 ± 1.13	14.16	12.2 ± 0.18	12.40	12.53 ± 0.37	12.08
Tether SLD	0.98 ± 0.30	1.35	1.15 ± 0.14	1.24	0.69 ± 0.13	1.20
Tether hydration	6.41 ± 1.02	5.82	9.26 ± 0.59	6.90	5.57 ± 1.55	3.98
Tether roughness	6.43 ± 0.94	3.85	3.21 ± 0.16	3.52	4.30 ± 0.22	4.56
Inner HC thickness	15.9 ± 1.23	16.43	12.3 ± 0.22	12.32	13.1 ± 0.59	13.59
Inner HC SLD	-0.31 ± 0.06	-0.21	-0.34 ± 0.04	-0.31	-0.31 ± 0.06	-0.38
Inner HC hydration	2.06 ± 1.06	3.61	5.48 ± 0.43	4.85	1.26 ± 0.87	0.80
Inner HC roughness	5.93 ± 1.48	3.82	4.61 ± 0.96	3.63	6.19 ± 1.27	6.20
Outer HC thickness	15.9 ± 1.22	16.32	12.3 ± 0.19	12.50	12.8 ± 0.50	12.35
Outer HC SLD	-0.34 ± 0.04	-0.40	-0.05 ± 0.04	0.01 ± 0.05	0.12 ± 0.07	-0.05 ± 0.04
Outer HC hydration	2.19 ± 0.79	0.08 ± 0.06	4.13 ± 0.69	4.52 ± 0.39	2.78 ± 1.78	1.35 ± 0.93
Outer HC roughness	6.57 ± 1.79	7.66 ± 1.53	6.59 ± 1.77	6.97 ± 1.87	6.73 ± 1.52	6.82 ± 1.81
Outer HG thickness	8.40 ± 0.30	8.03 ± 0.00	9.35 ± 0.84	8.12 ± 0.09	7.29 ± 0.85	8.46
Outer HG SLD	2.83 ± 0.36	2.13 ± 0.08	3.21 ± 0.35	2.17 ± 0.15	3.35 ± 0.40	2.26 ± 0.10
Outer HG hydration	60.2 ± 3.68	10.6 ± 0.47	72.8 ± 1.73	34.1 ± 0.73	69.3 ± 3.92	24.5 ± 2.68
Outer HG roughness	3.35 ± 0.25	3.09 ± 0.08	6.83 ± 0.46	6.93 ± 0.58	4.55 ± 0.37	3.63 ± 0.43

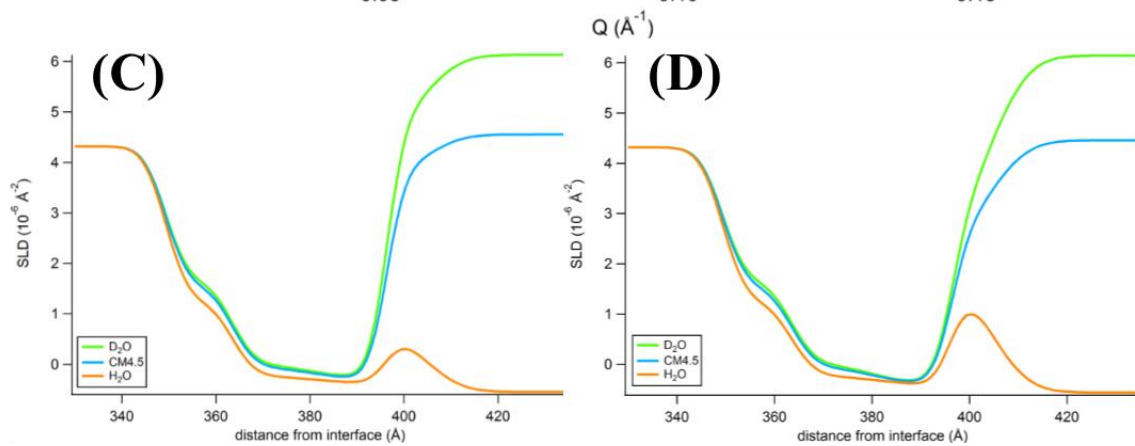
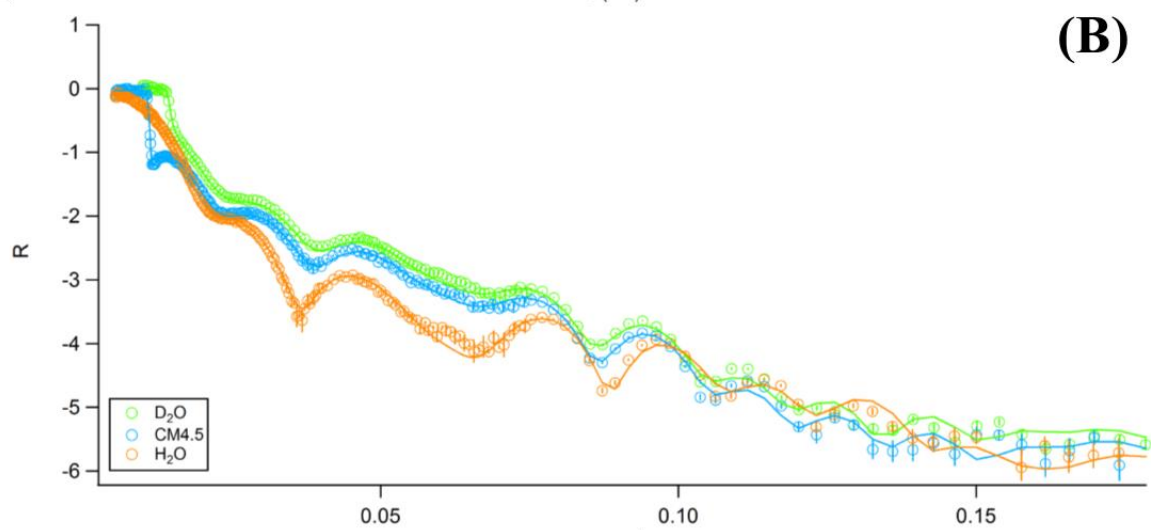
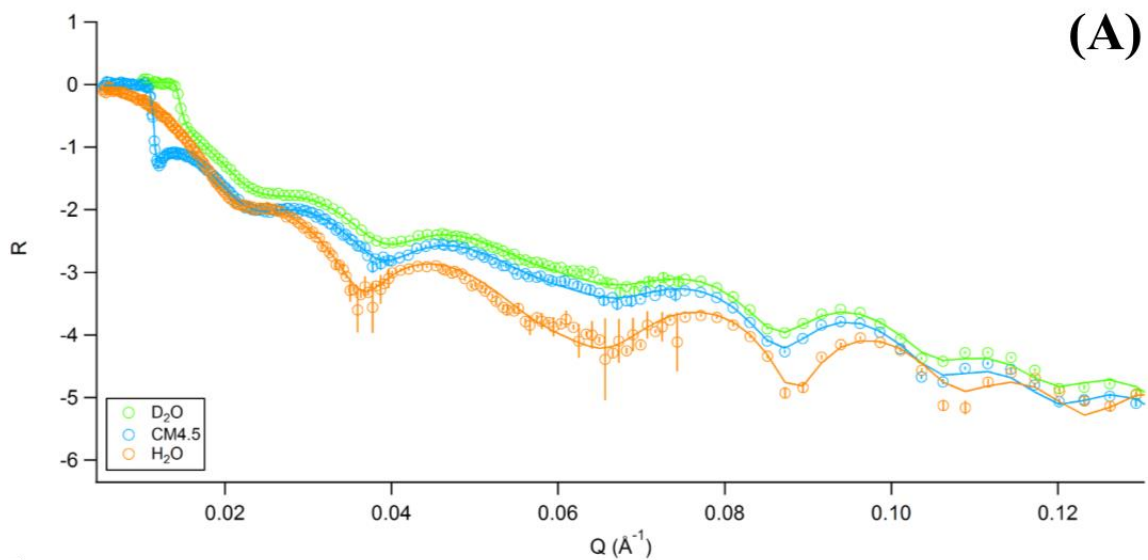


Figure S 5.1: Reflectivity plot of bilayer (A), bilayer after exposure to 10 mg/mL Colistin (B), SLD plot of bilayer (C) and SLD plot of bilayer after exposure to 10 mg/mL Colistin (D) for the sample at 100% DPhyTL and RcLPS.

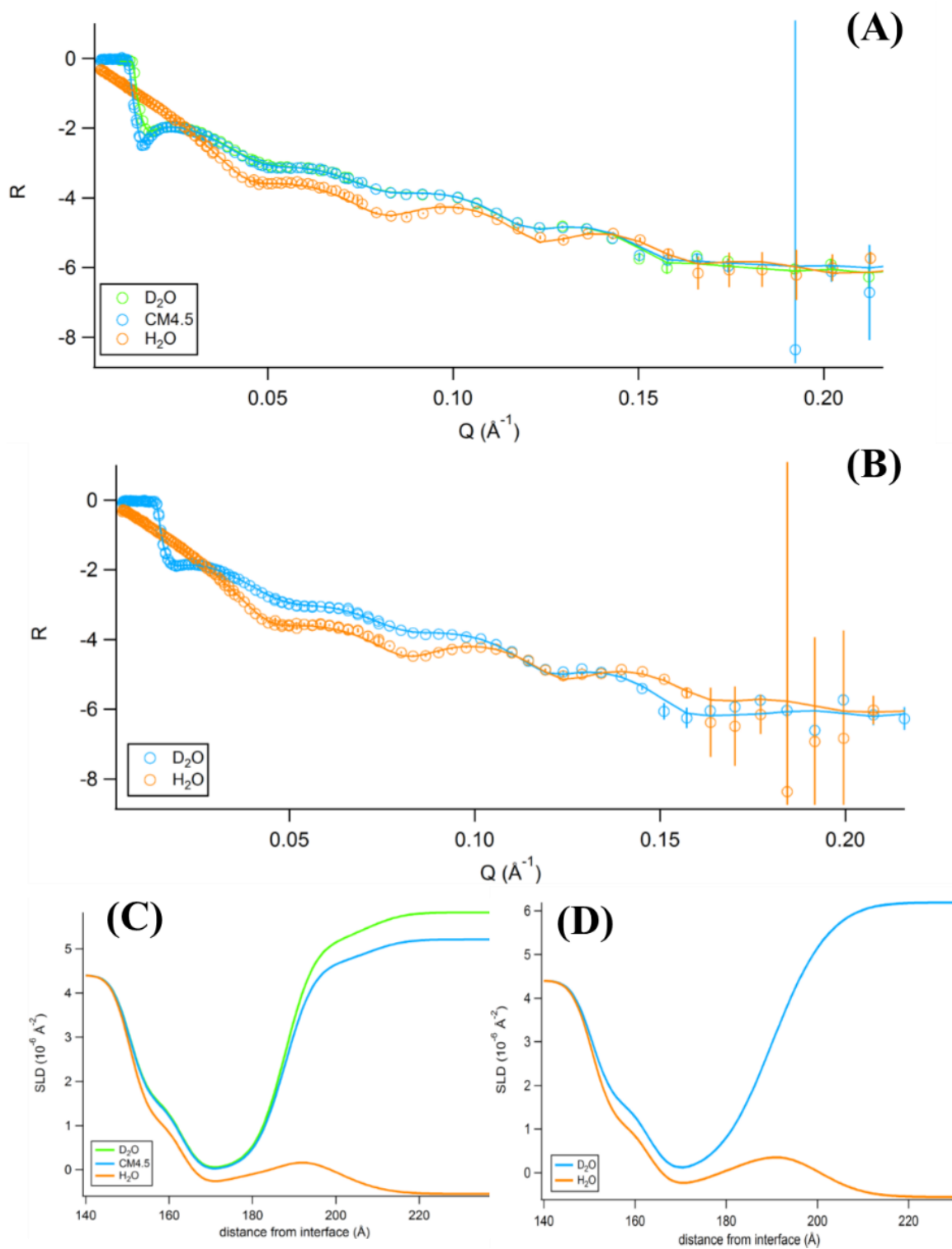


Figure S 5.2: Reflectivity plot of bilayer (A), bilayer after exposure to 10 mg/mL Colistin (B), SLD plot of bilayer (C) and SLD plot of bilayer after exposure to 10 mg/mL Colistin (D).

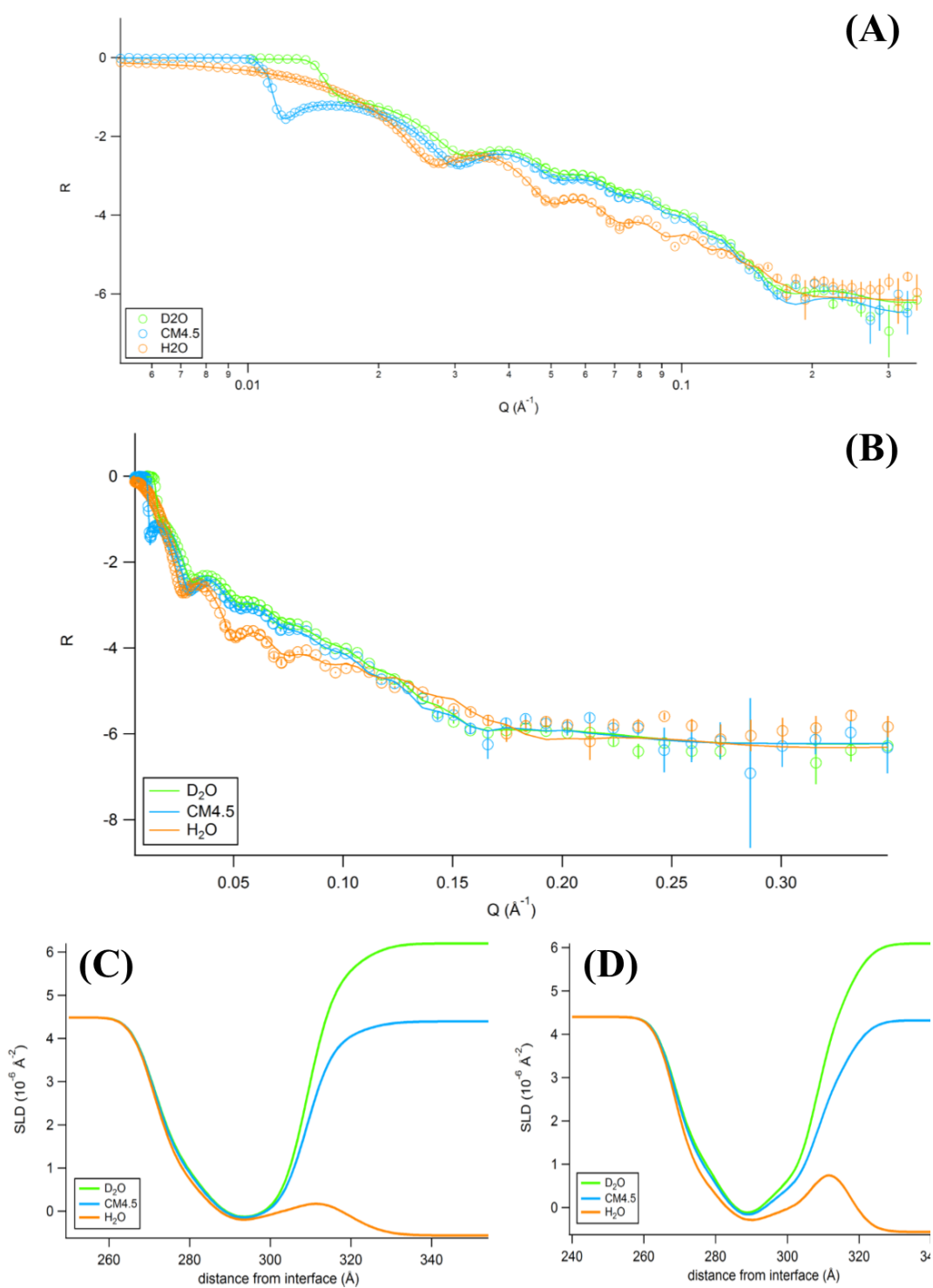


Figure S 5.3: Reflectivity plot of bilayer (A), bilayer after exposure to 10 mg/mL Colistin (B), SLD plot of bilayer (C) and SLD plot of bilayer after exposure to 10 mg/mL Colistin (D) for the sample at 100% DPhyTL and 94% RcLPS.

Table S 5.3: All parameters of sparsely tethered bilayers and bilayers with 10 mg/mL Colistin. SLD given in 10^{-6} \AA^{-2} , Thickness and roughness given in \AA and hydration given in volume-%.

	80% DPhyTL, 98% RcLPS		80% DPhyTL, 94% RcLPS	
	Bilayer	Bilayer + 10 mg/mL Colistin	Bilayer	Bilayer + 10 mg/mL Colistin
scale factor	0.96 ± 0.01	0.93	0.93 ± 0.01	0.90 ± 0.01
backing SLD	6.23 ± 0.01	6.15	6.24 ± 0.01	6.15 ± 0.02
backing roughness	7.71 ± 0.25	7.36	6.44 ± 1.07	6.06
SiO2 thickness	45.5 ± 0.65	40.76	48.5 ± 0.60	44.93
SiO2 SLD	3.47	3.47	3.47	3.47
SiO2 roughness	3.49 ± 0.38	3.09	4.35 ± 0.83	3.99
Cr thickness	5.22 ± 0.17	6.96	5.38 ± 0.30	9.12
Cr SLD	3.02 ± 0.01	3.02	3.02 ± 0.01	3.02
Cr Roughness	3.47 ± 0.38	3.86	5.58 ± 0.47	6.65
Au thickness	239.2 ± 0.73	243.21	226.5 ± 0.92	226.49
Au SLD	4.49 ± 0.01	4.49	4.49 ± 0.01	4.46
Au roughness	7.93 ± 0.06	7.73	7.90 ± 0.08	7.9
Tether thickness	8.33 ± 0.25	8.11	6.38 ± 0.29	6.65
Tether SLD	0.96 ± 0.25	0.59	1.12 ± 0.24	0.8
Tether hydration	11.1 ± 2.51	6.08	11.1 ± 2.32	10.72
Tether roughness	4.83 ± 0.41	5.27	4.52 ± 0.74	4.09
Inner HG thickness	6.32 ± 0.24	6.34	6.35 ± 0.27	6.62
Inner HG SLD	1.33 ± 0.28	1.19	1.64 ± 0.69	1.67
Inner HG hydration	17.4 ± 2.73	18.2	10.1 ± 3.37	7.4
Inner HG roughness	7.95 ± 1.48	6.64	7.46 ± 1.88	7.56
Inner HC thickness	10.1 ± 0.83	15.66 ± 2.67	12.6 ± 0.51	13.0 ± 0.51
Inner HC SLD	0.23 ± 0.02	0.02 ± 0.1	0.26 ± 0.05	0.04 ± 0.05
Inner HC hydration	1.76 ± 1.12	0.87 ± 0.72	2.38 ± 1.37	0.70 ± 0.63
Inner HC roughness	4.52 ± 0.42	3.83 ± 2.26	3.99 ± 0.92	0.74 ± 0.50
Outer HC thickness	15.7 ± 0.96	8.92 ± 2.80	12.6 ± 0.46	13.7 ± 0.82
Outer HC SLD	0.01 ± 0.01	0.02 ± 0.55	0.41 ± 0.13	0.68 ± 0.09
Outer HC hydration	2.24 ± 1.21	2.55 ± 2.54	2.83 ± 1.25	4.62 ± 1.73
Outer HC roughness	6.35 ± 1.44	13.8 ± 3.47	6.13 ± 1.81	18.9 ± 2.45
Outer HG thickness	7.34 ± 0.27	10.2 ± 2.81	13.8 ± 2.66	15.78 ± 0.20
Outer HG SLD	2.05 ± 0.04	1.95 ± 0.60	2.57 ± 0.53	2.33 ± 0.15
Outer HG hydration	63.8 ± 0.98	47.1 ± 18.0	78.4 ± 5.04	62.2 ± 3.21
Outer HG roughness	5.43 ± 0.51	5.37 ± 2.30	7.26 ± 0.93	4.40 ± 0.34

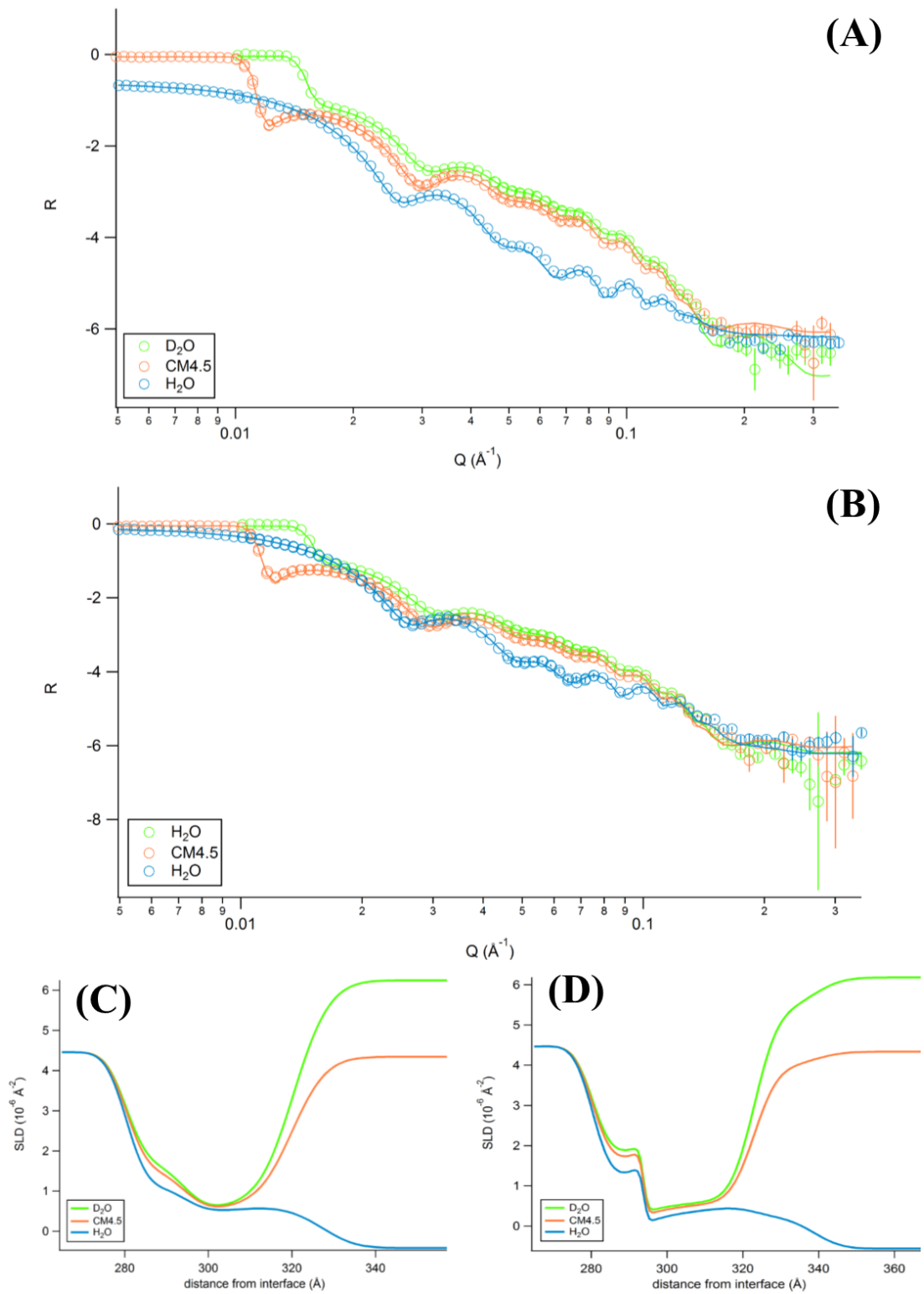


Figure S 5.4: Reflectivity plot of bilayer (A), bilayer after exposure to 10 mg/mL Colistin (B), SLD plot of bilayer (C) and SLD plot of bilayer after exposure to 10 mg/mL Colistin (D) for the sample at 80% DPhyTL and 98% R_cLPS.

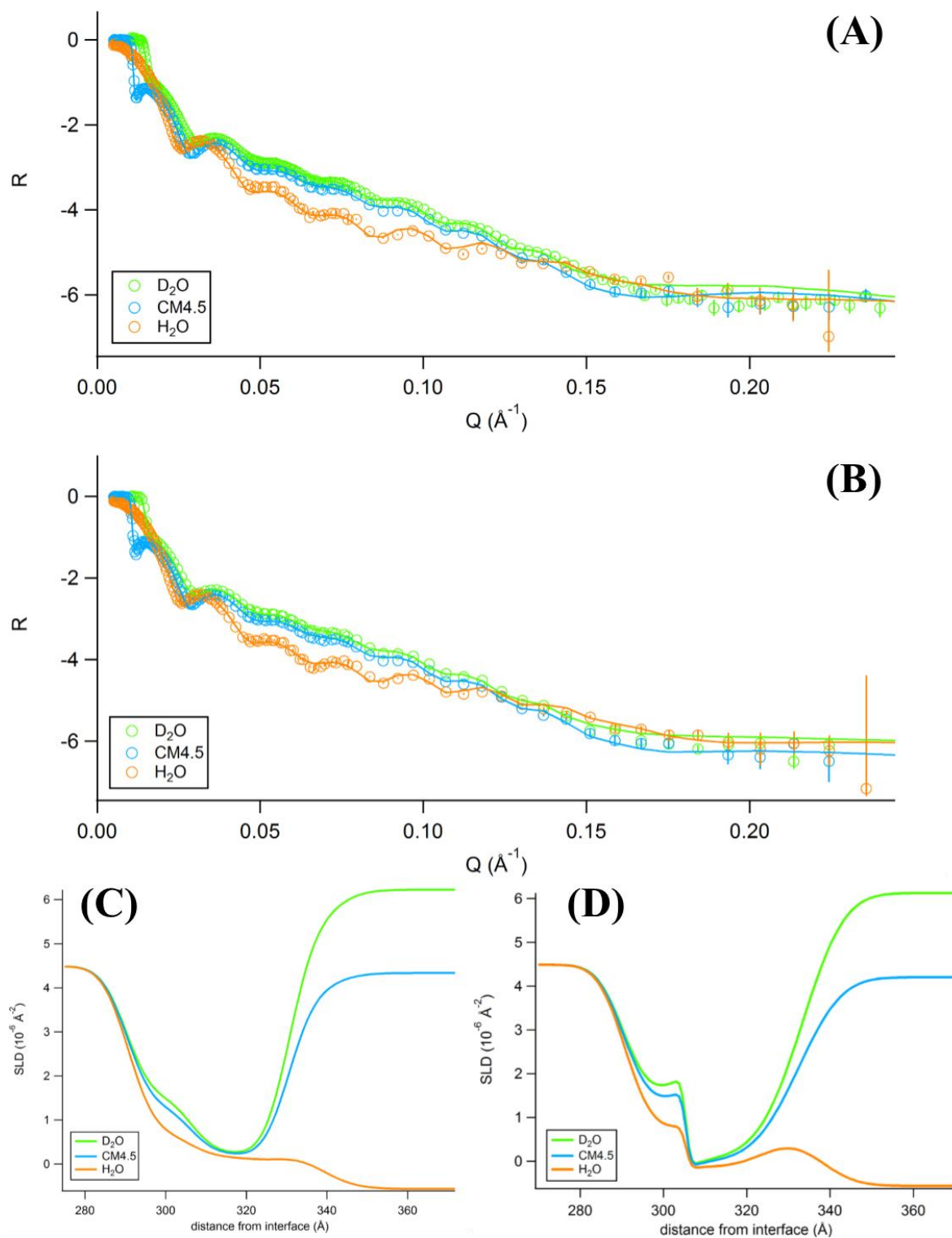


Figure S 5.5: Reflectivity plot of bilayer (A), bilayer after exposure to 10 mg/mL Colistin (B), SLD plot of bilayer (C) and SLD plot of bilayer after exposure to 10 mg/mL Colistin (D) for the sample at 80% DPhyTL and 94% RCLPS.

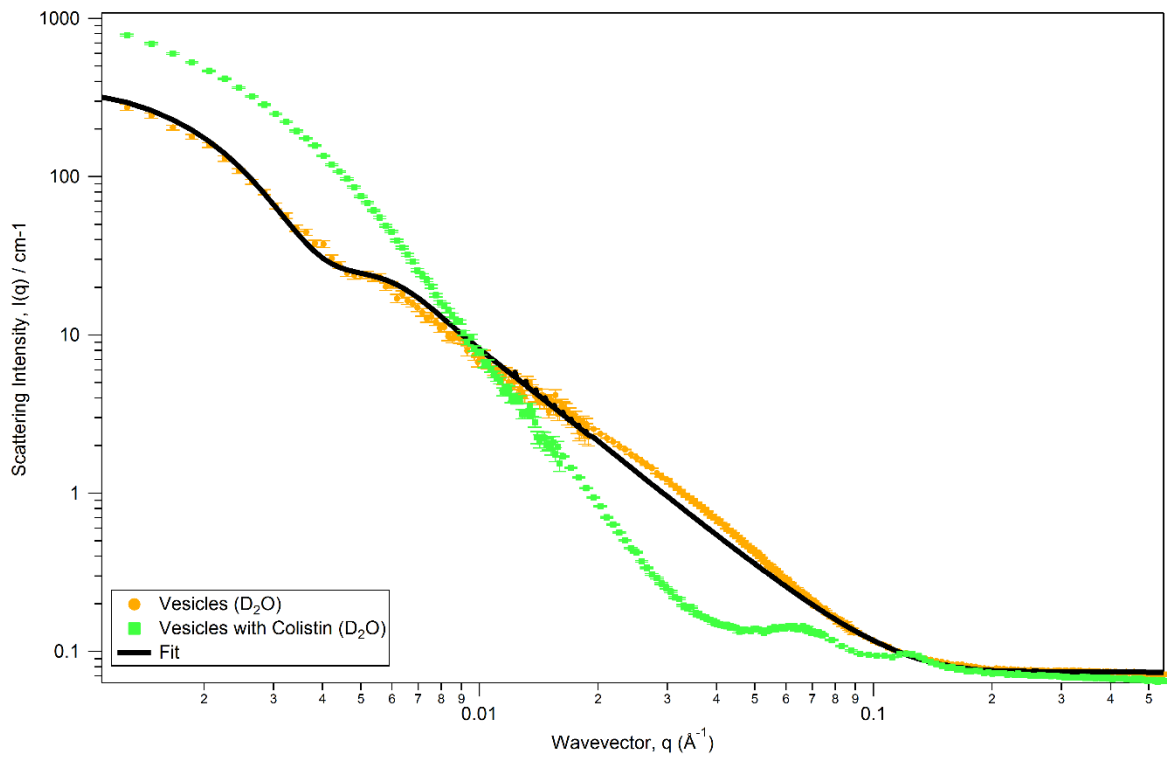


Figure S 5.6: Small angle neutron scattering (SANS) plot of vesicles comprised of lipopolysaccharides obtained from *Pseudomonas aeruginosa* prior to (orange) and after addition of 10 mg/mL Colistin.(green) and fit (black).

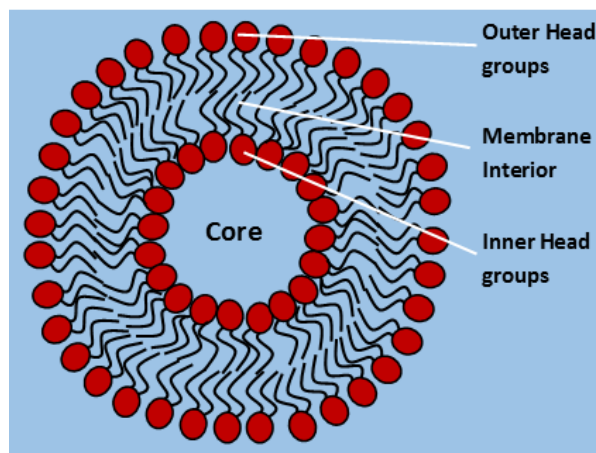


Figure S 5.7: Schematic of LPS model used to fit SANS data comprised of the water-filled core, the inner head groups (red), a hydrocarbon membrane interior (black) and the outer head groups (red).

Table S 5.4: SANS parameters of LPS-vesicles prior to exposure of Colistin. Parameters were fitted manually, therefore no error is available.

Core radius (Å)	570.0
Core polydispersity	0.295
Core SLD (10^{-6} \AA^{-2})	6.30
Inner head groups thickness (Å)	16
Inner head groups SLD (10^{-6} \AA^{-2})	4.10
Membrane interior thickness (Å)	9
Membrane interior SLD (10^{-6} \AA^{-2})	-0.4
Outer head groups (Å)	8
Outer head groups SLD (10^{-6} \AA^{-2})	3.90
Solvent SLD (10^{-6} \AA^{-2})	6.18
Background (cm^{-1})	7.40×10^{-2}

5.6.2 Electrochemical impedance spectroscopy data

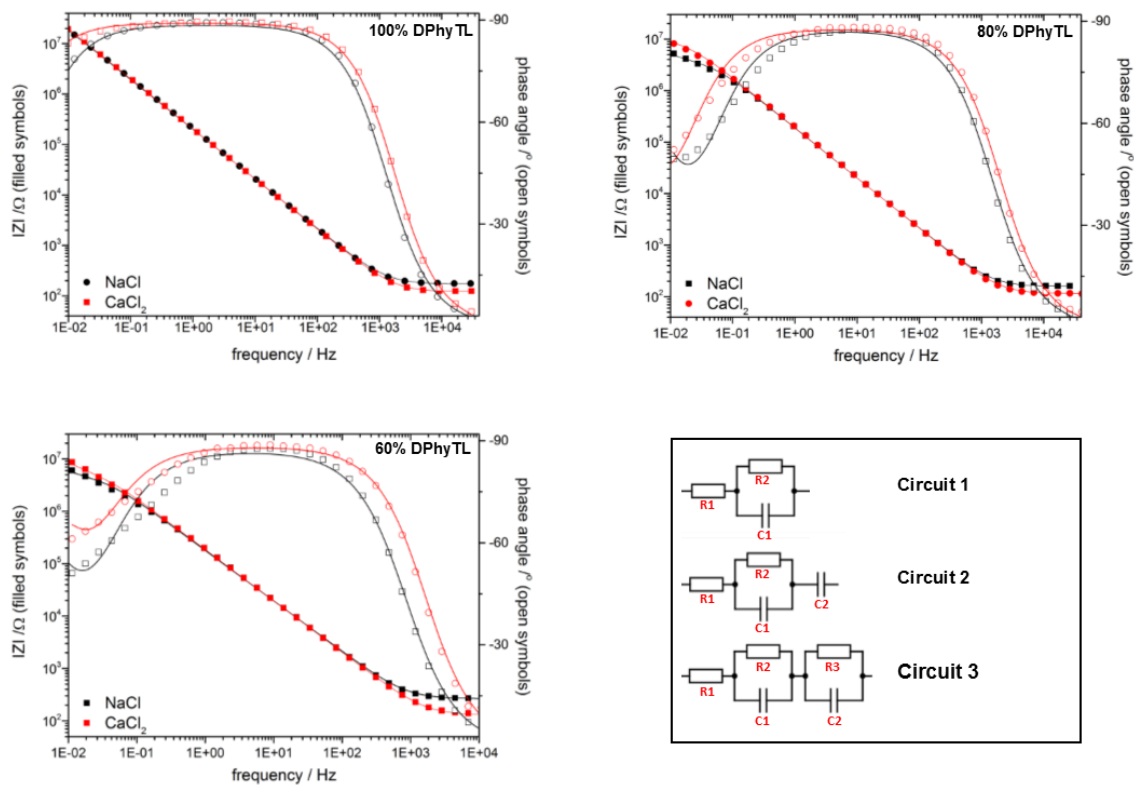


Figure S 5.8: Bode plots of DPhyPC-tBLMs under NaCl and CaCl_2 and schematics of the different circuits used to fit EIS data. R1 is the electrolyte resistance in all circuits, R2 the bilayer resistance and C1 the bilayer capacitance. In circuit 2, C2 represents the capacitance of the gold interface. In circuit 3, the sub-membrane reservoir is populated with ion to an extent that the spacer segment of the bilayer has a resistance and capacitance value.

Table S 5.5: All EIS parameters of Fully tethered LPS-tBLMs of various compositions exposed to EDTA and NaCl electrolytes and Valinomycin. Resistances are given in $M\Omega.cm^2$ and capacitances are given in $\mu F.cm^{-2}$

100% RcLPS					
	Bilayer		Spacer		Equivalent
	Resistance	Capacitance	Resistance	Capacitance	
CaCl	26.2 ± 18.4	3.50 ± 0.22			1
NaCl	11.6 ± 0.42	3.38 ± 0.03			1
30 mM	7.55 ± 2.14	2.99 ± 0.04			1
CaCl ₂	23.6 ± 1.60	3.08 ± 0.04			1
98% RcLPS					
	Resistance	Capacitance	Capacitance		
Bilayer	58.8 ± 4.15	0.79 ± 0.01			1
NaCl	34.9 ± 2.29	0.78 ± 0.01			1
30 mM	36.6 ± 5.38	0.73 ± 0.001			1
CaCl ₂	66.3 ± 4.37	0.71 ± 0.01			1
94% RcLPS					
	Resistance	Capacitance			
Bilayer	31.0 ± 2.08	1.09 ± 0.02			1
NaCl	37.3 ± 2.05	1.03 ± 0.02			1
3 mM edta	34.4 ± 1.77	1.00 ± 0.01			1
CaCl ₂	50.6 ± 3.04	0.96 ± 0.01			1
100% DPhyPC					
	Resistance	Capacitance			
Bilayer (in	160.3 ± 9.39	0.83 ± 0.01			1
NaCl	10.7 ± 3.57	1.28 ± 0.35			1
CaCl ₂	92.3 ± 5.22	0.84 ± 0.01			1

Table S 5.6: All EIS parameters for fully tethered LPS-tBLMs of various compositions after exposure to Colistin sulfate. Resistances are given in $M\Omega.cm^2$ and capacitances are given in $\mu F.cm^{-2}$

100% RcLPS			
	Bilayer		Equivalent
	Resistance	Capacitance	
Bilayer	138.1 ± 13.5	0.8 ± 0.01	1
10 mg/ml Colistin 18 h	196.5 ± 29.4	0.9 ± 0.01	1
10 mg/ml Colistin 48 h	119.6 ± 15.3	0.9 ± 0.01	1
20 mg/ml Colistin 48 h	108.4 ± 2.3	0.9 ± 0.01	1
98% RcLPS			
	Bilayer		
	Resistance	Capacitance	
Bilayer	101.9 ± 11.6	0.8 ± 0.01	1
10 mg/ml Colistin 18 h	91.0 ± 19.0	0.8 ± 0.01	1
10 mg/ml Colistin 48 h	83.6 ± 18.7	0.8 ± 0.01	1
20 mg/ml Colistin 48 h	71.6 ± 18.5	0.8 ± 0.01	1
94% RcLPS			
	Bilayer		
	Resistance	Capacitance	
Bilayer	100.6 ± 10.0	0.81 ± 0.01	1
10 mg/ml colistin 18 h	73.4 ± 7.41	0.85 ± 0.001	1
10 mg/ml colistin 72 h	76.2 ± 1.85	0.93 ± 0.001	1

Table S 5.7: All EIS parameters of sparsely tethered LPS-tBLMs (80% DPhyTL) under EDTA, NaCl and after exposure to valinomycin. Resistances are given in $M\Omega.cm^2$ and capacitances are given in $\mu F.cm^{-2}$

100% RcLPS					
	Bilayer		Spacer		Equivalent Circuit
	Resistance	Capacitance	Resistance	Capacitance	
Bilayer	3.52 ± 0.49	1.25 ± 0.09			1
NaCl	1.73 ± 0.12	1.25 ± 0.09			1
30 mM	0.001 ± 0.0001	1.24 ± 0.23	0.50 ± 0.02	7.26 ± 0.25	3
CaCl ₂	17.5 ± 0.81	0.77 ± 0.01			1
98% RcLPS					
	Bilayer		Spacer		
	Resistance	Capacitance	Resistance	Capacitance	1
Bilayer	1.75 ± 0.3	1.11 ± 0.6		3.16 ± 0.6	1
NaCl	3.54 ± 1.05	1.20 ± 1.05		2.9 ± 1.05	1
30 mM Edta	2.61 ± 0.37	0.98 ± 0.06		6.46 ± 2.47	1
CaCl ₂	4.87 ± 0.57	0.86 ± 0.05		11.1 ± 7.81	1
94% RcLPS					
	Bilayer		Spacer		
	Resistance	Capacitance	Capacitance		
Bilayer	1.24 ± 0.45	1.66 ± 0.23	2.68 ± 0.59		2
NaCl	0.22 ± 0.04	1.47 ± 0.13	3.38 ± 0.27		2
30 mM edta	1.88 ± 0.61	1.22 ± 0.18	3.24 ± 1.17		2
CaCl ₂	3.37 ± 1.11	1.12 ± 0.19	3.14 ± 1.37		2
100% DPhyPC					
	Bilayer		Spacer		
	Resistance	Capacitance	Capacitance		
Bilayer	1.79 ± 0.24	4.07 ± 0.34	12.4 ± 3.0		2
CaCl ₂	3.48 ± 0.83	3.73 ± 0.78	15.2 ± 11.8		2

Table S 5.8: All parameters of sparsely tethered LPS-tBLMs after exposure to 10 mg/mL Colistin sulfate. Resistances are given in $M\Omega.cm^2$ and capacitances are given in $\mu F.cm^{-2}$

100% RcLPS				
	Bilayer		Spacer	Equivalent
	Resistance	Capacitance	Capacitance	
Bilayer	5.71 ± 0.0001	1.16 ± 0.67	2.25 ± 2.29	2
10 mg/mL Colistin 18 h	0.01 ±	38.2 ± 0.18		1
CaCl rinse 18 h	0.04 ±	46.1 ± 0.49		1
98% RcLPS				
	Bilayer			
	Resistance	Capacitance		
Bilayer	1.75 ± 0.22	3.14 ± 0.45		1
10 mg/mL Colistin 18 h	4.19 ± 1.77	3.02 ± 1.88		1
10 mg/mL Colistin 76 h	5.01 ± 0.71	6.49 ± 2.53		1
94% RcLPS				
	Bilayer		Spacer	
	Resistance	Capacitance	Capacitance	
Bilayer	1.24 ± 0.45	1.66 ± 0.23	2.68 ± 0.59	2
10 mg/mL Colistin 18 h	2.26 ± 0.35	20.9 ± 0.45	3.40 ± 0.36	2
CaCl ₂ rinse	0.93 ± 0.04	17.0 ± 0.17		1

6 Enhancing Antibiotics with Nanoparticles

The model membrane architecture developed in chapter 5 was found to be susceptible to the antibacterial compound Colistin sulfate which is known to damage the cell wall and destroy bacteria. Having established the viability of this membrane platform as a means to study the behaviour of membrane-targeting compounds, it can now be used to test novel approaches to damage the membrane of gram-negative bacteria.

6.1 Introduction to antimicrobial gold nanoparticles

It may be possible to achieve enhanced treatment efficacy by combining currently used antibiotics with membrane-targeting nanoparticles. Gold nanoparticles are relatively benign in mammalian cells, although more studies are required to confirm this.[1] It is likely that the toxicity of gold nanoparticles to the host as well as their antibacterial properties vary significantly with their size, shape and functionalisation.

For example, Nanoparticles with a diameter of 5 nm caused the formation of temporary non-lethal membrane lesions in both gram-negative and gram-positive organism.[2] When the particle size was reduced to 2 nm, the effect on gram-positive bacteria was lethal, with 80% of exposed cells suffering cell lysis. However, only 20% of gram-negative cells were affected. The high resistance of gram-negative bacteria to the effects of cationic gold nanoparticles is likely a result of the highly resistant dual membrane structure that is unique to these organisms. Increasing the hydrophobicity[3] or surface charge[4] of the gold nanoparticles resulted in significantly improved growth inhibition of several multi-drug resistant species of both Gram-negative and Gram-positive bacteria.

The effect of the nanoparticles on the biophysical properties of lipid bilayers exposed to gold nanoparticles has thus far not been studied, as these experiments are challenging to carry out on living cells. Insight into the effect on the membrane structure and electrical properties would inform future efforts to design antibacterial nanoparticles and therapies. Furthermore, even if the structural changes to the membrane caused by the exposure to nanoparticles are themselves not lethal to the organism, they may still increase the susceptibility of the membrane to the effect of other antimicrobial compounds. Presented here are some initial studies on the effect of cationic gold nanoparticles with a diameter of 5 nm on sparsely tethered LPS-tBLMs.

6.2 Materials and methods

Chemicals: Rc-strain Lipopolysaccharides from the J5 mutant of *E. coli*, Poly(dimethylallylammoniumchloride) (35% by weight in aqueous 1mM NaCl solution) and colistin sulfate were purchased from Sigma Aldrich and used without further purification. Gold nanoparticles were purchased from NanoComposix and used without further purification. Ultrapure water (18.2 M Ω cm resistance, obtained from a WaterPro PS reverse osmosis system by Labconco) was used for all experiments.

Preparation of coated nanoparticles: The nanoparticles were prepared by Melanie Fuller at Flinders University by incubating the nanoparticles with 5 mg/mL PDADMAC in 1 mM aqueous NaCl for 90 minutes followed by centrifugation at 18,000 g for 10 minutes, after which the supernatant was removed, and the nanoparticles were resuspended in ultrapure water. Centrifugation and resuspension were repeated twice more before the nanoparticles were used for further experiments.

Bilayer formation: All EIS experiments in this chapter were carried out using a membrane architecture of 94% RcLPS and 6% DPhyPC assembled on a monolayer of 80% DPhyTL and 20% mercaptoethanol. Silicon substrates were cleaned using a 1:1:5 mixture of aqueous NH₃/H₂O₂/MilliQ for 1h at 70° C, rinsed thoroughly with water and ethanol (Sigma Aldrich) and dried under a stream of nitrogen. A 5 nm chromium adhesion layer was deposited by sputter coating (with a current of 100 mA) followed by 20 nm gold (10 mA). The substrates were then rinsed with ethanol and inserted into an 0.1 mM ethanolic solution of a DPhyTL and mercaptoethanol mixture for 18 hours allowing for the formation of a tethered monolayer.

The substrates were then removed from the solution and rinsed thoroughly with ethanol and dried under a stream of nitrogen. Bilayers were formed by fusion of vesicles with the pre-formed monolayer. Vesicles containing 6% DPhyPC and 94% RcLPS from *E. coli* at a total concentration of 1 mg/mL were used. The lipids were dissolved in chloroform and evaporated under a stream of nitrogen for 15 minutes or until completely dry. 1 mL water was added to the dried lipid film and the lipid-water mixture was sonicated at 45°C for 1h and extruded 30 times through 200nm track-etched polycarbonate filter membranes. The vesicles can be stored at -20° C for later use but should be extruded prior to each use. 10 μ L/mL vesicles solution was added to the monolayer to an aqueous solution of 100 mM CaCl₂ (electrode area: 0.283 cm²). Bilayer formation was left to occur for 18h at 25°C and the resulting membranes were rinsed with 5 cell volumes of 100 mM CaCl₂. Colistin sulfate was dissolved in water and incubated with the lipid bilayer for 18 hours prior to measurements.

6.3 The effect of gold nanoparticles on LPS-tBLMs

The particles used here were citrate-capped gold nanoparticles with a diameter of 5 nm purchased coated with the positively charged polymer Poly(diallyldimethylammonium chloride) (PDADMAC), shown in Figure 6.1. Zeta potential measurements were used to confirm that the nanoparticles had been successfully coated with the polymer. The citrate-capped gold nanoparticles had a zeta potential of -21.2 ± 4.91 mV, which increased to 36.7 ± 7.5 mV after coating with PDADMAC.

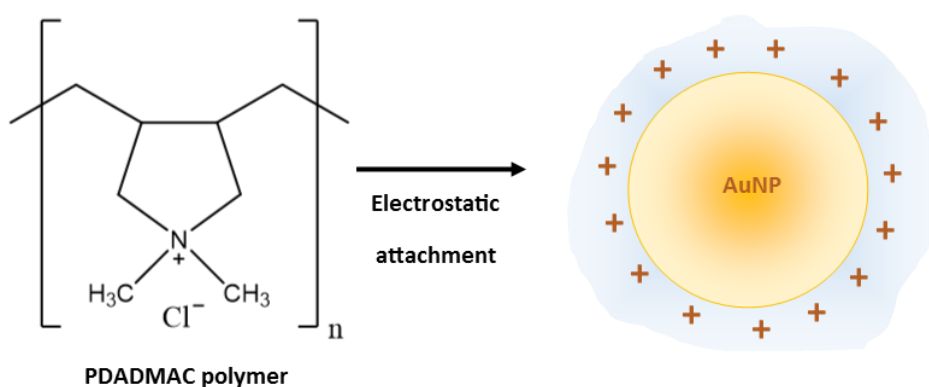


Figure 6.1: The PDADMAC polymer is electrostatically attached to citrate-capped gold nanoparticles suspended in water, resulting in positively charged nanoparticles.

Figure 6.2 shows UV-vis spectra of citrate-capped (uncoated) gold nanoparticles and nanoparticles coated with PDADMAC. There is a small shift in maximum absorbance from 514 nm for uncoated gold nanoparticles to 535 nm for coated gold nanoparticles.

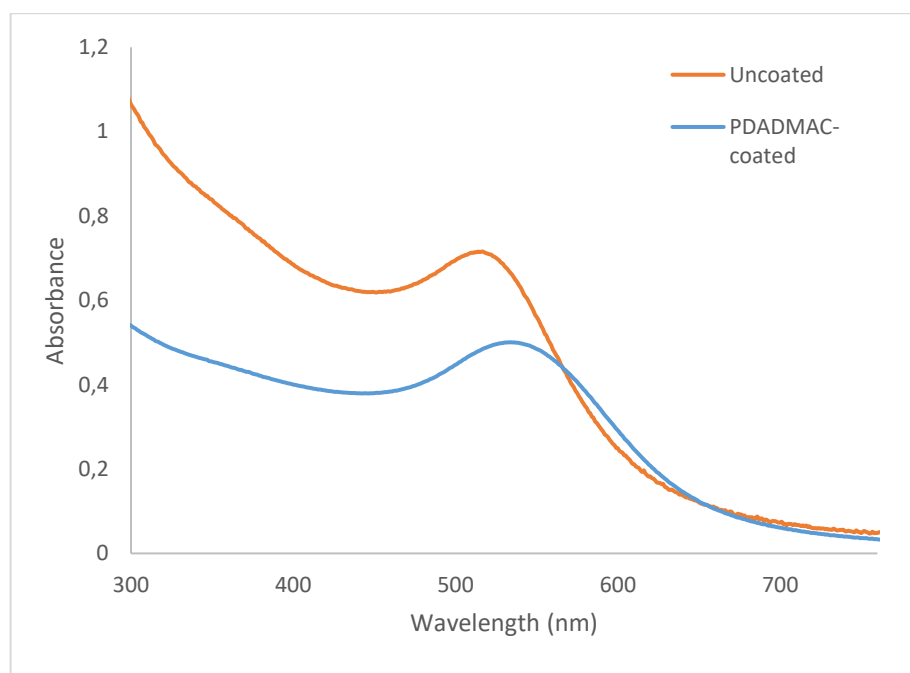


Figure 6.2: UV-vis spectra of uncoated (orange) and PDADMAC-coated (blue) nanoparticles.

An estimate of the concentration of PDADMAC-coated gold nanoparticles can be made by using the absorbance of the nanoparticles purchased from NanoComposix (with a stated concentration of 0.05 mg/mL) and compare their absorbance to that of the nanoparticles after incubation with PDADMAC. Assuming a uniform diameter of 5 nm, a concentration of 0.05 mg/mL corresponds to 4.95×10^{12} particles/mL. The nanoparticles were incubated with PDADMAC polymer and separated from the solution by centrifugation, resulting in a concentration of 0.035 mg/mL or 3.46×10^{12} particles/mL, or 5.7 nM. For convenience, the volume of nanoparticle stock solution is stated here instead of the total concentration of nanoparticles.

To investigate the effect of gold nanoparticles on an LPS-tBLM, PDADMAC-coated nanoparticles suspended in ultrapure water (18.2 M Ω , sourced from a WaterPro PS reverse osmosis system by Labconco) were added to a lipid bilayer in a 100 mM CaCl₂ bathing solution. Nanoparticle concentrations are stated in μ L/mL of a stock solution with a concentration of 3.46×10^{12} particles/mL. Electrical data of bilayers exposed to increasing concentrations of gold nanoparticles are shown in Table 6.1. Bode plots of the EIS data are shown in Figure 6.3.

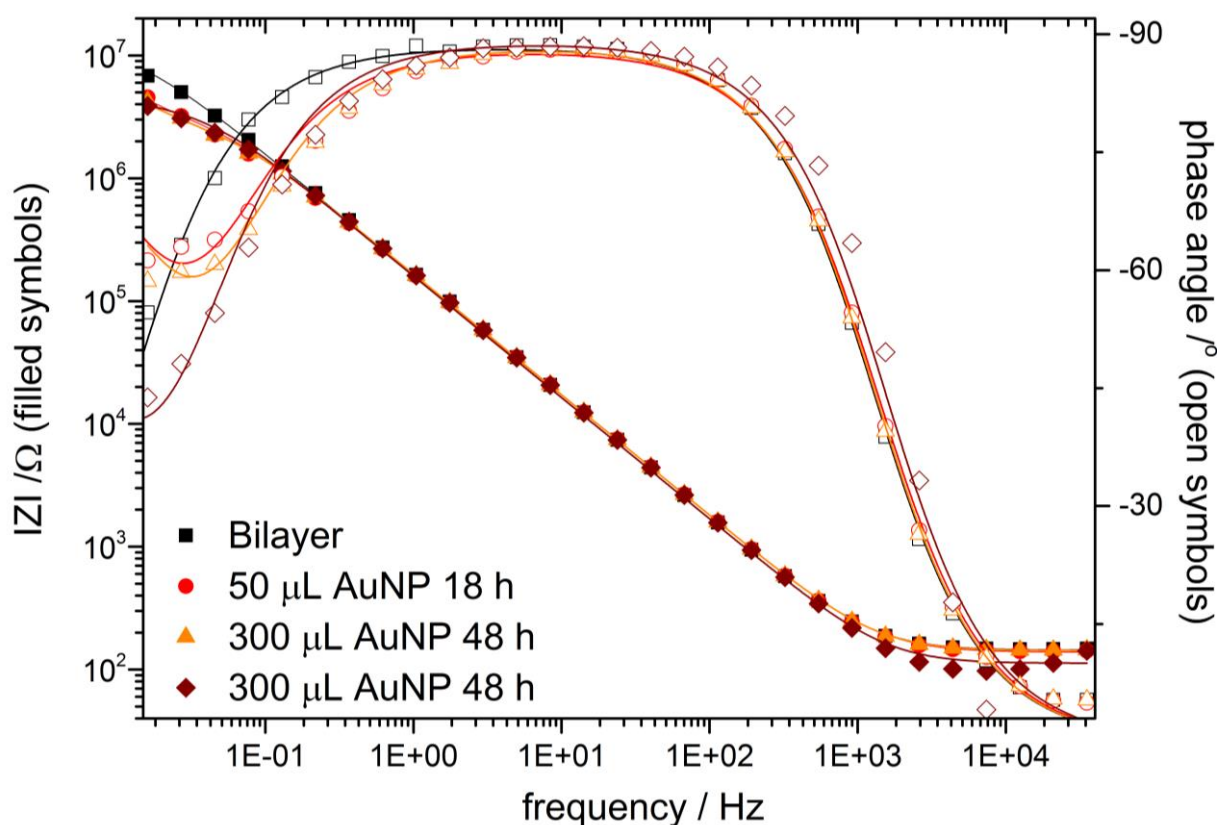


Figure 6.3: Bode plots of LPS-tBLMs exposed to 50 $\mu\text{L}/\text{mL}$ gold nanoparticles (a) and a mixture of 50 $\mu\text{L}/\text{mL}$ gold nanoparticles and 10 mg/mL Colistin sulfate (b).

There was a decrease in membrane resistance by around one order of magnitude from 12 $\text{M}\Omega\text{cm}^2$ to ca. 2 $\text{M}\Omega\text{cm}^2$ after the bilayer was incubated with 50 $\mu\text{L}/\text{mL}$ nanoparticle solution for 18 hours. Increasing nanoparticle concentration or incubation time did not caused additional decreases in membrane resistance.

Table 6.1: Effect of 50-300 $\mu\text{L}/\text{mL}$ gold nanoparticles on the electrical properties of an LPS-tBLM

	Resistance ($\text{M}\Omega\text{cm}^2$)	Capacitance (μFcm^{-2})
Bilayer	12.5 ± 0.39	0.99 ± 0.01
50 $\mu\text{L}/\text{mL}$ AuNP	2.02 ± 0.45	1.58 ± 0.19
300 $\mu\text{L}/\text{mL}$ AuNP	1.88 ± 0.37	1.45 ± 0.16
300 $\mu\text{L}/\text{mL}$ AuNP	3.49 ± 1.22	1.18 ± 0.21

Gold nanoparticles by themselves only have a minor effect to LPS membranes, as extensive damage would have resulted in large changes in membrane resistance or capacitance. While some of the stabilising calcium ions are likely displaced by the binding of nanoparticles to the membrane, the particles also provide a positive charge near the membrane surface, mitigating the repulsion between the phosphate groups of LPS.

It is possible that the binding nanoparticles cause the formation of lesions (shown schematically in Figure 6.4) where LPS molecules surrounding the nanoparticle are drawn slightly towards the nanoparticle without being removed entirely from the bilayer. As membranes are likely not completely homogenous, some areas of the membrane (possibly areas already containing membrane defects) may be affected more than others, creating defects that enable charge transport. This effect should be further investigated with neutron scattering.

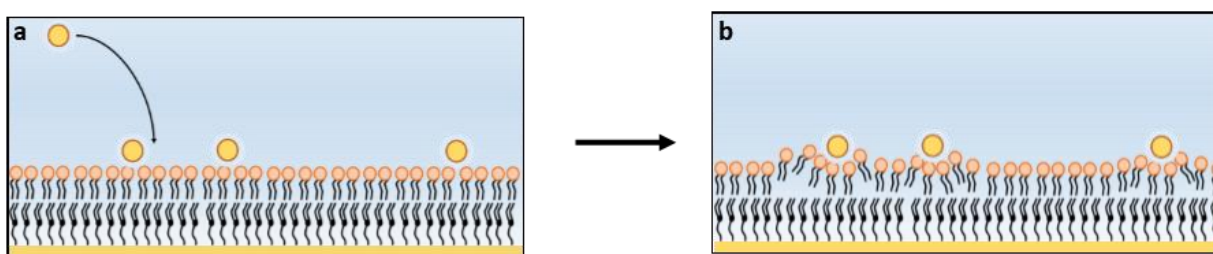


Figure 6.4: The binding of gold nanoparticles to the lipid bilayer may cause the formation of lesions in the lipid membrane without removing LPS molecules from the bilayer.

The structural disturbance to the lipid membrane caused by the nanoparticles could then result in increased susceptibility of the membrane to the effects of an antibiotic such as Colistin sulfate, which acts by inserting into the outer leaflet of the lipid membrane to cause structural damage to the lipid bilayer.[5]

Combining the effect of membrane-targeting antibiotics with nanoparticles, particularly if there is a synergistic effect between the compounds, may be an effective strategy to combat drug resistance. In addition to treating otherwise incurable infections, a synergistic effect between antibiotic compounds might also reduce the dosage required to treat the patient. This might reduce side effects in the patient and also decrease the cost of the treatment. Preliminary results on the combination of Colistin with cationic gold nanoparticles are presented in chapter 6.5.

6.4 Combining nanoparticles with antibiotics

Increasing concentrations of nanoparticles were combined with 10 mg/mL Colistin sulfate, a concentration of antibiotic known to cause significant damage the lipid bilayer (see chapter 5). Figure 6.5 shows Bode plots of LPS-tBLMs incubated with a combination of 50 $\mu\text{L}/\text{mL}$ gold nanoparticles with 10 mg/mL Colistin sulfate.

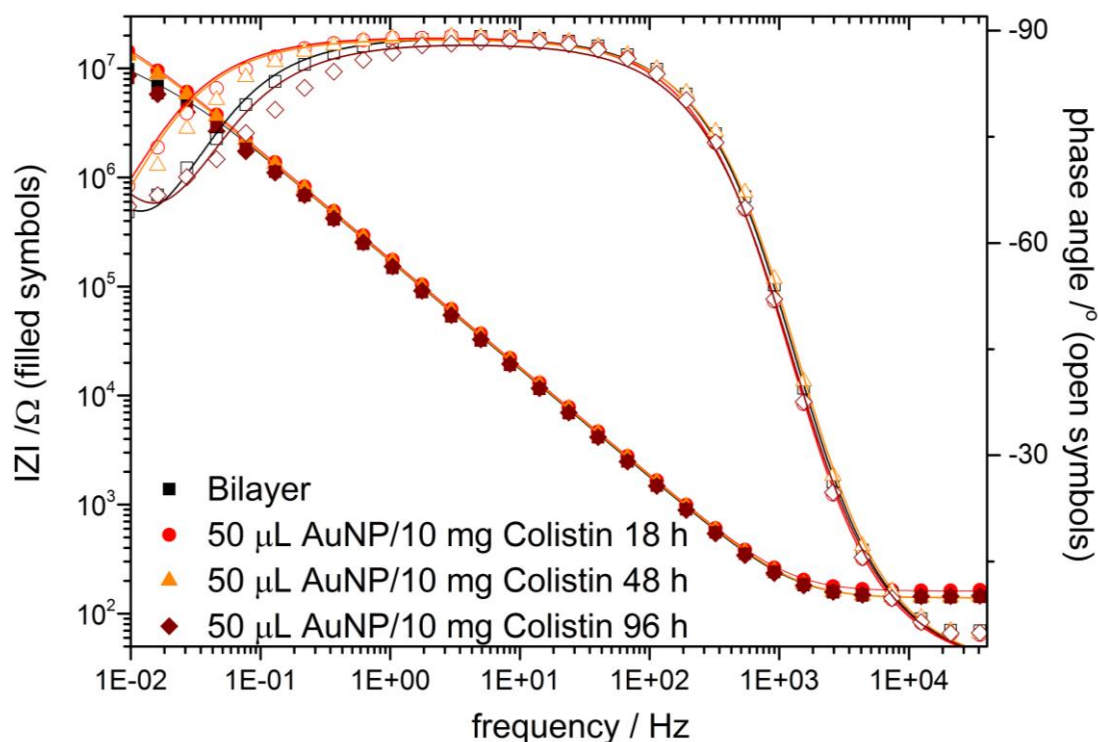


Figure 6.5: Bode plots of LPS-tBLMs treated with combination of 50 $\mu\text{L}/\text{mL}$ gold nanoparticles and 10 mg/mL Colistin sulfate for 18-96 hours.

A combination of 50 $\mu\text{L}/\text{mL}$ gold nanoparticles with 10 mg/mL Colistin sulfate did not cause increased damage to the membrane compared to the effect only nanoparticles did (see Table 6.2). Furthermore, instead of the decrease in membrane resistance caused by the addition of only 50 $\mu\text{L}/\text{mL}$ nanoparticles, there was a small increase in bilayer resistance upon addition of Colistin to the bilayer. It is possible that Colistin initially bound to the defects in the membrane formed by the binding of gold nanoparticles, thereby blocking charge transport pathways, but there were insufficient defect sites at this concentration of nanoparticles to cause increased Colistin activity.

Table 6.2: Effect of 50 $\mu\text{L/mL}$ gold nanoparticles on LPS-tBLM when combined with 10 mg/mL Colistin Sulfate

	Resistance ($\text{M}\Omega$)	Capacitance (μF)
Bilayer	5.29 ± 1.21	1.55 ± 0.26
50 $\mu\text{L/mL}$ AuNP 10 mg/mL Colistin 18	17.6 ± 4.72	1.34 ± 0.34
50 $\mu\text{L/mL}$ AuNP 10 mg/mL Colistin 48 h	17.3 ± 5.20	1.37 ± 0.36
50 $\mu\text{L/mL}$ AuNP 10 mg/mL Colistin 96 h	3.61 ± 1.18	1.83 ± 0.40

As there was no increased effectiveness of the antibiotic when combining 50 $\mu\text{L/mL}$ gold nanoparticles with Colistin, the nanoparticle concentration was increased to 100 $\mu\text{L/mL}$. Bode plots of the effect of gold nanoparticles combined with Colistin sulfate are shown in Figure 6.6 and electrical data are shown in Table 6.3.

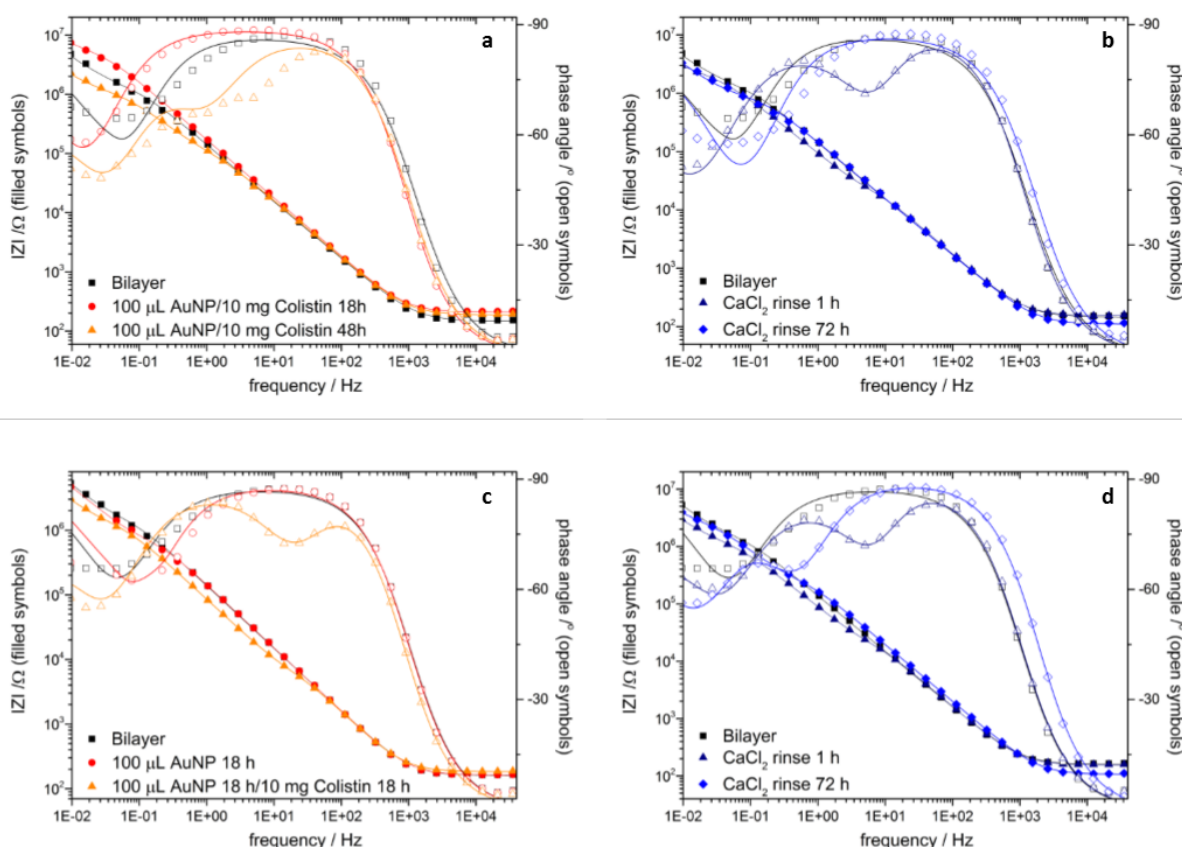


Figure 6.6: Bode plots of an LPS-tBLM exposed to 100 $\mu\text{L/mL}$ gold nanoparticles and 10 mg/mL Colistin (a) and subsequent rinsing of that membrane (b), and an LPS-tBLM exposed to gold nanoparticles only for 18 h prior to the addition of gold nanoparticles (c) and subsequent rinsing of that membrane (d).

Bilayers were either incubated with a combination of Colistin and nanoparticles for 18 h or pre-treated with gold nanoparticles for 18 h prior to the addition of Colistin. The combination 100 $\mu\text{L}/\text{mL}$ cationic nanoparticles with 10 mg/mL Colistin for 18 h caused the membrane resistance to triple, similar to the effect observed previously when combining 50 $\mu\text{L}/\text{mL}$ gold nanoparticles with Colistin. However, if left to incubate for 48 h, membrane resistance decreased by two orders of magnitude. This effect could be reversed by rinsing with CaCl_2 , but recovery was slow, requiring a period of 72 h.

Nanoparticles likely attached to the membrane initially, causing the formation of defects. Colistin then bound to the defect sites, blocking charge transport through the defects. Over a period of 48 hours, additional Colistin molecules possibly inserted into the membrane at defect sites and promoted the formation of larger defects allowing charge transport. Rinsing of the bilayer probably partially or completely removed the nanoparticles and antibiotic, allowing the membrane to recover.

Incubating the lipid bilayer with gold nanoparticles and adding Colistin only after a period of 18 h caused a reduction membrane resistance by three orders of magnitude. As there is no competition between the binding of Colistin and nanoparticles to the membrane, it is possible that more nanoparticles bind and form defect sites susceptible to Colistin.

The effect on the lipid membrane was partially reversible, with bilayer resistance recovering by two orders of magnitude over time when stored under CaCl_2 for 72 h. However, there is some permanent damage to the lipid membranes as the resistance is an order of magnitude below its original level.

There was no significant change in membrane capacitance in these experiments, therefore it is unlikely that the outer leaflet was partially or completely removed by these treatments.

Table 6.3: Effect on the electrical properties of an LPS-tBLM exposed to mixtures of 100 $\mu\text{L}/\text{mL}$ gold nanoparticles and 10 mg/mL Colistin sulfate

	Resistance ($\text{M}\Omega$)	Capacitance (μF)
Bilayer	0.84 ± 0.13	1.93 ± 0.11
100 $\mu\text{L}/\text{mL}$ AuNP 18h + 10 mg/mL Colistin 18 h	4.02 ± 0.39	1.40 ± 0.08
100 $\mu\text{L}/\text{mL}$ AuNP 18h + 10 mg/mL Colistin 48 h	0.05 ± 0.03	2.42 ± 0.30
CaCl₂ rinse 1 h	0.01 ± 0.0001	1.73 ± 0.19
CaCl₂ rinse 72 h	0.62 ± 0.08	1.60 ± 0.08
Bilayer	0.98 ± 0.22	2.03 ± 0.20
100 $\mu\text{L}/\text{mL}$ AuNP 18 h	0.49 ± 0.07	1.84 ± 0.08
100 $\mu\text{L}/\text{mL}$ AuNP + 10 mg/mL Colistin 18h	0.002 ± 0.0003	2.22 ± 0.32
CaCl₂ rinse 1 h	0.01 ± 0.0007	1.80 ± 0.19
CaCl₂ rinse 72 h	0.14 ± 0.01	1.50 ± 0.04

To determine if more significant damage could be caused to the membrane, the nanoparticle concentration was then increased to 200 $\mu\text{L}/\text{mL}$. Bode plots of lipid bilayers exposed to 200 μL gold nanoparticles and 10 mg/mL Colistin are shown in Figure 6.7 and Table 6.4.

As before, the effects were explored of immediately combining nanoparticles and Colistin as well as pre-treating the bilayer with nanoparticles for 18 h prior to the addition of the antibiotic.

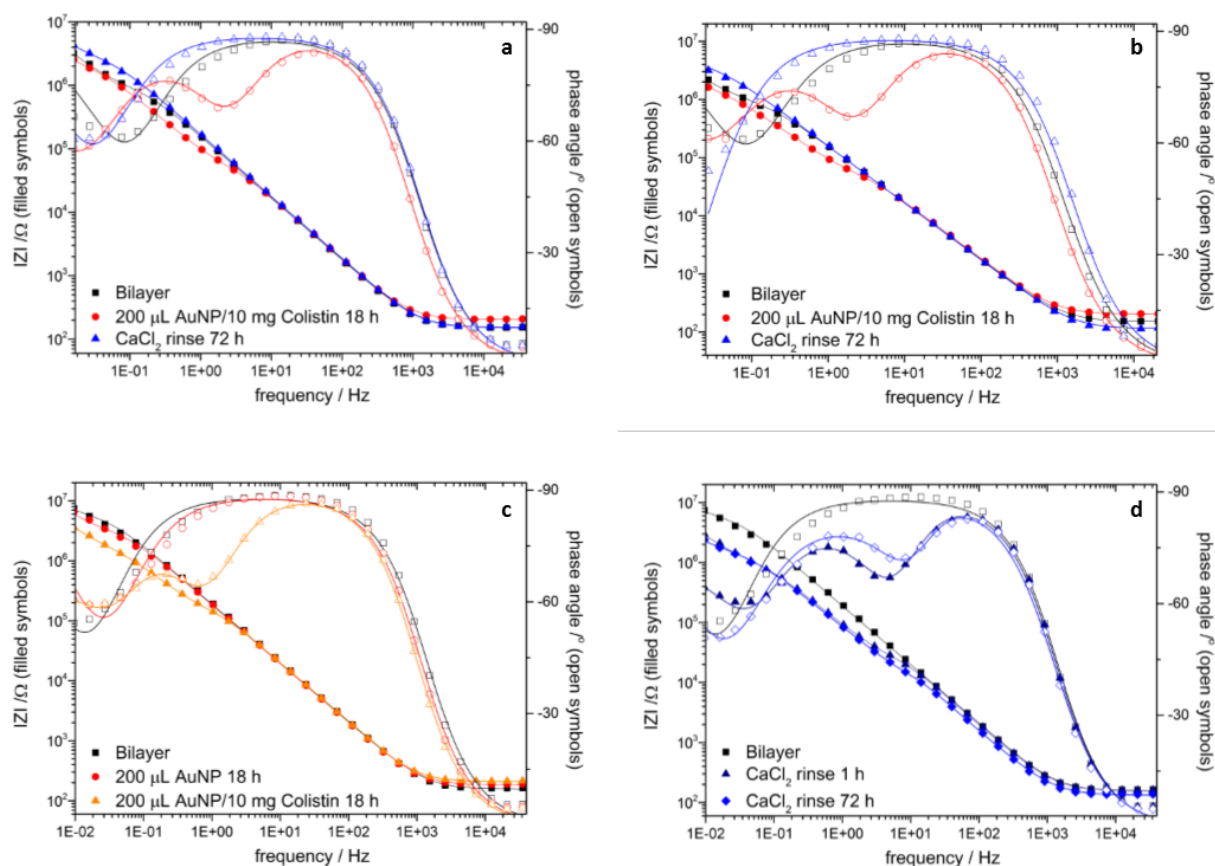


Figure 6.7: Bode plots of LPS-tBLMs exposed to 200 $\mu\text{L}/\text{mL}$ gold nanoparticles combined with 10 mg/mL Colistin Sulfate and rinsing of the system with CaCl_2 (a), which was then repeated after rinsing on the same membrane (b) and exposure of the LPS-tBLM to 200 $\mu\text{L}/\text{mL}$ gold nanoparticles only before the addition of colistin for 18 h (c) and rinsing of the membrane (d).

Adding nanoparticles and Colistin simultaneously caused a reversible reduction in membrane resistance by around two orders of magnitude. The increased nanoparticle concentration to 200 $\mu\text{L}/\text{mL}$ did not cause additional membrane damage when combined with Colistin. The effect also remained fully reversible, suggesting that only temporary structural changes were caused in the membrane. The removal of Colistin and nanoparticles from the system allowed the membrane to repair the defects over a period of 72 h. This treatment can be repeated with the same effect after the membrane has recovered.

When the bilayer was first incubated with 200 $\mu\text{L}/\text{mL}$ gold nanoparticles for 18 h before the addition of the antibiotic, the resistance of the membrane was irreversibly reduced by three orders of magnitude.

Table 6.4: Electrical properties of LPS-tBLMs exposed to 200 $\mu\text{L}/\text{mL}$ gold nanoparticles and 10 mg/mL Colistin sulfate

	Resistance ($M\Omega$)	Capacitance (μF)
Bilayer	0.63 ± 0.08	1.68 ± 0.07
200 $\mu\text{L}/\text{mL}$ AuNP 10 mg/mL Colistin 18 h	0.02 ± 0.001	1.79 ± 0.07
CaCl₂ rinse 1 h	1.98 ± 0.29	1.47 ± 0.11
200 $\mu\text{L}/\text{mL}$ AuNP 10 mg/mL Colistin 18 h	0.02 ± 0.002	1.63 ± 0.06
Bilayer	4.48 ± 0.67	1.17 ± 0.09
200 $\mu\text{L}/\text{mL}$ AuNP 18 h	2.45 ± 0.37	1.27 ± 0.09
200 $\mu\text{L}/\text{mL}$ AuNP + 10 mg/mL Colistin 48h	0.08 ± 0.01	1.43 ± 0.04
CaCl₂ 1 h	0.01 ± 0.001	1.25 ± 0.10
CaCl₂ 72 h	0.003 ± 0.001	1.45 ± 0.35

The addition of 200 $\mu\text{L}/\text{mL}$ gold nanoparticles likely created enough membrane defects that Colistin could permanently insert into the membrane and partially solubilise lipids. It is possible that the increased defect formation enables Colistin to penetrate the bilayer further than was enabled by lower nanoparticle concentrations such that it can no longer be washed from the bilayer when the system is rinsed. The membrane resistance decreased further even when it was stored under CaCl₂ in the absence of antibiotics or nanoparticles.

Due to the limited amount of nanoparticle solution that was available, further increases in nanoparticle concentration could not be explored. It would be interesting to further explore the effect that exposure to nanoparticles has on the susceptibility of the membrane to antibiotics such as Colistin. The shape of the nanoparticles may also have a significant impact on their toxicity to cell membranes. For example, gold nanorods coated with PDADMAC are not toxic to HeLa cell lines (a commonly used cell line with which the toxicity of various compounds can be studied), and do not cause abnormalities in gene expression in these cell lines.[1]

The effect of nanoparticles on the membrane when combined with antibiotics significantly differs from the effect of only Colistin on the LPS-tBLMs that was shown in Chapter 5. When treating the bilayers with the antibiotic only, an increase in membrane roughness (with a corresponding change in membrane capacitance) was observed, but no change of membrane resistance. The change of capacitance was attributed to the formation of lesions in the outer leaflet of the bilayer.

The reduction of membrane resistance and the absence of any increase in membrane capacitance when combining nanoparticles with the antibiotic suggests that the nanoparticles alter the mechanism by which the antibiotic damages the membrane. It is possible that the formation of lesions caused by the addition of nanoparticles pre-disposes the formation of pore-like defects where Colistin solubilises the lipopolysaccharides at the defect sites. However, a thorough understanding of the effect of combining nanoparticles with antibiotics can only be gained *via* neutron scattering experiments.

6.5 Conclusion

Cationic gold nanoparticles can bind to the lipid bilayer, causing the formation of a small number of membrane defects. This effect did not increase with nanoparticle concentration or incubation time. The combination of gold nanoparticles with Colistin caused more significant damage to the lipid bilayer than either gold nanoparticles or Colistin individually, but the effects were reversible when both antibiotic and nanoparticle were added to the membrane simultaneously. Exposing the bilayer to a high concentration of nanoparticles for 18 h prior to the addition of Colistin sulfate resulted in permanent irreversible damage to membrane, resulting in further deterioration of membrane properties even after the bilayer was rinsed to remove nanoparticles and antibiotics.

6.6 References

1. Alkilany, A.M. and C.J. Murphy, *Toxicity and cellular uptake of gold nanoparticles: what we have learned so far?* Journal of Nanoparticle Research, 2010. **12**(7): p. 2313-2333.
2. Hayden, S.C., et al., *Aggregation and Interaction of Cationic Nanoparticles on Bacterial Surfaces.* Journal of the American Chemical Society, 2012. **134**(16): p. 6920-6923.
3. Li, X., et al., *Functional Gold Nanoparticles as Potent Antimicrobial Agents against Multi-Drug-Resistant Bacteria.* ACS Nano, 2014. **8**(10): p. 10682-10686.
4. Feng, Z.V., et al., *Impacts of gold nanoparticle charge and ligand type on surface binding and toxicity to Gram-negative and Gram-positive bacteria.* Chemical Science, 2015. **6**(9): p. 5186-5196.
5. Falagas, M.E., S.K. Kasiakou, and L.D. Saravolatz, *Colistin: the revival of polymyxins for the management of multidrug-resistant gram-negative bacterial infections.* Clinical infectious diseases, 2005. **40**(9): p. 1333-1341.
6. Pelletier, M.R., et al., *Unique structural modifications are present in the lipopolysaccharide from colistin-resistant strains of Acinetobacter baumannii.* Antimicrobial agents and chemotherapy, 2013. **57**(10): p. 4831-4840.
7. Moffatt, J.H., et al., *Colistin resistance in Acinetobacter baumannii is mediated by complete loss of lipopolysaccharide production.* Antimicrobial agents and chemotherapy, 2010. **54**(12): p. 4971-4977.
8. Hsia, C.-Y., et al., *A Molecularly Complete Planar Bacterial Outer Membrane Platform.* Scientific Reports, 2016. **6**: p. 32715.
9. Balouiri, M., M. Sadiki, and S.K. Ibensouda, *Methods for in vitro evaluating antimicrobial activity: A review.* Journal of Pharmaceutical Analysis, 2016. **6**(2): p. 71-79.
10. Bölin, I., L. Norlander, and H. Wolf-Watz, *Temperature-inducible outer membrane protein of Yersinia pseudotuberculosis and Yersinia enterocolitica is associated with the virulence plasmid.* Infection and Immunity, 1982. **37**(2): p. 506-512.
11. Vogt, J. and G.E. Schulz, *The structure of the outer membrane protein OmpX from Escherichia coli reveals possible mechanisms of virulence.* Structure, 1999. **7**(10): p. 1301-1309.
12. Koebnik, R., K.P. Locher, and P. Van Gelder, *Structure and function of bacterial outer membrane proteins: barrels in a nutshell.* Molecular Microbiology, 2000. **37**(2): p. 239-253.
13. Ziervogel, B.K. and B. Roux, *The Binding of Antibiotics in OmpF Porin.* Structure (London, England : 1993), 2013. **21**(1): p. 76-87.
14. Yu, E.W., J.R. Aires, and H. Nikaido, *AcrB Multidrug Efflux Pump of Escherichia coli: Composite Substrate-Binding Cavity of Exceptional Flexibility Generates Its Extremely Wide Substrate Specificity.* Journal of Bacteriology, 2003. **185**(19): p. 5657-5664.
15. Kowal, J.Ł., et al., *Functional surface engineering by nucleotide-modulated potassium channel insertion into polymer membranes attached to solid supports.* Biomaterials, 2014. **35**(26): p. 7286-7294.
16. Civjan, N.R., et al., *Direct solubilization of heterologously expressed membrane proteins by incorporation into nanoscale lipid bilayers.* Biotechniques, 2003. **35**(3): p. 556-563.
17. Holt, S.A., et al., *An ion-channel-containing model membrane: structural determination by magnetic contrast neutron reflectometry.* Soft Matter, 2009. **5**(13): p. 2576-2586.

6.7 Supplementary information

The equivalent circuits used to model EIS data are shown in Figure S 6.1: Equivalent circuits used to fit EIS data in this chapter. The full set of fitting parameters for all EIS data in this chapter can be found in Table S 6.1, Table S 6.2 and Table S 6.3.

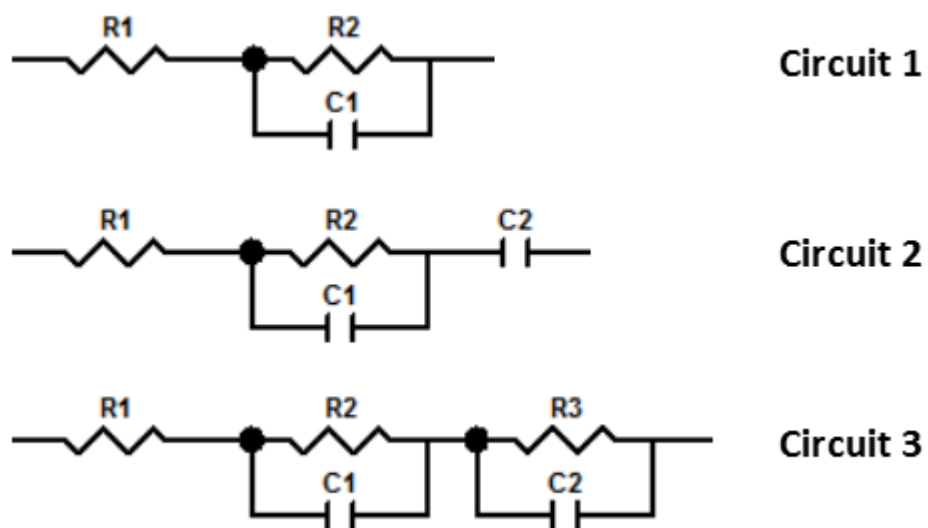


Figure S 6.1: Equivalent circuits used to fit EIS data in this chapter

Table S 6.1: All parameters of LPS-tBLMs treated with 50 $\mu\text{L}/\text{mL}$ Gold nanoparticles and a combination of 50 $\mu\text{L}/\text{mL}$ nanoparticles and 10 mg/mL Colistin sulfate. Resistances given in $\text{M}\Omega\cdot\text{cm}^2$ and capacitances in $\mu\text{F}\cdot\text{cm}^{-2}$

	Bilayer				Spacer				Circuit #
	Resistance	Error	Capacitance	Error	Resistance	Error	Capacitance	Error	
Bilayer	0.84	0.13	1.93	0.11			3.13	0.25	2
100 μL AuNP 18h 10 mg colistin 18 h	4.02	0.39	1.40	0.08			3.00	0.33	2
100 μL AuNP 18h 10 mg colistin 48 h	0.05	0.03	2.42	0.30	0.80	0.31	3.00	0.74	3
CaCl 1 h	0.01	0.00	1.73	0.19	1.69	0.23	2.64	0.22	3
CaCl 72 h	0.62	0.08	1.60	0.08	0.00	0.00	4.14	0.38	3
Bilayer	0.98	0.22	2.03	0.20			2.95	0.38	2
100 μL AuNP 18h	0.49	0.07	1.84	0.08			3.02	0.21	2
100 μL AuNP + 10 mg colistin 48h	0.00	0.00	2.22	0.32	0.90	0.15	3.12	0.31	3
CaCl 1 h	0.01	0.00	1.80	0.19	0.76	0.10	3.35	0.22	3
CaCl 72 h	0.14	0.01	1.50	0.04	1.78	0.35	2.90	0.43	3

Table S 6.2: All parameters of LPS-tBLMs treated with a combination of 100 $\mu\text{L}/\text{mL}$ nanoparticles and 10 mg/mL Colistin sulfate as well as membranes pre-treated with 100 $\mu\text{L}/\text{mL}$ Gold nanoparticles prior to the addition of the antibiotic. Resistances given in $\text{M}\Omega\cdot\text{cm}^2$ and capacitances in $\mu\text{F}\cdot\text{cm}^{-2}$

	Bilayer				spacer			Circuit #
	Resistance	Error	Capacitance	Error	Capacitance	Error		
Bilayer	12.5	0.39	0.99	0.01				1
50 $\mu\text{L}/\text{mL}$ AuNP 18 h	2.02	0.45	1.58	0.19	2.84	0.56		2
300 $\mu\text{L}/\text{mL}$ AuNP 18 h	1.88	0.37	1.45	0.16	3.09	0.65		2
300 $\mu\text{L}/\text{mL}$ AuNP 96 h	3.49	1.22	1.18	0.21	6.99	6.78		2
Bilayer	5.29	1.21	1.55	0.26	2.48	0.61		2
50 $\mu\text{L}/\text{mL}$ AuNP + 10 mg/mL Colistin 18 h	17.6	4.72	1.34	0.34	2.75	1.35		2
50 $\mu\text{L}/\text{mL}$ AuNP + 10 mg/mL 48 h	17.3	5.20	1.37	0.36	2.95	1.60		2
50 $\mu\text{L}/\text{mL}$ AuNP + 10 mg/mL h	3.61	1.18	1.83	0.40	2.54	0.72		2

Table S 6.3: All parameters of LPS-tBLMs treated with a combination of 100 $\mu\text{L}/\text{mL}$ nanoparticles and 10 mg/mL Colistin sulfate as well as membranes pre-treated with 100 $\mu\text{L}/\text{mL}$ Gold nanoparticles prior to the addition of the antibiotic. Resistances given in $\text{M}\Omega.\text{cm}^{-2}$ and capacitances in $\mu\text{F}.\text{cm}^{-2}$

	Bilayer				Spacer				Circuit #
	Resistance	Error	Capacitance	Error	Resistance	Error	Capacitance	Error	
Bilayer	4.48	0.67	1.17	0.09			3.39	0.74	2
200 ul AuNP 18h	2.45	0.37	1.27	0.09			3.08	0.51	2
200 ul AuNP + 10 mg colistin 48h	0.08	0.01	1.43	0.04	1.03	0.30	3.26	0.66	3
CaCl 1 h	0.01	0.00	1.25	0.10	0.64	0.07	3.47	0.18	3
CaCl 72 h	0.00	0.00	1.45	0.35	12.14	0.21	2.96	0.29	3
Bilayer	0.63	0.08	1.68	0.07			2.91	0.18	2
200 ul AuNP 10 mg colistin 18 h	0.02	0.00	1.79	0.07	1.40	0.29	2.96	0.45	3
CaCl 1 h	1.98	0.29	1.47	0.11	0.00	0.00	2.91	0.40	3
200 ul AuNP 10 mg colistin 18 h	0.02	0.00	1.63	0.06	0.88	0.14	3.70	0.37	3
NaCl 1 h	0.00	0.00	1.20	0.48	0.61	0.22	4.11	0.84	3

7 Summary, Future Directions and Outlook

7.1 Summary

Due to the central role performed by membrane-related processes and membrane proteins in the functioning of all organisms, it is vital that the range of tools and approaches available to study these processes continues to be enhanced. However, no single model membrane architecture can be sufficient to study all membrane proteins and processes as there is an extraordinarily diverse range of lipid membranes in nature. Rather, a diverse range of model membrane types is needed to ensure that a suitable architecture can be found for each study. The central topic of this thesis was to enhance the variety of available model membrane architectures.

Chapter 4: Membrane Structure and Hydration described the synthesis and structural analysis of new membrane architectures aiming to improve sub-membrane hydration. Replacement of the ethylene glycol segment of DPhyTL with ester linkages of various lengths did not result in improved sub-membrane hydration. This indicates that both the packing density and chemical composition of the tethering segment impact sub-membrane hydration, as in all cases when using 100% anchorlipid, the sub-membrane hydration did not increase.

However, the change in tether chemistry caused extended retention of ions in the sub-membrane space. Instead of being replaced immediately upon exchanging the electrolyte, the ions were slowly transported out of the sub-membrane space over a period of 24h along the concentration gradient when the lipid membrane was incubated with MilliQ. When the inner leaflet was assembled from mixtures of 40-60% anchorlipid diluted with mercaptoethanol to form sparsely tethered lipid bilayer membranes, the sub-membrane hydration was increased from 5% to 25%.

Continuing on from this work, **Chapter 5: Membrane Architectures Mimicking Gram-Negative Bacteria** showed the adaptation of tBLM architectures to mimic the outer membrane structure of gram-negative bacteria by creating tBLMs in which the outer leaflet is comprised of bacterial lipopolisaccharides (LPS) or a mixture of LPS and phospholipid to create an LPS-tBLM. These membrane architectures were developed to obtain a new means of studying the effect of antibiotic drugs and substances on the outer membrane of gram-negative bacteria, as they are among the most dangerous pathogens due to their ability to rapidly evolve resistance to antibiotics.

LPS-tBLMs comprised of 100% Lipopolysaccharides formed readily on SAMs assembled from 100% DPhyTL, with resistances of 10-30 $M\Omega\text{cm}^2$, these membranes were not susceptible to the effects of antibiotics. This is likely a result of the low fluidity of these membranes due to the densely packed inner leaflet. The susceptibility of the membrane to the effects of antibiotics was increased by using a sparsely tethered inner leaflet prepared from a solution containing a 4:1 mixture of DPhyTL/mercaptoethanol, and by including a small amount of the phospholipid DPhyPC in the membrane. This sparsely tethered LPS-tBLM architecture responds to Colistin by forming lesions, similar to the effects observed in bacterial membranes. The formation of lesions was indicated by a significant increase in membrane roughness upon exposure to Colistin sulfate.

This model system can be used to quickly assess the activity of new antibiotics targeting the cell membrane in a controlled environment. Because the lipid bilayers are self-assembled and can be monitored using electrochemical methods, they avoid many of the problems associated with other methods of testing new antibiotics that require the culturing of bacterial colonies or broth cultures in the presence of the drug candidate. These methods are time-consuming, and it can be difficult to obtain reliable data. The development of an LPS-tBLM is the first step in designing a microfluidic chip containing an array of membrane patches. This array of membranes could be used to screen large compound libraries for their ability to damage the bacterial membrane such that only the most promising drug candidates are selected for more time-consuming studies.

In addition, the development of an easy to assemble model of the outer membrane of gram-negative bacteria enables a wide range of future studies. These studies include improving the current knowledge around the mechanism of action of membrane-targeting antibiotics, enhancing the development of novel antibacterial treatments and enabling the study of membrane proteins from gram-negative bacteria in a more realistic environment.

Chapter 6: Synergistic interactions of nanomaterials and antibiotics presents some promising preliminary work investigating the effect of cationic gold nanoparticles on LPS-tBLMs and the possibility of synergistic effects between cationic gold nanoparticles and the membrane targeting antibiotic Colistin sulfate. Lastly, an outlook is presented exploring the potential of this membrane technology to serve as a platform to carry out rapid and automated large-scale screening for membrane-targeting drug candidates.

7.2 Future developments

7.2.1 Exploring the effect of membrane structure and composition on antibiotic susceptibility

In chapter 5, the structure and behaviour of tBMLs containing RcLPs (an LPS molecule with an oligosaccharide segment of moderate length) were explored. It is possible that changes in the length of the oligosaccharide segment have a significant impact on the strength with which calcium ions are bound to the membrane surface as well as the bilayers' susceptibility to antibiotics such as Colistin or derivatives of Colistin such as Polymyxin B. Knowledge about the efficacy of Colistin against varying LPS structures will be of significant benefit in drug development, enabling the optimisation of antibiotics towards different LPS structures for better treatment outcomes for patients.

There is a large degree of variation between the size and structure of LPS molecules between bacterial strains (see Figure 7.1 for a general schematic). It is likely that the structure of the LPS molecule has a significant impact on the susceptibility of a bacterial strain to membrane-targeting antibiotics.

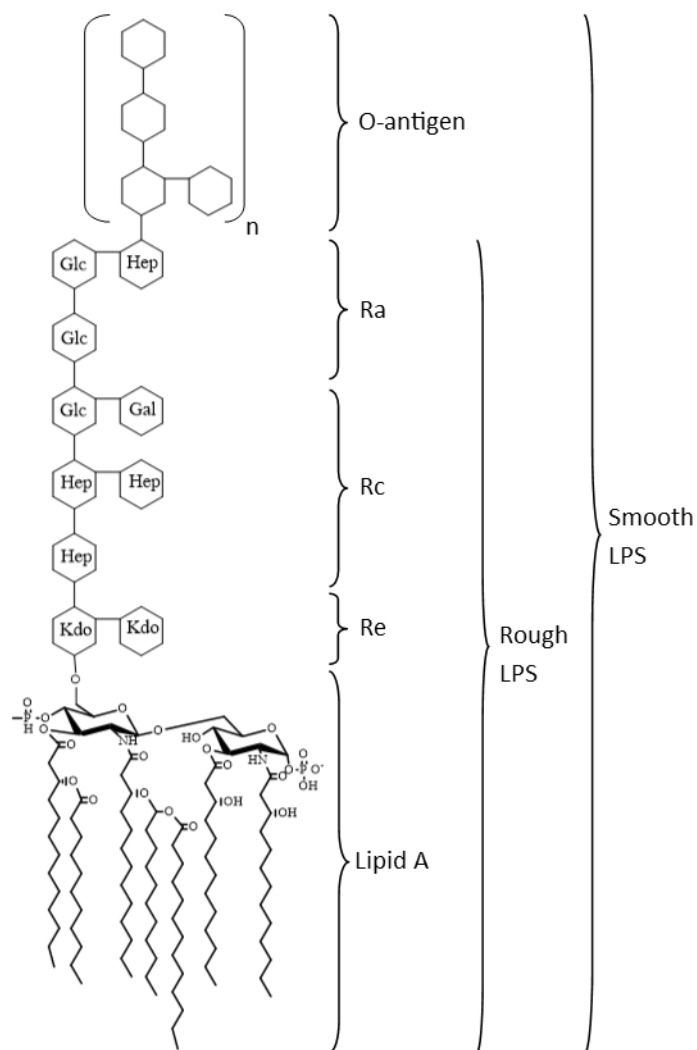


Figure 7.1: General schematic of an LPS molecule. The structure of LPS molecules varies significantly, both in the composition of the Lipid A segment and the length of the sugar chains.

In addition to exploring the properties of bilayers formed with LPS extracted from various strains (and their derivatives), it has also been shown that bacteria are capable of changing the structure of the outer membrane to resist treatment with Colistin. They achieve this either by adding positively charged residues to the Lipid A segment[1], altering its susceptibility to binding of Colistin, or by completely removing all LPS from the outer membrane[2]. By evolving to avoid the effects of Colistin, however, the bacteria may become vulnerable to other antibiotics they were previously able to resist. Using model membranes to study the susceptibility of the membranes to other compounds will significantly enhance the efficiency of developing treatment strategies for Colistin-resistant bacteria.

The main disadvantage of using purified LPS extracted from bacteria is that the purification process is expensive and time consuming, with the product costing several tens of thousands of dollars per gram of purified LPS. The purification procedure will need to be performed for every new bacterial species to carry out a systematic study of LPS structures and their behaviour. Thus, there will be a significant delay between the discovery of a new type of resistant bacteria, and the development of effective treatment methods.

Instead, it is possible to produce lipid bilayers comprised of outer membrane vesicles (OMVs, lipid vesicles naturally formed by GNB during cell division), which already have been shown to form solid-supported lipid bilayers by vesicle fusion.[3] It is likely that methodologies can be developed that allow bilayer formation by adding bacterial OMVs to pre-formed DPhyTL monolayers.

7.2.2 Large scale antibiotic screening

Currently, screening for novel antibiotics is carried out predominantly with a large number of cell culture growth and proliferation assays, either using the broth dilution method or by monitoring cell growth on an agarose plate, to assess the impact of the drug candidate on bacterial growth.[4] The drug candidates that prevent bacterial growth most effectively are then selected for further studies.

These methodologies are highly susceptible to small changes in growth conditions and can be difficult to reproduce. Furthermore, while they can be automated, some methods become costly when scaled up or require expensive equipment.[4] The efficiency of drug discovery would be greatly enhanced if only the most promising drug candidates were selected for this process. This could be achieved by developing a microfluidic chip containing hundreds or thousands of individually addressable membrane patches (see Figure 7.2). Each of these patches can serve to test a different drug candidate, enabling the screening of very large compound libraries with minimal effort prior to carrying out cell culture studies to determine the MIC of the drug candidates.

The main advantage of using membranes prepared exclusively by self-assembly is the fact that they can be used in a microfluidic chip, which would not be possible if the bilayer was assembled by Langmuir-Blodgett/Schaefer dipping.

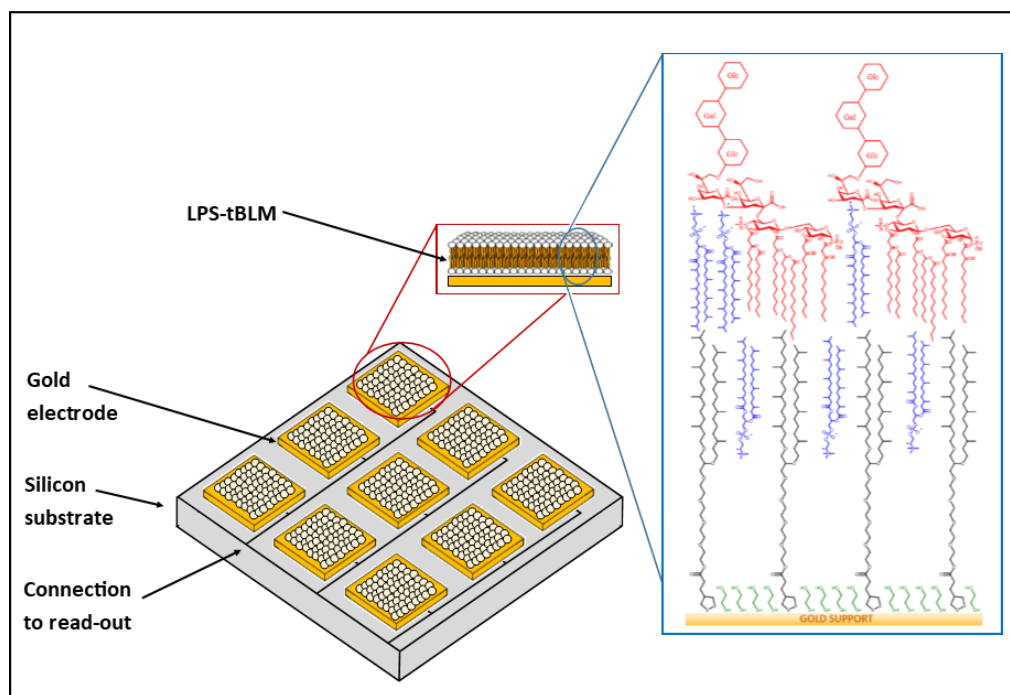


Figure 7.2: A microfluidic chip containing an array of gold electrodes functionalised with LPS-tBLMs.

The gold electrodes supporting the membranes contained within the chip can be manufactured with well-established lithographic methodologies on silicon substrates. The electrodes will then be covered with a microfluidic channel system, likely made from poly(dimethylsiloxane) as it is one of the most suitable materials used for these applications. Once the chip has been manufactured it should be stored under an inert atmosphere until required, at which point the electrodes are first functionalised with an anchorlipid followed by the addition of a distal leaflet *via* vesicle fusion. Ultimately, it is possible that using such a chip, model membranes can be assembled from outer membrane vesicles (vesicles produced by bacteria during the cell growth process) obtained from drug-resistant clinical isolates and a personalised treatment can be developed for the patient.

7.2.3 A platform to study bacterial membrane proteins

Bacterial membrane proteins are an important aspect of bacterial pathogenicity[5, 6] and their ability to sequester nutrients from their environment[6, 7]. Providing a controlled membrane-like environment matching their natural surroundings will significantly simplify the study of membrane components, particularly membrane proteins, while maintaining their native structure and function.

Outer membrane protein F (OmpF), for example, is a pore protein located in the outer membrane of *E. coli*, which is essential for nutrient uptake of the organism.[8] It is also used by the antibiotic Ampicillin (which inhibits cell wall synthesis) to enter the cell. Biophysical characterisation of the binding event of ampicillin to the channel under various conditions may lead to the development of new strategies to enhance treatment efficacy or to combat drug resistance. Resistance to Ampicillin can be partially attributed to a down-regulation of the expression of OmpF[9], but the most significant factor is a membrane protein known as AcrB Multidrug Efflux Pump.[10] This protein is able to eject harmful compounds from the bacterial cell to prevent cell death, enabling the bacteria to survive in the presence of Ampicillin. Biophysical studies of the AcrB protein may highlight possible means of blocking the efflux pump or inhibiting its function with a new or existing drug. This compound could then be combined with Ampicillin, enabling the treatment of infections that would otherwise be resistant to Ampicillin

The lipid vesicles used to form LPS-tBLMs are typically prepared from a dried suspension, which could denature or damage any incorporated protein. This method is therefore not suitable to create protein-functionalised LPS tBLMs. However, if protein-containing vesicles are formed during the protein purification steps, these vesicles can also be used for tBLM formation. Alternatively, detergent-stabilised proteins can also be added to pre-formed planar membranes with the use of bio-beads.[11, 12] It is also possible to immobilise a membrane protein on the substrate and subsequently assemble a lipid bilayer around the protein.[13] Attaching the protein to a solid support may cause impaired function of the protein or denature it, so an alternative approach is to form the outer leaflet of the tBLM *via* Langmuir-Blodgett film transfer of a lipid monolayer containing the membrane protein of interest on a gold surface functionalised with a DPhyTL-SAM (or a diluted SAM).

7.3 Conclusion

In addition to studying the effects of known membrane-targeting antibiotics, the LPS-tBLM developed in this project has the potential to serve as a platform to develop new antibiotic treatments for drug resistant infections. Some promising work has been shown in chapter 6, demonstrating novel approaches combining nanoparticles and antibiotics to provide enhanced membrane-damaging potential. In addition to investigating the effects of membrane-targeting compounds, these model membranes also provide a controlled environment in which the effect of drug candidates on the function of membrane proteins in their native form and function can be studied.

7.4 References

1. Pelletier, M.R., et al., *Unique structural modifications are present in the lipopolysaccharide from colistin-resistant strains of Acinetobacter baumannii*. Antimicrobial agents and chemotherapy, 2013. **57**(10): p. 4831-4840.
2. Moffatt, J.H., et al., *Colistin resistance in Acinetobacter baumannii is mediated by complete loss of lipopolysaccharide production*. Antimicrobial agents and chemotherapy, 2010. **54**(12): p. 4971-4977.
3. Hsia, C.-Y., et al., *A Molecularly Complete Planar Bacterial Outer Membrane Platform*. Scientific Reports, 2016. **6**: p. 32715.
4. Balouiri, M., M. Sadiki, and S.K. Ibsouda, *Methods for in vitro evaluating antimicrobial activity: A review*. Journal of Pharmaceutical Analysis, 2016. **6**(2): p. 71-79.
5. Bölin, I., L. Norlander, and H. Wolf-Watz, *Temperature-inducible outer membrane protein of Yersinia pseudotuberculosis and Yersinia enterocolitica is associated with the virulence plasmid*. Infection and Immunity, 1982. **37**(2): p. 506-512.
6. Vogt, J. and G.E. Schulz, *The structure of the outer membrane protein OmpX from Escherichia coli reveals possible mechanisms of virulence*. Structure, 1999. **7**(10): p. 1301-1309.
7. Koebnik, R., K.P. Locher, and P. Van Gelder, *Structure and function of bacterial outer membrane proteins: barrels in a nutshell*. Molecular Microbiology, 2000. **37**(2): p. 239-253.
8. Ziervogel, B.K. and B. Roux, *The Binding of Antibiotics in OmpF Porin*. Structure (London, England : 1993), 2013. **21**(1): p. 76-87.
9. Harder, K.J., H. Nikaido, and M. Matsushashi, *Mutants of Escherichia coli that are resistant to certain beta-lactam compounds lack the ompF porin*. Antimicrobial agents and chemotherapy, 1981. **20**(4): p. 549-552.
10. Yu, E.W., J.R. Aires, and H. Nikaido, *AcrB Multidrug Efflux Pump of Escherichia coli: Composite Substrate-Binding Cavity of Exceptional Flexibility Generates Its Extremely Wide Substrate Specificity*. Journal of Bacteriology, 2003. **185**(19): p. 5657-5664.
11. Kowal, J.L., et al., *Functional surface engineering by nucleotide-modulated potassium channel insertion into polymer membranes attached to solid supports*. Biomaterials, 2014. **35**(26): p. 7286-7294.
12. Civjan, N.R., et al., *Direct solubilization of heterologously expressed membrane proteins by incorporation into nanoscale lipid bilayers*. Biotechniques, 2003. **35**(3): p. 556-563.
13. Holt, S.A., et al., *An ion-channel-containing model membrane: structural determination by magnetic contrast neutron reflectometry*. Soft Matter, 2009. **5**(13): p. 2576-2586.